Heat Transfer Analysis in Ciliary Transport of MHD Flow

By

Naeema Manzoor

Reg. No. 51-FBAS/PHDMA/F15

Department of Mathematics and Statistics

Faculty of Basic and Applied Sciences

International Islamic University, Islamabad

2020

Heat Transfer Analysis in Ciliary Transport of MHD Flow

By

Naeema Manzoor

Supervised by

Dr. Khadija Maqbool

Department of Mathematics and Statistics

Faculty of Basic and Applied Sciences

International Islamic University, Islamabad

2020

Heat Transfer Analysis in Ciliary Transport of MHD Flow

By

Naeema Manzoor

A Thesis

Submitted in the Partial Fulfilment of the

Requirements for the degree of

DOCTOR OF PHILOSOPHY

IN

MATHEMATICS

Supervised by

Dr. Khadija Maqbool

Department of Mathematics and Statistics

Faculty of Basic and Applied Sciences

International Islamic University, Islamabad

2020

Author's Declaration

I, **Naeema Manzoor** Reg. No. **51-FBAS/PHDMA/F15** hereby state that my Ph.D. thesis titled: **Heat Transfer Analysis in Ciliary Transport of MHD Flow** is my own work and has not been submitted previously by me for taking any degree from this university, **International Islamic University, Sector H-10, Islamabad, Pakistan** or anywhere else in the country/world.

At any time if my statement is found to be incorrect even after my Graduation the university has the right to withdraw my Ph.D. degree.

Name of Student: ***(Naeema Manzoor)***
Reg. No. **51-FBAS/PHDMA/F15**
Dated: **01/01/2021**

Plagiarism Undertaking

I solemnly declare that research work presented in the thesis titled: **Heat Transfer Analysis in Ciliary Transport of MHD Flow** is solely my research work with no significant contribution from any other person. Small contribution/help wherever taken has been duly acknowledged and that complete thesis has been written by me.

I understand the zero tolerance policy of the HEC and University, **International Islamic University, Sector H-10, Islamabad, Pakistan** towards plagiarism. Therefore, I as an Author of the above titled thesis declare that no portion of my thesis has been plagiarized and any material used as reference is properly referred/cited.

I undertake that if I am found guilty of any formal plagiarism in the above titled thesis even after award of Ph.D. degree, the university reserves the rights to withdraw/revoke my Ph.D. degree and that HEC and the University has the right to publish my name on the HEC/University Website on which names of students are placed who submitted plagiarized thesis.

Student/Author Signature: _____

Name: **(Naeema Manzoor)**

Certificate of Approval

This is to certify that the research work presented in this thesis, entitled: **Heat Transfer Analysis in Ciliary Transport of MHD Flow** was conducted by **Ms. Naeema Manzoor,** Reg. No. **51-FBAS/PHDMA/F15** under the supervision of **Dr. Khadija Maqbool** no part of this thesis has been submitted anywhere else for any other degree. This thesis is submitted to the **Department of Mathematics & Statistics, FBAS, IIU, Islamabad** in partial fulfillment of the requirements for the degree of **Doctor of Philosophy in Mathematics, Department of Mathematics & Statistics, Faculty of Basic & Applied Science, International Islamic University, Sector H-10, Islamabad, Pakistan.**

Student Name: Naeema Manzoor **Signature: _____**

Examination Committee:

a) External Examiner 1:
Name/Designation/Office Address **Signature: _____**

Prof. Dr. Sohail Nadeem
Professor of Mathematics,
Department of Mathematics,
Quaid-i-Azam University, Islamabad,

b) External Examiner 2:
Name/Designation/Office Address) **Signature: _____**

Dr. Nabeela Kousar
Associate Professor
Department of Mathematics,
Air University, Islamabad.

c) Internal Examiner:
Name/Designation/Office Address) **Signature: _____**

Dr. Ambreen Afsar Khan
Assistant Professor

Supervisor Name:
Dr. Khadija Maqbool **Signature: _____**

Name of HOD:
Dr. Ambreen Afsar Khan **Signature: _____**

Name of Dean:
Prof. Dr. Muhammad Irfan Khan **Signature: _____**

Dedication

I dedicate this dissertation to a man who sacrificed his life for me, whom himself was deprived of education but he went beyond all means to ensure that I have access to the best education. His love for knowledge and learning is the foundation of my qualifications. The love he instilled me for education and learning is what kept me motivated throughout my academic career.

My Father, Manzoor Hussain Karimi, the man responsible for what I am today.

Acknowledgements

Words are insufficient to describe my gratefulness and appreciation to the ALLAH Almighty, the creator of the universe, who gave me strength, ability, courage and patience to successfully complete my thesis. I pay tributes to the Holy Prophet Muhammad (PBUH), whose personality showed the right path to mankind and His teachings make us ponder to explore the world.

I would like to extend my gratitude to my respected supervisor **Dr. Khadija Maqbool**, for their patient guide, enthusiastic encouragement and useful critiques of this research work. This thesis would not be possible without her worthy comments, suggestions, advice and assistance for keeping my progress on schedule. I pay my respects to all my teachers who enabled me for making my dream true.

I would have never accomplished all this without love, support and encouragement of my family especially parents. I am also thankful to my **Ph.D. class fellows especially Hadia Tariq** who always helped with all aspects of academia.

I am also very thankful to the Higher Education Commission, Pakistan for providing me the opportunity to avail the International Research Support Initiative Program, which enhanced and improved my capabilities for research and provided the opportunity for further international collaboration.

In the end, I am grateful to Allah for bestowing me with such a wonderful husband, **Abdul Saboor**, whose love, care, encouragement, support, relentlessness, patience and sacrifices have been a pillar of strength for me during the time-consuming process to this thesis.

Naeema Manzoor

Preface

A complex feature observed on biological surfaces is the ciliary transport in the existence of magnetic and thermal field. Cilia are small but complex additional structures that protrude from the walls of the vessels. Cilia with an average length of around 0.1 mm can easily fold and thus contribute to many advanced biophysical transport mechanisms. They usually emerge in large density dies, unlike the flagella, which generally exists in nature as pairs or single structures. The ciliary flogging mechanisms (metachronism) which control the direction of the induced propulsion, therefore differ considerably from the flagellar flogging. They manifest whip-like movements that appear in plants, cells, sea creatures and physiological organs. They play a huge part across the spectrum and biological properties e.g. embryonic mechanotransduction processes, tracheal aerodynamics, ventricular cerebrospinal fluid dynamics, coral reef systems, etc. The mathematical modeling of moving cilia has significance to estimate the various variables that are effected in this mechanism. Although experiments together with mathematical model of ciliary transport estimates the role of frequency, length, velocity and number of cilia in fluid dynamics and provide the awareness of ciliary importance in occurrence of diseases (related to cilia). Motivated by these facts, the cynosure of current thesis is based on the study of different fluid flow originate by the ciliary movement in a magnetic and thermal field with different effects like Hall effect, ion slip effect, magnetic field effect, viscous dissipation effect and inertial effects in different geometries and mathematical tools. Under such assumptions, the governing equations of above mentioned biological flows are modelled using continuity, momentum and energy equation. To analyze the effect of ion-slip and Hall current, generalized Ohm's law and Maxwell's equation are used. The resulting partial differential equations are developed with or without long wavelength approximation. The resulting linear and nonlinear system of equation has been evaluated by the perturbation method, Adomian decomposition method, Homotopy perturbation method and Fourier series expansion method. The effects of emerging parameters are shown through graphs plotted by the software Mathematica. The impacts of physical parameters such as Hartmann number, ion-slip parameter, Hall parameter, porosity parameter, Weissenberg number, slip parameter, cilia length, power law index, fluid parameters and Brinkman

number are illustrated by the graphs. It is found that cilia has to work more efficiently in the existence of magnetic field and heat transport in the fluid can be enhanced by the ciliary activity. This thesis comprises eight chapters which are described in following manners.

The introduction of fluid mechanics, basic information about cilia, non-dimensional numbers, fundamental laws, governing equations and explanation of methodology pertinent to the problems presented in chapters are included in chapter one.

Chapter two develops the mathematical model of magnetohydrodynamic (MHD) flow through the infinite length of ciliated porous planer surface. The governing partial differential equations are evaluated by Fourier series expansion method. The exact solution has been found which is used to find the velocity of propulsion of wave. The application of ciliary propulsion is also explained in this chapter. The behavior of physical variables are estimated by graphical results. This study is published in **Journal of Magnetism and Magnetic Materials, (2019) doi.org/10.1016/j-jmmm.2019.02.074.**

Chapter three extended the work presented in chapter two where influence of Hall and ion-slip on the metachronal flogging of cilia to flow the Newtonian fluid has been obtained. The finding are discussed and displayed by the graphs. This investigation is published in **Journal of porous media (2020) 23, 943-954.**

The rheological behavior of the fluid simulated with the non-Newtonian fluid under the action of magnetic field has been considered in chapter four. Mathematical modeling is evaluated for the flow of viscoelastic physiological fluid with Johnson-Segalman constitutive model in channel. The channel is ciliated internally and flow occur due to whip-like motion of cilia. The governing equations are simplified and solved analytically. The series solution is found by the perturbation method. The effect of important parameters on velocity field, pressure rise and pressure gradient are interpreted graphically. This work is published in **Computer Methods in Biomechanics and Biomedical Engineering, (2019) 22, 685-695.**

Chapter five illustrates the mathematical modeling of ciliary transport of electrically conducting inertial flow in a two dimensional channel implanted in a porous medium. The fluid obey the law of second grade constitutive model. The partial differential equations are non-linear and complex due to the inertial effect. The stream function, velocity profile and pressure gradient are commutated graphically for several values of involved

parameters. The analytical solution of complex partial differential equation is obtained by Homotopy perturbation method (HPM). The comparison of velocities due to symplectic and antiplectic metachronal wave are achieved graphically. This analysis is submitted for publication in **Mathematical Biosciences**.

In chapter six, force convective viscoelastic physiological Jeffery fluid model is contemplated through the ciliated channel. The Darcy law for porous medium is also used to model the problem. To obtain the impact of magnetohydrodynamic (MHD), magnetic field is applied normally. The viscous dissipation is also incorporated in the energy equation. The non-linear governing equations are evaluated by the Adomian decomposition method. The impact of interested parameters on temperature profile, velocity, pressure rise and pressure gradient are plotted by the graphs. The streamlines for the effect of various parameters are shown graphically. This effort is published in **Heat Transfer—Asian Research, (2018) 1–26.**

Chapter seven is devoted to analyze the mixed convective flow of electrically conducting generalized Newtonian fluid in a vertical ciliated channel. The behavior of the fluid is simulated with the Carreau constitutive model. The momentum and energy equations are simplified by using the low Reynolds number and small wavelength approximations. The emerging complicated boundary value problem is solved by Adomian decomposition method (ADM). The pressure rise, axial velocity, pressure gradient and temperature profile are obtained graphically for various values of interested variables. The material of this chapter is submitted for publication in **Journal of Thermal Analysis and Calorimetry**.

Chapter eight involves the convective flow of Carreau fluid through the two dimensional ciliated tube with ohmic heating. The Generalized Ohm's law is used to obtain the impact of Hall current and ion-slip on the fluid flow. The non-linear momentum equation and non-homogeneous energy equation are solved analytically. The Homotopy perturbation method has been used to compute the axial pressure gradient, axial velocity, streamlines and the temperature profile. The interested variables based on physiologically relevant data are graphically shown and discussed in detail. The results emerged in this chapter (chap. eight) are submitted for publication in **European journal of physics**.

Nomenclature

$\boldsymbol{V}$	Velocity field vector
u, v	Wave frame longitudinal and transverse velocity
x, y	Wave frame rectangular coordinates
$\widehat{U}, \widehat{V}$	Fixed frame longitudinal and transverse velocity
$\widehat{X}, \widehat{Y}$	Fixed frame rectangular coordinates
$\widehat{R}, \widehat{Z}$	Cylindrical coordinates of fixed frame
$\widehat{U}, \widehat{W}$	longitudinal and transverse velocity in fixed frame
$\hat{P}, \hat{p}$	Pressure in fixed and wave frame
$\boldsymbol{I}$	Identity tensor
$\boldsymbol{S}$	Cauchy stress tensor
$\boldsymbol{J}$	Current density
$\boldsymbol{B}$	Magnetic field
$\boldsymbol{E}$	Electric filed
$\boldsymbol{b_f}$	Body force
$\boldsymbol{R}$	Darcy's resistance
T	Fluid temperature
c_p	Specific heat
ω	Cyclotron frequency
h	Half length of channel
t	Time
n	Power law index

k	Non-dimensional porosity parameter
$\mathcal{K}$	Permeability of porous medium
$\mathcal{M}$	Hartmann number
c	Wave speed
l	Wave amplitude
Q	Volume flow rate
Re	Reynolds number
Pr	Prandtl number
Ec	Eckert number
Br	Non-dimensional Brinkman number
Gr	Grashof number
k_1	Thermal conductivity
s_0	Unit area
e_{ij}	Rate of strain tensor
We	Weissenberg number
$\boldsymbol{D}$	Symmetric part of the velocity gradient
$\boldsymbol{W}$	Skew symmetric part of the velocity gradient
$\boldsymbol{a}$	Rheological slip parameter
m	Relaxation time
c_f	Skin friction coefficient

Greek Letters

ρ	Fluid density
λ	Wavelength
λ_1, λ_2	viscoelastic parameters
β	Non-dimensional wave number
β_t	Coefficient of thermal expansion
β_e	Hall parameter
β_i	Ionslip parameter
ε	Cilia length
α	Eccentricity of elliptical path
σ_{ij}	Stresses exerted by the organisms on the fluid
μ_m	Magnetic permeability
ψ	Stream function
$\dot{\gamma}$	Shear rate
Φ	Viscous dissipation
σ	Thermal conductivity of the fluid
φ	Porosity media
μ	Viscosity of fluid
μ_∞	Infinite shear rate viscosity
μ_0	Zero shear rate viscosity
θ	Dimensionless temperature
$\boldsymbol{\Gamma}$	Time constant

τ_0	Electron collision time
$\boldsymbol{\tau}$	Extra stress tensor

Contents

Chapter 1

Introduction

1.1 Fluid Mechanics

1.1.1 History and applications

Fluid mechanics studies fluid in rest or motion. Leonardo Da Vinci (1452-1519) pioneered it by building the first chambered canal lock near Milan. Amongst his most remarkable work, his study was on flights of birds. He studied the complex movements of flight of birds, air flow and designed models for a flying machine which resembles a modern day helicopter. His torch was carried forward by Galileo, Euler, Torricelli, Newton, D' Alembert and Bernoulli's family. Their observations and experiments made the study of fluid mechanics ponder on.

Fluid is working as a medium in all the fields of science and technology, in almost all the actions a person does. For instance the design of all means of transportation including subsonic and supersonic aircraft, surface ships, submarines, automobile, pumps, fans, blowers, compressors, and turbines require applications of fluid mechanics. Even the circulatory system of the body is based on the law of fluid mechanics.

1.1.2 Types of Fluids

Fluid mechanics is further divided into Newtonian fluids (stress and deformation rate vary linearly) and the non-Newtonian fluids (stress and strain rate vary nonlinearly). Some common Newtonian fluids include air, water and gasoline while the most familiar non-Newtonian fluids include toothpaste, ketchup, emulsions and Lucite paints.

1.2 Cilia and its Working

Cilia are the slender 1-10μm long organelles, these organelles are present on surface of many microorganisms and on the different cells inside the human and animal bodies to perform the variety of essential activities. The ciliary activity helps to move the complete cell body or minute particles in fluid medium, or the cilia are static in epithelium and allow the fluid flow across the epithelium. There are two different cilia

(motile and non-motile). **Motile cilia** are moving and exists in groups on an organism whereas **non-motile cilia** are stationary and found on a cell body. All protozoan ciliates possess motile cilia. They utilize the cilia not only for transportation, also to feed themselves. Examples include the mytilus, veligers of molluscs, vorticella, annelid trochophores, coleps and echinoderm larvae which all rely on cilia to get their destination. In mammals, cilia are involved in the normal physiology of the entire respiratory tract, especially in the mechanism of lubrication and clearance of its surface, and in body defenses against foreign particulate matter. In genital tract, cilia play a vital role in the passage of spermatozoa and in the conduction of ova.

1.2.1 Ciliary Structure

Cilia has complex internal structure called axenemes given in Fig. 1.1. Cilia is composed of protein filaments called microtubules. The cross-sectional area of cilia shows the arrangement of these microtubules. In moving cilia, it consists of 9 doublet pair of microtubules organized in a circular manner around two central microtubules called 9+2 arrangement. It also contain radial spokes, dynein arm and nexin links for different functions. Primary cilia consists of 9+0 (absence of two central microtubules) arrangement of microtubules.

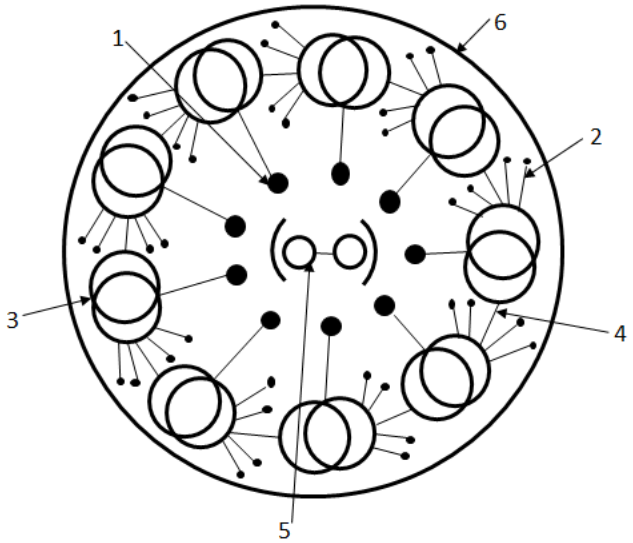

Fig. 1.1: The axoneme: 1-radial spoke, 2-dynein arms, 3-outer doublets, 4-nexin links, 5-central capsule, 6-plasma membrane.

1.2.3 Ciliary Movement

A cilium, collectively called cilia, exhibit two phase stroke, power stroke (effective stroke) and recovery stroke. Power stroke in which a cilium swings in full extension weakly, while in a recovery stroke it reach to the base and slowly return to the original position. The high friction effective stroke is followed by low friction recovery stroke. Cilium undergoes a cyclic motion with these two strokes, which generates force to induced relative motion between the cell and its surrounding fluid. Since cilia are close together on a single organism and move in coordination. This coordination produce a collective behavior of cilia beating which forms a wave, called metachronal wave. This wave can have different types, depending on the direction of propagation with effective stroke. If both (wave and power stroke) are in same direction, it is **symplectic** metachronal wave, or in opposite direction, called **antiplectic** metachronal wave, or perpendicular to each other, known as **diplectic** metachronal wave.

1.2.4 Pumping

A characteristics feature of ciliary transport in which cilia pumps the fluids from smaller pressure to larger pressure under certain conditions is known as pumping. This **pumping** can be **negative or positive** depending on negative and positive flow rate, respectively. If both pumping and pressure rise are positive, it is known as **ciliary pumping**. If pumping is positive but pressure rise is negative, it is **augmented pumping or co-pumping**. If pumping is negative and pressure rise is positive, it is **retrograde pumping**.

1.2.5 Trapping

Trapping is known as the circular bolus formed by the closed stream lines and move ahead along the metachronal wave of the ciliary flow. Basically, it helps to understand the behavior of flow pattern.

1.3 Some Basics Definitions

1.3.1 Surface Forces

The forces which are directly in contact with surface (internal or external) of the body. It decompose into normal force, i.e. act perpendicularly over the area and shear force, i.e. act tangentially over the area.

1.3.2 Body Forces

Forces that act on the entire volume of body but not in contact with the body e.g. forces due to magnetic field, electric filed and gravity.

1.3.3 Pressure Gradient

It is the rapid rate of change of pressure (i.e. applied force per unit area) in a specific area towards a peculiar direction. Mathematical form can be obtained by applying gradient operator to the pressure function.

1.3.4 Stream Lines

Streamlines describe the path of flow that is created by the fluid particles as it move with the flow and velocity at every point tangent to the path line.

1.3.5 Stream Function

The stream function, ψ, for which velocity components of incompressible fluid flow is expressed in derivative form and is used to represents the trajectory of flow so that it can be visualized graphically. Mathematically,

$$u = \frac{\partial \psi}{\partial y}, \quad v = -\frac{\partial \psi}{\partial x}, \tag{1.1}$$

where u and v are longitudinal and transverse velocities.

1.3.6 Volume Flow Rate

It offers the amount of fluid that passes through a unit area in unit time. It is also known as volumetric flow rate and usually represented by Q.

1.3.7 Hall Current and Ion-Slip Effect

The Hall current is the production of voltage difference when a current carrying conductor through an electric field is placed in a perpendicular direction of applied magnetic field, it is used to analyze the nature of conduction process in metals and semiconducting materials whereas an ion-slip effect is a relative drift that produced between ions, electrons and neutral particles due to the force exerted by the magnetic and electric field in the presence of high Hall parameter.

1.4 Heat Transfer

Heat transfer is also known as thermal energy. The form of energy which flow from one region to another or between the systems and surroundings as a result of temperature differences. Heat is transferred primarily through three modes conduction, convection are radiation.

Conduction (through surface): The continue process of energy transfer through the collision of warmer or high energetic particles to the cooler or low energetic particles until all particles get the same temperature.

Convection (through liquids): Convective heat transfer (or convection) is the study of processes which involves the heat transport by the flow of fluids. Heat transfer through fluid is thermal field and ensure energy balance of the system. The convective heat transfer is further divided into forced convection, free convection and mixed convection.

1.5 Laws of Fluid Mechanics

The fundamental laws of fluid mechanics which describe the fluid behavior are **mass, momentum and energy conversations** and are applicable in all the problems whether we realized it or not.

1.5.1 Continuity Equation

Law of conservation of mass is mathematically represented by the continuity equation. This Law states that neither mass can be generated nor demolished or the mass is conserved. For compressible fluid, the continuity equation is defined as follow

$$\frac{d\rho}{dt} + \rho\boldsymbol{\nabla}.\boldsymbol{V} = 0, \tag{1.2}$$

Where ρ is the density of fluid, $\boldsymbol{V}$ is the velocity field vector and $\frac{d}{dt}$ is the material time derivative which is defines as

$$\frac{d}{dt} = \frac{\partial}{\partial t} + \boldsymbol{V}.\boldsymbol{\nabla}. \tag{1.3}$$

Thus combining Eq. (1.2) and Eq. (1.3), we get

$$\frac{d\rho}{dt} + \boldsymbol{\nabla}.(\rho \boldsymbol{V}) = 0. \tag{1.4}$$

The continuity equation for incompressible fluid is defined as follow

$$\boldsymbol{\nabla}.\boldsymbol{V} = 0. \tag{1.5}$$

1.5.2 Momentum Equation

The law of conservation of momentum is governed by the following equation

$$\rho\left(\frac{\partial \boldsymbol{V}}{\partial t} + (\boldsymbol{V}.\boldsymbol{\nabla})\mathbf{V}\right) = -\boldsymbol{\nabla}P + \boldsymbol{\nabla}.\boldsymbol{\tau} + \rho \boldsymbol{b_f}, \tag{1.6}$$

in which $\boldsymbol{V}$, is the velocity field vector, ρ, is the density of fluid, P, is the pressure force, $\boldsymbol{\tau}$, is the extra stress tensor and $\boldsymbol{b_f}$ represents the body force.

1.5.3 Energy Equation

The convective heat transfer problem requires a solution for the temperature distribution through the flow. The equation for achieving this ultimate form is the energy equation. Mathematically we can write

$$\rho c_p\left(\frac{dT}{dt}\right) = k\boldsymbol{\nabla}^2 T + \boldsymbol{\tau}.\boldsymbol{L} + \rho r, \tag{1.7}$$

where T is the temperature, $\boldsymbol{\tau}$ is the extra stress tensor**,** r is radial heating**,** k is the thermal conductivity and c_p is the specific heat.

1.5.4 Generalized Ohm's Law

The current density $\boldsymbol{J}$ for Hall and ion-slip effect is interpreted by the generalized Ohm's law as follow

$$\boldsymbol{J} = \sigma(\boldsymbol{E} + \boldsymbol{V} \times \boldsymbol{B}) - \frac{\beta_e}{B_0}(\boldsymbol{J} \times \boldsymbol{B}) + \frac{\beta_e \beta_i}{B_0}\big((\boldsymbol{J} \times \boldsymbol{B}) \times \boldsymbol{B}\big), \tag{1.8}$$

where Hall parameter $\beta_e = \omega_e \tau_e$ in which ω_e is cyclotron frequency, τ_e is electron collusion time. σ is the fluid conductivity, β_i is ion-slip parameter, magnetic field $\boldsymbol{B} = B_i + B_0$, B_i and B_0 are induced and constant applied magnetic field, respectively, and $\boldsymbol{E}$ represents the electric field. In the current thesis, no applied voltage (i.e. $\boldsymbol{E} = 0$) is assumed and B_i is negligible.

1.6 Dimensionless Numbers

1.6.1 Hartmann Number

It is elucidated the ratio of electromagnetic forces to the viscous forces. It appears in the magnetohydrodymics flow problems. Mathematically,

$$\mathcal{M} = B_0 l \sqrt{\frac{\sigma}{\mu}}, \tag{1.9}$$

where B_0, l , σ, μ are magnetic field intensity, mean width of channel/tube, fluid conductivity and fluid viscosity, respectively.

1.6.2 Porosity Parameter

It is the ratio of volume pores in the medium to the volume of bulk fluid in the medium. Mathematically,

$$\frac{1}{\mathcal{K}} = \frac{\varphi l^2}{k}. \tag{1.10}$$

1.6.3 Reynolds Number

The most essential dimensionless parameter to determine whether the flow is laminar i.e. similar pattern flow that occur at low Reynolds number, or turbulent flow i.e. fluid does not know the next flow pattern and occur at high Reynolds number. It is expressed as a ratio of inertial to the viscous forces and is denoted by Re. Its mathematical form is as follow

$$Re = \frac{\rho U_f l}{\mu}. \tag{1.11}$$

1.6.4 Wave Number

The important dimensionless number for wavy flow is the ratio of mean width of channel to the wavelength (i.e. metachronal wave in this thesis) represent the wave number. Mathematically,

$$\beta = \frac{l}{\lambda}. \tag{1.12}$$

1.6.5 Weissenberg Number

The ratio of elastic forces to the viscous forces is actually the Weissenberg number. This dimensionless number is used to study the non-Newtonian viscoelastic fluid. Basically, it described the degree of deformation in simple shear flow. It is usually denoted by Wi or We (in this thesis, we use We). Mathematically, it is defined as

$$We = \frac{mU_f}{l}. \tag{1.13}$$

1.6.6 Prandtl Number

It describes the ratio of momentum to thermal diffusivity and measure the heat transfer between moving fluid and solid surface if Prandtl number (denoted by Pr) goes to unity, it corresponds to flow for which both, momentum and thermal dissipation, are at the same rate. Heat diffuses quickly if Pr is very small ($Pr \ll 1$) and slowly if Pr is large ($Pr \gg 1$) relative to the velocity boundary layer, respectively. Mathematically,

$$Pr = \frac{\mu c_p}{k_1}. \tag{1.14}$$

1.6.7 Eckert Number

It is the ratio of advective mass transfer to the heat dissipation potential. This dimensionless number is used to characterize the effect of self-heating in the presence of viscous dissipation term in the energy equation. It simply shows the relation between enthalpy and kinetic energy of the flow and is denoted by E_c. Mathematical representation is as follow

$$E_c = \frac{{U_f}^2}{c_p \Delta T}. \tag{1.15}$$

1.6.8 Brinkman Number

This dimensionless number specifies the viscous dissipation in the fluid flow. It is expressed as a ratio of viscous heat generation to the heat transfer rate and is essential for short distance velocity changes flow i.e. lubricant flow. It is denoted by Br in the product of Eckert and Prandtl number i.e. $Br = EcPr$.

1.6.9 Grashof Number

The ratio of buoyancy forces due to convective heat transfer to the viscous forces is known as Grashof number. This non-dimensional parameter is a measure of free or natural convection. Mathematically, the Grashof number is defines as

$$Gr = \frac{g\beta\Delta T l^3}{\nu^2}, \tag{1.16}$$

in which g denotes the gravitational acceleration, β denotes the volume expansion, L be the characteristics length, ΔT is the change in temperature and ν is for the viscous forces. It is also used to deduce the nature of convective boundary layer thickness. The laminar boundary layer occurs at low Grashof number and turbulent boundary layer arises at high Grashof number.

1.7 Literature Review

The study of ciliary flow is very rich in history. The light microscopic scientist, namely, 'Antoni van Leeuwenhoek' observed for the first time, motion of the little legs or thin feet of microorganisms in 1674-1675 [1]. Although, in 1786, Otto Friedrich Müller was the first to use the term 'cilia' for these organelles [2]. Originally, the cilia were discovered by their motile function, and, it was assumed the only function of cilia for the long time.

Later, in the 2nd half of the 19th century, some researchers [3, 4, 5] observed the stationary cilia, and, the first scientist to ever notice these organelles in mammalian cells including was Zimmermann. But his research and Zimmermann's name for these organelles were soon forgotten. In 1986, it was renamed to primary cilia [6]. In the last century, small attention was paid to this distinctive class of non-motile cilia and it remained a mystery.

The study of these organelles was limited due to deficient resolution of light microscope of nineteen and early twenty century. The problem of resolution resumed after the invention of electron microscope and causes the expansion in ciliary study. The contribution of Keith Porter in elucidation of ciliary structure [7] is highly appreciated. He described complete pattern of axoneme for both moving and stationary cilia which is discussed in subsection 1.2.1.

The comprehensive study of ciliary motion of microorganisms in 1950-1969 was given by, Taylor [8], Reynold's [9], Tuck [10], Lighthill [11], Sleigh [12, 13], for finite and infinite length models. They made calculation for the motion of single cilium and discussed the case of high concentration of cilia lying on the microorganism, which resembled the Gray's comment. Blake [14, 15] represent that comparison of the velocities of propulsion for the finite and infinite length model and reveals that propulsive velocity of infinite model is twice that are found for the finite model. During 1970s, Blake [15] and Brennen [16, 17] used the envelope model to study the locomotion of ciliated microorganisms later Katz [18] and Lardner [19] presented the propulsion of fluid due to cilia in mammalian reproductive systems and then Blake [20] used this model to study both female and male reproductive system. In 1980s, Sanderson, Sleigh [21], Fulford, Blake [22], Agarwal [23] and Sleigh [24] described the motion of mucus-propelling cilia of mammalian respiratory system. They presented the understanding of the mechanism of mucociliary transport and to provide an awareness of its importance in lung defense. By 1990s, it is seemed that with each passed years the field of cilia [25-29] reached a state of maturity, with incremental advances in the study. Ciliary systems are rather complex and most of the analysis in this domain are based on simplification of assumptions concerning the interaction of fluid and the cilia i.e. long wavelength and low Reynolds number assumptions. These assumptions are only applicable for physiological processes. Some recent investigations based on these assumptions can be found in [30-35].

Many physiological process in which the mechanism of ciliary transport play a major role, includes the movement of ovum in the fallopian tube [36, 37, 38], the mucus transport in the respiratory track [39, 40, 41] and the movement of spermatozoa in the ductus efferent of the male reproductive track [42,43, 44], etc. There are many diseases that may occur due to failure of ciliary system in human body such as lobar pneumonia, asthma, acute tracheobronchitis, postoperative atelectasis, influenzal pneumonia, bronchiectasis and bronchopneumonia, which were discussed by Hilding [45, 46]. Also, Afzelius [47] discussed diseases related to defective cilia such as immotile-cilia syndrome, situs inversus totalis, male infertility, female infertility or fertility, anosmia, hydrocephalus, retinitis pigmentosa. Due to its numerous importance, the study of motile cilia has key role in biofluid dynamics.

Magnetohydrodynamics (MHD) is an important area in modern smart (intelligent) bionic systems. It can be applied successfully to control flux, direction and other characteristics of the flow of electrically conducting fluids. MHD features in numerous medical technologies e.g. MRI, GMR, EMG, IMF, etc. wherein it allows the precise and non-invasive therapy of many physiological conditions. In biological propulsion, magnetohydrodynamic flows have been addressed for a variety of bionic systems including ciliated magneto hydraulics in soft robotics [48], respiratory magnetic treatment [49], peristaltic magnetofluid [50, 51, 52], magnetic blood pumps [53, 54], magneto-robotic microswimmers [55].

The role of MHD in mucociliary flow is highly beneficial, therefore Maan et al. [56] modelled the fractional Burgers' fluid to study the mocuciliary transport process and compare velocity for two types of metachronal wave (symplectic and antiplectic). Results are obtained by using fractional Adomian decomposition method reveal that antiplectic wave are efficient to transport the fluid than symplectic wave. Further, Bhatti et al. [57] studied the impact of magnetohydrodynamics (MHD) on ciliary motion of Casson fluid model embedded in the porous medium. The problem is modelled and simplified by applying the long wave length and low Reynolds number approximation. Closed form solution is obtained and results show that MHD and particles volume fractions decrease the fluid velocity. Same results concluded for the Newtonian fluid model considered by Elkhair et al. [58] without applying long wave length and low Reynolds number approximation. They also demonstrated that axial fluid velocity is efficient without ciliated boundary as compared to ciliated boundary whereas an opposite result shown near the boundary wall. Siddique et al. [59] studied the MHD viscous flow for the ciliary system in the porous planar channel (i.e. they considered mucus as a porous medium) and investigated that in case of mucus congestion in respiratory track magnetic field can be applied to clear the throat passage. Ramesh et al. [48] studied the cilia assisted magneto hydrodynamic flow of couple stress physiological fluid which can be used in medical devices such as MHD micro scale robots and biomimetic pump. Closed form solution is obtained and complicated numerical solution are evaluated by MATLAB. Results show that velocity is defeated in the core region by increasing magnetic parameter.

Magnetic field is also widely used for artificial cilia in microfluidic flow and mixing. These cilia can also be used for cells transportation, antifouling surfaces, biochemically

targets, proteins and chemical agents' sensing. Vilfan et al. [60] demonstrated the fluid motion by creating the self-assembled artificial cilia using the chains of super paramagnetic beads. Here the use of magnetic field to actuate the beating cilia in a simple non-reciprocal beating manner which causes nearly a uniform motion above the surface of cilia. Guager et al. [61] described the numerical modelling of fluid transport that occur due to motion of artificial cilia. These artificial cilia are made up of super paramagnetic elastic filament that are actuated by applied magnetic field. The magnetic or the electric field is used for better control over the artificial cilia.

Thermal analysis of biological systems is a vibrant area of modern biomechanics and biomedical engineering. Thermal science is divided into biological thermodynamics, classical thermodynamics, equilibrium and non-equilibrium thermodynamics, statistical thermodynamics, and heat transfer. The human body may be considered as an open system (heat engine). The fundamental law used in thermal conduction is Fourier law. Heat regulation is essential to all mammals and furthermore thermal analysis has found many exciting new applications in modern biomedical engineering. These include heat flow in blood [62], thermal tumors treatment [63], thermal treatment on food processing [64], heat transfer in treatment of eye [65], heat diffusion in dynamics of swallowing [66], air thermal control [67], cardiovascular system transport [68], thermal treatment of skin burns [69], thermo-bio convection [70], heat transfer in tissue (micro vascular) [71] and human thermal comfort [72]. Other applications of heat transfer in biological systems include laser radiation of tissue, thawing and freezing process for preserving the biological material, cryosurgery, infrared radiators, and microwave methods. Computational and mathematical thermal analysis is considered as a critical modern tool in biological flows. Mathematical simulation imparts a powerful and inexpensive methodology for robust analysis of mass and heat transfer. There to study the heat transfer, Mill et al. [73] deliberated the effect of elliptical beating motion of cilia on the heat transfer in the micro channel containing fluid and deduced that cilia enhance the transport of heat in the fluid. Akbar et al. [74-75] observed the influence of Hartmann layer and the analysis of heat transfer on transportation of copper nanofluids due to the metachronal wave of beating cilia. Recently, the heat transfer in bio fluid flow in curved channel due to metachronal flogging of cilia with variable viscosity (i.e. temperature dependent viscosity) is debated by Sadaf [76]. She observed that pressure gradient is larger for variable viscosity than that of constant viscosity.

Sadaf and Nadeem [77] found the exact solution of the same work in the existence of radial magnetic field also Adomian decomposition method has been applied on the mixed convective electromagnetic fluid flow in the vertical ciliated channel with variable viscosity by Farooq et al. [78]. Mathematical modeling of heat transfer and effect of MHD (transverse) through efferent ducts of male reproductive part with variable viscosity is elucidated by Imran et al. [79]. This study is useful to know the importance of cilia in fluid flow through male reproductive tract and movement of sperm and ovum in fallopian tube.

1.8 Research Methodology

We will use some analytical techniques to solve the linear and nonlinear problems appearing in the next chapters. Some of the these suitable techniques are described below

- Fourier series expansion method
- Perturbation method
- Adomian decomposition method
- Homotopy perturbation method

1.8.1 Fourier Series Expansion Method

An approximate solution can be found using Fourier series expansion method, for this a function $\varphi(x)$ represented as follows

$$\varphi(x) = a_0 + \sum_{n=1}^{\infty}(a_n cosnx + b_n sinnx), \qquad (1.17)$$

in which a_0, a_n and b_n are Fourier coefficients can be determined by the definition of orthogonality. This method is applicable for almost all kind of wave function. The Fourier series has many applications in physical sciences that uses sinusoidal signals in medical, applied mathematics, engineering, physics and chemistry.

1.8.2 Perturbation Method

This well-known method is widely applied to evaluate the nonlinear problems analytically. To approximate the perturbation solution [80], we assume $\boldsymbol{b}$ is a small or

large variable then the unknown function $\boldsymbol{u}$ of the differential equation can be express as

$$u = u_0 + u_1 b + u_2 b^2 + u_3 b^3 + \cdots \tag{1.18}$$

and substitute in differential equation to alter the nonlinear equation into numbers of linear problems depending on the large or small parameter of the equation and then solution is approximated by the sum of sub linear equation's solution. This technique has its vital role in development of science and engineering.

1.8.3 Adomian Decomposition Method

The Adomian decomposition method (ADM) [81, 82] is an efficient solution for linear and nonlinear, initial and boundary value problem. ADM doesn't need any restrictive assumptions such as linearization. Nonlinear differential equation can be written in the following form

$$u(x) = f(x) - L^{-1}(Ru) - L^{-1}(Nu), \tag{1.19}$$

in which unknown function u decompose into a sum of an infinite number of components and calculated in a recursive manner, $f(x)$ is inhomogeneous term, L is the inverse operator of linear highest order derivative, Ru is the linear part of the equation and can be decompose in the infinite sum of component of u_m where $m = 0, 1, 2, 3$ ..., and Nu represent the nonlinear part of the equation and can be decompose into an infinite series of Adomian polynomials A_m where $m = 0, 1, 2, 3$ ..., which are based on trigonometric and algebraic identities and on Taylor series. Finally, the partial sum of the equation is the solution of required equation.

1.8.4 Homotopy Perturbation Method

The Homotopy perturbation technique [83] is a powerful and efficient technique to find the approximate solution of linear and nonlinear equation. HPM combines the two different methods that are perturbation and Homotopy method, it reduces the limitations that may alter the physical manner of the model under discussion. This method is applicable when the exact solution of an equation is not possible. It start with the initial approximation which can be freely selected with possible unknown constants. The Homotopy structure can be written in the following form

$$\mathbb{H}(v,q) = (1-q)[L(v) - L(w_0)] + q[A(v) - f(r)] = 0, \qquad (1.10)$$

in which L is the linear part, A can be decompose into a linear and nonlinear part, u_0 is the initial guess which satisfy the considered equation and $q \in [0,1]$ is an embedding parameter.

Homptopy perturbation method leads to an expression for the desire solution in terms of a formal power series. In this way, a strict nonlinear equation reduce into solvable linear and nonlinear equation.

Chapter 2

Magnetohydrodynamic Flow Induced by Ciliary Movement

In this chapter, we have assessed the impact of magnetohydrodynamic (MHD) through a ciliated porous sheet of infinite length and flow occurs due to metachronal beating of cilia. The present problem is modelled under the small Reynolds number approximation and exact solution of partial differential equations have been found by the Fourier series expansion method. The impact of physical parameters along the characteristics of ciliary motion are illustrated by the graphs and discussed in detail.

2.1 Mathematical Modeling

Consider the two dimensional electrically conducting incompressible viscous fluid flow through a porous medium in a ciliated sheet. The fluid flow emerges due to the continuous flogging of cilia which appears as the metachronal wave due to small phase difference between the neighboring cilia. The fluid is flowing in the horizontal direction i.e. along the X-axes and magnetic field B_0 is applied perpendicular to the flow i.e. along Y-axes. The geometry of current problem is displayed in Fig. 2.1. The governing equations of conservation of mass and momentum along Maxwell's equations for magnetohydrodynamics and Darcy's law for porous medium can be written as

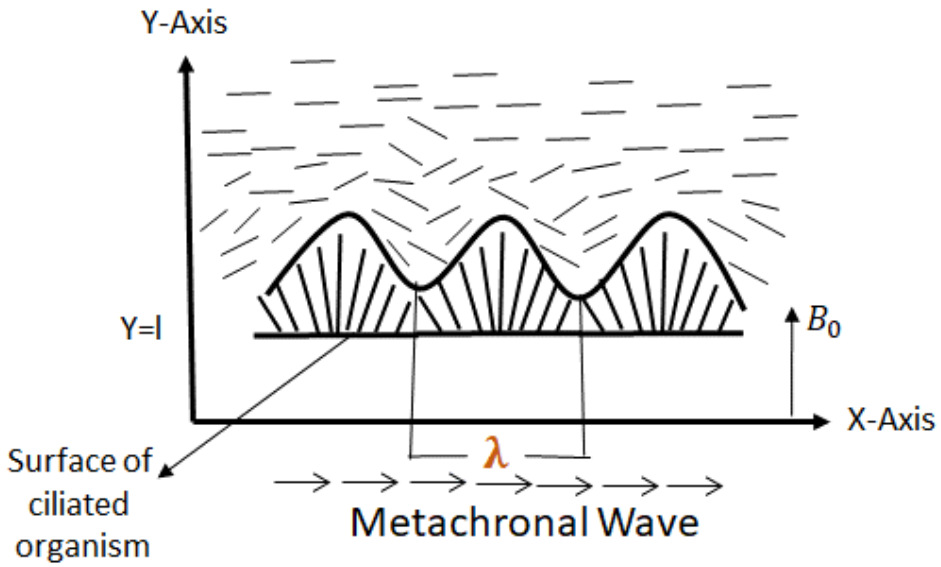

Fig. 2.1: Geometry of the problem

$$\frac{\partial U}{\partial X}+\frac{\partial V}{\partial Y}=0, \tag{2.1}$$

$$\mu\left(\frac{\partial^2 U}{\partial X^2}+\frac{\partial^2 U}{\partial Y^2}\right)-\sigma B_0 U-\frac{\mu\varphi}{k}U=\frac{\partial P}{\partial X}, \tag{2.2}$$

$$\mu\left(\frac{\partial^2 V}{\partial X^2}+\frac{\partial^2 V}{\partial Y^2}\right)-\frac{\mu\varphi}{k}V=\frac{\partial P}{\partial Y}, \tag{2.3}$$

where U, V, X, Y and P are velocity components, Cartesian coordinates and pressure in fixed frame, respectively, and μ, σ, φ, k and B_0 are fluid viscosity, electric conductivity, porosity media, permeability of porous medium and magnetic field.

The fixed and the wave frames are related by the following expressions

$$u=U-\mathfrak{c},\quad x=X-\mathfrak{c}t,\quad v=V,\quad y=Y\quad p=P. \tag{2.4}$$

Using Eq. (2.4) into Eqs. (2.1)-(2.3), following expressions can be obtained

$$\frac{\partial u}{\partial x}+\frac{\partial v}{\partial y}=0, \tag{2.5}$$

$$\mu\left(\frac{\partial^2 u}{\partial x^2}+\frac{\partial^2 u}{\partial y^2}\right)-\sigma B_0 u-\frac{\mu\varphi}{k}(u+\mathfrak{c})=\frac{\partial p}{\partial x}, \tag{2.6}$$

$$\mu\left(\frac{\partial^2 v}{\partial x^2}+\frac{\partial^2 v}{\partial y^2}\right)-\frac{\mu\varphi}{k}v=\frac{\partial p}{\partial y}, \tag{2.7}$$

Eqs. (2.5)-(2.7) are the governing equations of motion for MHD incompressible viscous fluid flow in porous medium. We have three equations and three unknowns u, v and p. Thus we can find the exact solution using Fourier series expansion method.

Where u and v in term of stream function are defined as follow

$$u = \frac{\partial \psi}{\partial y}, \quad v = -\frac{\partial \psi}{\partial x}. \tag{2.8}$$

The two dimensional function $\psi(x, y)$ in the form of Fourier series expansion is expressed as follows

$$\psi(x, y) = \sum_{n=0}^{\infty} (f_n cosnx + g_n sinnx)\psi_n(y), \tag{2.9}$$

Where f_n and g_n are known as the Fourier coefficients.

The velocity boundary conditions at $y = l$ i.e. the mean width of the sheet in the frame of reference moving in crests are

$$u(x, l) = A_0 + \sum_{n=1}^{\infty} (A_n cosnx + B_n sinnx)\psi_n(y), \tag{2.10}$$

$$v(x, l) = \sum_{n=1}^{\infty} (C_n cosnx + D_n sinnx)\psi_n(y), \tag{2.11}$$

in which A_n, B_n, C_n and D_n are known as Fourier coefficients.

The two dimensional fluid flow is symmetric along the centerline of the sheet i.e. the upper and lower half planes has same problem. So for convenience, we only take the upper portion of plane.

Now convert system of PDE given in Eqs. (2.6) & (2.7) into single PDE by eliminating the pressure and using the stream function defined in Eq. (2.8), we get

$$\nabla^4 \psi + \frac{\varphi}{k} \nabla^2 \psi - \frac{\sigma B_0}{\mu} \frac{\partial^2 \psi}{\partial y^2} = 0, \tag{2.12}$$

where

$$\nabla^4 = \frac{\partial^4 \psi}{\partial x^4} + \frac{\partial^4 \psi}{\partial y^4} + 2 \frac{\partial^4 \psi}{\partial x^2 \partial y^2}, \tag{2.13}$$

$$\nabla^2 = \frac{\partial^2 \psi}{\partial x^2} + \frac{\partial^2 \psi}{\partial y^2}. \tag{2.14}$$

Invoking Eq. (2.9) into Eq. (2.12), we get following form of single ODE

$$\psi_n{}^{iv}(y) - \left(2n^2 + \frac{\varphi}{k} + \mathcal{M}^2\right)\psi_n{}''(y) + n^2\left(n^2 + \frac{\varphi}{k}\right)\psi_n(y) = 0, \tag{2.15}$$

where

$$\mathcal{M}^2 = \frac{\sigma B_0}{\mu}. \tag{2.16}$$

2.2 Solution of the Problem

The solution of the ordinary differential equation is

$$\psi_n(y) = \mathscr{a}e^{L_1 y} + \mathscr{b}e^{-L_1 y} + \mathfrak{d}e^{L_2 y} + \mathscr{f}e^{-L_2 y}, \tag{2.17}$$

where

$$L_1 = \sqrt{\frac{1}{2}\left(2n^2 + \frac{\varphi}{k} + \mathcal{M}^2 + \sqrt{\left(\frac{\varphi}{k} + \mathcal{M}^2\right)^2 + 4\mathcal{M}^2 n^2}\right)}, \tag{2.18}$$

$$L_2 = \sqrt{\frac{1}{2}\left(2n^2 + \frac{\varphi}{k} + \mathcal{M}^2 - \sqrt{\left(\frac{\varphi}{k} + \mathcal{M}^2\right)^2 + 4\mathcal{M}^2 n^2}\right)}, \tag{2.19}$$

where L_1, L_2 are constants that depend upon physical parameters $\varphi, k, \mathcal{M}$ and n defined in Eqs. (2.18) and (2.19) and $\mathscr{a}$, $\mathscr{b}$, $\mathfrak{d}$ and $\mathscr{f}$ are constant to be determined.

We have considered the infinite length model containing cilia but $\psi_n(y)$ is finite. Thus as $y \to \infty$, we have $\mathscr{a} = \mathfrak{d} = 0$, hence

$$\psi_n(y) = \mathscr{b}e^{-L_1 y} + \mathscr{f}e^{-L_2 y}, \tag{2.20}$$

Placing the value of $\psi_n(y)$ into Eq. (2.8) and using the boundary conditions given in Eqs. (2.9) and (2.10), we get solution for stream function

$$\psi(x,y) = \alpha_0 e^{-l_1 y} + \beta_0 + \sum_{n=1}^{\infty}(\alpha_n e^{L_1 y} + \beta_n e^{L_2 y})cosnx$$

$$+ \sum_{n=1}^{\infty}(\gamma_n e^{L_1 y} + \delta_n e^{L_2 y})sinnx, \tag{2.21}$$

which is the representative solution for the stream function in which β_0 is the arbitrary parameter and we can find the following values with the assistance of boundary conditions in Eq. (2.9) and (2.10).

$$l_1 = \sqrt{\frac{\varphi}{k} + M^2}, \;\; \alpha_0 = \frac{A_0}{l_1 e^{-l_1 l}},$$

$$\alpha_n = \frac{L_2 D_n + nA_n}{n(L_2 - L_1)e^{-L_1 l}}, \quad \beta_n = \frac{L_1 D_n + nA_n}{n(L_2 - L_1)e^{-L_2 l}},$$

$$\gamma_n = \frac{L_2 B_n - nC_n}{n(L_2 - L_1)e^{-L_1 l}}, \quad \delta_n = \frac{L_1 B_n - nC_n}{n(L_2 - L_1)e^{-L_2 l}}. \tag{2.22}$$

Following form of the velocity gives the solution of Eq. (2.15)

$$u(x,y) = A_0 e^{-l_1(y-l)} - \sum_{n=1}^{\infty} \left(L_1 L_{11} e^{-L_1(y-l)} - L_2 L_{21} e^{-L_2(y-l)}\right) cosnx$$
$$- \sum_{n=1}^{\infty} \left(L_1 L_{12} e^{L_1(y-l)} - L_2 L_{22} e^{L_2(y-l)}\right) sinnx, \tag{2.23}$$

$$v(x,y) = \sum_{n=1}^{\infty} \left(nL_{11} e^{-L_1(y-l)} - nL_{21} e^{-L_2(y-l)}\right) sinnx$$
$$- \sum_{n=1}^{\infty} \left(nL_{12} e^{L_1(y-l)} - nL_{22} e^{L_2(y-l)}\right) cosnx. \tag{2.24}$$

Where

$$L_{11} = \frac{L_2 D_n + nA_n}{n(L_2 - L_1)}, \quad L_{21} = \frac{L_1 D_n + nA_n}{n(L_2 - L_1)},$$

$$L_{12} = \frac{L_2 B_n - nC_n}{n(L_2 - L_1)}, \quad L_{22} = \frac{L_1 B_n - nC_n}{n(L_2 - L_1)}. \tag{2.25}$$

With the aid of Eqs. (2.6) and Eq. (2.7), we get following pressure distribution

$$p = \mu \sum_{n=1}^{\infty} \left(\frac{n}{L_1}\left(n^2 - {L_1}^2 + \frac{\varphi}{k}\right) L_{11} e^{-L_1(y-l)}\right.$$
$$\left. - \frac{n}{L_2}\left(n^2 - {L_2}^2 + \frac{\varphi}{k}\right) L_{21} e^{-L_2(y-l)}\right) sinnx$$
$$- \mu \sum_{n=1}^{\infty} \left(\frac{n}{L_1}\left(n^2 - {L_1}^2 + \frac{\varphi}{k}\right) L_{12} e^{L_1(y-l)}\right.$$
$$\left. - \frac{n}{L_2}\left(n^2 - {L_2}^2 + \frac{\varphi}{k}\right) L_{22} e^{L_2(y-l)}\right) cosnx + C, \tag{2.26}$$

where C is the constant of integration.

Now we will calculate rate of working per unit area of the sheet which can be expressed by the following integral

$$P = \int_{S_0}^{S} u_i \sigma_{ij} n_j ds, \tag{2.27}$$

where

$$\sigma_{ij} = p\delta_{ij} - 2\mu e_{ij}, \tag{2.28}$$

or

$$P = 2\pi \int_{-\pi}^{\pi} \left(u\sigma_{xy} + v\sigma_{yy}\right)_{(x,l)} dx, \tag{2.29}$$

where

$$\sigma_{xy} = -\mu\left(\frac{\partial u}{\partial y} + \frac{\partial v}{\partial x}\right), \quad \sigma_{yy} = p - 2\mu\frac{\partial v}{\partial y}. \tag{2.30}$$

Using Eqs. (2.10), (2.11) and (2.30) into Eq. (2.29), working rate takes the following form

$$P = \frac{\mu}{2}\left(2{A_0}^2 l_1 + \sum_{n=1}^{\infty}(L_1 + L_2)\left({A_n}^2 + {B_n}^2 + \left(n^2 + \frac{\varphi}{k}\right)\frac{{C_n}^2 + {D_n}^2}{L_1 L_2}\right)\right.$$
$$\left. + \sum_{n=1}^{\infty}(B_n C_n - A_n D_n)\left(2n - \frac{L_1 L_2}{n} - \left(n^2 + \frac{\varphi}{k}\right)\frac{n}{L_1 L_2}\right)\right). \tag{2.31}$$

2.3 Surface of Organism

The oscillation of cilium is periodic so we can represent the surface envelope of the organism, for symplectic metachronal wave with frequency $\frac{\sigma}{2\pi}$ and wavelength $\frac{2\pi}{\hbar}$, in a fixed frame by Fourier series as follow

$$X_0 = X + \varepsilon\sum_{n=1}^{N}\left(a_n sinn(\hbar X - \sigma t) - b_n cosn(\hbar X - \sigma t)\right), \tag{2.32}$$

$$Y_0 = l + \varepsilon\sum_{n=1}^{N}\left(c_n sinn(\hbar X - \sigma t) - d_n cosn(\hbar X - \sigma t)\right), \tag{2.33}$$

Also surface in wave frame can be expressed as follow

$$x_0 = x + \varepsilon\sum_{n=1}^{N}(a_n sinnx - b_n cosnx), \tag{2.34}$$

$$y_0 = l + \varepsilon\sum_{n=1}^{N}(c_n sinnx - d_n cosnx), \tag{2.35}$$

As we consider the no slip condition for the extensible sheet, so by taking the derivatives of Eq. (2.34) and Eq. (2.35) w.r.t t i.e. $\frac{\partial x_0}{\partial t}$ and $\frac{\partial y_0}{\partial t}$, we get the following form of longitudinal velocity $u(x_0, y_0)$ and transverse velocity $v(x_0, y_0)$, respectively

$$u(x_0, y_0) = \sigma + \sigma\varepsilon \sum_{n=1}^{N} n(a_n cosnx + b_n sinnx), \quad (2.36)$$

$$v(x_0, y_0) = \sigma\varepsilon \sum_{n=1}^{N} n(c_n cosnx + d_n sinnx), \quad (2.37)$$

To acquire velocity coefficients in Eqs. (2.9) & (2.10), the following Taylor's series expansion is applied for the velocity component about (x, l),

$$\hat{V}(x, l) = \hat{V}(x_0, y_0) - \sum_{\substack{k=1 \\ k=m+n}}^{p1} \binom{k}{m} \frac{(x_0 - x)^n (y_0 - l)^n}{k!} \frac{\partial^k \hat{V}}{\partial x^m \partial y^n} + O(\epsilon^{p1+2}). \quad (2.38)$$

To get the order of accuracy, we applied the iterative technique for velocity component of Taylor series expansion. To proceed this technique, we take the 1st order approximation i.e. $O(\epsilon)$ of Taylor's series and equate $\hat{V}(x, l) = (u(x, l), v(x, l), 0)$ and $\hat{V}(x_0, y_0) = (u(x_0, y_0), v(x_0, y_0), 0)$ which gives the following approximation for A_0, A_n, B_n, C_n and D_n.

$$A_0 = \sigma, \;\; A_n = \varepsilon\sigma n a_n, \;\; B_n = \varepsilon\sigma n b_n, \;\; C_n = \varepsilon\sigma n c_n, \;\; D_n = \varepsilon\sigma n d_n, \quad (2.39)$$

for all $n = 1, 2, \ldots, N$.

To obtain the next approximation we have to go to the second order approximation i.e. $O(\epsilon^2)$ of two dimensional Taylor's series. For this we need to simplify the velocity component in x-direction only, thus the 2nd approximation gives

$$\mathfrak{U} = \sigma + \frac{\sigma\varepsilon^2}{2} \sum_{n=1}^{\infty} \Big(n^2 {a_n}^2 + n^2 {b_n}^2 + n(L_1 + L_2)(b_n c_n - a_n d_n) - L_1 L_2 \big({c_n}^2 + {d_n}^2 \big) \Big), \quad (2.40)$$

which is the velocity of propulsion of second approximation.

2.4 Application to Ciliary Propulsion

Each individual cilium usually has a consistent rhythm that often appear by the propagation of tip of cilia. Generally the cilium is straighten out during the power stroke in the beat known as recovery stroke (beat back) the cilium sneaks back to its initial point in the bend position so that the significant portion of the each cilium is moving tangential to the fluid rather than perpendicular to it as in the effective stroke. Generally the recovery stroke is longer than the effective stroke. The cilia exhibit metachronal

wave (in which cilium beats slightly out of the phase). The direction of the wave propagation may have almost any orientation relative to the direction of power stroke. For this model, we need symplectic wave in which the metachronal wave propagation and the power stroke are in the same direction.

The mathematical representation of considered envelope model for symplectic metachronal wave can be represented as.

$$x_0 = x + \beta cos(x + ct) + \gamma sin(x + ct), \tag{2.41}$$

$$y_0 = l + bsin(x + ct), \tag{2.42}$$

where β and b are major and minor axes of elliptical path and γ is due to the inclination of cilia tip to body axes.

Differentiating Eqs. (2.41) & (2.42) w.r.t t, and comparing with Eqs. (2.36) & (2.37), we get

$$a_n = \frac{\gamma}{n\varepsilon}, \quad b_n = \frac{\beta}{n\varepsilon}, \quad c_n = \frac{b}{n\varepsilon}, \quad d_n = 0, \tag{2.43}$$

for all $n = 1, 2, \dots, N$.

Substituting Eqs. (2.41) & (2.42) into Eq. (2.39) and Eq. (2.29), we get the following 2nd order velocities and the 1st order rate of working

$$\mathfrak{U} = \sigma + \frac{\sigma}{2}\sum_{n=1}^{\infty}\left(\gamma^2 + \beta^2 - (L_1 + L_2)\frac{b\beta}{n} - L_1L_2\frac{b^2}{n^2}\right), \tag{2.44}$$

$$P = \frac{\mu\sigma^2}{2}\left(2l_1 + \sum_{n=1}^{\infty}(L_1 + L_2)\left(\gamma^2 + \beta^2 + \left(n^2 + \frac{\varphi}{k}\right)\frac{b^2}{L_1L_2}\right) - \sum_{n=1}^{\infty} b\beta\left(2n - \frac{L_1L_2}{n} - \left(n^2 + \frac{\varphi}{k}\right)\frac{n}{L_1L_2}\right)\right). \tag{2.45}$$

If we consider instantaneous model with $b \neq 0$, β and γ zero, one can obtain the following velocity of propulsion in non dimensional form

$$\mathfrak{U} = \sigma - \frac{\sigma}{2}\sum_{n=1}^{\infty} L_1L_2\frac{b^2}{n^2}, \tag{2.46}$$

whereas for $\beta \neq 0$, b and γ are zero, one can obtain the following velocity of propulsion in non- dimensional form

$$\mathfrak{U} = \sigma + \frac{\sigma}{2}\sum_{n=1}^{\infty}\beta^2. \tag{2.47}$$

2.5 Results and Discussion

In this section we have described the graphical results of velocity components in Fig. 2.2 and Fig. 2.3, working rate per unit area in Fig. 2.4 and the stream function in Fig. 2.5 and Fig. 2.6 under the influence of Hartmann number which is the ratio of electromagnetic force to the viscous force and porosity parameter that represents the ratio of volume of pores to the volume of bulk fluid in the medium. Fig. 2.2 and Fig. 2.3 show that the effect of both parameters diminished as fluid moves away from boundary layer thickness. But this contraction become faster in horizontal velocity than vertical velocity. The consequence of Hartmann number on the velocity components, u and v, can be seen through Fig. 2.2a and Fig. 2.2b. To see this influence we considered the electromagnetic force equal, double, triple and four times to the viscous forces. The horizontal velocity attains its maximum value near the boundary layer thickness i.e. at $y = 1.2$ while vertical velocity is maximum around $y = 1.6$ for all values of Hartmann number. The magnetic force create resistance for the fluid flow, if it is applied normal to flow. Thus it can be notice from Fig. 2.2a that velocity reduces as the value of Hartmann number increases while Fig. 2.2b shows a dual behavior i.e. velocity decreases near the boundary layer and transition occur at $y = 2.2$ and velocity rises with increase in Hartmann number. Fig. 2.3 depicts that the influence of porosity parameter on u and v is same i.e. velocity increases for the ratio (which define the porosity parameter) 1%, 5%, 10% and 50%. The maximum change is attained in both velocities for all the values of porosity parameter near the boundary layer thickness, the horizontal velocity reaches to its peak, at $y = 1.2$, while vertical movement attains its peak around $y = 1.6$. The influence of Hartmann number and porosity parameter on pressure distribution can be seen by Fig. 2.4a and Fig. 2.4b, respectively. As the resistance occur in the ciliary flow due to the implication of magnetic field, cilia have to work more efficiently in the Hartmann boundary layer region to speed up the flow. Thus, it can be noted from Fig. 2.4a, that more power is required as the Hartmann number increases. But if the ratio that define the porosity parameter changes from 1% to 50% we have to decrease power for high speed of ciliary flow. The impact of Hartmann number and porosity parameter on the trapped bolus can be seen by Fig. 2.5 and Fig. 2.6, respectively. Trapping is known as the circular bolus formed by the closed stream lines and move ahead along the metachronal wave of the ciliary flow. Basically, it helps to understand the behavior of flow pattern. Thus form Fig. 2.5a-c, we can see

the behavior of ciliary flow in the existence of magnetic field. As the Hartmann number results the reduction in velocity which indicates reduction in the number and size of trapped bolus. Fig. 2.6a-c indicate the trapping phenomena in the existence of porous medium. As the porous medium causes the thinning of boundary layer, so the velocity accelerate and trapped bolus rises by increasing the ratio of volume fraction from 1%-3%.

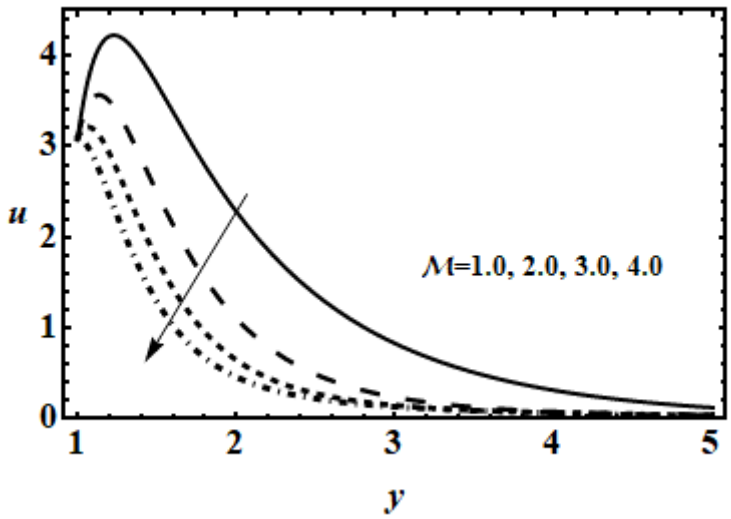

Fig. 2.2a: Influence of Hartmann number on longitudinal velocity $u(x, y)$ for $\beta = 0.5,\ \gamma = 0,$ $\sigma = 1,\ \mu = 1,\ b = 0.5,\ l = 1,\ \varphi = 0.1,\ k = 10.$

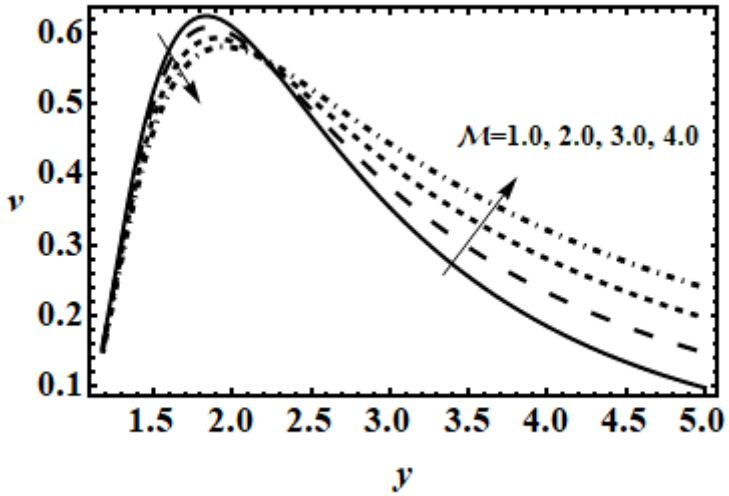

Fig. 2.2b: Influence of Hartmann number on transverse velocity $v(x, y)$ for $\beta = 0.5,\ \gamma = 0,$ $\sigma = 1,\ \mu = 1,\ b = 0.5,\ l = 1,\ \varphi = 0.1,\ k = 10.$

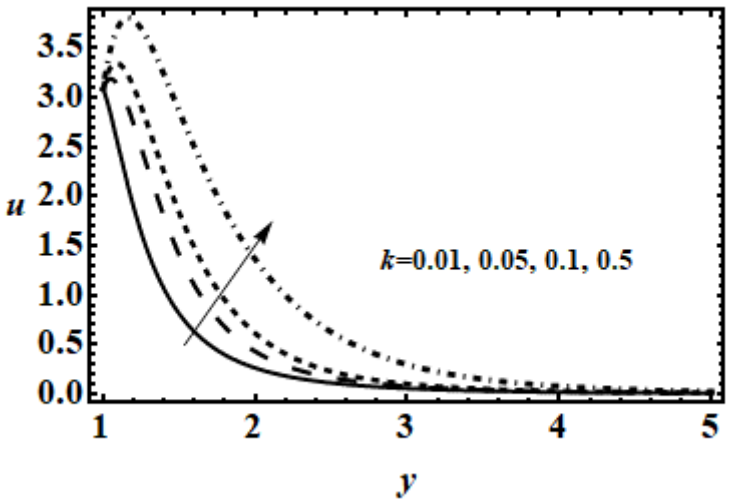

Fig. 2.3a: Influence of porosity parameter on longitudinal velocity $u(x,y)$ for $\beta = 0.5,\ \gamma = 0,\ \sigma = 1,\ \mu = 1,\ b = 0.5,\ l = 1,\ \varphi = 0.1,\ \mathcal{M} = 1.$

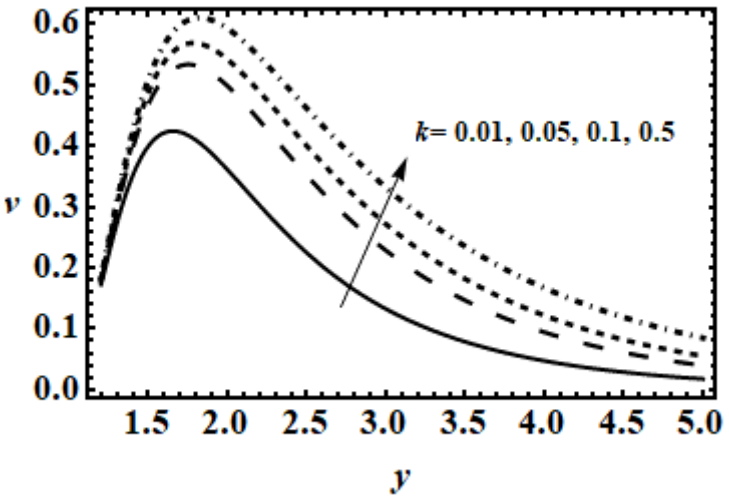

Fig. 2.3b: Influence of porosity parameter on transverse velocity $v(x,y)$ for $\beta = 0.5,\ \gamma = 0,\ \sigma = 1,\ \mu = 1,\ b = 0.5,\ l = 1,\ \varphi = 0.1,\ \mathcal{M} = 1.$

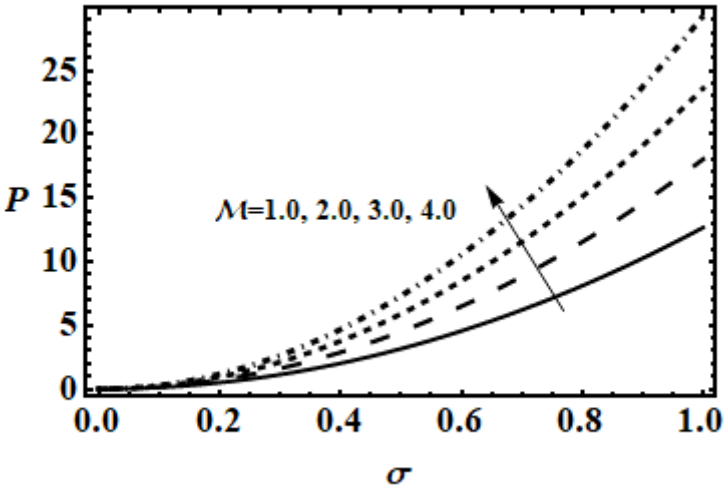

Fig. 2.4a: Influence of Hartmann number on longitudinal velocity $u(x, y)$ for $\beta = 0.5,\ \gamma = 0,\ \sigma = 1,\ \mu = 1,\ b = 0.5,\ l = 1,\ \varphi = 0.1,\ k = 10$.

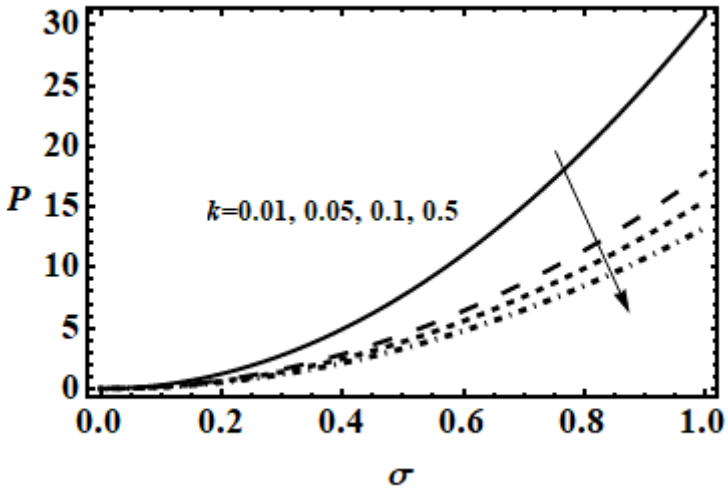

Fig. 2.4b: Influence of Hartmann number on transverse velocity $v(x, y)$ for $\beta = 0.5,\ \gamma = 0,\ \sigma = 1,\ \mu = 1,\ b = 0.5,\ l = 1,\ \varphi = 0.1,\ \mathcal{M} = 1$.

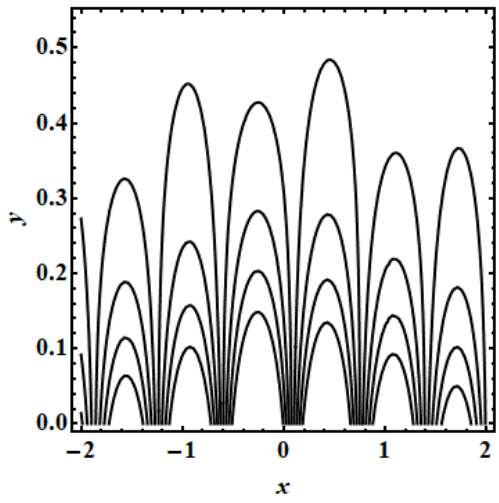

(a) $\mathcal{M} = 1$

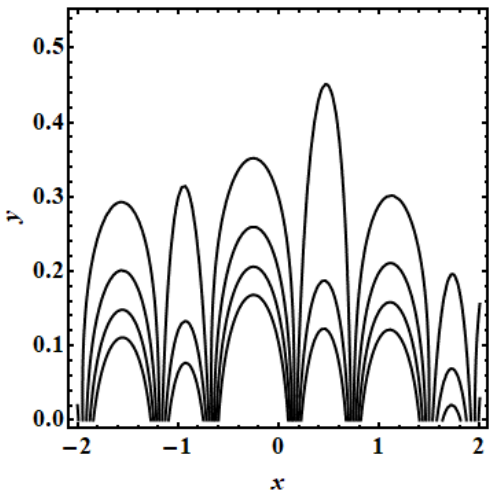

(b) $\mathcal{M} = 6$

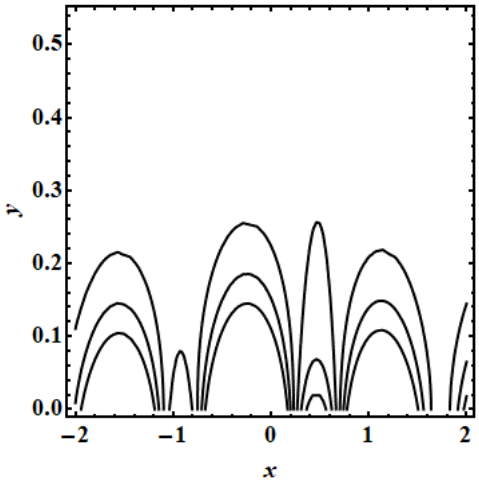

(c) $\mathcal{M} = 9$

Fig. 2.5: Influence of Hartmann number $\mathcal{M}$ on stream function for $\beta = 0.25,\ \gamma = 0.25,\ \alpha = 1,\ \mu = 1,\ b = 0.5,\ l = 1,\ \varphi = 0.1, k = 10.$

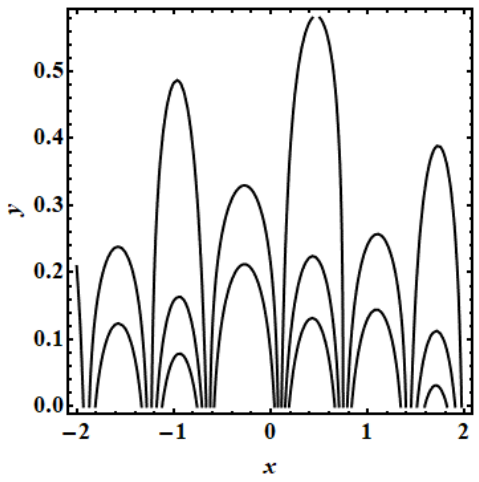

(a) $k = 0.01$

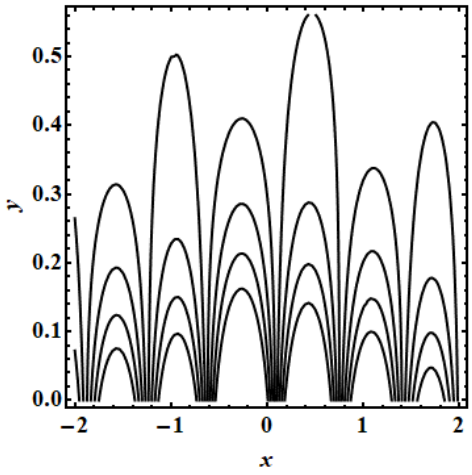

(b) $k = 0.02$

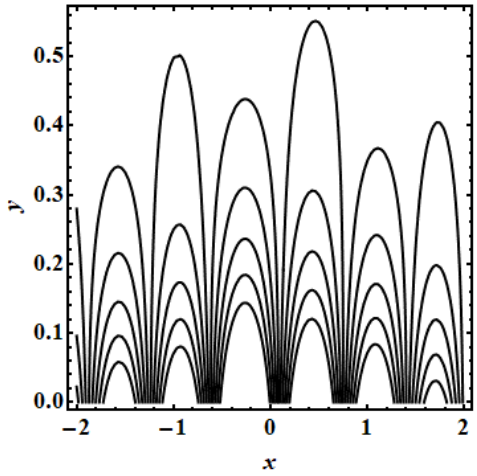

(c) $k = 0.03$

Fig. 2.6: Influence of porosity parameter k on stream function for $\beta = 0.25,\ \gamma = 0.25,\ \alpha = 1,\ \mu = 1,\ b = 0.5,\ l = 1,\ \varphi = 0.1,\ \mathcal{M} = 1.$

2.6 Conclusion

The existing study have shown the effects of MHD and porous medium for the infinite length of cilia model. If $\mathcal{M} \to 0$ and $\frac{1}{k} \to 0$, i.e. the non-existence of magnetic field and porous medium, the present study can be deduced to the study of Blake [14]. Key points of the present chapter are as follows.

- The implication of magnetic field indicate that the horizontal component of the velocity decelerates for the increasing value of magnetic field and dual behavior is observed for the vertical component of the velocity field.
- The presence of porous medium shows that velocity profile rises by rising the volume fraction parameter from 1% to 50%.
- The impact of Hartmann number and volume fraction parameter show that fluid is required large amount of power for the flow in the existence of magnetic field and less amount of power is required in the existence of porous medium.
- Present study is very helpful to treat the diseases in respiratory track as in case of congestion, fluid in respiratory track become thick and to make the bio fluid thin magnetic pills are required that will increase the transverse velocity and throat passage can be cleared and patient can breathe easily.

Chapter 3

Series Solution of Cilia Induced MHD Flow in a Porous Medium under the Hall Current and Ionslip Effect

This chapter is the expansion of previous chapter. We have studied the impact of Hall current and ionslip on the flow created by the metachoronal wave of cilia in the infinite length model of porous ciliated sheet. Following the procedure of chapter 2, results can be observed by the graphs and discussed in section 3.3.

3.1 Mathematical Formulation

We have assumed the magnetohydrodynamic (MHD) viscous fluid flow passed on a two-dimensional sheet implanted in a porous medium. The flow is produced by ciliary movement which generates the metachronal wave. The fluid is flowing in the X and Y-direction and the metachronal wave is produced in the X-direction. The constant magnetic field is applied normally to the flow i.e. in Z-direction.

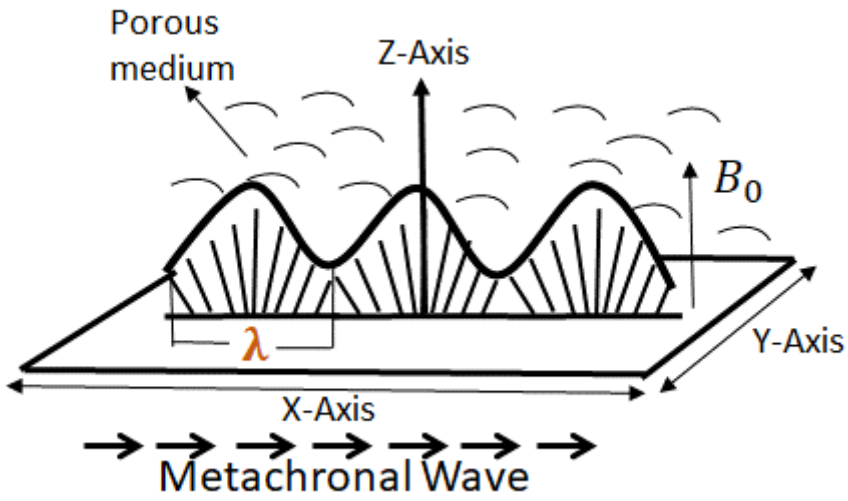

Fig. 3.1: Geometry of problem

To observe the effect of Hall current and ionslip we will use the following generalized Ohm's law.

$$\boldsymbol{J} = \sigma(\boldsymbol{E} + \boldsymbol{V} \times \boldsymbol{B}) - \frac{w_e \tau_e}{B_0}(\boldsymbol{J} \times \boldsymbol{B}) + \frac{w_e \tau_e \beta_i}{{B_0}^2}\big((\boldsymbol{J} \times \boldsymbol{B}) \times \boldsymbol{B}\big), \tag{3.1}$$

Where $\boldsymbol{J} = \big(J_x,\ J_y, 0\big)$ is the current density, $\boldsymbol{E} = \big(E_x,\ E_y, 0\big)$ is the electric field which is constant everywhere in the flow field, $\boldsymbol{B} = (0,\ 0, B_0)$ is the applied magnetic field. Choose (x, y) and (X, Y) coordinates into wave frame and in fixed frame, which are related as follow

$$u = U - \mathfrak{c}, \quad x = X - \mathfrak{c}t, \quad v = V, \quad y = Y, \ \ p = P \tag{3.2}$$

Solving Eq. (3.1), we obtain the following components of current density vector.

$$J_x = \frac{\sigma\left(\alpha_e(E_x - B_0 v) + \beta_e\left(E_y + B_0(u + \mathfrak{c})\right)\right)}{{\alpha_e}^2 + {\beta_e}^2}, \tag{3.3}$$

$$J_y = \frac{\sigma\left(\alpha_e\left(E_y - B_0(u + \mathfrak{c})\right) + \beta_e(E_x + B_0 v)\right)}{{\alpha_e}^2 + {\beta_e}^2}, \tag{3.4}$$

where $\beta_i = \omega_e \tau_e$ and $\alpha_e = 1 + \beta_i \beta_e$.

The law of conservation of momentum and mass in the presence of porous medium, Hall and ionslip effects imply the following equations in wave frame

$$\frac{\partial u}{\partial x} + \frac{\partial v}{\partial y} = 0, \tag{3.5}$$

$$\frac{\partial p}{\partial x} = \mu\left(\frac{\partial^2 u}{\partial x^2} + \frac{\partial^2 u}{\partial y^2}\right) + \frac{\sigma B_0\left(\alpha_e\left(E_y - B_0(u + \mathfrak{c})\right) + \beta_e(E_x + B_0 v)\right)}{{\alpha_e}^2 + {\beta_e}^2} - \frac{\mu\varphi}{k}(u + c), \tag{3.6}$$

$$\frac{\partial p}{\partial y} = \mu\left(\frac{\partial^2 v}{\partial x^2} + \frac{\partial^2 v}{\partial y^2}\right) - \frac{\sigma B_0\left(\alpha_e(E_x - B_0 v) + \beta_e\left(E_y + B_0(u + \mathfrak{c})\right)\right)}{{\alpha_e}^2 + {\beta_e}^2} - \frac{\mu\varphi}{k} v. \tag{3.7}$$

Fourier series expansion of the stream function $\psi(x,y)$ is given as follows

$$\psi(x,y)=\sum_{n=0}^{\infty}(f_n cosnx+g_n sinnx)\psi_n(y), \tag{3.8}$$

also the velocity components and the stream function are related by the following expression

$$u(x,y)=\frac{\partial\psi}{\partial y},\ \ v(x,y)=-\frac{\partial\psi}{\partial x}. \tag{3.9}$$

The velocity boundary conditions at $y=l$ are

$$u(x,l)=A_0+\sum_{n=1}^{\infty}(A_n cosnx+B_n sinnx)\psi_n(y), \tag{3.10}$$

$$v(x,l)=\sum_{n=1}^{\infty}(C_n cosnx+D_n sinnx)\psi_n(y), \tag{3.11}$$

Eliminating pressure gradient and using Eq. (3.9), Eq. (3.6) and Eq. (3.7) take the following form

$$\nabla^4\psi+\left(\frac{\sigma {B_0}^2\alpha_e}{\mu\left({\alpha_e}^2+{\beta_e}^2\right)}+\frac{\varphi}{k}\right)\nabla^2\psi-\frac{\sigma B_0}{\mu}\frac{\partial^2\psi}{\partial y^2}=0. \tag{3.12}$$

Using Eq. (3.8) into Eq. (3.12), we get following form

$$\begin{aligned}{\psi_n}^{iv}(y)-\left(2n^2+\frac{\sigma {B_0}^2\alpha_e}{\mu\left({\alpha_e}^2+{\beta_e}^2\right)}+\frac{\varphi}{k}\right){\psi_n}''(y)\\ +n^2\left(n^2+\frac{\sigma {B_0}^2\alpha_e}{\mu\left({\alpha_e}^2+{\beta_e}^2\right)}+\frac{\varphi}{k}\right)\psi_n(y)=0,\end{aligned} \tag{3.13}$$

3.2 Solution of Problem

Solution of the ordinary differential equation (3.13) is

$$\psi_n(y)=ae^{\sqrt{n^2+A}y}+\mathscr{b}e^{-\sqrt{n^2+A}y}+\mathfrak{d}e^{ny}+\mathscr{f}e^{-ny}, \tag{3.14}$$

As $y\to\infty$, $a=\mathfrak{d}=0$, so we have

$$\psi_n(y)=\mathscr{b}e^{-\sqrt{n^2+A}y}+\mathscr{f}e^{-ny}, \tag{3.15}$$

where

$$A = \frac{\mathcal{M}^2 \alpha_e}{\left(\alpha_e{}^2 + \beta_e{}^2\right)} + \frac{\varphi}{k} \quad \text{and} \quad \mathcal{M}^2 = \frac{\sigma B_0}{\mu}, \tag{3.16}$$

and the solution in the form of stream function is given by

$$\psi(x,y) = \alpha_0 e^{-\sqrt{A}y} + \beta_0 + \sum_{n=1}^{\infty} \left(\alpha_n e^{\sqrt{n^2+A}y} + \beta_n e^{ny}\right) cosnx$$

$$+ \sum_{n=1}^{\infty} \left(\gamma_n e^{\sqrt{n^2+A}y} + \delta_n e^{ny}\right) sinnx, \tag{3.17}$$

where β_0 is arbitrary constant and

$$\alpha_0 = \frac{A_0}{\sqrt{A}e^{-\sqrt{A}l}}, \quad \alpha_n = \frac{A_n + D_n}{n\left(\sqrt{n^2+A} - n\right)e^{-\sqrt{n^2+A}_1 l}},$$

$$\beta_n = \frac{\sqrt{n^2+A}D_n + nA_n}{n\left(\sqrt{n^2+A} - n\right)e^{-nl}}, \quad \gamma_n = \frac{C_n - B_n}{n\left(\sqrt{n^2+A} - n\right)e^{-\sqrt{n^2+A}l}},$$

$$\delta_n = \frac{nB_n - \sqrt{n^2+A}C_n}{n\left(\sqrt{n^2+A} - n\right)e^{-nl}}. \tag{3.18}$$

With the help of Eqs. (3.10), (3.11) and Eq. (3.17) following velocity component u and v are obtained

$$u(x,y) = A_0 e^{-\sqrt{A}(y-l)}$$
$$- \sum_{n=1}^{\infty} \left(\sqrt{n^2+A}L_{11}e^{-\sqrt{n^2+A}(y-l)} - nL_{21}e^{-n(y-l)}\right) cosnx$$
$$- \sum_{n=1}^{\infty} \left(\sqrt{n^2+A}L_{12}e^{\sqrt{n^2+A}(y-l)} - nL_{22}e^{n(y-l)}\right) sinnx, \tag{3.19}$$

$$v(x,y) = \sum_{n=1}^{\infty} \left(nL_{11}e^{-\sqrt{n^2+A}(y-l)} - nL_{21}e^{-n(y-l)}\right) sinnx$$
$$- \sum_{n=1}^{\infty} \left(nL_{12}e^{-\sqrt{n^2+A}(y-l)} - nL_{22}e^{-n(y-l)}\right) cosnx, \tag{3.20}$$

where

$$L_{11} = -\frac{A_n + D_n}{n\left(\sqrt{n^2+A} - n\right)}, \quad L_{21} = \frac{nA_n + \sqrt{n^2+A}D_n}{n\left(\sqrt{n^2+A} - n\right)},$$

$$L_{12} = \frac{C_n - B_n}{\left(\sqrt{n^2 + A} - n\right)}, \quad L_{22} = \frac{nB_n - \sqrt{n^2 + A}C_n}{\left(\sqrt{n^2 + A} - n\right)}. \tag{3.21}$$

The following expression is found for pressure from Eqs. (3.6) and Eq. (3.7)

$$\begin{aligned} p = \mu\sqrt{A}A_0\beta_e e^{-\sqrt{A}(y-l)} & \\ & + \mu\sum_{n=1}^{\infty}\left(\left(n\left(n^2 - \sqrt{n^2 + A}^2 - A\alpha_e\right)\frac{L_{11}}{\sqrt{n^2 + A}}\right.\right. \\ & \left.\left. + A\beta_e L_{12}\right)e^{-\sqrt{n^2+A}(y-l)} - \frac{A}{n}(\alpha_e L_{21} + \beta_e L_{22})e^{-n(y-l)}\right)sinnx \\ & + \mu\sum_{n=1}^{\infty}\left(\left(n\left(n^2 - \sqrt{n^2 + A}^2 - A\alpha_e\right)\frac{L_{12}}{\sqrt{n^2 + A}}\right.\right. \\ & \left.\left. - A\beta_e L_{12}\right)e^{-\sqrt{n^2+A}(y-l)} + \frac{A}{n}(\alpha_e L_{22} + \beta_e L_{21})e^{-n(y-l)}\right)cosnx \\ & + C. \end{aligned} \tag{3.22}$$

where C is the constant of integration.

Now following Eqs. (2.27)-(2.30) of chapter 2, we can calculate work rate as follows

$$\begin{aligned} P = \frac{\mu}{2}\Bigg(& 2{A_0}^2\sqrt{A} \\ & + \sum_{n=1}^{\infty}\left(\sqrt{n^2 + A} + n\right)\Bigg({A_n}^2 + {B_n}^2 + nB_nC_n \\ & - \frac{n^2 - A\alpha_e}{n\sqrt{n^2 + A}}\left({C_n}^2 - {D_n}^2\right)\Bigg) \\ & + \sum_{n=1}^{\infty}\frac{n\sqrt{n^2 + A}}{\sqrt{n^2 + A} - n}\left(B_nC_n - A_nD_n - {C_n}^2 - {D_n}^2 - 2A\beta_e(A_nC_n\right. \\ & \left. + B_nD_n)\right) \\ & - \sum_{n=1}^{\infty}\left(\sqrt{n^2 + A} - n + \frac{n^2 - A\alpha_e}{\sqrt{n^2 + A} - n}\right)(B_nC_n - A_nD_n)\Bigg). \end{aligned} \tag{3.23}$$

Following the sections 2.3, we get the expression for velocity of propulsion $\mathfrak{U}$ and working rate P as follow

$$\mathfrak{U} = \sigma + \frac{\sigma}{2}\sum_{n=1}^{\infty}\left(\gamma^2 + \beta^2 - \frac{\sqrt{n^2 + A}}{n}b^2 - \frac{\sqrt{n^2 + A} + n}{n}\beta b\right), \tag{3.24}$$

$$P = \frac{\mu\sigma^2}{2}\left(2\sqrt{A} + \sum_{n=1}^{\infty}\left(\sqrt{n^2+A}+n\right)\left(\gamma^2+\beta^2-\frac{n^2-A\alpha_e}{n\sqrt{n^2+A}}b^2\right)\right.$$
$$-\sum_{n=1}^{\infty} b\beta\left(\sqrt{n^2+A}-n-\frac{n\sqrt{n^2+A}}{\sqrt{n^2+A}-n}+\frac{n^2-A\alpha_e}{\sqrt{n^2+A}}\right)$$
$$\left.-\sum_{n=1}^{\infty}\frac{nb}{\sqrt{n^2+A}-n}\left(\sqrt{n^2+A}b+2A\beta_e\gamma-n\right)\right). \qquad (3.25)$$

3.3 Results and Discussion

In this section impact of various parameters of interest are explored graphically. Effect of Hall parameter β_e, ionslip parameter β_i, Hartmann number $\mathcal{M}$, porosity parameter k are plotted for stream function and velocity profile. Figs. 3.2-3.5 have been presented for velocity components u and v against y for the different values of involved parameters. It is noted from Fig. 3.2-3.3 that horizontal and vertical velocity components mounted with the escalating values of Hall parameter β_e and ionslip parameter β_i, respectively. But the vertical velocity component increases slowly. The increase in Hall and ionslip parameters results a decrease in fluid resistance in the direction of wave therefore velocity profile along the metachronal wave increases by increasing Hall and ionslip parameter. Fig. 3.4 shows that magnetic field resist the fluid flow in x and y direction as Lorentz force due to magnetic field opposes the fluid flow. Fig. 3.5 show that both horizontal and the vertical velocity increases in the presence of porous medium as the porous medium in ciliary movement accelerate the velocity profile.

Stream lines owing to ciliary motion are shown in Figs. 3.6-3.7. It is noted that bolus formed by the fluid flow rises by increasing the values of porosity parameter i.e. porosity parameter play an essential role to expedite the fluid flow. Reverse behavior is noted due to increase in magnetic parameter i.e. it decelerated the fluid flow therefore bolus size reduces.

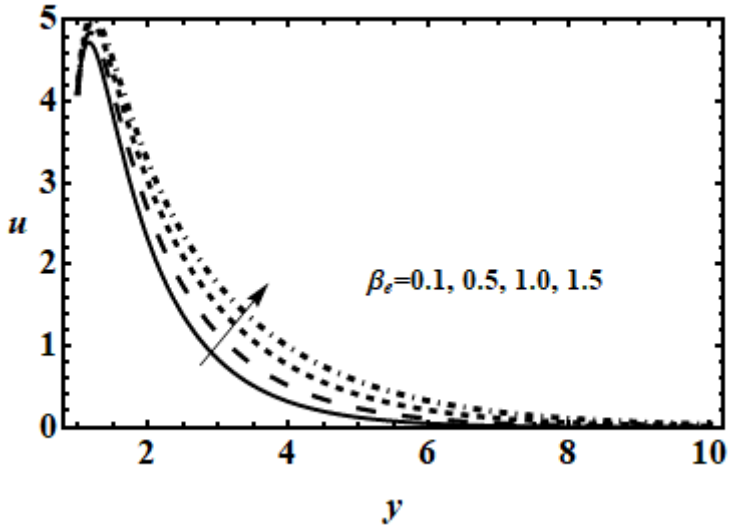

Fig. 3.2a: Influence of Hall parameter on longitudinal velocity $u(x, y)$ for $\beta = 0.5,\ \gamma = 0,$ $\sigma = 1,\ \mu = 1,\ b = 0.5,\ l = 1,\ \varphi = 0.1,\ k = 10,\ \beta_i = 1.$

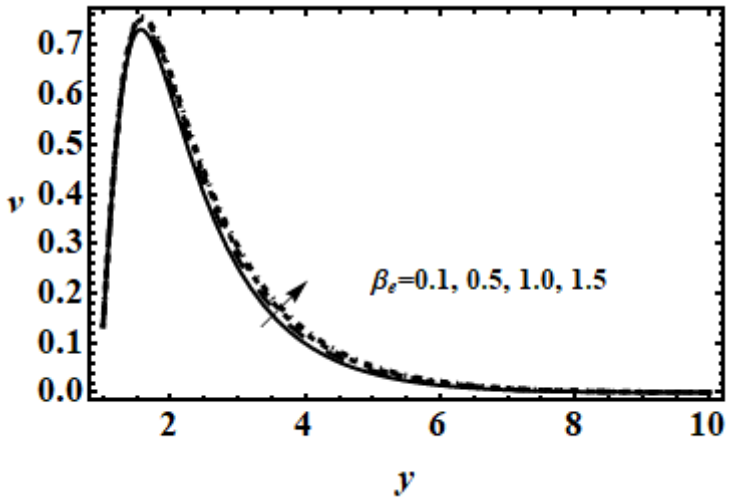

Fig. 3.2b: Influence of Hall parameter on transverse velocity $v(x, y)$ for $\beta = 0.5,\ \gamma = 0,$ $\sigma = 1,\ \mu = 1,\ b = 0.5,\ l = 1,\ \varphi = 0.1,\ \mathcal{M} = 1,\ k = 10,\ \beta_i = 1.$

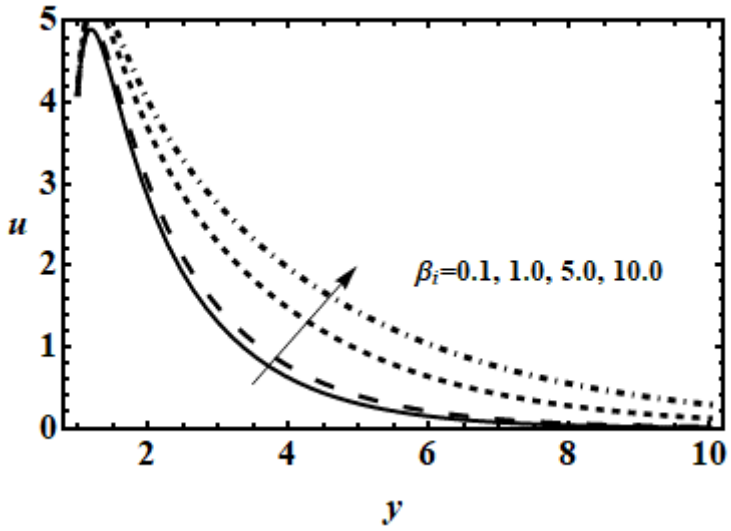

Fig. 3.3a: Influence of ionslip parameter on longitudinal velocity $u(x, y)$ for $\beta = 0.5,\ \gamma = 0,$ $\sigma = 1,\ \mu = 1,\ b = 0.5,\ l = 1,\ \varphi = 0.1,\ \mathcal{M} = 1,\ k = 10,\ \beta_e = 1.$

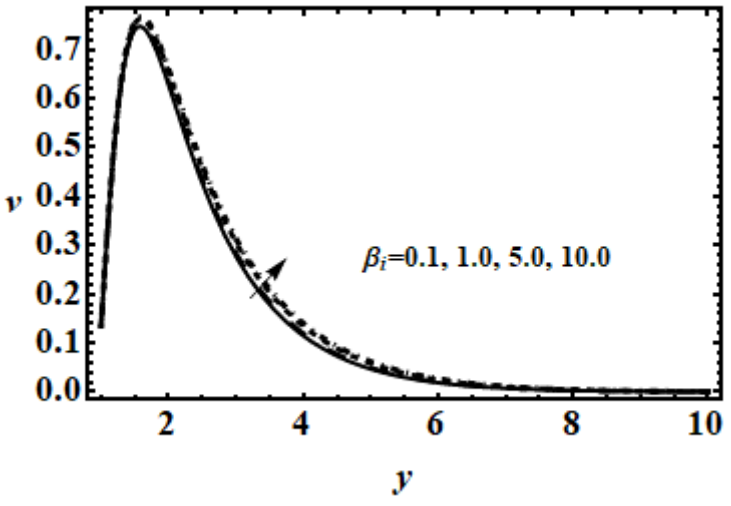

Fig. 3.3b: Influence of ionslip parameter on transverse velocity $v(x, y)$ for $\beta = 0.5,\ \gamma = 0,$ $\sigma = 1,\ \mu = 1,\ b = 0.5,\ l = 1,\ \varphi = 0.1,\ \mathcal{M} = 1,\ k = 10,\ \beta_e = 1.$

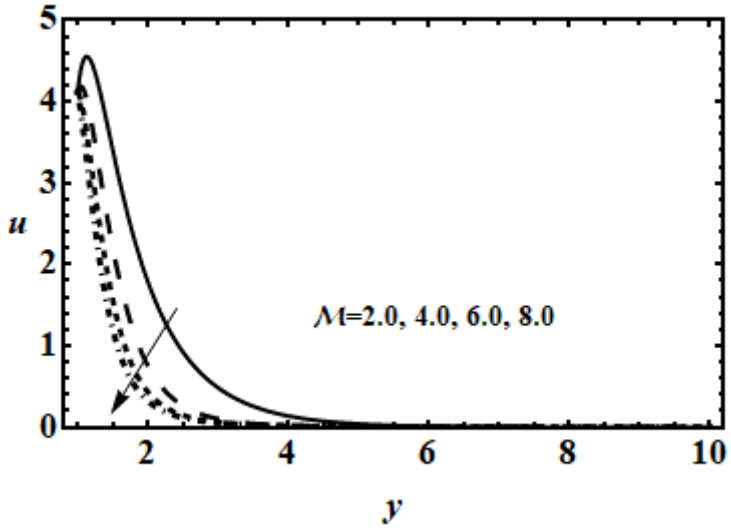

Fig. 3.4a: Influence of Hartmann number on longitudinal velocity $u(x, y)$ for $\beta = 0.5,\ \gamma = 0,\ \sigma = 1,\ \mu = 1,\ b = 0.5,\ l = 1,\ \varphi = 0.1,\ k = 10,\ \beta_e = 1,\ \beta_i = 1.$

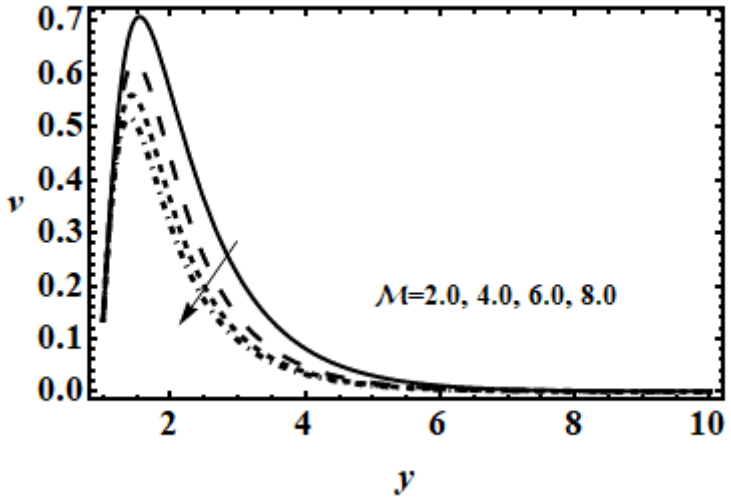

Fig. 3.4b: Influence of Hartmann number on transverse velocity $v(x, y)$ for $\beta = 0.5,\ \gamma = 0,\ \sigma = 1,\ \mu = 1,\ b = 0.5,\ l = 1,\ \varphi = 0.1,\ k = 10,\ \beta_e = 1,\ \beta_i = 1.$

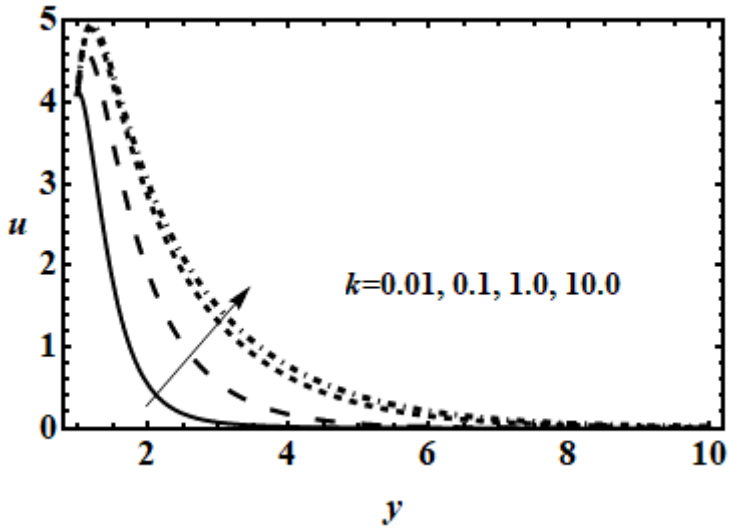

Fig. 3.5a: Influence of porosity parameter on longitudinal velocity $u(x,y)$ for $\beta = 0.5,\ \gamma = 0,\ \sigma = 1,\ \mu = 1,\ b = 0.5,\ l = 1,\ \varphi = 0.1,\ \mathcal{M} = 1,\ \beta_e = 1,\ \beta_i = 1.$

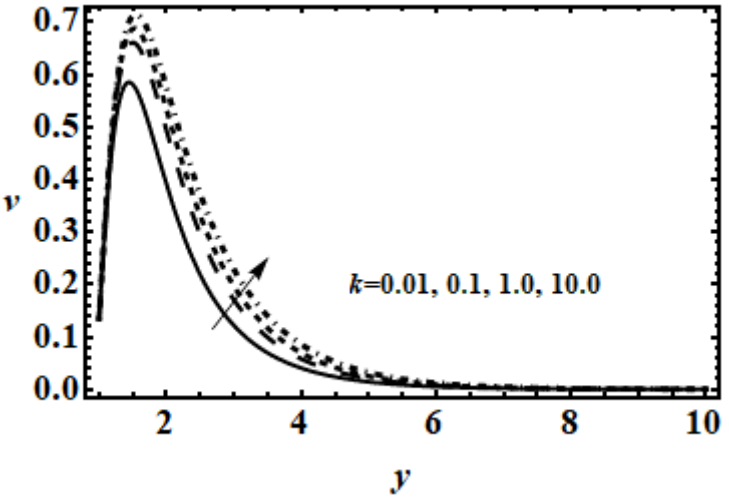

Fig. 3.5b: Influence of porosity parameter on transverse velocity $v(x,y)$ for $\beta = 0.5,\ \gamma = 0,\ \sigma = 1,\ \mu = 1,\ b = 0.5,\ l = 1,\ \varphi = 0.1,\ \mathcal{M} = 1,\ \beta_e = 1,\ \beta_i = 1.$

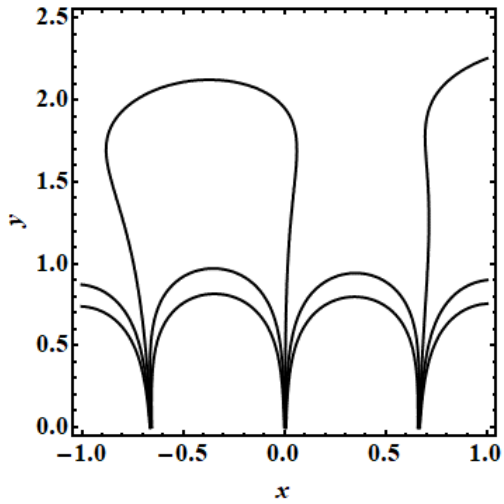

(a) $\mathcal{M}$ =1

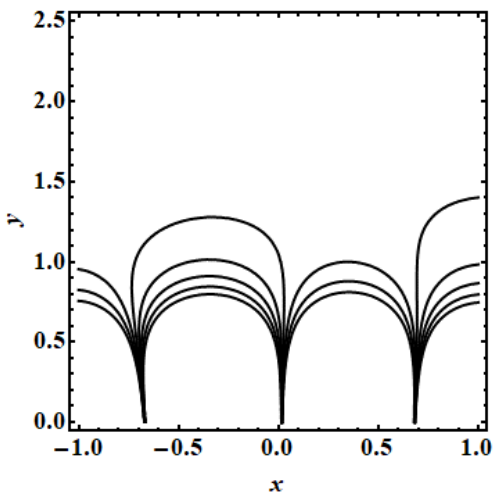

(b) $\mathcal{M}$ =5

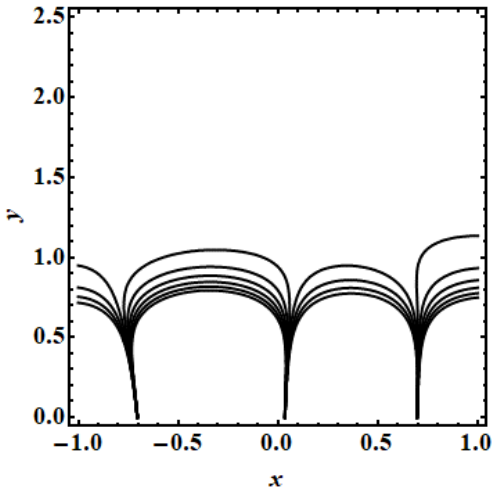

(c) $\mathcal{M}$ =10

Fig. 3.6: Influence of Hartmann number $\mathcal{M}$ on stream function for $\beta = 0.25,\ \gamma = 0.25,\ \alpha = 1,\ \mu = 1,\ b = 0.5,\ l = 1,\ \varphi = 0.1,\ k = 10,\ \beta_e = 1,\ \beta_i = 1.$

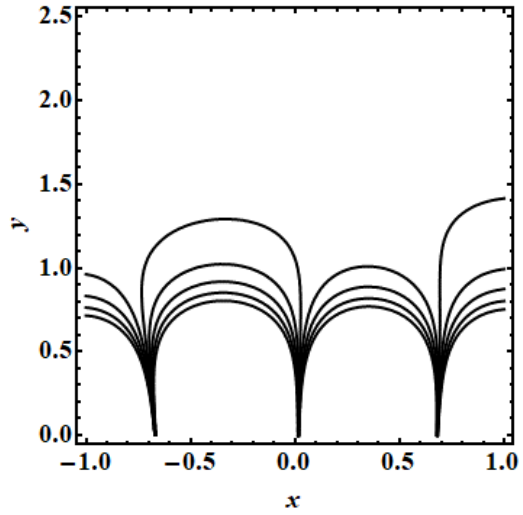

(a) k =0.01

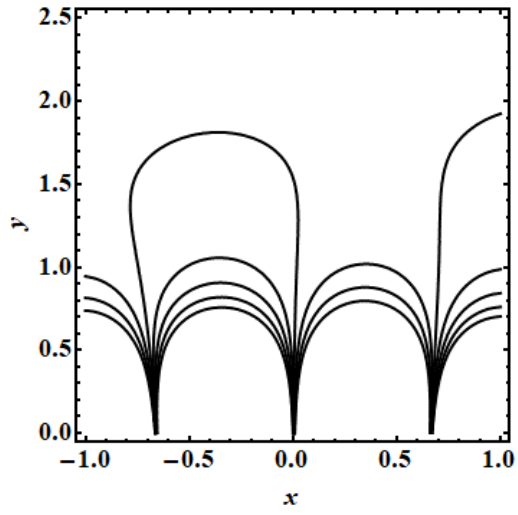

(b) k =0.05

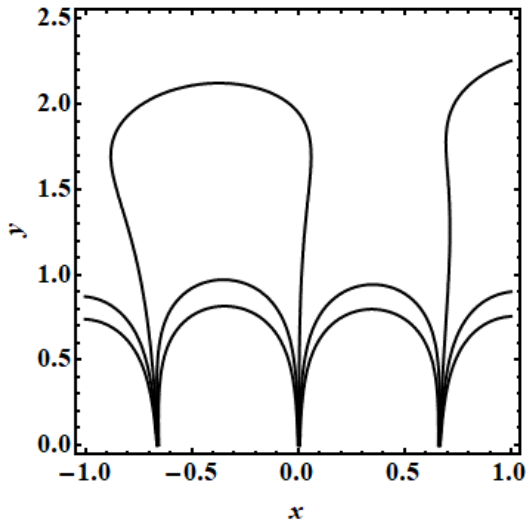

(c) k =0.1

Fig. 3.7: Influence of porosity parameter $\mathcal{k}$ on stream function for $\beta = 0.25,\ \gamma = 0.25,\ \alpha = 1,\ \mu = 1,\ b = 0.5,\ l = 1,\ \varphi = 0.1,\ \mathcal{M} = 1,\ \beta_e = 1,\ \beta_i = 1.$

3.4 Conclusion

In this study we have developed a mathematical model of velocity profile, stream function, pressure and work rate in the existence of Hall current and ionslip effect is developed. The flow is produced by the ciliated surface in which cilia tip form a metachronal wave. The metachronal wave suggest the envelope of cilia which helps to find the velocity, stream function and pressure. The Navier Stoke's equations in 2-dimensional and 2-directional are transformed into bi harmonic partial differential equation and evaluated by Fourier series expansion method. The resulting velocity profile and stream function involve the magnetic parameter $\mathcal{M}$, porosity parameter k, ionslip parameter β_i and Hall parameter β_e. Following observations are found for the velocity and stream function.

- Horizontal and vertical velocity is mounted by increasing Hall parameter β_e
- Ionslip parameter β_i showed the increasing effect on the horizontal and vertical velocity but the effect on horizontal velocity is more significant as compared to the vertical velocity.
- Magnetic parameter $\mathcal{M}$ retarded the motion in the horizontal and vertical direction.
- The velocity profile in x and y direction decreases by increasing the porosity parameter k.
- Contour plots of stream function show that when accelerated flow is required, porosity, Hall and ion slip effect should be incorporated whereas for the decelerated flow magnetic field should be applied in the perpendicular direction of the flow.
- Current study can be used for the treatment of diseases caused by the inactive cilia like asthma by pulmonary cilia and loss of memory due to cilia caused the movement of cerebrospinal fluid.

Chapter 4

Ciliary Flow of MHD Johson-Segalman Fluid in a Channel

In this chapter, a mathematical model for the cilia-generated propulsion of an electrically-conducting non-Newtonian fluid in a channel, under the action of magnetic field is discussed. The rheological behavior of the fluid is simulated with the Johnson-Segalman constitutive model which allows internal wall slip. Under the classical lubrication approximation, the boundary value problem is non-dimensionalized and solved analytically with a perturbation technique. The influence of the geometric, rheological (slip and Weissenberg number) and magnetic parameters on pressure rise, velocity and the pressure gradient (evaluated via the stream function in symbolic software) are presented graphically and interpreted at length.

4.1 Mathematical Modeling

Assume an incompressible MHD Johnson-Segalman fluid flow through a symmetric ciliated channel of width 2L, under the action of a transverse magnetic field B_0. The X-axis is taken along the direction of metachronal wave. The model is shown in Fig. 4.1. Cilia are continuously beating with recovery and effective strokes and the tip of the cilia follow the elliptical path centered at (X_0, l). The position of the cilia is given by the following parametric representation.

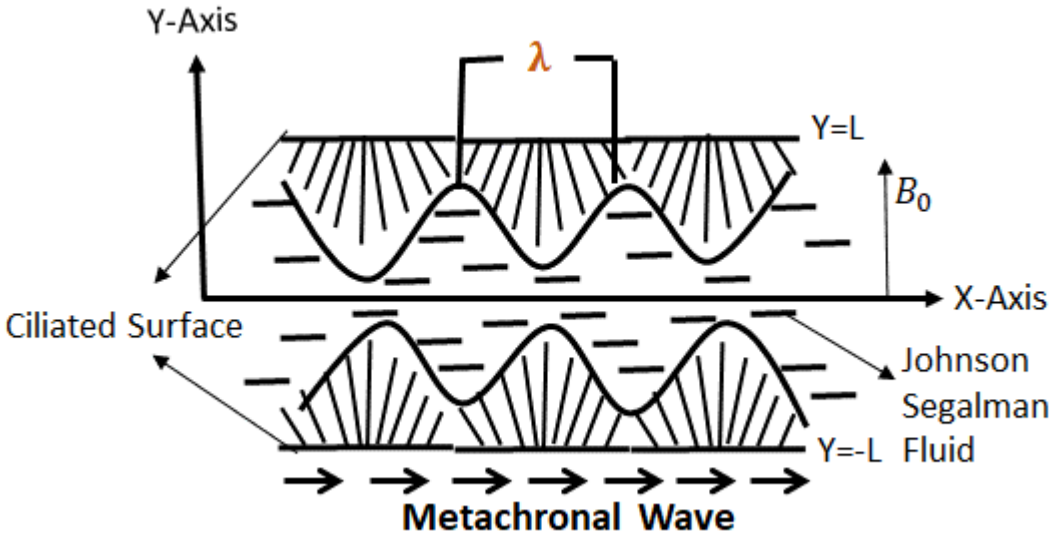

Fig. 4.1: Geometry of Problem

$$\hat{X} = F(\hat{X}, \hat{t}) = X_0 + \varepsilon l\alpha sin\left(\frac{2\pi}{\lambda}\right)(\hat{X} - c\hat{t}), \tag{4.1}$$

$$\hat{Y} = H(\hat{X}, \hat{t}) = l + l\varepsilon cos\left(\frac{2\pi}{\lambda}\right)(\hat{X} - c\hat{t}) = \pm L, \tag{4.2}$$

Here $l\varepsilon\alpha$ is the major axis in the $\hat{X}$-direction and $l\varepsilon$ is its minor axis in the $\hat{Y}$-direction. After determining the location of the cilia tips, we may calculate the horizontal and vertical velocity components. The horizontal velocity $\hat{U}$ is obtained by the time derivative at $\hat{X}$ and vertical velocity $\hat{V}$ is obtained by taking time derivative of vertical coordinate $\hat{Y}$ i.e.

$$\hat{U} = \frac{\frac{2\pi}{\lambda}\left(\varepsilon cl\alpha cos\left(\frac{2\pi}{\lambda}\right)(\hat{X} - c\hat{t})\right)}{1 - \frac{2\pi}{\lambda}\left(\varepsilon l\alpha cos\left(\frac{2\pi}{\lambda}\right)(\hat{X} - c\hat{t})\right)}, \tag{4.3}$$

$$\hat{V} = \frac{\frac{2\pi}{\lambda}\left(\varepsilon cl\alpha sin\left(\frac{2\pi}{\lambda}\right)(\hat{X} - c\hat{t})\right)}{1 - \frac{2\pi}{\lambda}\left(\varepsilon l\alpha cos\left(\frac{2\pi}{\lambda}\right)(\hat{X} - c\hat{t})\right)}. \tag{4.4}$$

Using the MHD Johnson-Segalman fluid model [38, 50] the continuity and momentum equations in a fixed frame are defined as follows:

$$div\, \boldsymbol{V} = 0, \tag{4.5}$$

$$\rho \frac{d\boldsymbol{V}}{dt} = div\boldsymbol{\tau} + \rho \boldsymbol{b_f}, \tag{4.6}$$

$$\rho \boldsymbol{b_f} = \left(\sigma {B_0}^2 \widehat{U}, 0, 0\right), \tag{4.7}$$

$$\boldsymbol{\tau} = P\boldsymbol{I} + \mathbb{T} \text{ and } \mathbb{T} = 2\mu \boldsymbol{D} + \boldsymbol{S}, \tag{4.8}$$

$$\boldsymbol{S} + m\left(\frac{d\boldsymbol{S}}{dt} + \boldsymbol{S}(\boldsymbol{W} - a\boldsymbol{D}) + (\boldsymbol{W} - a\boldsymbol{D})^T \boldsymbol{S}\right) = 2\eta \boldsymbol{D}, \tag{4.9}$$

$$\boldsymbol{D} = \frac{1}{2}(\boldsymbol{L} + \boldsymbol{L}^T), \;\; \boldsymbol{W} = \frac{1}{2}(\boldsymbol{L} - \boldsymbol{L}^T), \tag{4.10}$$

$$\boldsymbol{L} = \text{grad}\boldsymbol{V}, \;\; \boldsymbol{V} = \left(\widehat{U}\left(\hat{X}, \hat{Y}, \hat{t}\right), \widehat{V}\left(\hat{X}, \hat{Y}, \hat{t}\right), 0\right), \tag{4.11}$$

where all the parameters, tensors and stresses which are used in Eqs. (4.1)-(4.10) are defined in nomenclature. When we take slip parameter equals one i.e. $a = 1$, then this fluid model reduced to Oldroyd-B model, if dynamics viscosity of Johnson Segalmann fluid is zero i.e. $\mu = 0$ and the slip parameter $a = 1$, we get Maxwell fluid model, if $\frac{1}{2} \leq a \leq 1$, this fluid will be rod climbing, and when relaxation time m =0 of Johnson Segalmann fluid, we get classical Navier-Stokes fluid. Now Eqs. (4.5) and (4.6) together with Eqs. (4.7)-(4.10) take the following form:

$$\frac{\partial \widehat{U}}{\partial \hat{X}} + \frac{\partial \widehat{V}}{\partial \hat{Y}} = 0, \tag{4.12}$$

$$\rho\left(\frac{\partial \widehat{U}}{\partial \hat{t}} + \widehat{U}\frac{\partial \widehat{U}}{\partial \hat{X}} + \widehat{V}\frac{\partial \widehat{U}}{\partial \hat{Y}}\right) = -\frac{\partial \hat{P}}{\partial \hat{X}} + \frac{\partial \hat{S}_{\hat{X}\hat{X}}}{\partial \hat{X}} + \frac{\partial \hat{S}_{\hat{X}\hat{Y}}}{\partial \hat{Y}} - \sigma {B_0}^2 \widehat{U}, \tag{4.13}$$

$$\rho\left(\frac{\partial \widehat{V}}{\partial \hat{t}} + \widehat{U}\frac{\partial \widehat{V}}{\partial \hat{X}} + \widehat{V}\frac{\partial \widehat{V}}{\partial \hat{Y}}\right) = -\frac{\partial \hat{P}}{\partial \hat{Y}} + \frac{\partial \hat{S}_{\hat{X}\hat{Y}}}{\partial \hat{X}} + \frac{\partial \hat{S}_{\hat{Y}\hat{Y}}}{\partial \hat{Y}}, \tag{4.14}$$

Here $\hat{S}_{\hat{X}\hat{X}}, \hat{S}_{\hat{X}\hat{Y}}$ and $\hat{S}_{\hat{Y}\hat{Y}}$ satisfy following equations

$$2\eta\frac{\partial \widehat{U}}{\partial \hat{X}} = \hat{S}_{\hat{X}\hat{X}} + m\left(\widehat{U}\frac{\partial}{\partial \hat{X}} + \widehat{V}\frac{\partial}{\partial \hat{Y}}\right)\hat{S}_{\hat{X}\hat{X}} - 2am\hat{S}_{\hat{X}\hat{X}}\frac{\partial \widehat{U}}{\partial \hat{X}} + m\left((1-a)\frac{\partial \widehat{V}}{\partial \hat{X}} - (1+a)\frac{\partial \widehat{U}}{\partial \hat{Y}}\right)\hat{S}_{\hat{X}\hat{Y}}, \tag{4.15}$$

$$\eta\left(\frac{\partial \widehat{U}}{\partial \hat{Y}} + \frac{\partial \widehat{V}}{\partial \hat{X}}\right) = \hat{S}_{\hat{X}\hat{Y}} + m\left(\widehat{U}\frac{\partial}{\partial \hat{X}} + \widehat{V}\frac{\partial}{\partial \hat{Y}}\right)\hat{S}_{\hat{X}\hat{Y}} + \frac{m}{2}\left((1-a)\frac{\partial \widehat{U}}{\partial \hat{Y}} - (1+a)\frac{\partial \widehat{V}}{\partial \hat{X}}\right)\hat{S}_{\hat{X}\hat{X}} + \frac{m}{2}\left((1-a)\frac{\partial \widehat{V}}{\partial \hat{X}} - (1+a)\frac{\partial \widehat{U}}{\partial \hat{Y}}\right)\hat{S}_{\hat{Y}\hat{Y}}, \tag{4.16}$$

$$2\eta\frac{\partial \widehat{V}}{\partial \hat{Y}} = \hat{S}_{\hat{Y}\hat{Y}} + m\left(\widehat{U}\frac{\partial}{\partial \hat{X}} + \widehat{V}\frac{\partial}{\partial \hat{Y}}\right)\hat{S}_{\hat{Y}\hat{Y}} - 2am\hat{S}_{\hat{Y}\hat{Y}}\frac{\partial \widehat{V}}{\partial \hat{Y}}$$

$$+m\left((1-a)\frac{\partial \widehat{U}}{\partial \widehat{Y}}-(1+a)\frac{\partial \widehat{V}}{\partial \widehat{X}}\right)\hat{S}_{\hat{X}\hat{Y}}, \tag{4.17}$$

The fixed and the wave frame are related as

$$\begin{aligned}&\hat{x}=\hat{X}-\mathrm{c}\hat{t},\quad \hat{u}=\widehat{U}-\mathrm{c},\quad \hat{y}=\hat{Y},\quad \hat{v}=\hat{V}\\&\hat{p}(\hat{x},\hat{y},\hat{t})=\hat{P}\left(\hat{X},\hat{Y},\hat{t}\right),\quad H\left(\hat{X},\hat{t}\right)=h(\hat{x}).\end{aligned} \tag{4.18}$$

With the help of Eq. (4.18), Eqs. (4.12)-(4.17) take the following form

$$\frac{\partial \hat{u}}{\partial \hat{x}}+\frac{\partial \hat{v}}{\partial \hat{y}}=0, \tag{4.19}$$

$$\rho\left(\hat{u}\frac{\partial \hat{u}}{\partial \hat{x}}+\hat{v}\frac{\partial \hat{u}}{\partial \hat{y}}\right)=-\frac{\partial \hat{p}}{\partial \hat{x}}+\frac{\partial \hat{S}_{\hat{x}\hat{x}}}{\partial x}+\frac{\partial \hat{S}_{\hat{x}\hat{y}}}{\partial y}-\sigma {B_0}^2(\hat{u}+c), \tag{4.20}$$

$$\rho\left(\hat{u}\frac{\partial \hat{v}}{\partial \hat{x}}+\hat{v}\frac{\partial \hat{v}}{\partial \hat{y}}\right)=-\frac{\partial \hat{p}}{\partial \hat{y}}+\frac{\partial \hat{S}_{\hat{x}\hat{y}}}{\partial \hat{x}}+\frac{\partial \hat{S}_{\hat{y}\hat{y}}}{\partial \hat{y}}, \tag{4.21}$$

Here $\hat{S}_{\hat{x}\hat{x}},\hat{S}_{\hat{x}\hat{y}}$ and $\hat{S}_{\hat{y}\hat{y}}$ satisfy following equations

$$\begin{aligned}2\eta\frac{\partial \hat{u}}{\partial \hat{x}}=\hat{S}_{\hat{x}\hat{x}}+m\left(\hat{u}\frac{\partial}{\partial \hat{x}}+\hat{v}\frac{\partial}{\partial \hat{y}}\right)\hat{S}_{\hat{x}\hat{x}}-2am\hat{S}_{\hat{x}\hat{x}}\frac{\partial \hat{u}}{\partial \hat{x}}\\+m\left((1-a)\frac{\partial \hat{v}}{\partial \hat{x}}-(1+a)\frac{\partial \hat{u}}{\partial \hat{y}}\right)\hat{S}_{\hat{x}\hat{y}},\end{aligned} \tag{4.22}$$

$$\begin{aligned}&\eta\left(\frac{\partial \hat{u}}{\partial \hat{y}}+\frac{\partial \hat{v}}{\partial \hat{x}}\right)=\hat{S}_{\hat{x}\hat{y}}+m\left(\hat{u}\frac{\partial}{\partial \hat{x}}+\hat{v}\frac{\partial}{\partial \hat{y}}\right)\hat{S}_{\hat{x}\hat{y}}\\&+\frac{m}{2}\left((1-a)\frac{\partial \hat{u}}{\partial \hat{y}}-(1+a)\frac{\partial \hat{v}}{\partial x}\right)\hat{S}_{\hat{x}\hat{x}}\\&+\frac{m}{2}\left((1-a)\frac{\partial \hat{v}}{\partial \hat{x}}-(1+a)\frac{\partial \hat{u}}{\partial \hat{y}}\right)\hat{S}_{\hat{y}\hat{y}},\end{aligned} \tag{4.23}$$

$$\begin{aligned}2\eta\frac{\partial \hat{v}}{\partial \hat{y}}=\hat{S}_{\hat{y}\hat{y}}+m\left(\hat{u}\frac{\partial}{\partial \hat{x}}+\hat{v}\frac{\partial}{\partial \hat{y}}\right)\hat{S}_{\hat{y}\hat{y}}-2am\hat{S}_{\hat{y}\hat{y}}\frac{\partial \hat{v}}{\partial \hat{y}}\\+m\left((1-a)\frac{\partial \hat{u}}{\partial \hat{y}}-(1+a)\frac{\partial \hat{v}}{\partial \hat{x}}\right)\hat{S}_{\hat{x}\hat{y}},\end{aligned} \tag{4.24}$$

The non-dimensional variables are elucidated as follows:

$$\begin{aligned}&x=\frac{\hat{x}}{\lambda},\quad y=\frac{\hat{y}}{l},\quad u=\frac{\hat{u}}{\mathrm{c}},\quad v=\frac{\lambda\,\hat{v}}{l\mathrm{c}},\quad t=\frac{\mathrm{c}\hat{t}}{\lambda},\\&h=\frac{\hat{h}}{l},\quad \beta=\frac{l}{\lambda},\quad S_{ij}=\frac{l}{\mu\mathrm{c}}\hat{S}_{\hat{\imath}\hat{\jmath}},\quad p=\frac{l^2\hat{p}}{\lambda(\mu+\eta)},\\&\mathcal{M}^2=\frac{\sigma {B_0}^2 l^2}{\mu},\quad Re=\frac{\rho\mathrm{c}l}{\mu},\quad We=\frac{m\mathrm{c}}{l},\end{aligned} \tag{4.25}$$

here $\mathcal{M}$, β, We and Re represents Hartmann number, wave number, Weissenberg number, Reynolds number, respectively. The two dimensional flow is represented by the following stream function

$$\hat{u} = \frac{\partial \psi}{\partial \hat{y}}, \quad \hat{v} = -\frac{\partial \psi}{\partial \hat{x}}. \tag{4.26}$$

With the assistance of Eqs. (4.25), (4.26) and the lubrication approximations (long wavelength relative to channel width and low Reynolds number), Eqs. (4.19)-(4.24) can be written as

$$\left(\frac{\mu+\eta}{\mu}\right)\frac{\partial p}{\partial x} = \frac{\partial S_{xy}}{\partial y} + \frac{\partial^3 \psi}{\partial y^3} - \mathcal{M}^2\left(\frac{\partial \psi}{\partial y} + 1\right), \tag{4.27}$$

$$\frac{\partial p}{\partial y} = 0, \tag{4.28}$$

$$S_{xx} \quad = We(1+a)\frac{\partial^2 \psi}{\partial y^2} S_{xy}, \tag{4.29}$$

$$\frac{\eta}{\mu}\frac{\partial^2 \psi}{\partial y^2} = S_{xy} + \frac{We}{2}(1-a)\frac{\partial^2 \psi}{\partial y^2} S_{xx} - \frac{We}{2}(1+a)\frac{\partial^2 \psi}{\partial y^2} S_{yy}, \tag{4.30}$$

$$S_{yy} = -We(1-a)\frac{\partial^2 \psi}{\partial y^2} S_{xy}, \tag{4.31}$$

Eliminating pressure gradient from Eq. (4.27) and Eq. (4.28), following expression can be obtained

$$\frac{\partial^2 S_{xy}}{\partial y^2} + \frac{\partial^4 \psi}{\partial y^4} - \mathcal{M}^2 \frac{\partial^2 \psi}{\partial y^2} = 0. \tag{4.32}$$

From Eqs. (4.29)-(4.31), the shear stress, S_{xy}, can be found as follows

$$S_{xy} = \frac{\frac{\eta}{\mu}\frac{\partial^2 \psi}{\partial y^2}}{1 + We^2(1-a^2)\left(\frac{\partial^2 \psi}{\partial y^2}\right)^2}. \tag{4.33}$$

Now placing Eq. (4.33) into Eqs. (4.32) and (4.27) yields

$$\frac{\partial^2}{\partial y^2}\left(\frac{\left(\frac{\eta}{\mu}+1\right)\frac{\partial^2 \psi}{\partial y^2} + We^2(1-a^2)\left(\frac{\partial^2 \psi}{\partial y^2}\right)^3}{1 + We^2(1-a^2)\left(\frac{\partial^2 \psi}{\partial y^2}\right)^2} - \mathcal{M}^2 \psi\right) = 0, \tag{4.34}$$

$$\left(\frac{\mu+\eta}{\mu}\right)\frac{\partial p}{\partial x} = \frac{\partial}{\partial y}\left(\frac{\frac{\eta}{\mu}\frac{\partial^2 \psi}{\partial y^2}}{1 + We^2(1-a^2)\left(\frac{\partial^2 \psi}{\partial y^2}\right)^2}\right) + \frac{\partial^3 \psi}{\partial y^3} - \mathcal{M}^2\left(\frac{\partial \psi}{\partial y} + 1\right), \tag{4.35}$$

In bionic pumping systems, volume flow rate is a key design quantity. The instantaneous volumetric flow rate in a fixed frame is given by

$$\hat{F} = \int_0^H \hat{U}(\hat{X}, \hat{Y}, \hat{t}) d\hat{Y}, \tag{4.36}$$

using the formula of transformation (fixed to wave) given in Eq. (4.18), we get

$$\hat{f} = \int_0^{\hat{h}} \hat{u}(\hat{x}, \hat{y}) d\hat{y}, \tag{4.37}$$

Now the fixed and wave frame for volume flow rate can be defined with the help of Eq. (4.36) and Eq. (4.37) as

$$\hat{F} = \hat{f} + c\hat{h}, \tag{4.38}$$

The time-mean flow, at a fixed position $\hat{X}$, over a period $\hat{\mathcal{T}}$ is defined as

$$Q = \frac{1}{\hat{\mathcal{T}}} \int_0^{\hat{\mathcal{T}}} \hat{F}\, d\hat{t}, \tag{4.39}$$

using Eq. (4.38) into Eq. (4.39), and integrating, we get

$$Q = \int_0^1 (\hat{f} + c\hat{h}) d\hat{x} = \hat{f} + c \int_0^1 \hat{h} d\hat{x}, \tag{4.40}$$

now with the help of Eq. (4.2), Eq. (4.18) and Eq. (4.40) become

$$Q = \hat{f} + cl. \tag{4.41}$$

Define the dimensionless form of time mean flow $\hat{Q}$ and F respectively as

$$\hat{Q} = \frac{Q}{cl}, \quad F = \frac{\hat{f}}{cl}, \tag{4.42}$$

we get

$$F = \int_0^h \frac{\partial \psi}{\partial y} dy = \psi(h) - \psi(0). \tag{4.43}$$

And

$$\hat{Q} = F + 1, \tag{4.44}$$

If we choose $\psi = 0$ at $y = 0$ then $\psi = F$ at $y = h$. The boundary conditions become as

$$\psi = 0, \quad \frac{\partial^2 \psi}{\partial y^2} = 0, \quad at \quad y = 0,$$

$$\psi = F, \quad \frac{\partial \psi}{\partial y} = \mathcal{u}_0, \ \ at \ \ y = h. \tag{4.45}$$

Where

$$F = \int_0^h \frac{\partial \psi}{\partial y} dy, \ \ \mathcal{u}_0 = -1 - 2\pi\varepsilon\alpha\beta \cos(2\pi x), \ \ h = 1 + \varepsilon \cos(2\pi x). \tag{4.46}$$

With the help of binomial theorem and neglecting higher powers of $\left(\frac{\partial^2 \psi}{\partial y^2}\right)$ i.e. $O\left(\left(\frac{\partial^2 \psi}{\partial y^2}\right)\right)^6$,

$$\frac{\partial^2}{\partial y^2}\left(\frac{\partial^2 \psi}{\partial y^2} + We^2 \kappa_2 \left(\frac{\partial^2 \psi}{\partial y^2}\right)^3 - \kappa_1 \mathcal{M}^2 \psi\right) = 0, \tag{4.47}$$

Eqs. (4.34) and (4.35) then take the following form

$$\frac{\partial p}{\partial x} = \frac{\partial}{\partial y}\left(\frac{\partial^2 \psi}{\partial y^2} + We^2 \kappa_2 \left(\frac{\partial^2 \psi}{\partial y^2}\right)^3\right) - \kappa_1 \mathcal{M}^2 \left(\frac{\partial \psi}{\partial y} + 1\right). \tag{4.48}$$

Here

$$\kappa_1 = \frac{\mu}{\mu + \eta}, \ \ \kappa_2 = \frac{(a^2 - 1)}{\mu + \eta}. \tag{4.49}$$

Here μ, η are viscosity coefficients of the Johnson-Segalman fluid, a is slip parameter.

4.4 Perturbation Solution

To solve the non-linear Eqs. (4.47) and (4.48) together with the boundary condition (4.45), a perturbation method is employed. Expanding the stream function ψ, pressure distribution p and flow rate F about the Weissenberg number We (assuming small Weissenberg number) leads to

$$\psi = \psi_0 + We^2 \psi_1 + \cdots, \tag{4.50}$$

$$p = p_0 + We^2 p_1 + \cdots, \tag{4.51}$$

$$F = F_0 + We^2 F_1 + \cdots, \tag{4.52}$$

Using the above equations in (4.47)-(4.48) we obtain the following systems

4.4.1 Zeroth Order System

$$\frac{\partial^2}{\partial y^2}\left(\frac{\partial^2 \psi_0}{\partial y^2} - \kappa_1 \mathcal{M}^2 \psi_0\right) = 0, \tag{4.53}$$

$$\frac{dp_0}{dx} = \frac{\partial}{\partial y}\left(\frac{\partial^2 \psi_0}{\partial y^2}\right) - \kappa_1 \mathcal{M}^2 \left(\frac{\partial \psi_0}{\partial y} + 1\right). \tag{4.54}$$

The associated boundary conditions are

$$\begin{aligned} &\psi_0 = 0, \quad \frac{\partial^2 \psi_0}{\partial y^2} = 0, \ \ at \ \ y = 0, \\ &\psi_0 = F_0, \quad \frac{\partial \psi_0}{\partial y} = u_0, \ \ at \ \ y = h. \end{aligned} \tag{4.55}$$

Solution of zeroth order system

Solution of zeroth order system given by Eqs. (4.53)-(4.55) is as follows

$$\begin{aligned} &\psi_0 \\ &= \frac{-\mathcal{M} y \cosh(\mathcal{M} h\sqrt{\kappa_1}) F_0 \sqrt{\kappa_1} + y \sinh(\mathcal{M} h\sqrt{\kappa_1}) u_0 + \sinh(\mathcal{M} h\sqrt{\kappa_1})(F_0 - h u_0)}{\sinh(\mathcal{M} h\sqrt{\kappa_1}) - \mathcal{M} \cosh(\mathcal{M} h\sqrt{\kappa_1}) h\sqrt{\kappa_1}}, \end{aligned} \tag{4.56}$$

Using Eqs. (4.54) and (4.56), the zeroth order pressure gradient is obtained as

$$\frac{dp_0}{dx} = \frac{\mathcal{M}^2 \kappa_1 \left(-\mathcal{M} \cosh(\mathcal{M} h\sqrt{\kappa_1})(h + F_0)\sqrt{\kappa_1} + \sinh(\mathcal{M} h\sqrt{\kappa_1})(1 + u_0)\right)}{-\sinh(\mathcal{M} h\sqrt{\kappa_1}) + \mathcal{M} \cosh(\mathcal{M} h\sqrt{\kappa_1}) h\sqrt{\kappa_1}}. \tag{4.57}$$

4.4.2 First Order System

$$\frac{\partial^2}{\partial y^2}\left(\frac{\partial^2 \psi_1}{\partial y^2} + We^2 \kappa_2 \left(\frac{\partial^2 \psi_0}{\partial y^2}\right)^3 - \kappa_1 \mathcal{M}^2 \psi_1\right) = 0, \tag{4.58}$$

$$\frac{\partial p_1}{\partial x} = \frac{\partial}{\partial y}\left(\frac{\partial^2 \psi_1}{\partial y^2} + We^2 \kappa_2 \left(\frac{\partial^2 \psi_0}{\partial y^2}\right)^3\right) - \kappa_1 \mathcal{M}^2 \left(\frac{\partial \psi_1}{\partial y} + 1\right). \tag{4.59}$$

The relevant boundary conditions are

$$\begin{aligned} &\psi_1 = 0, \quad \frac{\partial^2 \psi_1}{\partial y^2} = 0, \ \ at \ \ y = 0, \\ &\psi_1 = F_1, \quad \frac{\partial \psi_1}{\partial y} = 0, \ \ at \ \ y = h, \end{aligned} \tag{4.60}$$

Solution of first order system

Solving first order system as given by Eqs. (4.58)-(4.60), we obtain

$$\psi_1 = \frac{1}{64(\sinh(\mathcal{M}h\sqrt{\kappa_1}) - \mathcal{M}cosh(\mathcal{M}h\sqrt{\kappa_1})h\sqrt{\kappa_1})^4}\Bigg(\Big(8F_1\Big(8\sinh\big(\mathcal{M}y\sqrt{\kappa_1}\big)\big(\sinh\big(\mathcal{M}h\sqrt{\kappa_1}\big)\big)^3 + \mathcal{M}\sqrt{\kappa_1}\Big(-8y\cosh\big(\mathcal{M}h\sqrt{\kappa_1}\big)\big(\sinh\big(\mathcal{M}h\sqrt{\kappa_1}\big)\big)^3 + h(-3\big(\sinh(\mathcal{M}(y-3h)\sqrt{\kappa_1}\big) - \sinh\big(\mathcal{M}(y-h)\sqrt{\kappa_1}\big) - \sinh(\mathcal{M}(y+h)\sqrt{\kappa_1}\Big) + \sinh(\mathcal{M}(y+3h)\sqrt{\kappa_1}\Big)) + \mathcal{M}\sqrt{\kappa_1}(6y(\sinh\big(2\mathcal{M}\sqrt{\kappa_1}\big)^2 + h(-3\big(\cosh\big(\mathcal{M}(y-3h)\sqrt{\kappa_1}\big) + \cosh\big(m(y-h)\sqrt{\kappa_1}\big)\big) - 8\mathcal{M}\big(\cosh\big(\mathcal{M}h\sqrt{\kappa_1}\big)\big)^3\Big(h\sinh\big(\mathcal{M}y\sqrt{\kappa_1}\big) + 3y\sinh\big(\mathcal{M}h\sqrt{\kappa_1}\big)\Big)\sqrt{\kappa_1} + 8\mathcal{M}^2y\big(\cosh\big(\mathcal{M}h\sqrt{\kappa_1}\big)\big)^4h\kappa_1)))) - \mathcal{M}^4\kappa_1)\Big)^2\Big(-\cosh\big(\mathcal{M}(y-3h)\sqrt{\kappa_1}\big) + \cosh\big(\mathcal{M}(3y-h)\sqrt{\kappa_1}\big) - \cosh\big(\mathcal{M}(3y+h)\sqrt{\kappa_1}\big) + \mathcal{M}(2y\Big(-6\sinh\big(\mathcal{M}(y-h)\sqrt{\kappa_1}\big) - 8\sinh\big(2\mathcal{M}h\sqrt{\kappa_1}\big) + \big(\sinh\big(4\mathcal{M}h\sqrt{\kappa_1}\big) + 6\sinh\big(\mathcal{M}(y+h)\sqrt{\kappa_1}\big)\big) + h\Big(-3\sinh\big(\mathcal{M}(\mathrm{y}-3\mathrm{h})\sqrt{\kappa_1}\big) + \sinh\big(\mathcal{M}(3\mathrm{y}-\mathrm{h})\sqrt{\kappa_1}\big) + \sinh\big(\mathcal{M}(3\mathrm{y}++\mathrm{h})\sqrt{\kappa_1}\big) - 3\sinh\big(\mathcal{M}(\mathrm{y}+3\mathrm{h})\sqrt{\kappa_1}\big)\Big)\Big)\sqrt{\kappa_1} + 24\mathcal{M}^2h(y - y\cosh\big(\mathcal{M}h\sqrt{\kappa_1}\big)\cosh\big(mh\sqrt{\kappa_1}\big) + h\sinh(\mathcal{M}y\sqrt{\kappa_1})\sinh(\mathcal{M}h\sqrt{\kappa_1}))\kappa_1)\kappa_2(-F_0 + hu_0)^3\Big)\Bigg). \quad (4.61)$$

Using Eq. (4.61) into Eq. (4.59), we arrive at the first order pressure gradient

$$\frac{dp_1}{dx} = \frac{1}{32(\sinh(\mathcal{M}h\sqrt{\kappa_1}) - \mathcal{M}cosh(\mathcal{M}h\sqrt{\kappa_1})h\sqrt{\kappa_1})^4}\Bigg(\mathcal{M}^2\kappa_1\Big(-16cosh\big(2\mathcal{M}h\sqrt{\kappa_1}\big)(-1 + \mathcal{M}^4h^3(h+F_1){\kappa_1}^2) - 4cosh\big(4\mathcal{M}h\sqrt{\kappa_1}\big)\Big(1 + \mathcal{M}^2h\kappa_1\big(3F_1 + h(6 + \mathcal{M}^2h(h+F_1)\kappa_1)\big)\Big) - 8\mathcal{M}sinh\big(2\mathcal{M}h\sqrt{\kappa_1}\big)\sqrt{\kappa_1}\Big(F_1 - \mathcal{M}{F_0}^3{\kappa_1}^2\kappa_2 + h\big(4 + 3\mathcal{M}^4{F_0}^2{\kappa_1}^2\kappa_2u_0\big) - 3\mathcal{M}h^2\kappa_1(F_1 + \mathcal{M}F_0\kappa_1\kappa_2{u_0}^2) + \mathcal{M}^2h^3\kappa_1(-4 + \mathcal{M}^2\kappa_1\kappa_2{u_0}^3)\Big) + \mathcal{M}sinh\big(4\mathcal{M}h\sqrt{\kappa_1}\big)\sqrt{\kappa_1}\Big(4F_1 - \mathcal{M}^4{F_0}^3{\kappa_1}^2\kappa_2 + h\big(16 + 3\mathcal{M}^4{F_0}^2{\kappa_1}^2\kappa_2u_0\big) - 3\mathcal{M}h^2\kappa_1(-4F_1 + \mathcal{M}^2F_0\kappa_1\kappa_2{u_0}^2) + \mathcal{M}^2h^3\kappa_1(16 + \mathcal{M}^2\kappa_1\kappa_2{u_0}^3)\Big) + 12\Big(-1 + \mathcal{M}^2h\kappa_1\Big(F_1 - \mathcal{M}^4{F_0}^3{\kappa_1}^2\kappa_2 + h\big(2 + 3\mathcal{M}^4{F_0}^2{\kappa_1}^2\kappa_2u_0\big) - \mathcal{M}^2h^2\kappa_1(F_1 + 3\mathcal{M}^2F_0\kappa_1\kappa_2{u_0}^2) + \mathcal{M}^2h^3\kappa_1(-1 + \mathcal{M}^2\kappa_1\kappa_2{u_0}^3)\Big)\Big)\Big)\Big)\Bigg). \quad (4.62)$$

Now summarize the above results up to order We^2 and to achieve final results we introduce $F = F_0 + We^2F_1$ or $F_0 = F - We^2F_1$ in stream function ψ and pressure

gradient $\frac{dp}{dx}$ given in Eqs. (4.50) and (4.51). Where $\psi_0, \psi_1, \frac{dp_0}{dx}$ and $\frac{dp_1}{dx}$ are defined in Eqs. (4.56), (4.57), (4.61) and (4.62).

4.5 Results and Discussion

Figs. 4.2, 4.3 and 4.4 are plotted to visualize the effects of the key parameters i.e. Hartmann number, Weissenberg number, slip parameter and the cilia length, on the pressure rise, velocity and the pressure gradient keeping all other parameters fixed.

Figs. 4.2a-d illustrate the impact of Hartmann number $\mathcal{M}$, Weissenberg number We, slip parameter a and cilia length ε on the axial pressure p evolution with axial coordinate x i.e. pressure gradient. Fig. 4.2a shows that pressure is strongly affected by the Hartmann number. With the rise in Hartmann number there is a uniform decrease in pressure. A reduction in pressure is also induced with increasing slip parameter in Fig 4.2c. However pressure is boosted with elevation in Weissenberg number (Fig. 4.2c) and cilia length (Fig. 4.2d). There is a more uniform pressure distribution along the channel length with variation in Hartmann number (Fig. 4.2a) and the principal reduction in pressure is concentrated in the intermediate section of the channel; lower pressures ascend at entry and exit of the channel with maximum pressures in between, an important feature is required for efficient medical magnetic pumping performance.

Hartmann number appears in the Lorentz magnetohydrodynamic body force terms in Eqs. (4.47) and (4.48). This is a retarding force which opposes the flow and induces deceleration across the channel span (described later). Effectively pressure is suppressed with stronger magnetic field. The maximum pressure is achieved for the case $\mathcal{M} = 1$ wherein viscous and magnetic forces in the regime are equivalent in magnitude. For $\mathcal{M} > 1$ the magnetic drag force dominates the viscous hydrodynamic resistance. Figs. 4.2b-d indicate that the other parameters induce a more marked modification in pressure profiles in the vicinity of the entry and exit zones (low and high values of axial coordinate). The viscoelastic parameter i.e. Weissenberg number embodies the relative contribution of viscous forces to the elastic forces. For cases where the time-scale of a flow is significantly less than the relaxation time of the viscoelastic fluids, then elastic effects dominate the flow behavior. However, when time-scale exceeds the relaxation time, substantial elastic relaxation takes place and the viscous forces dominate the flow. The Johnson-Segalman fluid model is more sophisticated than other viscoelastic models and permits the non-monotonic variation

in shear stress with decrease/increase in the rate of deformation for simple shear flows. It is also capable of simulating slip effects and furthermore the spurt phenomenon i.e. an abnormal rise in volume throughput for a very weak elevation in the driving pressure gradient. With greater Weissenberg numbers the elastic effect dominates the behavior and this contributes to the enhancement in pressure. With greater slip effect the pressure is decreased significantly (Fig. 4.2c). The increase in pressure with greater cilia length is related to the enhanced transfer of force to the fluid in the channel with longer cilia geometry. This boosts the pressure in the central channel length area but depresses the pressure near the entry and exit locations.

Figs. 4.3a-d reveal the impact of the key parameters on axial velocity across the channel span i.e. with transverse coordinate, y. Evidently although symmetrical profiles in velocity are consistently computed, the parameters exhibit different effects. Fig. 4.3a and 4.3b show that by increasing Hartmann number and Weissenberg number velocity reduces in the central (core) region, $-0.32 < y < 0.32$ and rises near the walls in range, $y < -0.32$ and $y > 0.32$ of the channel. The contrary behavior can be observed with a rise in slip parameter and cilia length from Figs. 4.3c and 4.3d. Furthermore, inspection of the figures reveals that Hartmann number, Weissenberg number and slip parameter generate a more significant influence at the center as compared to walls of the channel.

The expression for the pressure rise is

$$\Delta p = \int_0^1 \frac{dp}{dx}\, dx, \tag{4.63}$$

To calculate the result of volume flow rate, we use the expression of Δp which involves integration of $\frac{dp}{dx}$. Due to the complexity of the expression given in the Eq. (4.63), the symbolic software, MATHEMATICA, has been implemented for the numerical integration. The results are shown in Figs. 4.4a-b, which present the evolution in average rise in the pressure against $\hat{Q}$ (time-averaged flux). The impact of magnetic parameter $\mathcal{M}$ on pressure rise is shown in Fig. 4.4a, which shows the retrograde pumping $\hat{Q} < 0, \Delta p > 0$ and the free pumping $\Delta p = 0$ uniformly change with the rise in Hartmann number. Fig. 4.4b and 4.4c, reveals the change of pressure rise against time average flux, for the different values of Weissenberg number We and the slip parameter a. It is noted that co-pumping rate reduces with the rising values of slip parameter and Weissenberg number. Fig. 4.4d, depicts the effect of cilia length ε on the

pressure rise. It is noticeable that the pumping and co-pumping rates increases with growing cilia length.

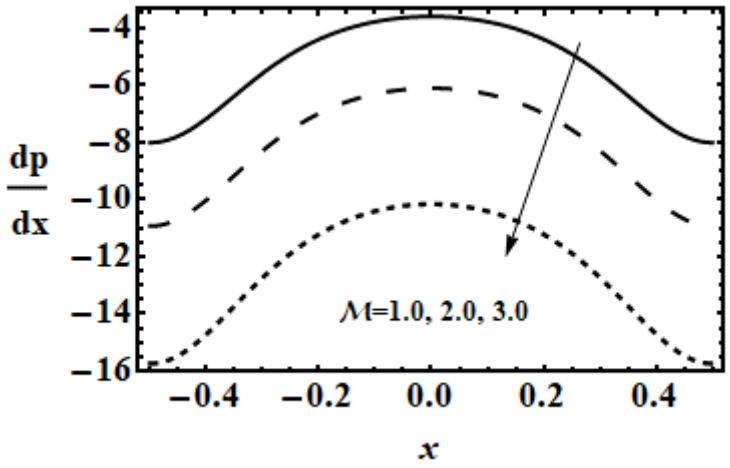

Fig. 4.2a: The effect of Hartmann number $\mathcal{M}$ on pressure gradient.

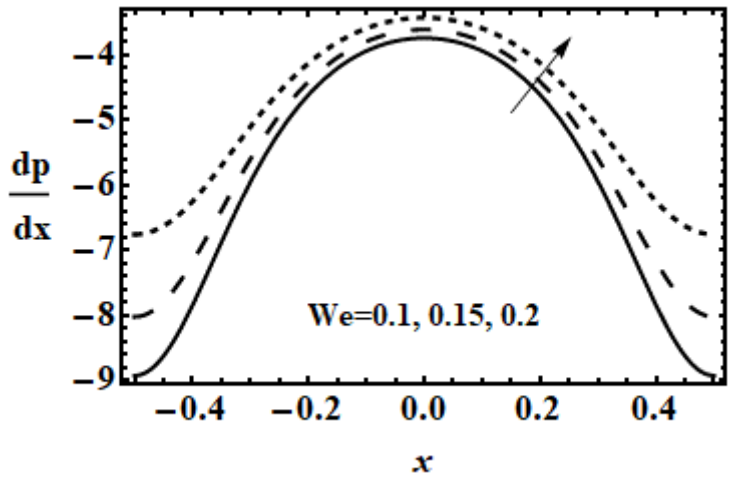

Fig. 4.2b: The effect of Weissenberg number We on pressure gradient.

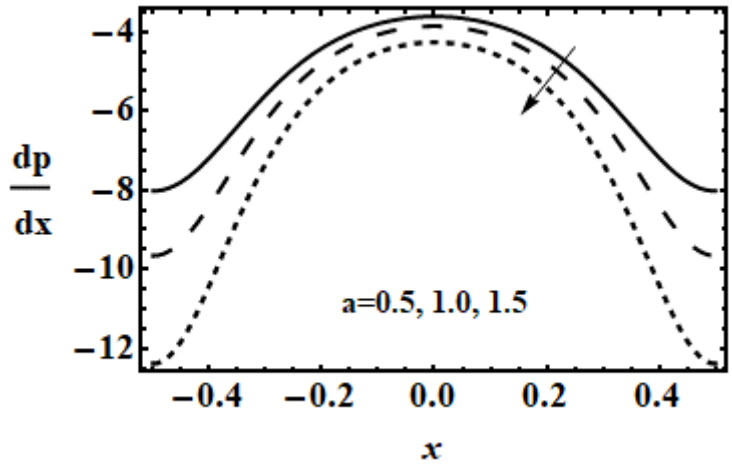

Fig. 4.2c: The effect of slip parameter a on pressure gradient.

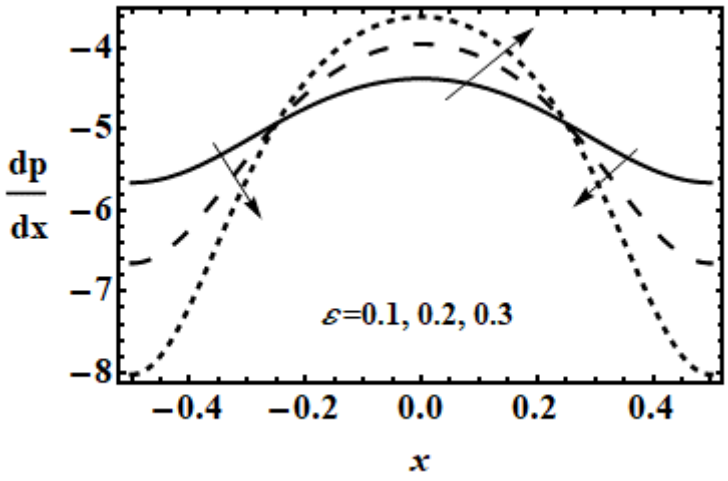

Fig. 4.2d: The effect of cilia length ε on pressure gradient.

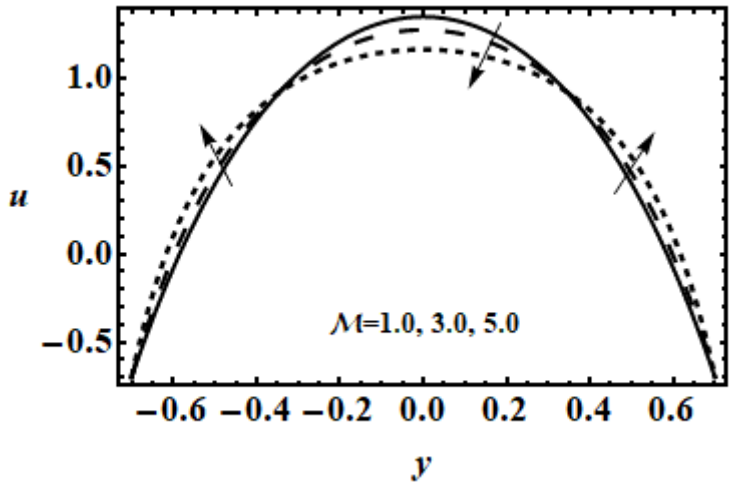

Fig. 4.3a: The effect of Hartmann number $\mathcal{M}$ on velocity.

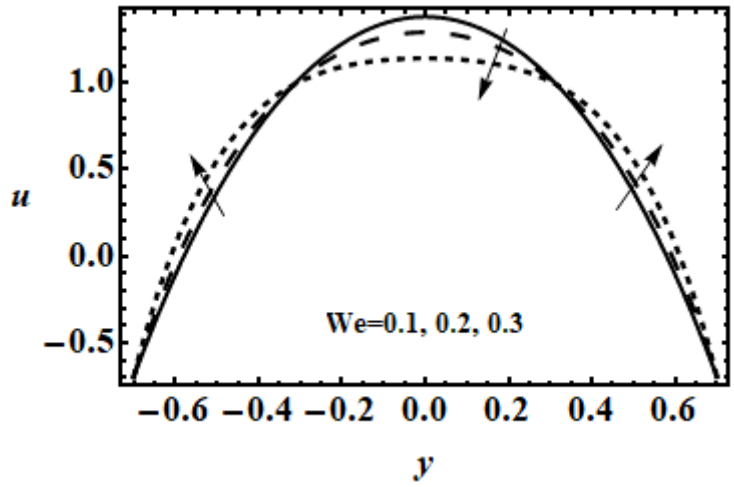

Fig. 4.3b: The effect of Weissenberg number We on velocity.

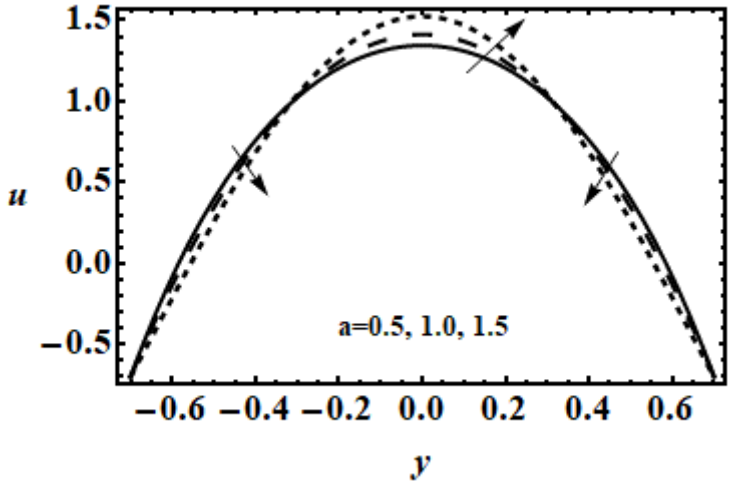

Fig. 4.3c: The effect of slip parameter a on velocity.

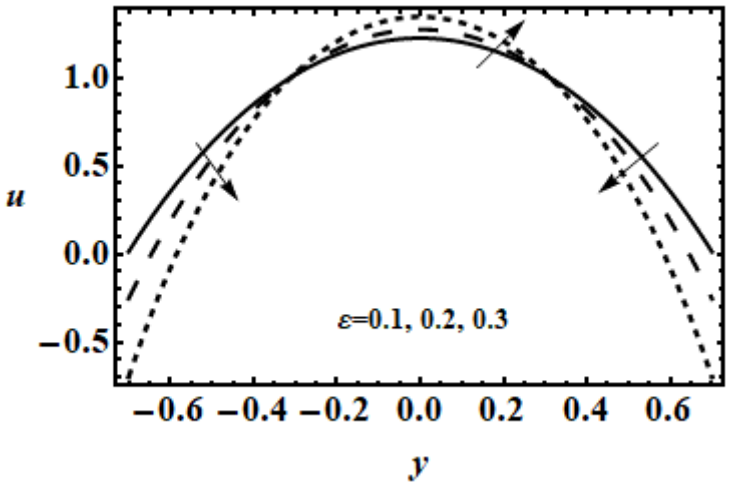

Fig. 4.3d: The effect of cilia length ε on velocity.

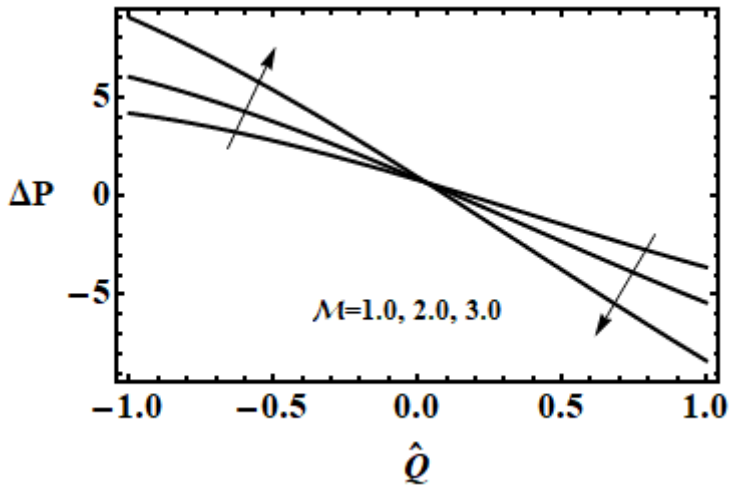

Fig. 4.4a: The effect of Hartmann number $\mathcal{M}$ on pressure rise.

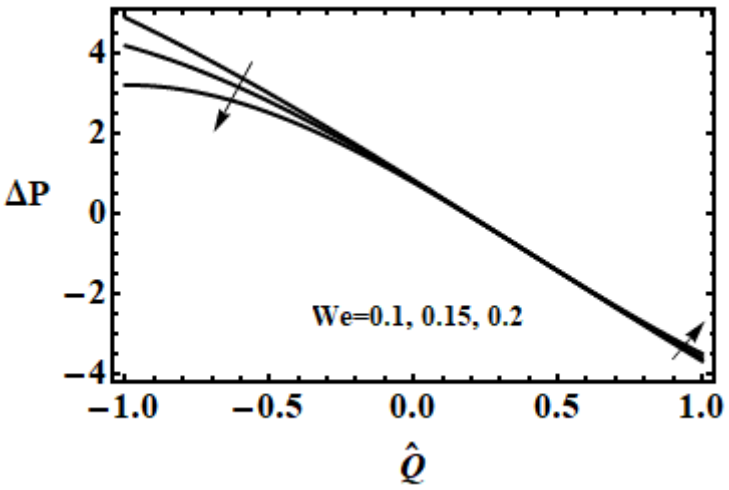

Fig. 4.4b: The effect of Weissenberg number We on pressure rise.

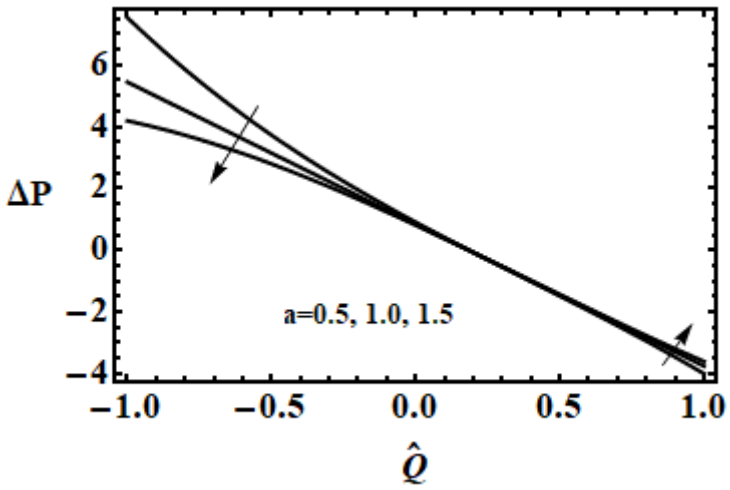

Fig. 4.4c: The effect of slip parameter a on pressure rise.

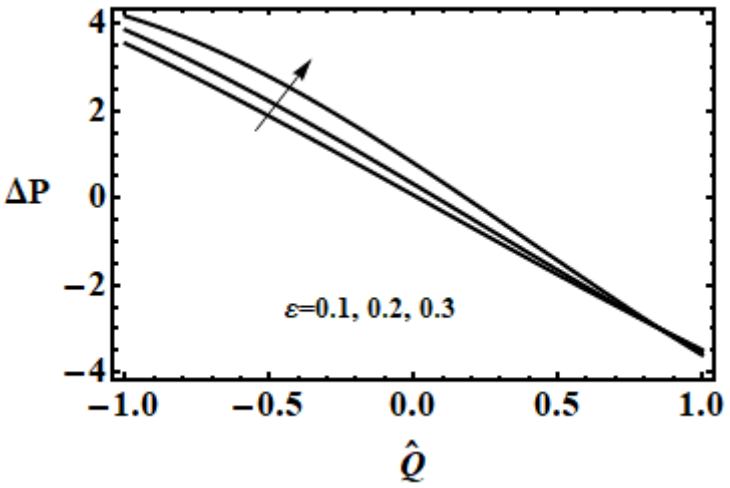

Fig. 4.4d: The effect of cilia length ε on pressure rise.

4.6 Conclusion

In this study, we have considered the ciliary transport of MHD Johnson-Segalman fluid in a 2D symmetric channel. The flow is produced by continuous beating of cilia in an elliptical path which generates the two-dimensional velocity field. The governing equations are simplified by using lubrication theory and converted into non-dimensional form via suitable transformations. A regular perturbation technique is used to solve non-linear PDEs with appropriate boundary conditions. Mathematica symbolic software is deployed to evaluate the series solutions and results are visualized graphically. The principal findings from this chapter may be concluded as follows:

- The pressure gradient is strongly affected by Weissenberg viscoelastic number We and cilia length ε.
- With increase in Weissenberg viscoelastic number We and cilia length ε larger pressure gradient is required to maintain the same flux through a narrow region as compared to a wider region of channel, whereas, smaller pressure gradient is required with rise in magnetic parameter $\mathcal{M}$ and slip parameter a.
- The velocity response is not the same throughout the channel. Velocity decreases in the central region by rising magnetic number $\mathcal{M}$ and Weissenberg number We and enhances with a rise in slip parameter a and cilia length ε.
- By increasing magnetic parameter $\mathcal{M}$ and cilia length ε pressure rise increases whereas it is reduced with larger values of Weissenberg number We and cilia length ε.
- The present investigation has neglected curvature, rotational and heat transfer effects which are also important in biomimetic pumps and these may be addressed in the future.

Chapter 5

Inertial Flow of MHD Second Grade Fluid in a Ciliated Channel

This study is presented for MHD second grade fluid in a ciliated channel embedded in a porous medium. The two dimensional flow is modelled with the inertial effects ($Re \neq 0$) which make the partial differential equation non-linear and complex. The Homotopy Perturbation Method (HPM), is used to solve the complex partial differential equation, which does not indispensable the assumption of small parameter like the perturbation method. The HPM solution is found by the help of software "Mathematica" and graphical results are shown in the last section.

5.1 Mathematical Formulation

Assume the ciliary flow of an incompressible second grade fluid in a symmetric channel embedded in a porous medium under the effect of constant applied magnetic field. To study the magnetohydrodynamics flow of second grade model having properties $\alpha_1 + \alpha_2 = 0$ and $\alpha_1 > 0$ through a ciliated porous channel, the Lorentz force and Darcy's law are considered with the two dimensional momentum equations. The flow occur due to ciliary motion as a cilium moves in an elliptical path and collectively produced a metachronal wave in X-direction of Cartesian coordinate system and Y-axis is normal to the wave propagation. The mathematical form of horizontal and vertical components of the elliptical path followed by the cilia are given in Eqs. 4.1 and 4.2.

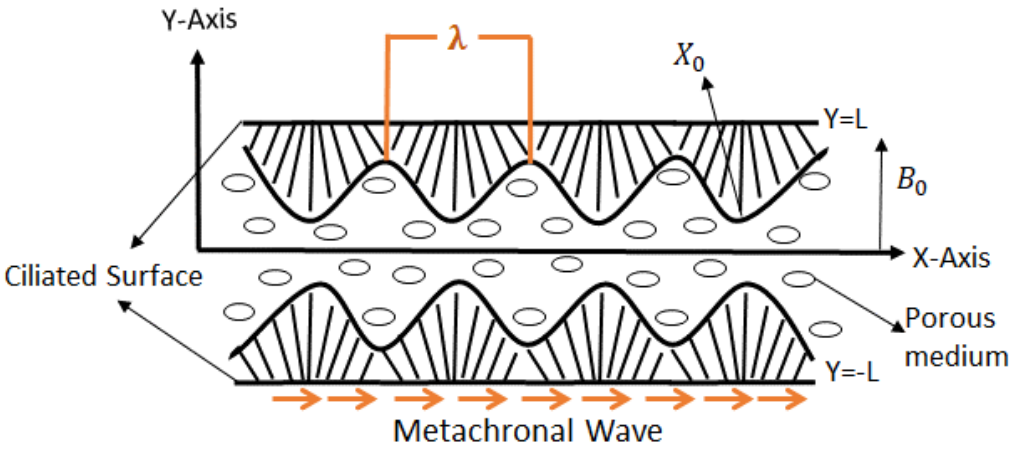

Figure 5.1: Geometry of Problem

The fixed and the wave frame are related as follow

$$\hat{x} = \hat{X} - c\hat{t}, \quad \hat{u} = \hat{U} - c, \quad \hat{y} = \hat{Y}, \quad \hat{v} = \hat{V}, \quad \hat{p}(\hat{x}, \hat{y}, \hat{t}) = \hat{P}(\hat{X}, \hat{Y}, \hat{t}), \tag{5.1}$$

where $(\hat{x}, \hat{y})$ and $(\hat{u}, \hat{v})$ are coordinates and velocity in wave frame and $(\hat{X}, \hat{Y})$ and $(\hat{U}, \hat{V})$ are coordinate and velocity in fixed frame. The non-dimensional variables are stated as

$$\begin{gathered} x = \frac{\hat{x}}{\lambda}, \quad u = \frac{\hat{u}}{c}, \quad y = \frac{\hat{y}}{l}, \quad v = \frac{\lambda \hat{v}}{lc}, \\ p = \frac{l^2 \hat{p}}{c\lambda\mu}, \quad t = \frac{c\,\hat{t}}{\lambda}, \quad h = \frac{L}{l}, \quad \beta = \frac{l}{\lambda}, \\ Re = \frac{\rho c l}{\mu}, \quad \frac{1}{\mathcal{K}} = \frac{\varphi \sigma^2}{k}, \quad \mathcal{M}^2 = \frac{\sigma {B_0}^2 l^2}{\mu}, \\ \lambda_1 = \frac{\alpha_1 c}{\mu l}, \quad \lambda_2 = \frac{\alpha_2 c}{\mu l}. \end{gathered} \tag{5.2}$$

Where p is pressure, h is mean width of channel, β is wave number, $\mathcal{M}$ is Hartmann number, $\mathcal{K}$ is porosity parameter, Re is Reynolds number, λ_1 and λ_2 are fluid parameters.

The non-dimensional equations of continuity and momentum for the second grade fluid model [84] in a moving system are as follows

$$\frac{\partial u}{\partial x} + \frac{\partial v}{\partial y} = 0, \tag{5.3}$$

$$Re\beta\left(u\frac{\partial u}{\partial x} + v\frac{\partial u}{\partial y}\right) = -\frac{\partial p}{\partial x} + \left(\beta^2\frac{\partial^2 u}{\partial x^2} + \frac{\partial^2 u}{\partial y^2}\right)$$

$$+\lambda_1\beta\left(\begin{array}{c}-v\left(\beta^2\frac{\partial^2}{\partial x^2}+\frac{\partial^2}{\partial y^2}\right)\left(\beta^2\frac{\partial v}{\partial x}-\frac{\partial u}{\partial y}\right)\\+\frac{\partial}{\partial x}\left(\begin{array}{c}u\left(\beta^2\frac{\partial^2 u}{\partial x^2}+\frac{\partial^2 u}{\partial y^2}\right)\\+\beta^2 v\left(\beta^2\frac{\partial^2 v}{\partial x^2}+\frac{\partial^2 v}{\partial y^2}\right)\end{array}\right)\end{array}\right)$$

$$+\frac{1}{4}(3\lambda_1+2\lambda_2)\frac{\partial}{\partial x}\left(\begin{array}{c}4\left(\beta\frac{\partial u}{\partial x}\right)^2+4\left(\beta\frac{\partial v}{\partial y}\right)^2\\+2\left(\beta^2\frac{\partial v}{\partial x}+\frac{\partial u}{\partial y}\right)^2\end{array}\right)$$

$$-\left(\mathcal{M}^2+\frac{1}{\mathcal{K}}\right)(u+1) \qquad (5.4)$$

$$Re\beta^3\left(u\frac{\partial v}{\partial x}+v\frac{\partial v}{\partial y}\right)=-\frac{\partial p}{\partial y}+\beta^2\left(\beta^2\frac{\partial^2 v}{\partial x^2}+\frac{\partial^2 v}{\partial y^2}\right)$$

$$+\lambda_1\beta\left(\begin{array}{c}u\left(\beta^2\frac{\partial^2}{\partial x^2}+\frac{\partial^2}{\partial y^2}\right)\left(\beta^2\frac{\partial v}{\partial x}-\frac{\partial u}{\partial y}\right)\\+\frac{\partial}{\partial y}\left(\begin{array}{c}u\left(\beta^2\frac{\partial^2 u}{\partial x^2}+\frac{\partial^2 u}{\partial y^2}\right)\\+\beta^2 v\left(\beta^2\frac{\partial^2 v}{\partial x^2}+\frac{\partial^2 v}{\partial y^2}\right)\end{array}\right)\end{array}\right)$$

$$+\frac{1}{4}(3\lambda_1+2\lambda_2)\frac{\partial}{\partial y}\left(\begin{array}{c}4\left(\beta\frac{\partial u}{\partial x}\right)^2+4\left(\beta\frac{\partial v}{\partial y}\right)^2\\+2\left(\beta^2\frac{\partial v}{\partial x}+\frac{\partial u}{\partial y}\right)^2\end{array}\right)$$

$$-\frac{1}{\mathcal{K}}\beta^2 v, \qquad (5.5)$$

The relevant boundary conditions are

$$u=\mathcal{u}_0=-1-2\pi\varepsilon\alpha\beta\cos(2\pi x),$$

$$v=2\pi\varepsilon\sin(2\pi x)+\beta(2\pi\varepsilon)^2\alpha sin(2\pi x)cos(2\pi x),$$

$$\text{at}\quad y=h=1+\varepsilon\sin(2\pi x). \qquad (5.6)$$

and the symmetry condition is

$$\frac{\partial u}{\partial y}=0,\quad \text{at}\ \ y=0, \qquad (5.7)$$

The stream function ψ is defined as

$$u=\frac{\partial\psi}{\partial y},\ \ v=-\frac{\partial\psi}{\partial x}. \qquad (5.8)$$

After eliminating the pressure gradient and ignoring β^2 and β^3 terms (long wavelength approximation), the governing equations in terms of ψ will take the following form

$$\frac{\partial^4\psi}{\partial y^4} - \left(\mathcal{M}^2 + \frac{1}{\mathcal{K}}\right)\frac{\partial^2\psi}{\partial y^2} = Re\beta\left(\frac{\partial\psi}{\partial y}\frac{\partial^3\psi}{\partial x\partial y^2} - \frac{\partial\psi}{\partial x}\frac{\partial^3\psi}{\partial y^3}\right) - \lambda_1\beta\left(\frac{\partial\psi}{\partial y}\frac{\partial^5\psi}{\partial x\partial y^4} - \frac{\partial\psi}{\partial x}\frac{\partial^5\psi}{\partial y^5}\right). \tag{5.9}$$

5.2 Volumetric Flow Rate and Boundary Conditions

The volumetric flow rate at a certain instant in a fixed frame is given by

$$\hat{F} = \int_0^H \hat{U}(\hat{X}, \hat{Y}, \hat{t})d\hat{Y}. \tag{5.10}$$

Using Eq. (5.1) in Eq. (5.10), we get

$$\hat{f} = \int_0^L \hat{u}(\hat{x}, \hat{y})d\hat{y}. \tag{5.11}$$

From Eqs. (5.10), (5.11) and (5.1), we get

$$\hat{F} = \hat{f} + \mathfrak{c}L. \tag{5.12}$$

The time mean flow, at a fixed position $\hat{X}$, over a period $\hat{\mathcal{T}}$ is defined as

$$Q = \frac{1}{\hat{\mathcal{T}}}\int_0^{\hat{\mathcal{T}}} \hat{F}d\hat{t}. \tag{5.13}$$

Using Eq. (5.12) into Eq. (5.13), and integrating, we get

$$Q = \int_0^1 (\hat{f} + \mathfrak{c}L)d\hat{x} = \hat{f} + \mathfrak{c}\int_0^1 Ld\hat{x}. \tag{5.14}$$

Now with the aid of Eq. (4.2), Eq. (5.1) and Eq. (5.14), we get

$$Q = \hat{f} + \mathfrak{c}l. \tag{5.15}$$

Define the dimensionless form of time mean flow $\hat{Q}$ and $\hat{F}$ respectively as

$$\hat{Q} = \frac{Q}{\mathfrak{c}l}, \quad F = \frac{\hat{f}}{\mathfrak{c}l}, \tag{5.16}$$

we get

$$\hat{Q} = F + 1, \tag{5.17}$$

7

where

$$F = \int_0^h \frac{\partial \psi}{\partial y} dy = \psi(h) - \psi(0). \tag{5.18}$$

If we choose $\psi = 0$ at $y = 0$ then $\psi = F$ at $y = h \; and$ other boundary conditions are

$$\begin{aligned} \psi = 0, \;\; \frac{\partial^2 \psi}{\partial y^2} = 0, \;\; at \;\; y = 0, \\ \psi = F, \;\; \frac{\partial \psi}{\partial y} = u_0, \;\; at \; y = h, \end{aligned} \tag{5.19}$$

where

$$F = \int_0^h \frac{\partial \psi}{\partial y} dy, \;\; u_0 = -1 - 2\pi\varepsilon\alpha\beta \cos(2\pi x), \;\; h = 1 + \varepsilon \cos(2\pi x). \tag{5.20}$$

5.3 Solution of Problem

To solve Eq. (5.9) along the boundary conditions (5.19), we use HPM.

Here we choose the linear operator L and the nonlinear operator N as

$$L = \frac{\partial^4 \psi}{\partial y^4} - \left(\mathcal{M}^2 + \frac{1}{\mathcal{K}}\right)\frac{\partial^2 \psi}{\partial y^2}, \tag{5.21}$$

$$\begin{aligned} N = Re\beta \left(\frac{\partial \psi}{\partial y}\frac{\partial^3 \psi}{\partial x \partial y^2} - \frac{\partial \psi}{\partial x}\frac{\partial^3 \psi}{\partial y^3}\right) \\ -\lambda_1 \beta \left(\frac{\partial \psi}{\partial y}\frac{\partial^5 \psi}{\partial x \partial y^4} - \frac{\partial \psi}{\partial x}\frac{\partial^5 \psi}{\partial y^5}\right). \end{aligned} \tag{5.22}$$

We established a homotopy $\psi[r, q]: \Omega \times [0,1] \to R$ which satisfy

$$\mathbb{H}(\psi, q) = (1 - q)[L(\psi) - L(w_0)] + q[L(\psi) + N(\psi) - g(r)] = 0, \tag{5.23}$$

Here w_0 is the initial guess and $q\epsilon[0,1]$ is the embedding parameter.

Also define the homotopy equation

$$\begin{aligned} (1 - q)\begin{bmatrix} \left(\frac{\partial^4 \psi}{\partial y^4} - \left(\mathcal{M}^2 + \frac{1}{\mathcal{K}}\right)\frac{\partial^2 \psi}{\partial y^2}\right) \\ -\left(\frac{\partial^4 w_0}{\partial y^4} - \left(\mathcal{M}^2 + \frac{1}{\mathcal{K}}\right)\frac{\partial^2 w_0}{\partial y^2}\right) \end{bmatrix} + q\begin{bmatrix} \frac{\partial^4 \psi}{\partial y^4} - \left(\mathcal{M}^2 + \frac{1}{\mathcal{K}}\right)\frac{\partial^2 \psi}{\partial y^2} \\ -Re\beta \left(\frac{\partial \psi}{\partial y}\frac{\partial^3 \psi}{\partial x \partial y^2} - \frac{\partial \psi}{\partial x}\frac{\partial^3 \psi}{\partial y^3}\right) \\ +\lambda_1 \beta \left(\frac{\partial \psi}{\partial y}\frac{\partial^5 \psi}{\partial x \partial y^4} - \frac{\partial \psi}{\partial x}\frac{\partial^5 \psi}{\partial y^5}\right) \end{bmatrix} \\ = 0, \end{aligned} \tag{5.24}$$

The associated boundary conditions are

$$\psi = 0, \quad \frac{\partial^2 \psi}{\partial y^2} = 0, \quad at \quad y = 0,$$
$$\psi = F, \quad \frac{\partial \psi}{\partial y} = \mathcal{u}_0, \quad at\ y = h \tag{5.25}$$

Decomposing stream function ψ and the flux F in following series

$$\psi = \psi_0 + q\psi_1 + \cdots, \tag{5.26}$$

$$F = F_0 + qF_1 + \cdots. \tag{5.27}$$

We choose initial guess

$$w_0 = \mathcal{u}_0 + \frac{(y^2 - h^2)}{2}\frac{dP_0}{dx}, \tag{5.28}$$

and making use of Eqs. (5.26)-(5.28) in Eqs. (5.24) and (5.25) and equating the same powers of q on both sides, we get the following equations

$$q^0 : \frac{\partial^4 \psi_0}{\partial y^4} - \left(\mathcal{M}^2 + \frac{1}{\mathcal{K}}\right)\frac{\partial^2 \psi_0}{\partial y^2} = \frac{\partial^4 w_0}{\partial y^4} - \left(\mathcal{M}^2 + \frac{1}{\mathcal{K}}\right)\frac{\partial^2 w_0}{\partial y^2}, \tag{5.29}$$

with the boundary conditions

$$\psi_0 = 0, \quad \frac{\partial^2 \psi_0}{\partial y^2} = 0, \quad \text{at} \quad y = 0,$$
$$\psi_0 = F_0, \quad \frac{\partial \psi_0}{\partial y} = \mathcal{u}_0, \quad \text{at}\ y = h, \tag{5.30}$$

$$q^1 : \frac{\partial^4 \psi_1}{\partial y^4} - \left(\mathcal{M}^2 + \frac{1}{\mathcal{K}}\right)\frac{\partial^2 \psi_1}{\partial y^2} = Re\beta\left(\frac{\partial \psi_0}{\partial y}\frac{\partial^3 \psi_0}{\partial x \partial y^2} - \frac{\partial \psi_0}{\partial x}\frac{\partial^3 \psi_0}{\partial y^3}\right)$$
$$-\lambda_1 \beta\left(\frac{\partial \psi_0}{\partial y}\frac{\partial^5 \psi_0}{\partial x \partial y^4} - \frac{\partial \psi_0}{\partial x}\frac{\partial^5 \psi_0}{\partial y^5}\right), \tag{5.31}$$

with boundary conditions

$$\psi_1 = 0, \quad \frac{\partial^2 \psi_1}{\partial y^2} = 0, \quad \text{at} \quad y = 0,$$
$$\psi_1 = F_1, \quad \frac{\partial \psi_1}{\partial y} = 0, \quad \text{at}\ y = h \tag{5.32}$$

Solving Eqs. (5.29)-(5.32), we get following expressions

$$\psi_0 = \frac{1}{2G^{\frac{3}{2}}cosh\left(\sqrt{G}h\right)h - 2Gsinh\left(\sqrt{G}h\right)}\Bigg[2\sqrt{G}\frac{dP_0}{dx}\Big(y - cosh\left[\sqrt{G}(y-h)\right]h\Big) + \sqrt{G}cosh\left[\sqrt{G}h\right]\left(\frac{dP_0}{dx}(y-h)(-2+Gyh) + 2GyF_0\right) + sinh\left[\sqrt{G}y\right]\left(2\frac{dP_0}{dx} - Gh^2\frac{dP_0}{dx} - 2GF_0 + 2G\mathcal{u}_0\right) - sinh\left[\sqrt{G}h\right]\left(\frac{dP_0}{dx}(2+Gy^2-2Gyh) + 2Gy\mathcal{u}_0\right) - 2\frac{dP_0}{dx}sinh\left[\sqrt{G}(y-h)\right]\Bigg], \tag{5.33}$$

$$\psi_1 = \frac{1}{8\left(-\sqrt{G}cosh\left[\sqrt{G}h\right]h + sinh\left[\sqrt{G}h\right]\right)^4}C_1(x,y)F_1 + \frac{\beta(Re - G\lambda)h'}{128G^{\frac{3}{2}}\begin{pmatrix}-\sqrt{G}cosh\left[\sqrt{G}h\right]h \\ +sinh\left[\sqrt{G}h\right]\end{pmatrix}^4}\left[C_2(x,y) + cosh\left[\sqrt{G}h\right]C_3(x,y)\right. + cosh\left[\sqrt{G}h\right]C_4(x,y) + cosh\left[\sqrt{G}h\right]C_5(x,y) + cosh\left[\sqrt{G}h\right]C_6(x,y) + cosh\left[\sqrt{G}h\right]C_7(x,y) + sinh\left[\sqrt{G}h\right]C_8(x,y) + sinh\left[\sqrt{G}h\right]C_9(x,y) + sinh\left[2\sqrt{G}h\right]A_{10}(x,y) + sinh\left[3\sqrt{G}h\right]C_{11}(x,y) + sinh\left[4\sqrt{G}h\right]C_{12}(x,y) + cosh\left[\sqrt{G}(y-h)\right]C_{13}(x,y) + cosh\left[\sqrt{G}(y+h)\right]C_{14}(x,y) + cosh\left[\sqrt{G}(y-2h)\right]C_{15}(x,y) + cosh\left[\sqrt{G}(y+2h)\right]C_{16}(x,y) + cosh\left[\sqrt{G}(y-3h)\right]C_{17}(x,y) + cosh\left[\sqrt{G}(y+3h)\right]C_{18}(x,y) + cosh\left[\sqrt{G}(y-4h)\right]C_{19}(x,y) + sinh\left[\sqrt{G}(y-h)\right]C_{20}(x,y) + sinh\left[\sqrt{G}(y+h)\right]C_{21}(x,y) + sinh\left[\sqrt{G}(y-2h)\right]C_{22}(x,y) + sinh\left[\sqrt{G}(y+2h)\right]C_{23}(x,y) + sinh\left[\sqrt{G}(y-3h)\right]C_{24}(x,y) + sinh\left[\sqrt{G}(y+3h)\right]C_{25}(x,y) + sinh\left[\sqrt{G}(y - 4h)\right]C_{26}(x,y)\Big], \tag{5.34}$$

where

$$G = \mathcal{M}^2 + \frac{1}{\mathcal{K}}, \tag{5.35}$$

where $C_1(x,y), C_2(x,y), C_3(x,y), \dots, C_{26}(x,y)$ are given in appendix.

Using Eqs. (5.33) and (5.34) into (5.26), we get the solution in the following form

$$\psi = \psi_0 + q\psi_1 + \cdots, \tag{5.36}$$

We introduce $F = F_0 + qF_1$ in stream function ψ given in Eq. (5.36). Now pressure gradient can be found in the following equations

$$\frac{\partial p}{\partial x} = Re\beta\left(\frac{\partial\psi}{\partial x}\frac{\partial^2\psi}{\partial y^2} - \frac{\partial\psi}{\partial y}\frac{\partial^2\psi}{\partial x\partial y}\right) + \frac{\partial^3\psi}{\partial y^3} + \lambda_1\beta\left(\frac{\partial\psi}{\partial y}\frac{\partial^4\psi}{\partial x\partial y^3} - \frac{\partial\psi}{\partial x}\frac{\partial^4\psi}{\partial y^4} + \frac{\partial^2\psi}{\partial x\partial y}\frac{\partial^3\psi}{\partial y^3} + \frac{\partial^3\psi}{\partial x\partial y^2}\frac{\partial^2\psi}{\partial y^2}\right) - \left(\mathcal{M}^2 + \frac{1}{\mathcal{K}}\right)\left(\frac{\partial\psi}{\partial y} + 1\right), \tag{5.37}$$

$$\frac{\partial p}{\partial y} = 2\lambda_1\beta\frac{\partial^2\psi}{\partial y^2}\frac{\partial^3\psi}{\partial y^3}. \tag{5.38}$$

Here one more interested physical quantity is the non-dimensional skin friction coefficient c_f which is defined at the height $y = h$ of the channel as

$$c_f = \frac{\tau_w}{\rho c^2}, \tag{5.39}$$

The dimensionless form of Eq. (5.39) is

$$\sqrt{Re}c_f = \tau_w, \tag{5.40}$$

where

$$\tau_w = \left[\frac{\partial^2\psi}{\partial y^2} + \lambda_1\beta\left(\frac{\partial\psi}{\partial y}\frac{\partial^3\psi}{\partial x\partial y^2} - \frac{\partial\psi}{\partial x}\frac{\partial^3\psi}{\partial y^3} + 2\frac{\partial^2\psi}{\partial x\partial y}\frac{\partial^2\psi}{\partial y^2}\right)\right]_{y=h}. \tag{5.41}$$

The above expression can be obtained by driving Eq. (5.36) into Eq. (5.39) and the numerical result which is found by using software MTHEMATICA, has been discussed in the next section.

5.4 Numerical Solution and Discussion

In this section effect of Hartmann number $\mathcal{M}$, fluid parameter λ_1, porosity parameter $\mathcal{K}$ and Reynolds number Re on pressure gradient, velocity field and trapping bolus are investigated. Figs. 5.2a-d reveal the impacts of interested parameters on horizontal velocity which show that influences of emerging parameters on ciliated flow are strong at the center region of the channel and decay near the channel's wall due to cilia anchored in the inner wall surface. The parabolic behavior of flow is caused by pressure gradient which is close to the core region of the channel due to the moving force caused by tip of cilia bed. Fig. 5.2a reveals the outcome of Hartmann number/magnetic parameter $\mathcal{M}$ on the horizontal velocity. The magnetic parameter is the ratio of electromagnetic forces to the viscous forces. Here we have considered the ratio 1, 2 and 3 that means electromagnetic forces are equal, double and triple to the viscous forces and help to retard the horizontal velocity as electromagnetic forces are applied transverse to the direction of flow. The viscoelastic fluid flow due to ciliary movement in the existence of viscous and inertial effects can be visualized due to the

magnetic field that is dominant over the viscous effect therefore impact of magnetic field in the normal direction is more powerful than the viscous effect which helps to retard the motion to observe the frequency of cilia beat. Fig. 5.2b depicts the impact of porosity parameter $\mathcal{K}$ on the horizontal component of the velocity. Porosity parameter is the ratio of pore volume to the bulk volume which is mostly less than one. It shows that if bulk volume decreases or pore volume increases then horizontal velocity increases close to core region of the channel, because increase in pore volume permit the fluid to flow through the porous space that results to enhance the velocity profile in the horizontal direction (x direction). Fig. 5.2c shows that velocity profile in longitudinal direction rises with the increasing value of viscoelastic parameter λ_1, because the fluid become thin and resistivity due to viscosity become weak. Fig. 5.2d shows that the Reynolds number Re is considered to be 1, 5 and 10. Since in this study we have considered the inertial effects due to Reynolds number, which causes to accelerate the fluid flow because inertial forces have large impact due to high speed as compared to the viscous forces.

The behavior of the vertical component of the velocity field is indicated in Figs. 5.3a-d. These figures show that velocity vanishes at the center of the channel and behave like a sinusoidal wave. These figures indicate the effect of Hartmann number $\mathcal{M}$, fluid parameter λ_1, porosity parameter $\mathcal{K}$ and Reynolds number Re. Figs. 5.3a-d show that vertical velocity enhances with the rising value of $\mathcal{M}$ (Hartmann number), λ_1 (fluid parameter), $\mathcal{K}$ (Porosity parameter) Re (Reynolds number) in upper half of the channel and same behavior is observed in the lower half of the channel in opposite direction due to symmetry of ciliated channel with effective and recovery stroke (to and fro motion). Figs. 5.4a-d illustrate that horizontal pressure gradient $\frac{\partial p}{\partial x}$ has a periodic nature. Figs. 5.4a-b show that favorable pressure gradient occurs with the rising value of Hartmann number $\mathcal{M}$ and with the rising value of porosity parameter $\mathcal{K}$, because Lorentz force due to magnetic field require more pressure to flow and porous medium requires less pressure for the fluid flow in the porous regime. However Figs. 5.4c-d show the dual behavior of pressure gradient with the growing value of fluid parameter λ_1 and Reynolds number Re. It can be depicted from Figs. 5.4c-d that pressure gradient show decline in the region $-1 < x < -0.5$ and $0 < x < 0.5$ while rises in the region $-0.5 < x < 0$ and $0.5 < x < 1$ with the growing value of λ_1 and Re due to the metachoronal wave motion in the horizontal direction.

The behavior of vertical pressure gradient is seen in Figs. 5.5a-d which is symmetric about the center line and behave like a sinusoidal wave. These figures show that vertical pressure gradient is favorable in the region $-0.5 < x < 0$ and adverse in the region $0 < x < 0.5$ with the growing value of λ_1 , $\mathcal{M}$ and $\mathcal{K}$ near the upper wall, and static pressure increases in the direction of flow due to forward and backward stroke.

The stream line plots can be seen for Hartmann number $\mathcal{M}$, fluid parameter λ_1, porosity parameter $\mathcal{K}$ and Reynolds number Re in Figs. 5.6a-5.9c by taking all other parameters $\alpha = 0.4,\ \beta = 0.4,\ \varepsilon = 0.1,\ Q = 0.9$. The impact of Hartmann number on stream lines is shown in Figs. 5.6a-c which illustrate that increasing value of Hartmann number $\mathcal{M}$ resist the flow, therefore bolus size reduces. It can be observed from Figs. 5.7a-c that bolus size increases with the rising value of porosity parameter $\mathcal{K}$ as it allows the fluid to flow through the medium. Figs. 5.8a-c indicate that increasing value of fluid parameter λ_1 help to increase the size of trapped bolus. Figs. 5.9a-c indicate that bolus size and the number of stream lines become larger due to the increasing amount of inertial forces compared to the viscous forces. Fig. 5.10a-b have been plotted for the comparison of velocity for both symplectic and antiplectic metachronal waves. It is noted that both velocities have same effect for symplectic and antiplectic waves by growing cilia length ε, but the magnitude of velocity for antiplectic metachronal wave is greater than the magnitude of velocity due to symplectic metachronal wave. Therefore for the high speed, researchers used the antiplectic patterns of the wave whereas for the low speed of ciliary flow they used the symplectic patterns. At the end, the impact of viscoelastic second grade fluid on the skin friction has been plotted in Fig. 5.11 for the growing length of cilia ε. This figure reveals the linear relation between the τ_w and λ_1, It is also noted that this linear relation become nonlinear as cilia length ε increases.

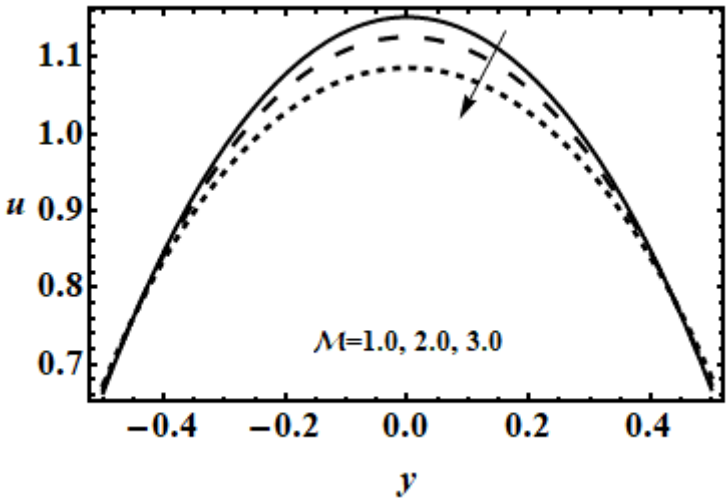

Fig. 5.2a: The effect of Hartmann number $\mathcal{M}$ on longitudinal velocity.

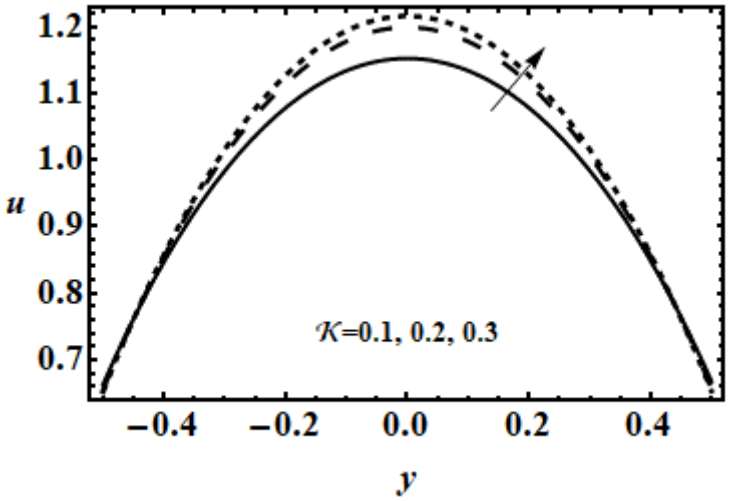

Fig. 5.2b: The effect of porosity parameter $\mathcal{K}$ on longitudinal velocity.

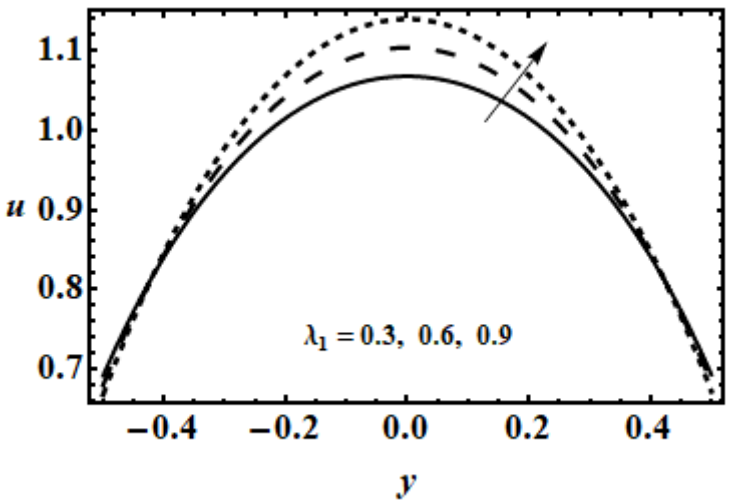

Fig. 5.2c: The effect of fluid parameter λ_1 on transverse velocity.

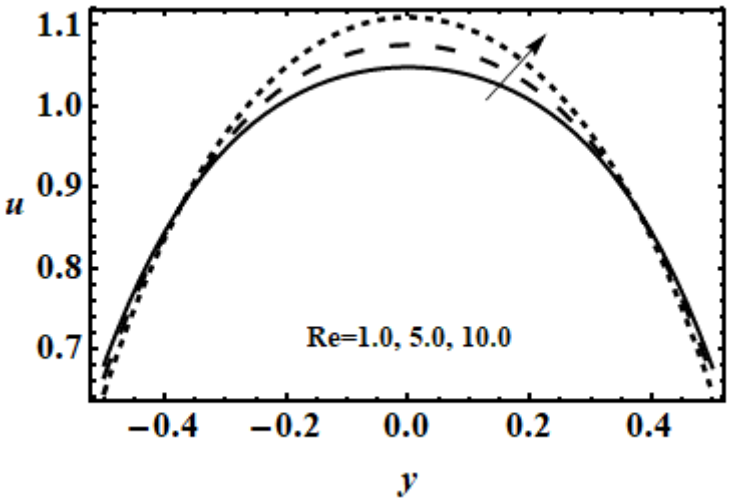

Fig. 5.2d: The effect of Reynolds number Re on transverse velocity.

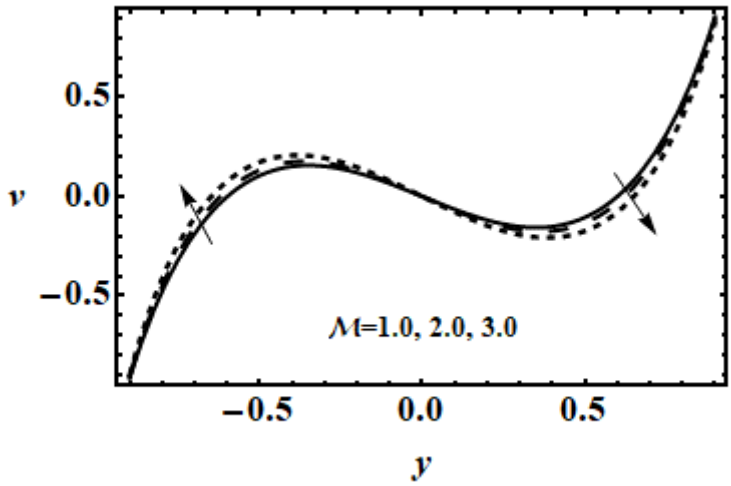

Fig. 5.3a: The effect of Hartmann number $\mathcal{M}$ on transverse velocity.

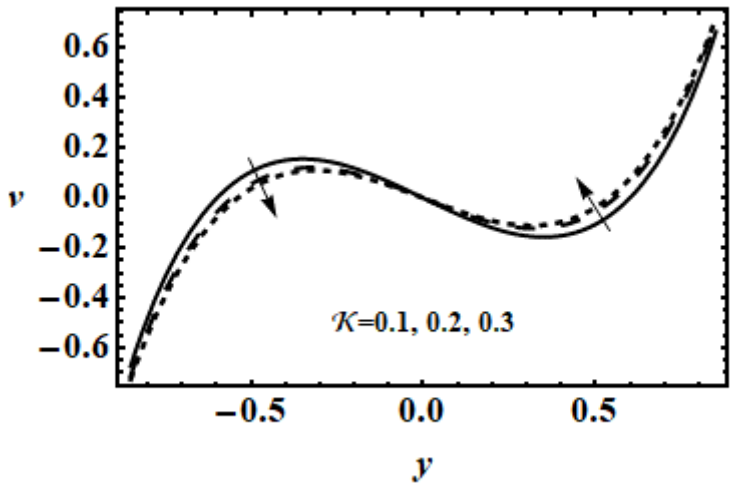

Fig. 5.3b: The effect of porosity parameter $\mathcal{K}$ on transverse velocity.

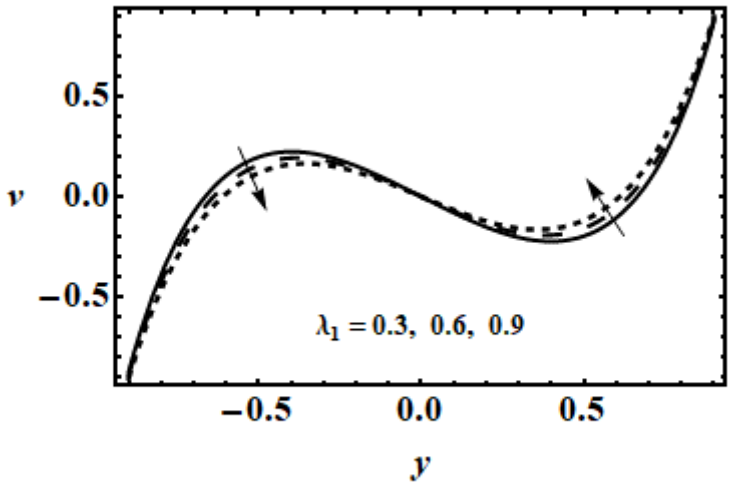

Fig. 5.3c: The effect of fluid parameter λ_1 on transverse velocity.

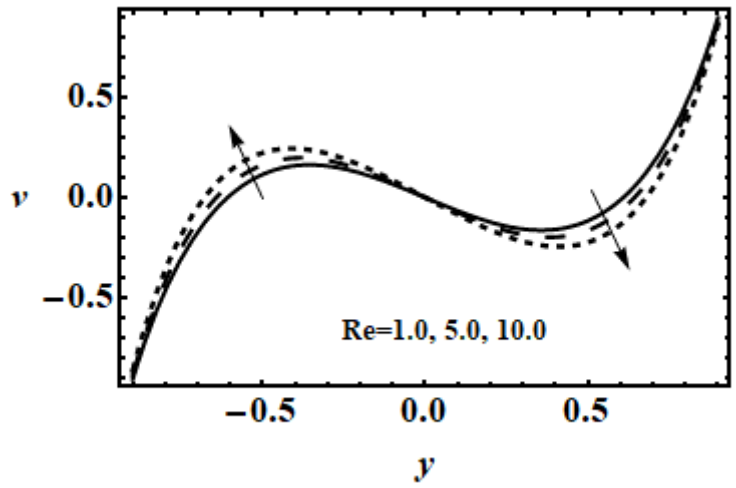

Fig. 5.3d: The effect of Reynolds number Re on transverse velocity.

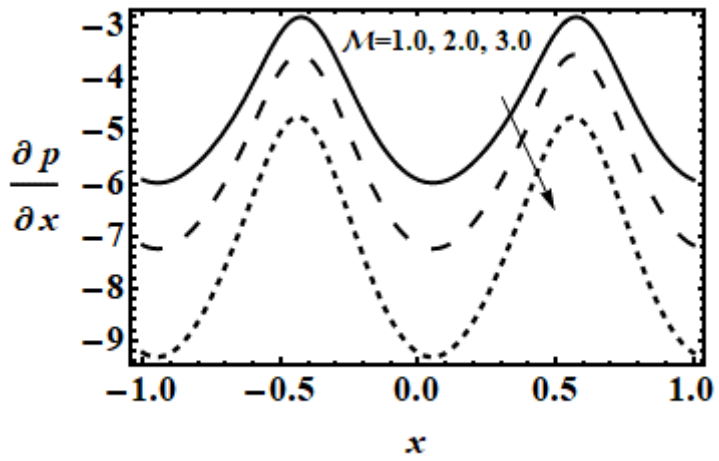

Fig. 5.4a: The effect of Hartmann number $\mathcal{M}$ on longitudinal pressure gradient.

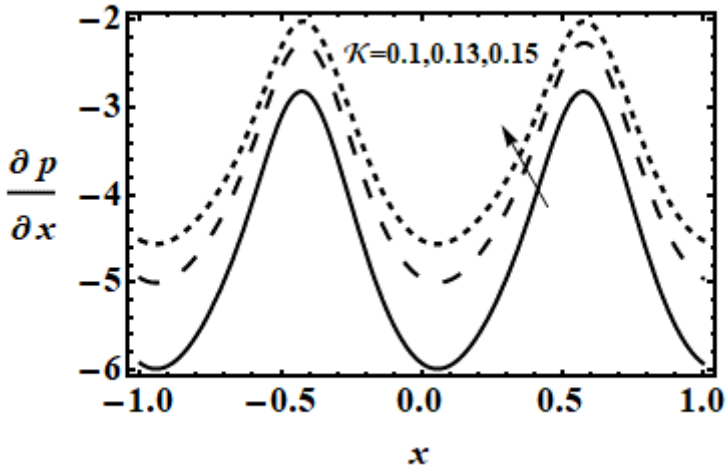

Fig. 5.4b: The effect of porosity parameter $\mathcal{K}$ on longitudinal pressure gradient.

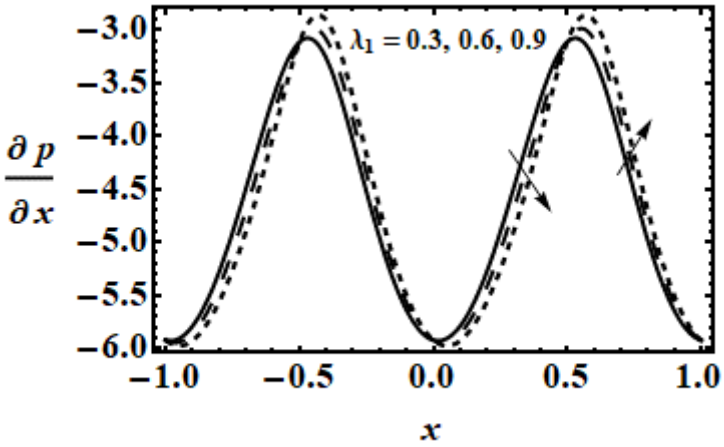

Fig. 5.4c: The effect of fluid parameter λ_1 on longitudinal pressure gradient.

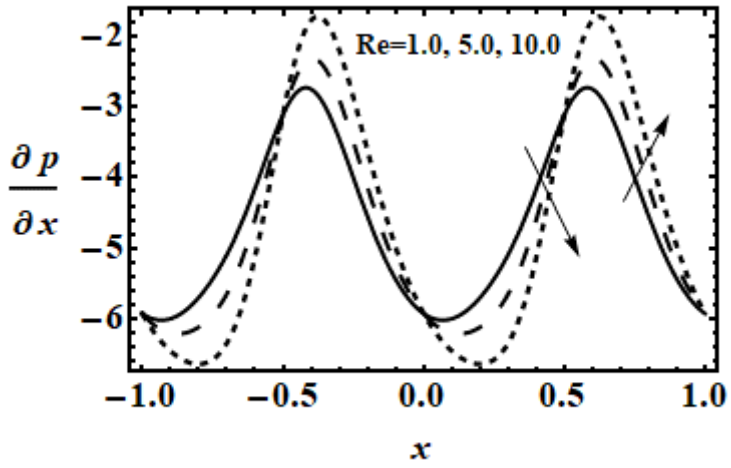

Fig. 5.4d: The effect of Reynolds number Re on longitudinal pressure gradient.

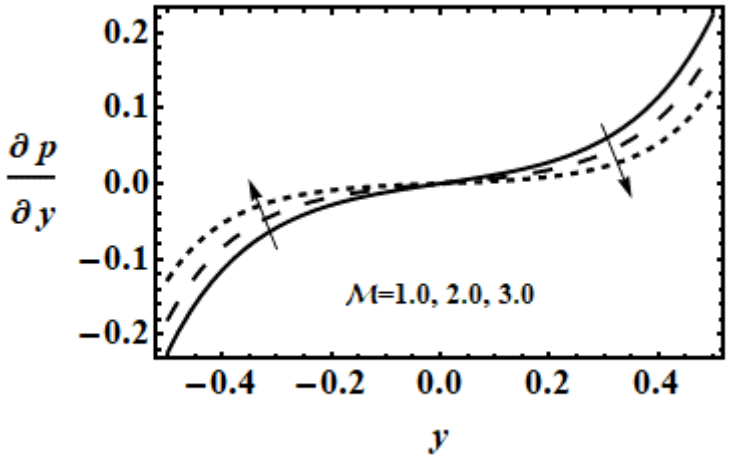

Fig. 5.5a: The effect of Hartmann number $\mathcal{M}$ on transverse pressure gradient.

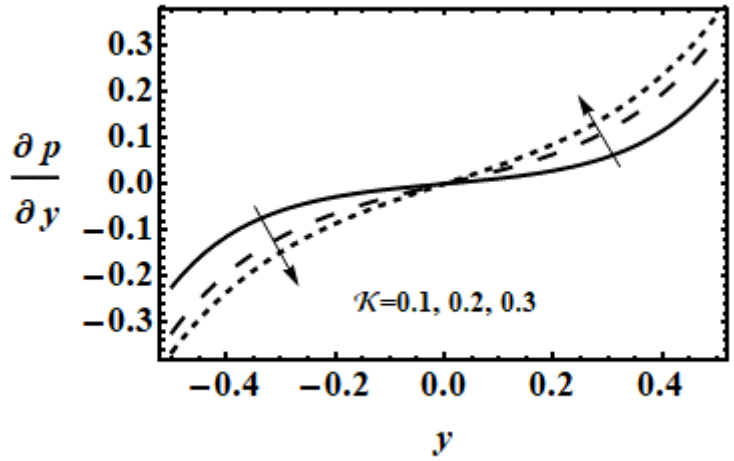

Fig. 5.5b: The effect of porosity parameter $\mathcal{K}$ on transverse pressure gradient.

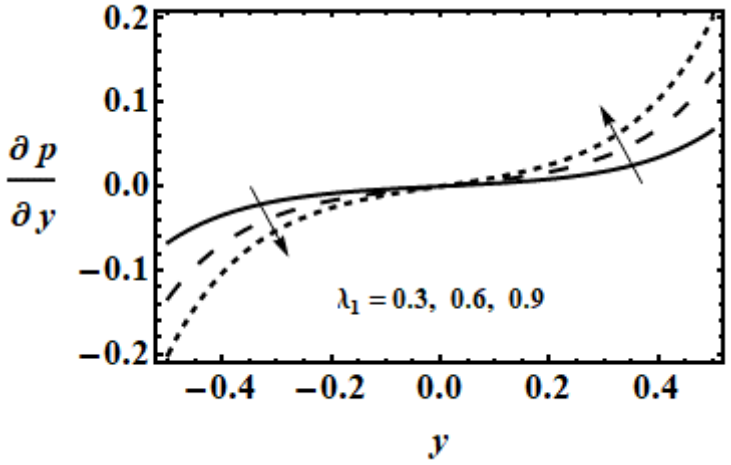

Fig. 5.5c: The effect of fluid parameter λ_1 on transverse pressure gradient.

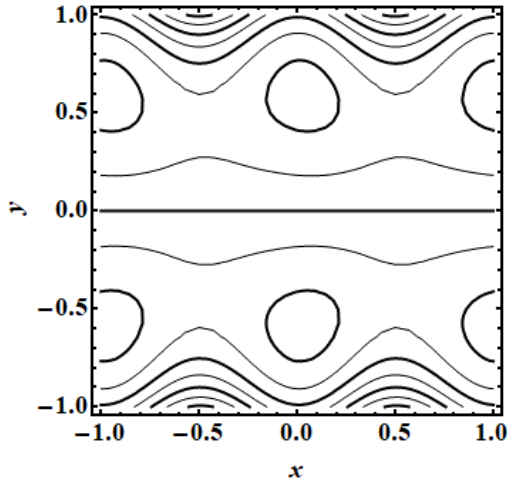

(a) $\mathcal{M} = 1.0$

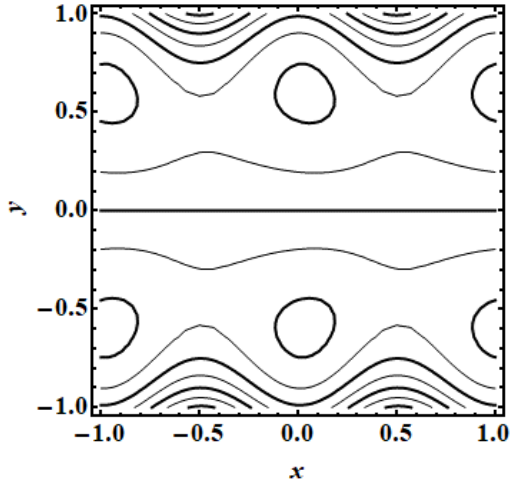

(b) $\mathcal{M} = 1.5$

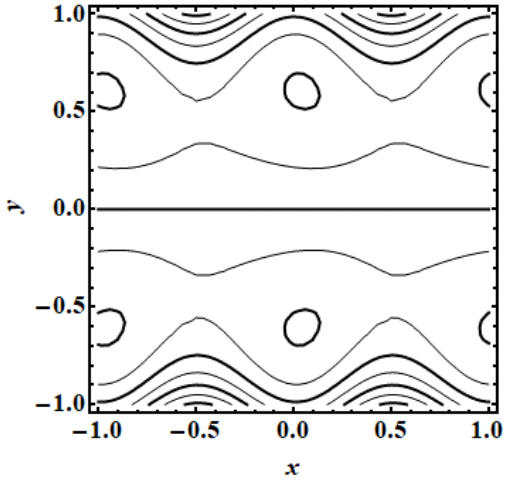

(c) $\mathcal{M} = 2.0$

Fig. 5.6: Influence of Hartmann number $\mathcal{M}$ on stream function

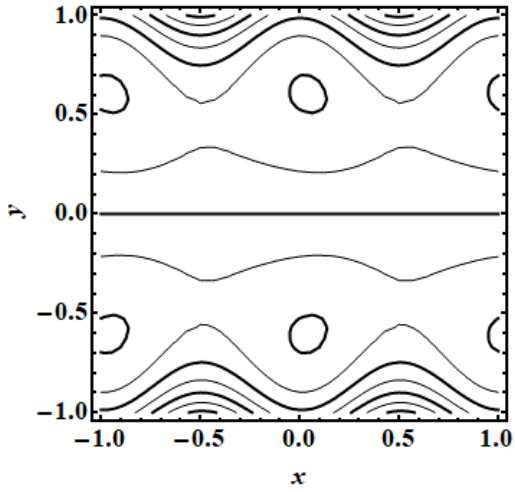

(a) $\mathcal{K} = 0.15$

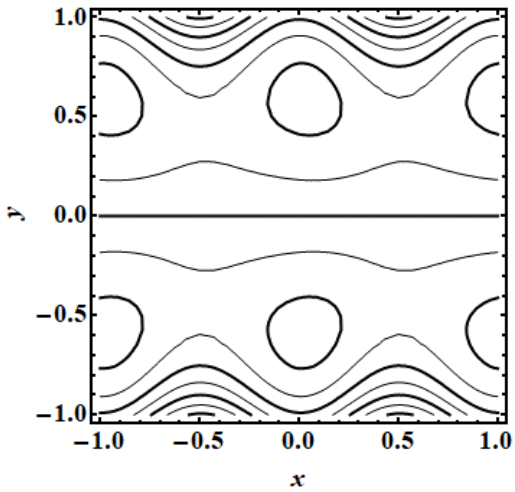

(b) $\mathcal{K} = 0.2$

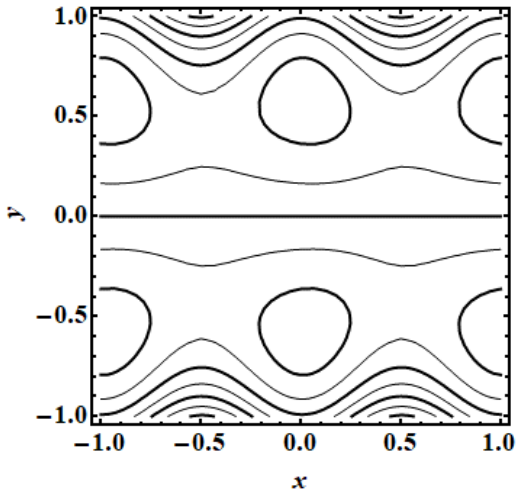

(c) $\mathcal{K} = 0.3$

Fig. 5.7: Influence of porosity parameter $\mathcal{K}$ on stream function

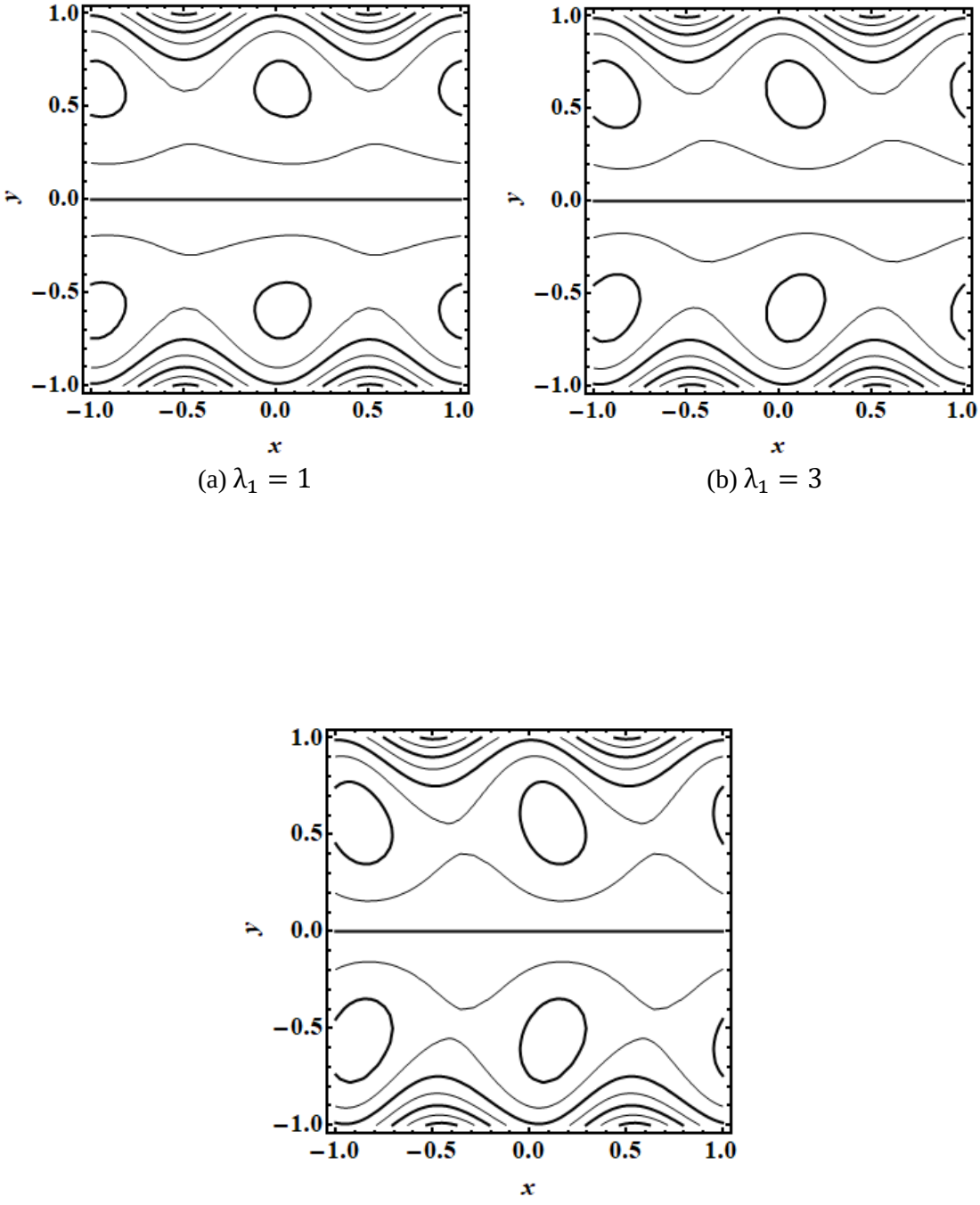

(a) $\lambda_1 = 1$ (b) $\lambda_1 = 3$

(c) $\lambda_1 = 5$

Fig. 5.8: Influence of fluid parameter λ_1 on stream function.

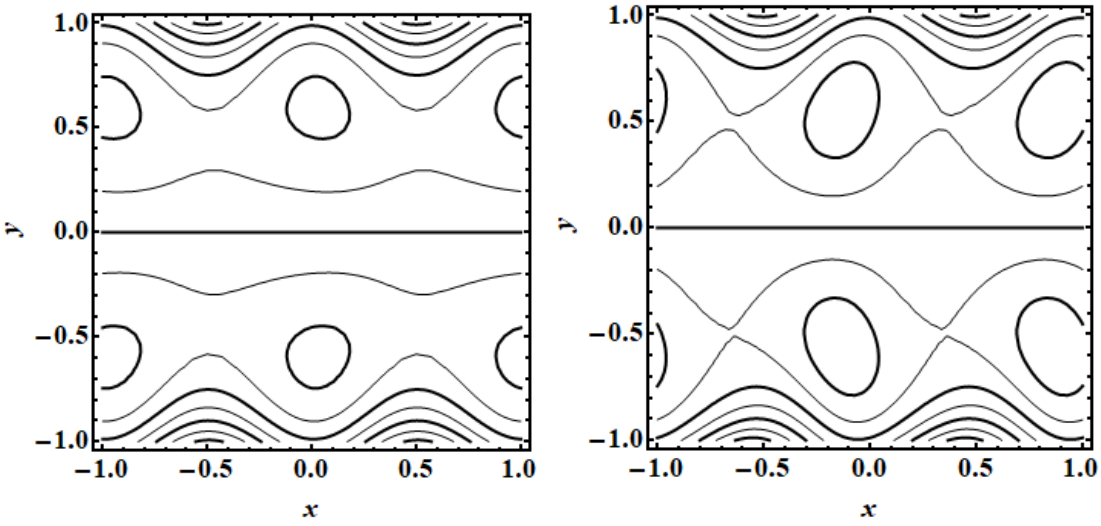

(a) $Re = 1$ (b) $Re = 50$

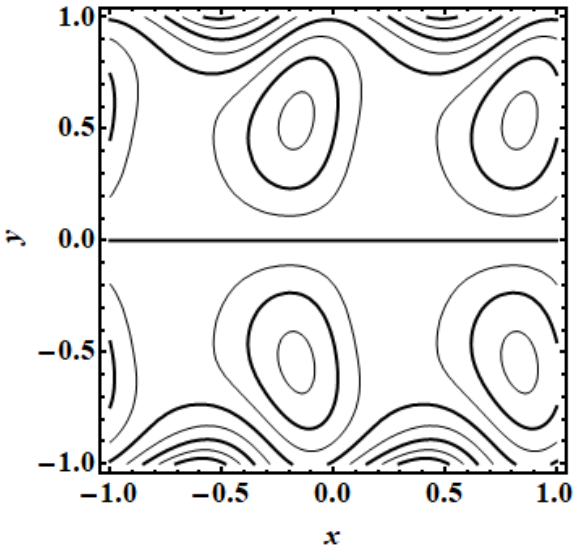

(c) $Re = 100$

Fig. 5.9: Influence of Reynolds number Re on stream function.

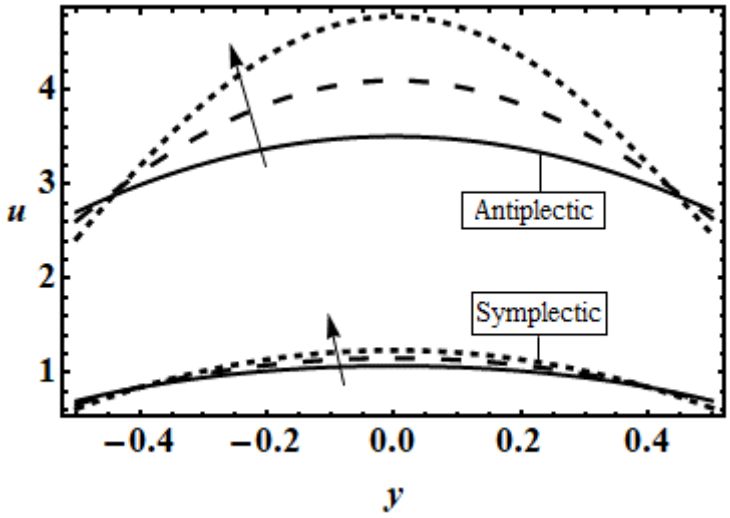

(a) u(x,y)

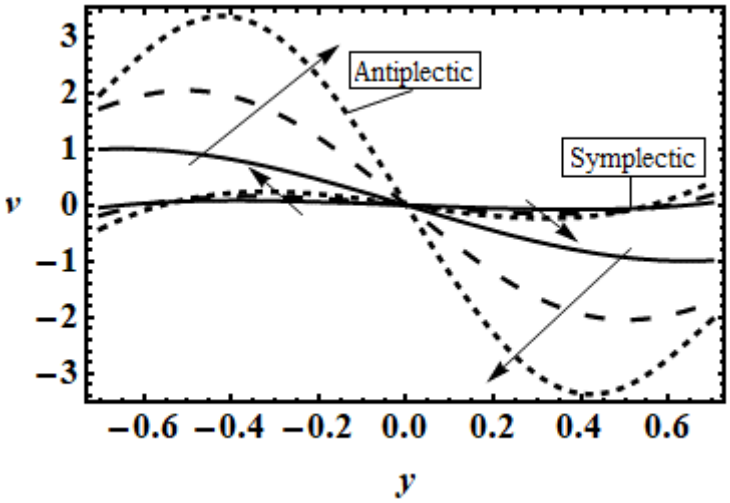

(b) v(x,y)

Fig. 5.10: Comparison of velocities for the effect of cilia length ε for both symplectic and antiplectic metachronal wave.

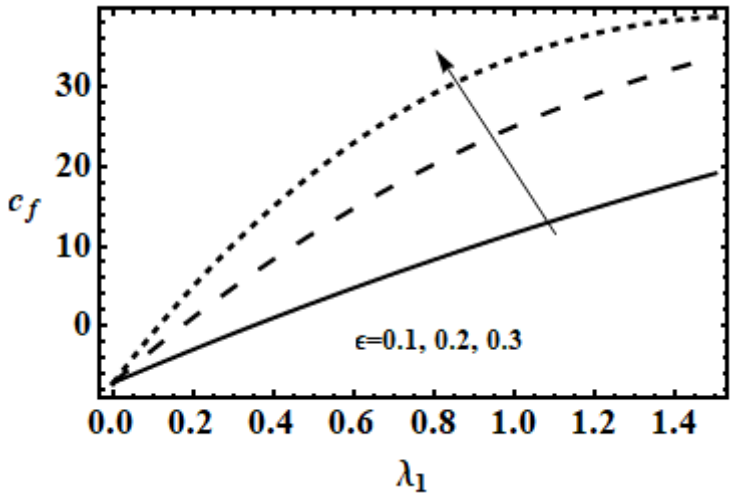

Fig. 5.11: Influence of cilia length ε on the skin friction.

5.5 Conclusion

In this study we have assumed the inertial flow of MHD 2nd grade fluid in a ciliated channel implanted in a porous medium. This study is presented first time with the effect of inertial forces $Re \neq 0$ in the existence of magnetic field and porous medium. The highly nonlinear equation is solved by the HPM and Software "Mathematica". From the Figs. 5.2-5.9 it is clear that code is validated for the emerging parameters Re, Hartmann number $\mathcal{M}$, fluid parameter λ_1 and porosity parameter $\mathcal{K}$ for the velocity, pressure gradient and stream function as showing the symmetric behaviour about y=0. From the graphs of stream functions it is cleared that path of ciliary movement is elliptic which is shown in graphs plotted by the code that is generated in software "Mathematica". The two dimensional and two directional flow is represented by non-linear PDEs which are solved by HPM. The study of second grade fluid with small Reynolds number approximation is recently presented by S. Hina [84] but not a single study is available in literature for inertial flow of 2nd grade fluid in a ciliated channel. If $\lambda_1, \rightarrow 0, Re \rightarrow 0$ and $\beta \rightarrow 0$ then present study can be validated with the study of A. M. Siddiqui [43] that is hydro magnetic ciliated flow of Newtonian fluid in a porous medium.

This study can be very useful for those researchers who are interested to observe the pressure and flow pattern of mucus in trachea and blood flow in fallopian tube during motion with the inertial effect. When the body is performing a job (exercise) then shear forces and inertial forces are very effective for the biological flows e.g. mucus in

trachea, blood in fallopian tube and cerebrospinal fluid due to ciliary movement.

The MHD flow of the 2nd grade fluid in a ciliated channel have shown following observations on velocity, pressure gradient and stream function.

- The horizontal velocity decreases with Hartmann number $\mathcal{M}$ and increases with Reynolds number Re, porosity parameter$\mathcal{K}$, and fluid parameter λ_1 at the centre of the channel. But velocity is small at the exit and entrance region and attain its maximum value at the center of the channel. Whereas, the vertical component of the velocity vanishes at the center of channel and move like a sinusoidal wave.
- Favorable pressure gradient in x direction uniformly increases for Hartmann number $\mathcal{M}$ and uniformly decreases with the porosity parameter $\mathcal{K}$ and it shows a dual behaviour for the fluid parameter λ_1 and the Reynolds numberRe, whereas, the vertical favorable pressure gradient is symmetric about the center of channel. It decreases for large value of Hartmann number $\mathcal{M}$ while increases for larger values of fluid parameter λ_1 and Reynolds number Re.
- Size of trapped bolus reduces with increasing value of Hartmann number $\mathcal{M}$ and expanded with increasing value of porosity parameter $\mathcal{K}$ and fluid parameter λ_1. However both the size and number of trapped bolus increases in a specific direction by increasing the value of Reynolds number Re due to high speed.

Chapter 6

Forced Convective Flow of MHD Jeffrey Bio Fluid in a Ciliated Channel

Physiological transportation often occur due to ciliated surfaces. In human body, the physiological fluids e.g. blood which contain hemoglobin consists of ionic constituents that make reaction with the magnetic forces when undergo to external (extra-corporeal) magnetic fields. Motivated by these applications, here, we have assumed the forced convective magnetohydrodynamic viscoelastic physiological fluid flow through a ciliated channel. Darcy porous medium drag force model has been used for the existence of deposits e.g. cholesterol, fats etc. Viscous dissipation is fitted in energy conversation equation to reveals the heat loss effects. The infinite series of pressure distribution, velocity and temperature have been constructed via ADM. The impact of interested physical parameters such as Brinkman number, Jeffrey first and second viscoelastic parameters, Hartmann number and permeability parameter on temperature, pressure gradient, velocity and stream function are visualized graphically.

6.1 Mathematical Formulation

The regime under investigation, as visualized in Fig. 6.1, examines the forced convective magnetohydrodynamic (MHD) flow of an incompressible physiological liquid through a ciliated channel of finite length L. The channel is ciliated internally, and contains a high-permeability porous medium (representative of deposits, debris etc. in biomedical vessels). A constant strength of magnetic field, B_0, is applied normal to the longitudinal axis of the channel.

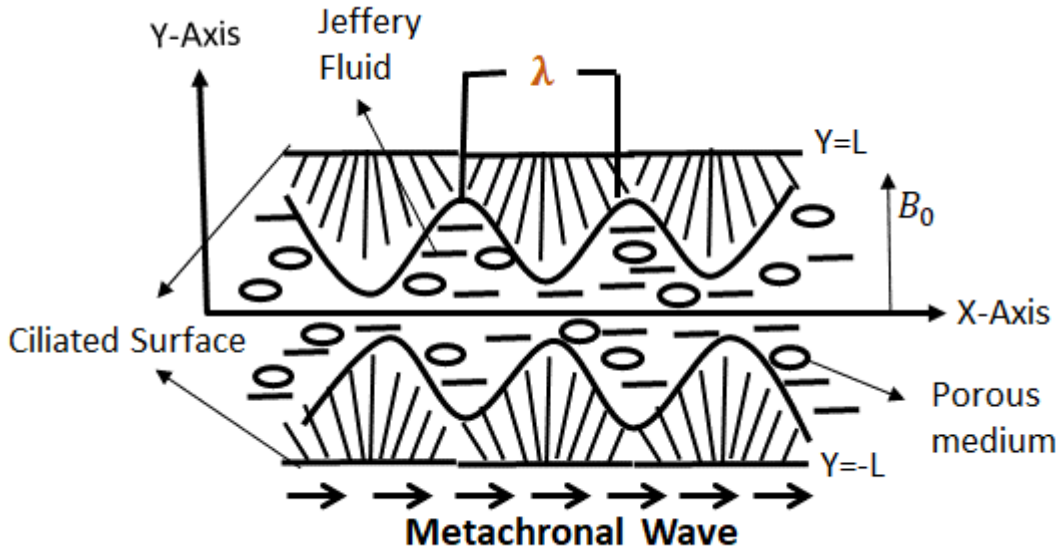

Fig. 6.1: Geometry of Problem

The collective motion of cilia generates a metachronal wave in the axial direction of channel having wave speed ɕ, and wavelength λ. The biofluid rheology is simulated with the robust Jeffrey elastic-viscous model [34] for which the constitutive equation is

$$\boldsymbol{\tau} = -p\boldsymbol{I} + \boldsymbol{S}, \tag{6.1}$$

where

$$\boldsymbol{S} = \frac{\mu}{1+\lambda_1}(\dot{\boldsymbol{\gamma}} + \lambda_2 \ddot{\boldsymbol{\gamma}}). \tag{6.2}$$

The momentum and energy equations in the fixed frame are given by

$$\frac{\partial \hat{U}}{\partial \hat{X}} + \frac{\partial \hat{V}}{\partial \hat{Y}} = 0, \tag{6.3}$$

$$\rho\left(\hat{U}\frac{\partial \hat{U}}{\partial \hat{X}} + \hat{V}\frac{\partial \hat{U}}{\partial \hat{Y}}\right) = -\frac{\partial \hat{P}}{\partial \hat{X}} + \frac{\partial S_{\hat{X}\hat{X}}}{\partial \hat{X}} + \frac{\partial S_{\hat{X}\hat{Y}}}{\partial \hat{Y}} + (J \times B)_{\hat{X}} + R_{\hat{X}}, \tag{6.4}$$

$$\rho\left(\hat{U}\frac{\partial \hat{V}}{\partial \hat{X}} + \hat{V}\frac{\partial \hat{V}}{\partial \hat{Y}}\right) = -\frac{\partial \hat{P}}{\partial \hat{Y}} + \frac{\partial S_{\hat{X}\hat{Y}}}{\partial \hat{X}} + \frac{\partial S_{\hat{Y}\hat{Y}}}{\partial \hat{Y}} + (J \times B)_{\hat{Y}} + R_{\hat{Y}}, \tag{6.5}$$

$$\rho c_p\left(\hat{U}\frac{\partial \hat{T}}{\partial \hat{X}} + \hat{V}\frac{\partial \hat{T}}{\partial \hat{Y}}\right) = S_{\hat{X}\hat{X}}\frac{\partial \hat{U}}{\partial \hat{X}} + S_{\hat{X}\hat{Y}}\left(\frac{\partial \hat{U}}{\partial \hat{Y}} + \frac{\partial \hat{V}}{\partial \hat{X}}\right) + S_{\hat{Y}\hat{Y}}\frac{\partial \hat{V}}{\partial \hat{Y}} + k_1\left(\frac{\partial^2 \hat{T}}{\partial \hat{X}^2} + \frac{\partial^2 \hat{T}}{\partial \hat{Y}^2}\right). \tag{6.6}$$

Where

$$S_{\hat{X}\hat{X}} = \frac{2\mu}{1+\lambda_1}\left[1+\lambda_2\left(\hat{U}\frac{\partial}{\partial\hat{X}}+\hat{V}\frac{\partial}{\partial\hat{Y}}\right)\right]\frac{\partial\hat{U}}{\partial\hat{X}}, \tag{6.7}$$

$$S_{\hat{X}\hat{Y}} = \frac{\mu}{1+\lambda_1}\left[1+\lambda_2\left(\hat{U}\frac{\partial}{\partial\hat{X}}+\hat{V}\frac{\partial}{\partial\hat{Y}}\right)\right]\left(\frac{\partial\hat{U}}{\partial\hat{Y}}+\frac{\partial\hat{V}}{\partial\hat{X}}\right), \tag{6.8}$$

$$S_{\hat{Y}\hat{Y}} = \frac{2\mu}{1+\lambda_1}\left[1+\lambda_2\left(\hat{U}\frac{\partial}{\partial\hat{X}}+\hat{V}\frac{\partial}{\partial\hat{Y}}\right)\right]\frac{\partial\hat{V}}{\partial\hat{Y}}, \tag{6.9}$$

$$(J\times B)_{\hat{X}} = -\sigma {B_0}^2,\ \ (J\times B)_{\hat{Y}} = 0, \tag{6.10}$$

$$R_{\hat{X}} = \frac{\mu\varphi}{k}\hat{U},\ \ R_{\hat{Y}} = \frac{\mu\varphi}{k}\hat{V}. \tag{6.11}$$

The envelope of the tips are as follow

$$\hat{X} = F(\hat{X},\hat{t}) = X_0 + \varepsilon l\alpha sin\left(\frac{2\pi}{\lambda}\right)(\hat{X}-\mathfrak{c}\hat{t}), \tag{6.12}$$

$$\hat{Y} = H(\hat{X},\hat{t}) = l + \varepsilon l cos\left(\frac{2\pi}{\lambda}\right)(\hat{X}-\mathfrak{c}\hat{t}) = \pm L. \tag{6.13}$$

The fixed and the wave frame are related as follow

$$\hat{x} = \hat{X}-\mathfrak{c}\hat{t},\ \ \hat{u} = \hat{U}-\mathfrak{c},\ \ \hat{y} = \hat{Y},\ \ \hat{v} = \hat{V},\ \ \hat{p}(\hat{x},\hat{y},\hat{t}) = \hat{P}(\hat{X},\hat{Y},\hat{t}). \tag{6.14}$$

The following non-dimensional variables are implemented

$$\begin{gathered} x = \frac{\hat{x}}{\lambda},\ \ u = \frac{\hat{u}}{\mathfrak{c}},\ \ y = \frac{\hat{y}}{l},\ \ v = \frac{\lambda\,\hat{v}}{l\mathfrak{c}}, \\ p = \frac{l^2\,\hat{p}}{\mathfrak{c}\lambda\mu},\ \ t = \frac{\mathfrak{c}\,\hat{t}}{\lambda},\ \ h = \frac{L}{l},\ \ \beta = \frac{l}{\lambda}, \\ Re = \frac{\rho c l}{\mu},\ \ \frac{1}{\mathcal{K}} = \frac{\varphi l^2}{k},\ \ \mathcal{M}^2 = \frac{\sigma {B_0}^2 l^2}{\mu}, \\ Pr = \frac{\mu c_p}{k_1},\ \ E_c = \frac{\mathfrak{c}^2}{c_p T_0},\ \ Br = PrE_c, \\ \theta = \frac{\hat{T}-T_0}{T_0}. \end{gathered} \tag{6.15}$$

With the help of Eqs. (6.7)-(6.15) and employing the low Reynolds number approximation from lubrication theory, Eqs. (6.3)-(6.6) take the following form:

$$\frac{\partial u}{\partial x}+\frac{\partial v}{\partial y} = 0, \tag{6.16}$$

$$\frac{\partial p}{\partial x} = \frac{1}{1+\lambda_1}\frac{\partial}{\partial y}\left(1+\lambda_2\beta\left(u\frac{\partial}{\partial x}+v\frac{\partial}{\partial y}\right)\right)\frac{\partial u}{\partial y} - \left(\mathcal{M}^2+\frac{1}{\mathcal{K}}\right)(u+1), \tag{6.17}$$

$$\frac{\partial p}{\partial y} = 0, \tag{6.18}$$

$$\frac{\partial^2\theta}{\partial y^2} = \frac{Br}{1+\lambda_1}\left(1+\lambda_2\beta\left(u\frac{\partial}{\partial x}+v\frac{\partial}{\partial y}\right)\right)\left(\frac{\partial u}{\partial y}\right)^2. \tag{6.19}$$

The associated boundary conditions can be emerge as

$$u(h) = \mathcal{u}_0 = -1 - 2\pi\varepsilon\alpha\beta\cos(2\pi x),$$

$$v(h) = 2\pi\varepsilon\sin(2\pi x) + \beta(2\pi\varepsilon)^2\alpha\sin(2\pi x)\cos(2\pi x),$$

$$\theta(h) = 0, \quad \text{at} \quad y = h,$$

$$\frac{\partial u}{\partial y} = 0, \quad \frac{\partial\theta}{\partial y} = 0, \quad \text{at} \quad y = 0, \tag{6.20}$$

here $h = 1 + \varepsilon\cos(2\pi x)$.

The stream function ψ is defined as

$$u = \frac{\partial\psi}{\partial y}, \quad v = -\frac{\partial\psi}{\partial x}. \tag{6.21}$$

Eqs. (6.16)-(6.19) in terms of ψ take the following form

$$\frac{\partial^4\psi}{\partial y^4} = \lambda_2\beta\frac{\partial^2}{\partial y^2}\left(\frac{\partial\psi}{\partial y}\frac{\partial}{\partial x} - \frac{\partial\psi}{\partial x}\frac{\partial}{\partial y}\right)\frac{\partial^2\psi}{\partial y^2} + \left(\mathcal{M}^2 + \frac{1}{\mathcal{K}}\right)(1+\lambda_1)\frac{\partial^2\psi}{\partial y^2}. \tag{6.22}$$

$$\frac{\partial^2\theta}{\partial y^2} = \frac{Br}{1+\lambda_1}\left(1+\lambda_2\beta\left(\frac{\partial\psi}{\partial y}\frac{\partial}{\partial x}' - \frac{\partial\psi}{\partial x}\frac{\partial}{\partial y}\right)\right)\left(\frac{\partial^2\psi}{\partial y^2}\right)^2. \tag{6.23}$$

The boundary conditions can be expressed as

$$\begin{gathered}\psi = 0, \quad \frac{\partial^2\psi}{\partial y^2} = 0, \quad \frac{\partial\theta}{\partial y} = 0, \quad at \quad y = 0,\\ \psi = F, \quad \frac{\partial\psi}{\partial y} = -1 - 2\pi\varepsilon\alpha\beta\cos(2\pi x), \quad \theta = 0,\\ \frac{\partial\psi}{\partial x} = 2\pi\varepsilon\sin(2\pi x) + \beta(2\pi\varepsilon)^2\alpha\sin(2\pi x)\cos(2\pi x), \quad at\ y = h.\end{gathered} \tag{6.24}$$

Here Q is the volumetric flow rate, and related to the flux by the following relation

$$Q = \int_0^h\left(\frac{\partial\psi}{\partial y} + 1\right)dy = F + h. \tag{6.25}$$

In fixed frame, the time mean volumetric flow rate is defined as

$$\hat{Q} = \frac{1}{T}\int_0^h (F+h)d\hat{t} = \int_0^1 (F+h)dt = F + 1. \tag{6.26}$$

6.2 Solution of the Problem

Many advanced computational and semi-computational methods may be employed to evaluate the transformed boundary value problem defined by Eqs. 6.22-6.24. These include homotopy methods, spectral methods, variational iterative methods and finite element methods. Here we have employed the Adomian decomposition method (ADM), introduced by American mathematician, Adomian [81]. Recent applications of this technique in complex biological flow problems include Bég et al. [85] (for smart lubrication squeeze films) and Bég [86] (swirling nanofluid bioreactors).

Re-writing Eqs. (6.22) and (6.23) in terms of Adomian operators we have

$$\psi = \varphi_0 + {L_1}^{-1}\left(-\lambda_2\beta\frac{\partial^2}{\partial y^2}\left(\frac{\partial\psi}{\partial y}\frac{\partial}{\partial x}-\frac{\partial\psi}{\partial x}\frac{\partial}{\partial y}\right)\frac{\partial^2\psi}{\partial y^2}\right) + {L_1}^{-1}\left(\left(\mathcal{M}^2+\frac{1}{\mathcal{K}}\right)(1+\lambda_1)\frac{\partial^2\psi}{\partial y^2}\right), \tag{6.27}$$

$$\theta = \varphi_1 - \frac{Br}{1+\lambda_1}{L_2}^{-1}\left(\left(1+\lambda_2\beta\left(\frac{\partial\psi}{\partial y}\frac{\partial}{\partial x}-\frac{\partial\psi}{\partial x}\frac{\partial}{\partial y}\right)\right)\left(\frac{\partial^2\psi}{\partial y^2}\right)^2\right). \tag{6.28}$$

Here the inverse operators are defined as

$${L_1}^{-1}(.) = \int\int\int\int(.)dy, \tag{6.29}$$

$${L_2}^{-1} = \int\int(.)dy, \tag{6.30}$$

The linear term $\psi(x,y)$ is decomposed in term of an infinite series of components through the following expression

$$\psi(x,y) = \sum_{n=0}^{\infty}\psi_n(x,y). \tag{6.31}$$

The nonlinear term $N\psi(x,y)$ can be decomposed into Adomian polynomials and satisfies

$$A_n = \frac{1}{n!}\frac{d^m}{d\lambda^m}\left[N\left(\sum_{i=0}^{\infty}\psi_i,\right)\right]_{\lambda=0}, \quad n = 0,1,2,3,\ldots. \tag{6.32}$$

This leads to

$$A_0 = -\frac{\partial\psi_0}{\partial x}\frac{\partial^5\psi_0}{\partial y^5} + \frac{\partial\psi_0}{\partial y}\frac{\partial^5\psi_0}{\partial x\partial y^4} + 2\frac{\partial^2\psi_0}{\partial y^2}\frac{\partial^4\psi_0}{\partial x\partial y^3} - 2\frac{\partial^4\psi_0}{\partial y^4}\frac{\partial^2\psi_0}{\partial x\partial y}, \tag{6.33}$$

$$A_1 = -\frac{\partial\psi_0}{\partial x}\frac{\partial^5\psi_1}{\partial y^5} - \frac{\partial\psi_1}{\partial x}\frac{\partial^5\psi_0}{\partial y^5} + \frac{\partial\psi_1}{\partial y}\frac{\partial^5\psi_0}{\partial x\partial y^4} + \frac{\partial\psi_0}{\partial y}\frac{\partial^5\psi_1}{\partial x\partial y^4} + 2\frac{\partial^2\psi_0}{\partial y^2}\frac{\partial^4\psi_1}{\partial x\partial y^3} + 2\frac{\partial^2\psi_1}{\partial y^2}\frac{\partial^4\psi_0}{\partial x\partial y^3} - 2\frac{\partial^4\psi_0}{\partial y^4}\frac{\partial^2\psi_1}{\partial x\partial y} - 2\frac{\partial^4\psi_1}{\partial y^4}\frac{\partial^2\psi_0}{\partial x\partial y}, \tag{6.34}$$

$$A_2 = -\frac{\partial\psi_0}{\partial x}\frac{\partial^5\psi_2}{\partial y^5} - \frac{\partial\psi_1}{\partial x}\frac{\partial^5\psi_1}{\partial y^5} - \frac{\partial\psi_2}{\partial x}\frac{\partial^5\psi_0}{\partial y^5} + \frac{\partial\psi_0}{\partial y}\frac{\partial^5\psi_2}{\partial x\partial y^4} + \frac{\partial\psi_1}{\partial y}\frac{\partial^5\psi_1}{\partial x\partial y^4} + \frac{\partial\psi_2}{\partial y}\frac{\partial^5\psi_0}{\partial x\partial y^4} + 2\frac{\partial^2\psi_0}{\partial y^2}\frac{\partial^4\psi_2}{\partial x\partial y^3} + 2\frac{\partial^2\psi_1}{\partial y^2}\frac{\partial^4\psi_1}{\partial x\partial y^3} + 2\frac{\partial^2\psi_2}{\partial y^2}\frac{\partial^4\psi_0}{\partial x\partial y^3} - 2\frac{\partial^4\psi_0}{\partial y^4}\frac{\partial^2\psi_2}{\partial x\partial y} - 2\frac{\partial^4\psi_1}{\partial y^4}\frac{\partial^2\psi_1}{\partial x\partial y} - 2\frac{\partial^4\psi_2}{\partial y^4}\frac{\partial^2\psi_0}{\partial x\partial y}. \tag{6.35}$$

and

$$\varphi_0 = c_1 + c_2 y + c_3\frac{y^2}{2!} + c_4\frac{y^3}{3!}, \tag{6.36}$$

$$\varphi_1 = d_1 + d_2 y. \tag{6.37}$$

Here $c_1,\ c_2,\ c_3, c_4\ ,\ d_1, d_2$ are integration constants and can be extracted with the assistance of boundary conditions given in Eq. (6.24). Now by decomposing the linear and the non-linear terms in the infinite series form, we get

$$\sum_{n=0}^{\infty}\psi_n = \varphi_{0,n} + {L_1}^{-1}\left(-\lambda_2\beta\frac{\partial^2}{\partial y^2}\left(\frac{\partial\psi_n}{\partial y}\frac{\partial}{\partial x} - \frac{\partial\psi_n}{\partial x}\frac{\partial}{\partial y}\right)\frac{\partial^2\psi_n}{\partial y^2}\right) + {L_1}^{-1}\left(\left(\mathcal{M}^2 + \frac{1}{\mathcal{K}}\right)(1+\lambda_1)\frac{\partial^2\psi_n}{\partial y^2}\right), \tag{6.38}$$

$$\sum_{n=0}^{\infty}\theta_n = \varphi_{1,n} - \frac{Br}{1+\lambda_1}{L_2}^{-1}\left(\left(1 + \lambda_2\beta\left(\frac{\partial\psi}{\partial y}\frac{\partial}{\partial x} - \frac{\partial\psi}{\partial x}\frac{\partial}{\partial y}\right)\right)\left(\frac{\partial^2\psi}{\partial y^2}\right)^2\right). \tag{6.39}$$

Following the ADM, we obtain

$$\psi_0 = \left(\frac{3F - hu(h)}{2h}\right) y - \left(\frac{F - hu(h)}{2h^3}\right) y^3, \tag{6.40}$$

$$\begin{aligned}\theta_0 = {} & \frac{1}{10h^4(1+\lambda_1)}\left[Br\begin{pmatrix} 27\beta F^3\lambda_2 h' + h(-42\beta F^2\lambda_2 u(h)h' \\ +h(-5h^4 + 18\beta F\lambda_2 u^2(h)h' \\ +3\beta\lambda_2(F - hu(h))(3F + 2hu(h))u'(h))) \end{pmatrix}\right] \\ & + \frac{Br}{2+2\lambda_1} y^2 \\ & + \frac{1}{2h^8(1+\lambda_1)}\begin{bmatrix} 3Br\beta\lambda_2(F - hu(h))(3F^2 - 3hFu(h) \\ +h^2u^2(h)h' + h^2Fu'(h)) \end{bmatrix} y^4 \\ & + \frac{1}{5h^{10}(1+\lambda_1)}\begin{bmatrix} 3Br\beta\lambda_2\big(F - hu(h)\big)^2 \times \big(3F - 2hu(h)\big)h' \\ +h^2u'(h)) \end{bmatrix} y^6, \end{aligned} \tag{6.41}$$

$$\begin{aligned}\psi_n = {} & {L_1}^{-1}\left(-\lambda_2\beta\frac{\partial^2}{\partial y^2}\left(\frac{\partial\psi_{n-1}}{\partial y}\frac{\partial}{\partial x} - \frac{\partial\psi_{n-1}}{\partial x}\frac{\partial}{\partial y}\right)\frac{\partial^2\psi_{n-1}}{\partial y^2}\right) \\ & + {L_1}^{-1}\left(\left(\mathcal{M}^2 + \frac{1}{\mathcal{K}}\right)(1+\lambda_1)\frac{\partial^2\psi_{n-1}}{\partial y^2}\right), \quad n \geq 1, \end{aligned} \tag{6.42}$$

$$\theta_n = -\frac{Br}{1+\lambda_1}{L_2}^{-1}\left(\left(1 + \lambda_2\beta\left(\frac{\partial\psi_n}{\partial y}\frac{\partial}{\partial x} - \frac{\partial\psi_n}{\partial x}\frac{\partial}{\partial y}\right)\right)\left(\frac{\partial^2\psi_n}{\partial y^2}\right)^2\right). \tag{6.43}$$

The solution in the ψ can be written as

$$\begin{aligned}\psi = \sum_{n=0}^{\infty}\psi_n(x,y) = {} & \psi_0 + \psi_1 + \psi_2 + \psi_3 + \cdots = A_{11}(x)y + A_{12}(x)y^3 \\ & + A_{13}(x)y^5 + A_{14}(x)y^7 + A_{15}(x)y^9 + \cdots, \end{aligned} \tag{6.44}$$

and the solution of temperature can be written as

$$\begin{aligned}\theta = {} & \theta_0 + \theta_1 + \theta_2 + \theta_3 + \cdots = B_1(x) + B_2(x)y^4 \\ & + B_3(x)y^6 + B_4(x)y^8 + B_5(x)y^{10} + B_6(x)y^{12} \\ & + B_7(x)y^{14} + B_8(x)y^{16} + B_9(x)y^{18} + B_{10}(x)y^{20} \\ & + B_{11}(x)y^{22} + B_{12}(x)y^{24} + \cdots. \end{aligned} \tag{6.45}$$

Here $A_{11}(x)$, $A_{12}(x)$... $B_{12}(x)$ are given in the appendix.

The pressure gradient $\left(\frac{dp}{dx}\right)$ after using Eq. (6.44) in Eq. (6.17) is as follows

$$\frac{dp}{dx} = \frac{1}{1+\lambda_1}\frac{\partial}{\partial y}\left(1 + \lambda_2\beta\left(\frac{\partial\psi}{\partial y}\frac{\partial}{\partial x} - \frac{\partial\psi}{\partial x}\frac{\partial}{\partial y}\right)\right)\frac{\partial^2\psi}{\partial y^2} - \left(\mathcal{M}^2 + \frac{1}{\mathcal{K}}\right)\left(\frac{\partial\psi}{\partial y} + 1\right), \tag{6.46}$$

Integrate Eq. (6.46) to obtain the pressure rise per wavelength as

$$\Delta p = \int_0^1 \frac{dp}{dx} dx. \tag{6.47}$$

However, the numerical value of the integral is evaluated using the symbolic software MATHEMATICA.

6.3 Results and Discussion

The influence of interested parameters on axial velocity $u(x, y)$, axial pressure gradient $\frac{dp}{dx}$, pressure rise Δp, temperature profile, stream function $\psi(x, y)$ are displayed graphically in Figs. 6.2-6.9.

Axial velocity

In Figs. 6.2a-6.2d the effect of Hartmann number $\mathcal{M}$, permeability parameter $\mathcal{K}$, Jeffrey 1st and 2nd viscoelastic parameters (λ_1, λ_2) on the horizontal velocity $u(x, y)$. It can be observed from this figure that behavior of velocity is not same at the center and near to the wall of channel due to presence of cilia in the interior channel wall. Figs. 6.2a and 6.2c depict that the horizontal velocity decreases in the region $-0.38 < y < 0.38$ otherwise significant variation is not seen with the increase in $\mathcal{M}$and $\lambda_1$because magnetic force and viscous force are strong at the center of the channel whereas the converse behavior can be seen in Figs. 6.2b and 6.2d with an increase in $\mathcal{K}$ and λ_2 as porosity and retardation time causes to increase the velocity near the center of the channel.

Pumping characteristics

Figs. 6.3a-d show that the pressure gradient has a periodic nature and attains its peak at core region of the channel then reduces rapidly as we progress from the core zone. Similar to velocity field the behavior of pressure gradient exhibits some variation throughout the region. It can be observed from Figs. 6.3a that pressure gradient is boosted at the center and depressed near the walls with increasing Hartmann number. The magnetic field effect is enhanced with rising Hartmann number and generates deceleration in the flow. The inverse relation between velocity and pressure manifests in an elevation in pressure gradient in the core flow. With increasing permeability $\mathcal{K}$, although velocity is enhanced (Fig. 6.2b), the converse effect is induced in pressure gradient (Fig. 6.3c). The Darcy resistance term in Eq. (6.22) is inversely proportional

to permeability. Increasing $\mathcal{K}$ values decrease the impedance to flow and result in an acceleration and a drop in the pressure gradient. Figs. 6.3c and 6.3d show that the first λ_1, and second λ_2 Jeffrey parameters induce respectively an enhancement and suppression in the pressure gradient, although the first parameter has a much more profound effect. The first parameter denotes the ratio of the relaxation to retardation times of the bio-rheological fluid whereas the second parameter designates purely retardation time. When $\lambda_1 = 1$ relaxation time is exactly equivalent to retardation time. However, we have considered some values less than unity which are more representative of physiological fluids [87]. For $\lambda_1 < 1$, the retardation time is greater than relaxation time which implies that the biofluid responds quicker with the removal of stress and returns faster to its unperturbed state. This influences pressure gradient (and velocity field).

Figs. 6.4a-c show the effect of various values of Hartmann number $\mathcal{M}$, permeability parameter $\mathcal{K}$, and the ratio of retardation to relaxation times λ_1 on pressure rise Δp versus $\hat{Q}$. A linear relation between pressure rise Δp and volumetric flow rate $\hat{Q}$ can be seen from these figures. Fig. 6.4a depicts that pressure rise increases with Hartmann number$\mathcal{M}$, in the region $-1.5 < \hat{Q} < -0.3$ because in this region resistive force due to magnetic field requires more pressure difference and reverse behavior is noted in the range $-0.4 < \hat{Q} < 1$ whereas, it decreases with greater permeability (lesser Darcian resistance) in the range $-1.5 < \hat{Q} < -0.4$ because permeability requires less pressure difference for the flow through the mentioned volume flux. The effect of λ_1 on pressure rise decreases in the region$-1.5 < \hat{Q} < -1.0$. However, the contrary effect is induced in the range $-1.5 < \hat{Q} < 1.0$ with increasing first Jeffrey viscoelastic parameter.

Temperature profile

Figs. 6.5a-e are plotted to analyze the outcome of Hartmann number $\mathcal{M}$, permeability parameter $\mathcal{K}$, Brinkman number Br, Jeffrey first parameter λ_1 and second parameter λ_2 on temperature distribution across the channel. The manner of the temperature profile is same as that of the velocity profile although the profiles are significantly more plateau-like in the interior region of the channel. Significantly less variation in profiles is observed near the channel walls. Increasing Hartmann number (Fig. 6.5a) induces a strong elevation in temperatures across the channel due to slow motion in the existence of magnetic field. The supplementary work expended by the biofluid is dragging against

the applied magnetic field, conversely increasing permeability parameter (Fig. 6.5b) leads to a reduction in temperature because porosity causes to reduce conductivity of the biofluid. The increase in medium permeability implies a decrease in solid matrix fibers in the medium. This reduces the material available for thermal conduction heat transfer and manifests in a cooling of the medium. Thermal conductivity of the fluid-saturated medium is clearly influenced with a modification in permeability and as the permeability increases the heat transfer rate to the walls will increase. Increasing first and second Jeffrey parameters (Figs. 6.5c and 6.5d) respectively decreases and enhances the temperature magnitudes in the medium. Retardation of the biofluid is therefore beneficial to heat transfer through the medium whereas relaxation opposes it. Fig.5e illustrates the impact of Brinkman number on the temperature profile. Brinkman number is the heat conduction from the boundary to the viscous fluid and characterizes the viscous dissipation term in the fluid flow. With rising the value of Brinkman number, the thermal conductivity of the fluid reduces so larger quantity of heat that can be transferred through the fluid. It is also noted that a higher temperature exists close to the interior region of the channel in comparison to the walls of the ciliated channel.

Streamlines

Figs. 6.6-6.9 reveal the impact of Hartmann number $\mathcal{M}$, permeability parameter $\mathcal{K}$, the Jeffrey 1st parameter λ_1 and 2nd parameter λ_2 on the stream function. Figs. 6.6a-c depicts that the number of trapped boluses decrease with Hartmann number. This is because magnetic force decelerate the velocity. It is noted from Figs. 6.7a-c that the amplitude of wave reduces with a rise in the permeability parameter since the flow is accelerated and this prevents the build-up of larger amplitudes generated by the metachronal wave motion. Figs. 6.8a-c highlight that the number of trapped boluses and their magnitudes are enhanced with increasing Jeffrey first viscoelastic parameter i.e. with greater rheological relaxation times. The boluses are strongly stretched in the vertical direction with greater values of λ_1. Finally, it is evident from Figs. 6.9a-c that the size of trapped boluses is also increased with greater retardation time values λ_2.

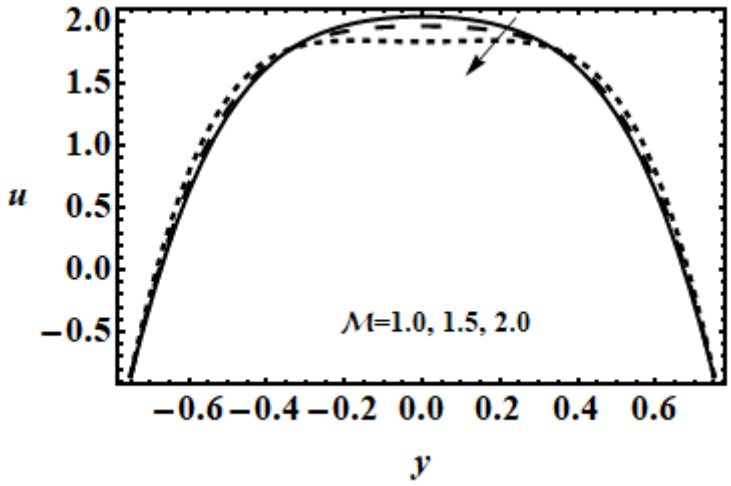

Fig. 6.2a: The effect of Hartmann number $\mathcal{M}$ on velocity.

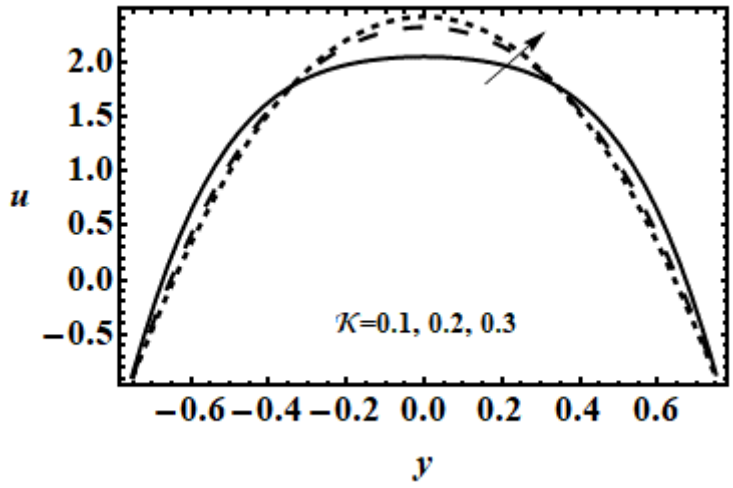

Fig. 6.2b: The effect of porosity parameter $\mathcal{K}$ on velocity.

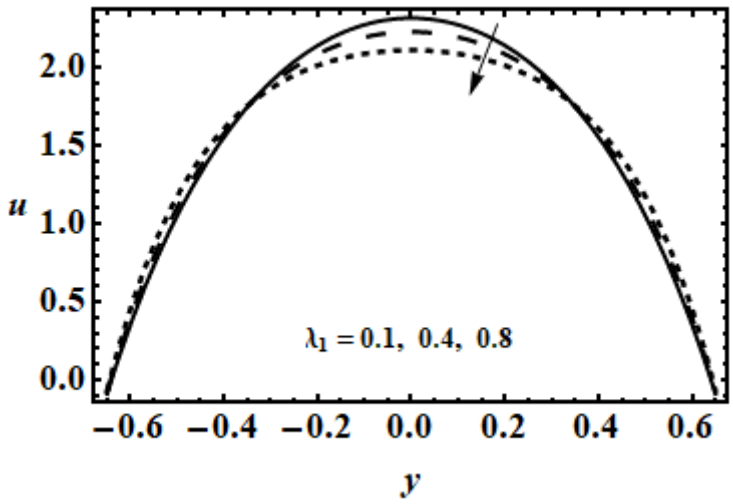

Fig. 6.2c: The effect of fluid parameter λ_1 on velocity.

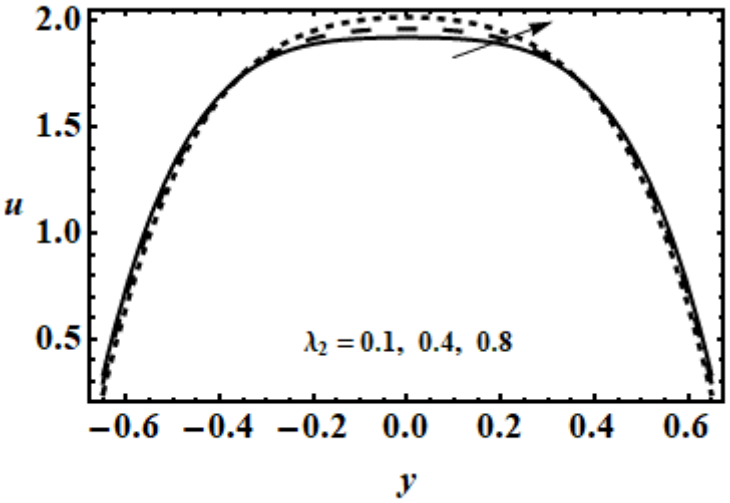

Fig. 6.2d: The effect of fluid parameter λ_2 on velocity.

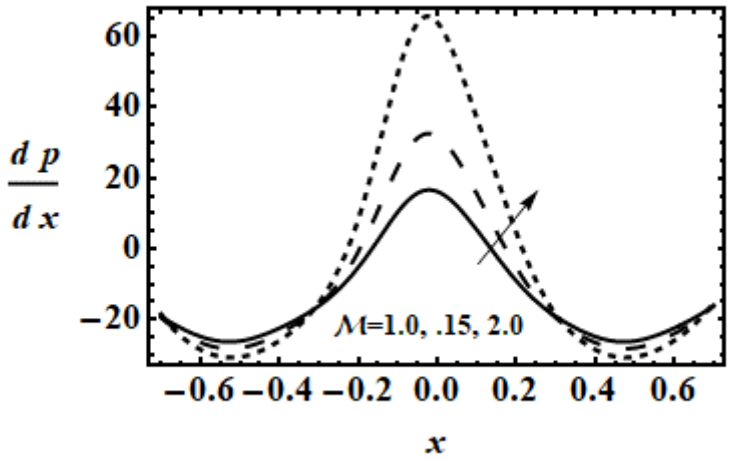

Fig. 6.3a: The effect of Hartmann number $\mathcal{M}$ on pressure gradient.

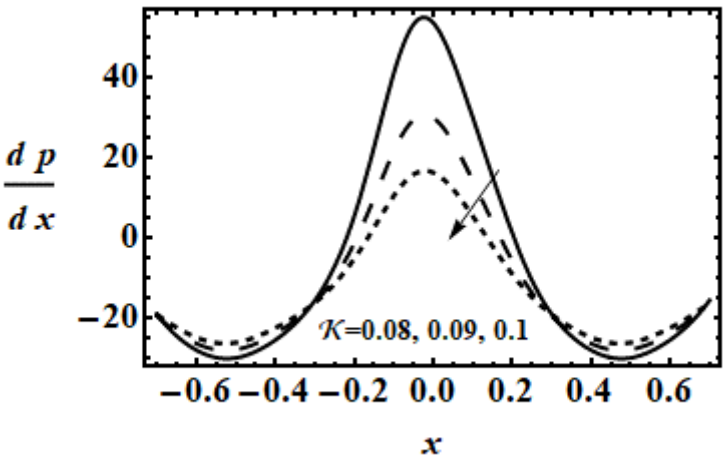

Fig. 6.3b: The effect of porosity parameter $\mathcal{K}$ on pressure gradient.

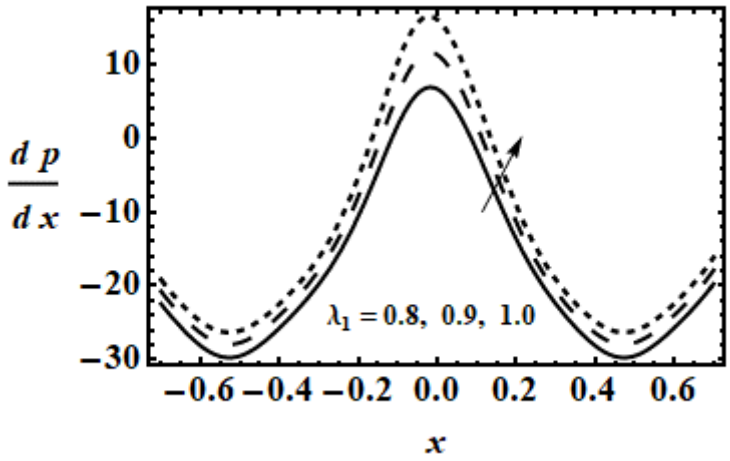

Fig. 6.3c: The effect of fluid parameter λ_1 on velocity.

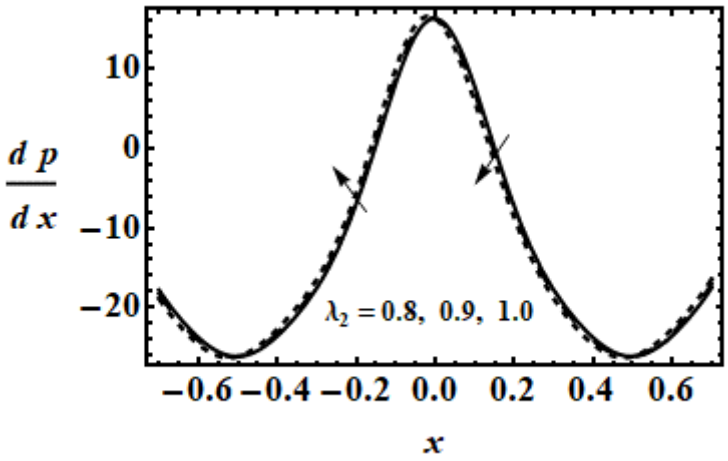

Fig. 3d: The effect of fluid parameter λ_2 on pressure gradient.

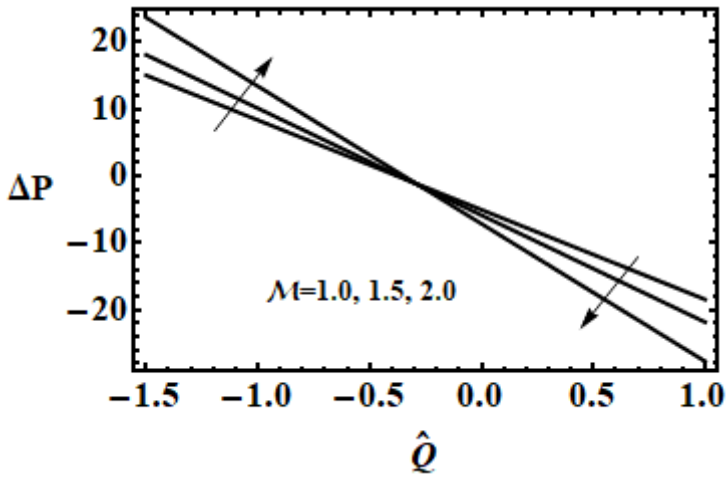

Fig. 6.4a: The effect of Hartmann number $\mathcal{M}$ on pressure rise Δp with time mean volumetric flow rate $\hat{Q}$.

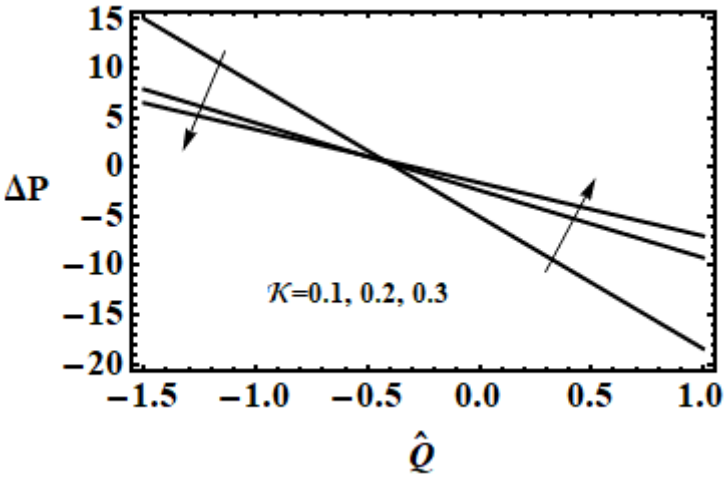

Fig. 6.4b: The effect of porosity parameter $\mathcal{K}$ on pressure rise Δp with time mean volumetric flow rate $\hat{Q}$.

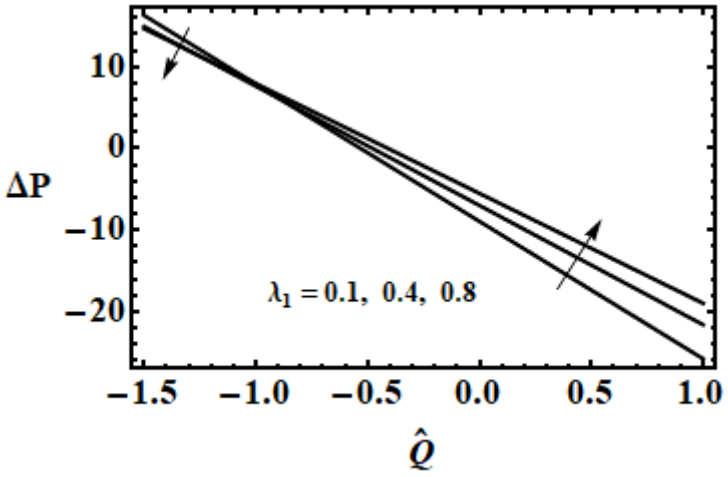

Fig. 6.4c: The effect of fluid parameter λ_1 on pressure rise Δp with volumetric flow rate $\hat{Q}$.

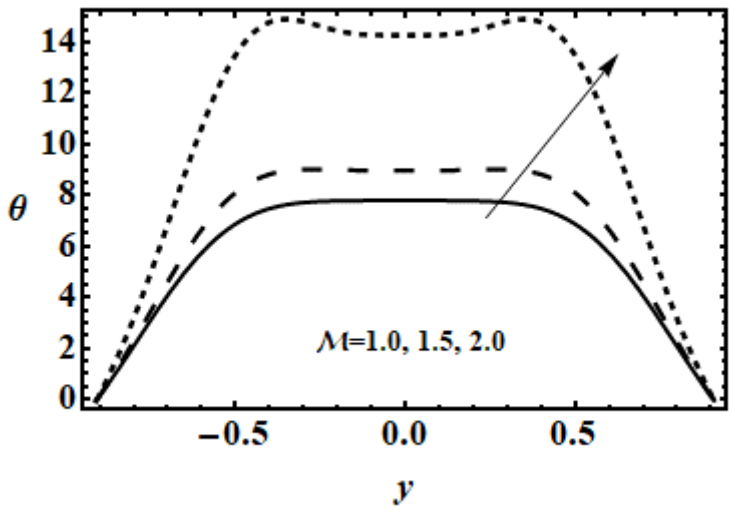

Fig. 6.5a: The effect of Hartmann number $\mathcal{M}$ on temperature profile.

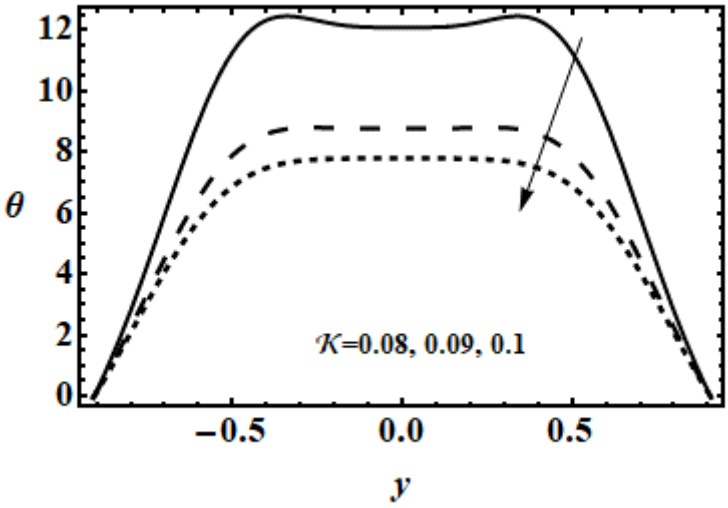

Fig. 6.5b: The effect of porosity parameter $\mathcal{K}$ on temperature profile.

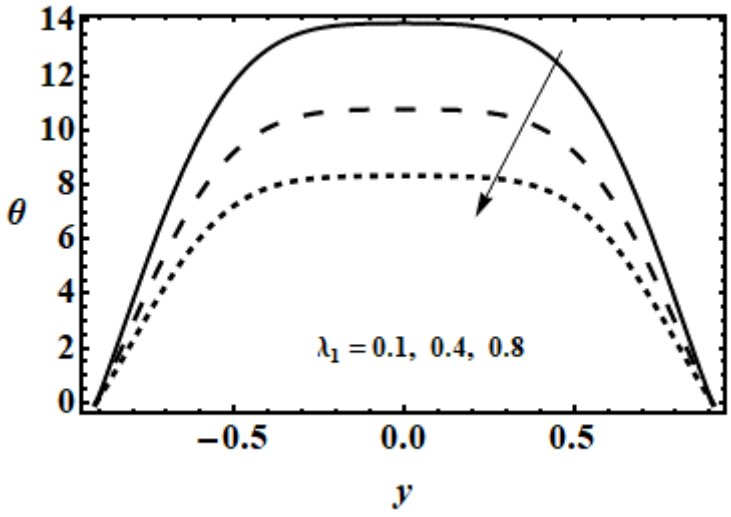

Fig. 6.5c: The effect of fluid parameter λ_1 on temperature profile.

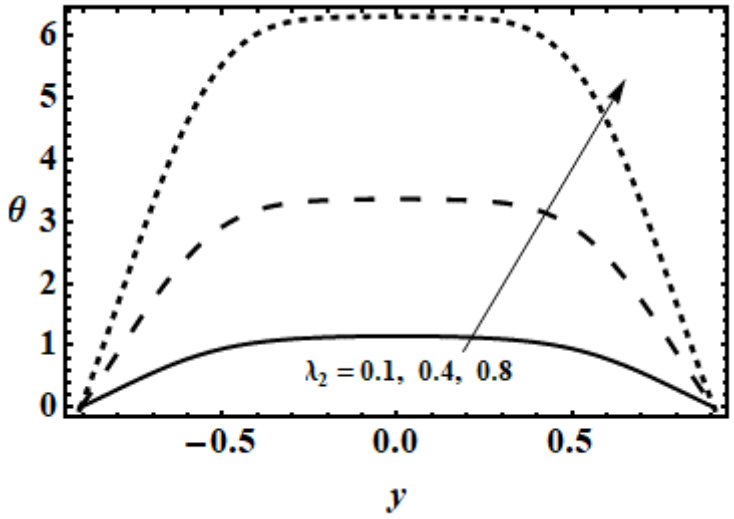

Fig. 6.5d: The effect of fluid parameter λ_2 on temperature profile.

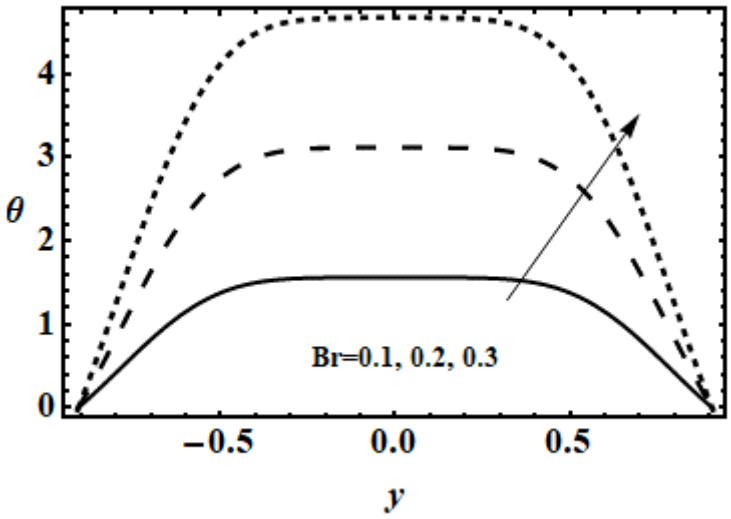

Fig. 6.5e: The effect of Brinkman number Br on temperature profile.

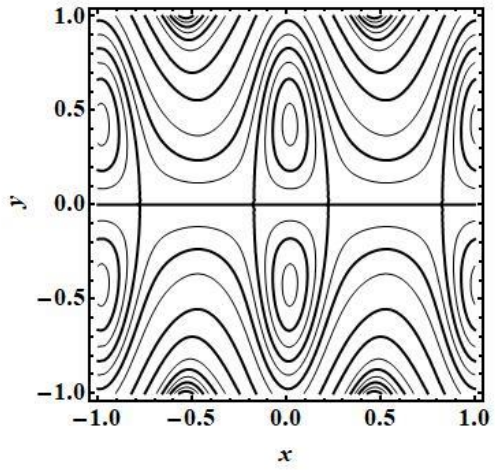

(a) $\mathcal{M} = 1.0$

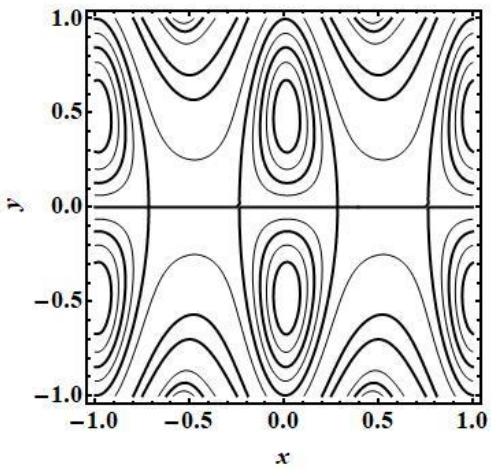

(b) $\mathcal{M} = 1.5$

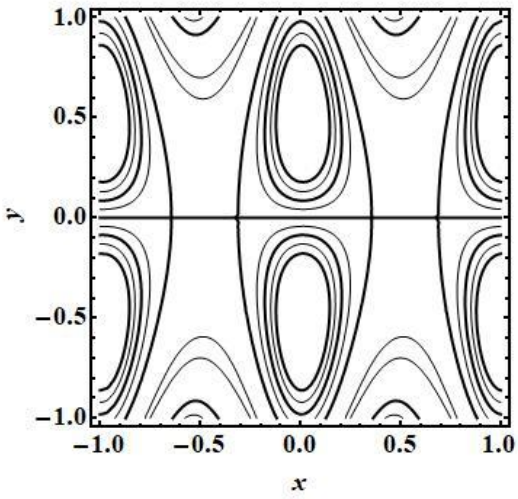

(c) $\mathcal{M} = 2.0$

Fig. 6.5: Influence of Hartmann number on stream function for $\alpha = 0.3;\ \beta = 0.1;\ \varepsilon = 0.3;\ \hat{Q} = 2;\ \mathcal{K} = 0.1;\ \lambda_1 = \lambda_2 = 1$.

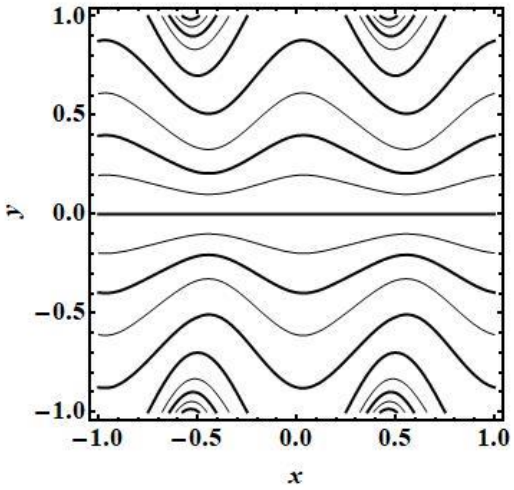

(a) $\mathcal{K} = 0.2$

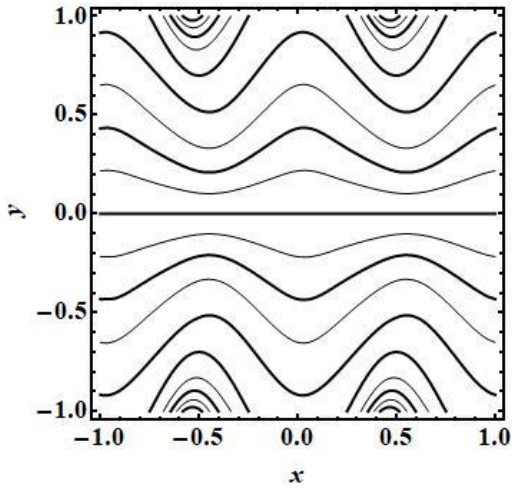

(b) $\mathcal{K} = 0.3$

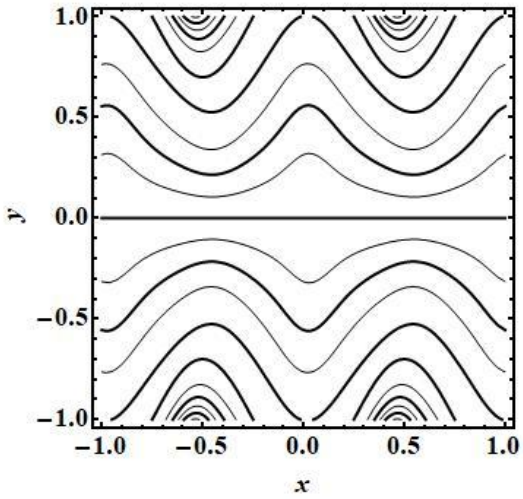

(c) $\mathcal{K} = 0.4$

Fig. 6.6: Influence of porosity parameter $\mathcal{K}$ on stream function for $\alpha = 0.3$; $\beta = 0.1$; $\varepsilon = 0.3$; $\hat{Q} = 2$; $\mathcal{M} = 1$; $\lambda_1 = \lambda_2 = 1$.

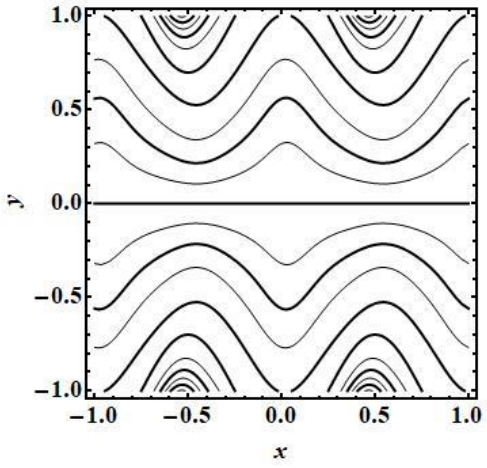

(a) $\lambda_1 = 0.1$

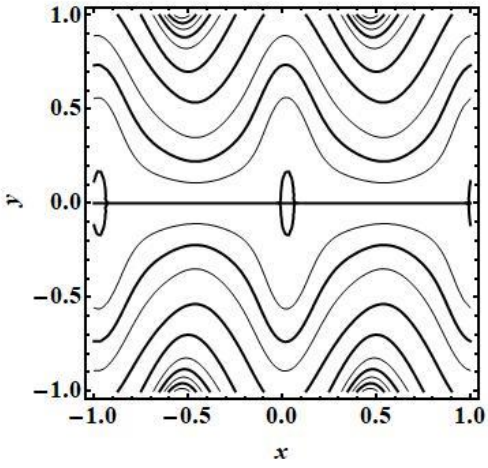

(b) $\lambda_1 = 0.4$

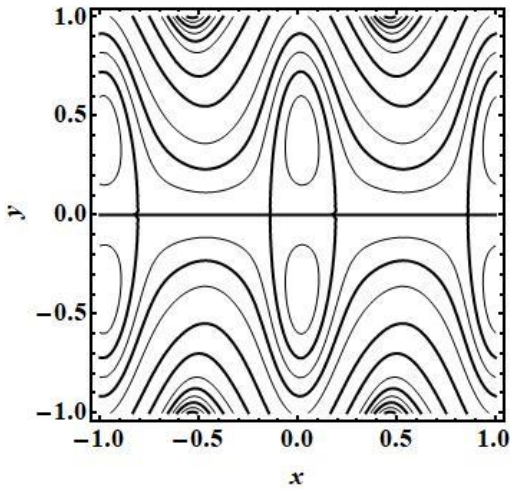

(c) $\lambda_1 = 0.8$

Fig. 6.7: Influence of fluid parameter λ_1 on stream function for $\alpha = 0.3$; $\beta = 0.1$; $\varepsilon = 0.3$; $\hat{Q} = 2$; $\mathcal{M} = 1$; $\mathcal{K} = 0.1$; $\lambda_2 = 1$.

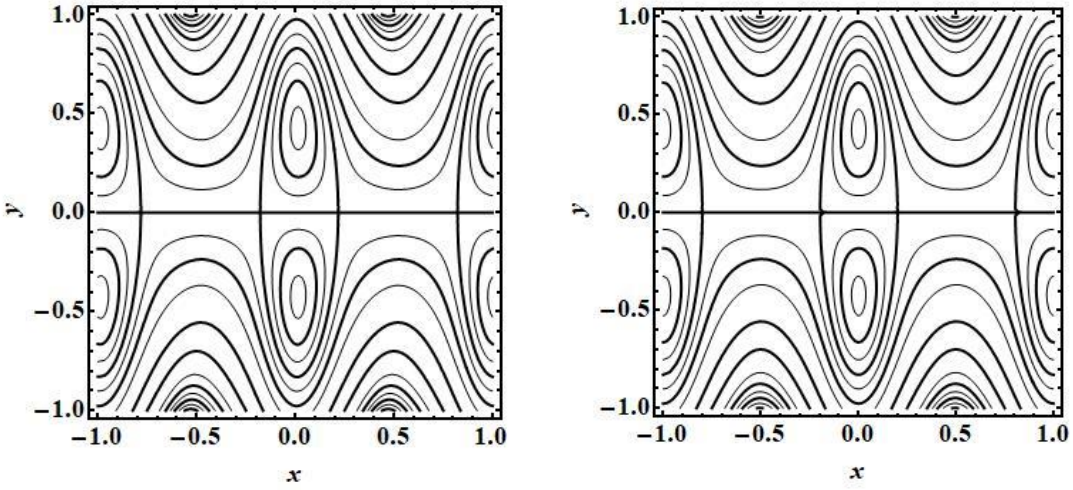

(a) $\lambda_2 = 0.1$ (b) $\lambda_2 = 0.4$

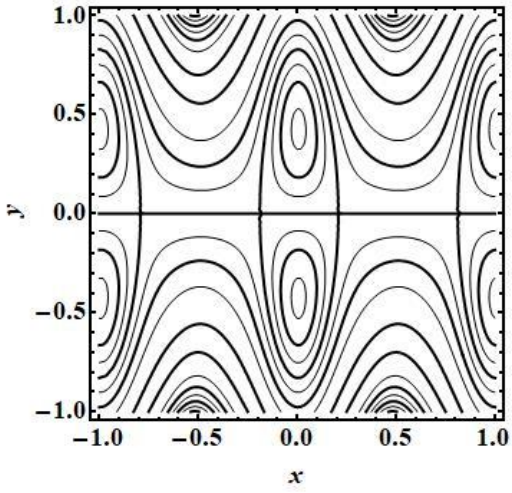

(c) $\lambda_2 = 0.8$

Fig. 6.8: Influence of fluid parameter λ_2 on stream function for $\alpha = 0.3;\ \beta = 0.1;\ \varepsilon = 0.3;\ \hat{Q} = 2;\ \mathcal{M} = 1;\ \mathcal{K} = 0.1;\ \lambda_1 = 1.$

6.4 Conclusion

A mathematical model has been presented for forced convective heat transfer in transport of a viscoelastic Jeffrey fluid through a ciliated channel containing a high permeability porous medium under the impact of a normal magnetic field. The flow is produced due to the metachronal wave generated by synchronized beating of cilia which follow an elliptical path. The transformed (fixed to wave frame) and non-dimensional boundary value problem (momentum and energy conservation equations and associated channel wall boundary conditions) have been solved with the semi-numerical Adomian decomposition method (ADM). Extensive details of the ADM solutions have been provided. The numerical evaluation of the power-series solutions is conducted in MATHEMATICA software with the approximately one hour of CPU time. In the present study if $\lambda_1, \lambda_2 \to 0$ then [43] can be obtained which assume that our results are correct. The present study can be used to discuss the problem caused by cholesterol in veins and arteries. The results show that:

- Velocity field, pressure gradient and temperature profile show a similar parabolic nature and attain maximum magnitudes at the midway of the conduit and further decrease rapidly at the walls of channel.
- The behavior of velocity field and pressure gradient is distinctly different throughout the channel.
- Velocity is decreased with increasing Hartmann number and Jeffrey 1st viscoelastic parameter in the core section of the channel whereas the flow is accelerated close to the walls.
- Velocity is elevated with rising permeability parameter and Jeffrey 2nd viscoelastic parameter (retardation parameter) in the core zone.
- Pressure gradient is increased with high Hartmann number whereas it is reduced with greater permeability parameter at the center of the channel.
- Temperature profile is maximized in the core section of the channel and diminished at the walls.
- Temperature is noted to be enhanced with rising Hartmann number and second Jeffrey parameter whereas it is reduced with permeability parameter and Jeffrey first parameter.

- Volume flow rate and pressure rise have shown the linear relationship between each other.
- Pressure rise is elevated with increasing permeability and Jeffrey 1st parameter whereas it decreases with an increase in Lorentz retarding force i.e. with greater Hartmann numbers.
- Number of trapped boluses decreases as Hartmann number is high.
- The amplitude of streamlines decreases with a rise in permeability parameter whereas the size and the number of trapped boluses increase with greater values of Jeffrey first and second viscoelastic parameters.
- The current study has neglected magnetic induction and mass transfer effects which are also important in fertility devices. These aspects will be addressed in the future.

Chapter 7

Influence of Heat Transfer on MHD Carreau Fluid Flow Due to Motile Cilia

Mucus transport mediated by motile cilia in the airway is an important defense mechanism for prevention of respiratory infections. As cilia motility can be affected by temperature difference and magnetic field, therefore, in this research we investigate the combined effects of magnetic field and buoyancy force due to temperature difference. In the present study mixed convective flow of a Carreau fluid model through a ciliated channel is modeled and analyzed by a symplectic metachoronal wave. The momentum and energy equation for the Carreau fluid are modeled and simplified by the stream function and small Reynolds number approximation. The transport moving boundary value problem is solved with no slip condition by Adomian decomposition method. The velocity profile, temperature profile and pressure distribution are obtained in the form of infinite series by ADM which is evaluated by software "MATHEMATICA". The influence of magnetic parameter, Carreau fluid parameter, Brinkman number and Weissenberg number on velocity, temperature and pressure gradient are presented via graphs. Hartmann number helps to decelerate the flow whereas Weissenberg number, Grashof number and Carreau fluid parameter are responsible for the accelerated flow. The temperature profile increases by increasing the values of Hartmann number, Weissenberg number, Carreau fluid parameter and Brinkman number.

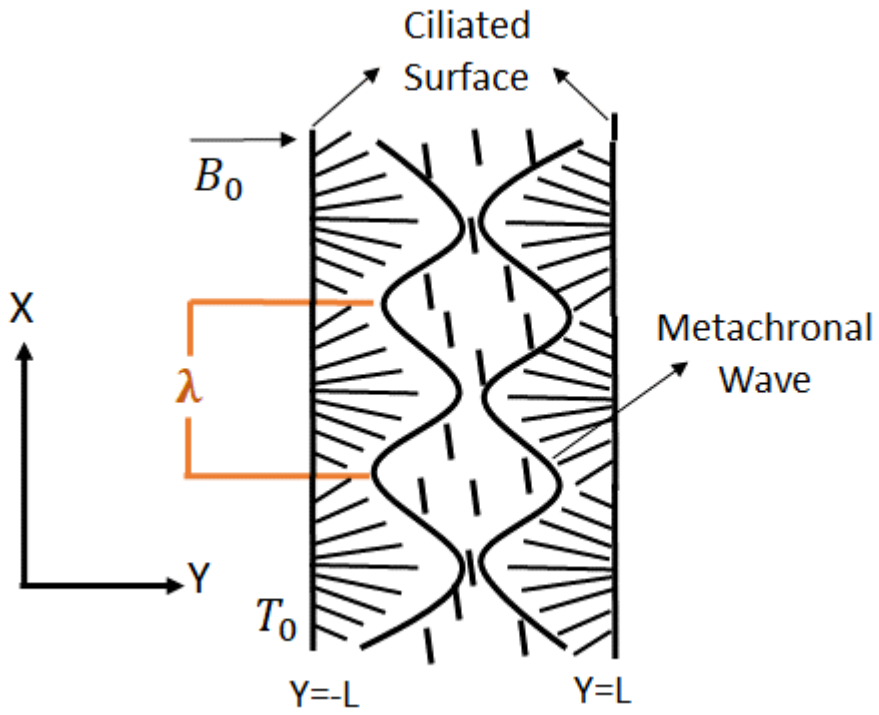

Fig. 7.1: Geometry of problem

7.1 Problem Formulation

Let us assume the ciliary flow of an incompressible rheological Carreau fluid in a symmetric vertical channel under the effect of constant magnetic field. To study the mixed convective flow of Carreau fluid through a ciliated channel, buoyancy forces due to temperature difference is considered. Viscous dissipation have a significant effect during the energy transfer. Therefore in convective heat transfer the viscous dissipation term is also considered in the modelling of mixed convective flow of MHD Carreau fluid in a ciliated channel. The mathematical form of the longitudinal and transverse components of the elliptical path followed by the cilia is as follow

$$\hat{X} = F(\hat{X}, \hat{t}) = X_0 + \varepsilon l \alpha sin\left(\frac{2\pi}{\lambda}\right)(\hat{X} - c\hat{t}), \tag{7.1}$$

$$\hat{Y} = H(\hat{X}, \hat{t}) = l + \varepsilon l cos\left(\frac{2\pi}{\lambda}\right)(\hat{X} - c\hat{t}) = \pm L. \tag{7.2}$$

The mass, momentum and the energy equations of an incompressible Carreau fluid model are as follow

$$div\, \boldsymbol{V} = 0, \tag{7.3}$$

$$\rho \frac{d\boldsymbol{V}}{dt} = div\boldsymbol{\tau} + \boldsymbol{b_f} + \rho g \beta_1 (T - T_0), \tag{7.4}$$

$$\rho c_p \frac{dT}{d\bar{t}} = k_1 \nabla^2 T + \Phi, \tag{7.5}$$

where the parameters $\boldsymbol{V}, \boldsymbol{S}, \boldsymbol{b_f}, \rho, g, \beta_1, T, T_0, c_p, k$ and Φ are defined in nomenclature. Here

$$\boldsymbol{\tau} = -P\boldsymbol{I} + \boldsymbol{S}, \tag{7.6}$$

in which $\boldsymbol{\tau}$ is the extra stress tensor of Carreau fluid [88] and can be written as

$$\boldsymbol{S} = -[\mu_\infty + (\mu_0 - \mu_\infty)][1 + (\Gamma\dot{\gamma})^2]^{\frac{n-1}{2}}\dot{\boldsymbol{\gamma}}, \tag{7.7}$$

where μ_0, μ_∞, Γ and $\dot{\boldsymbol{\gamma}}$ are defined in nomenclature and

$$\dot{\boldsymbol{\gamma}} = \frac{1}{2}\sum_i \dot{\gamma}_{ij} \sum_j \dot{\boldsymbol{\gamma}}_{ij} = \sqrt{\frac{1}{2}\Pi}, \tag{7.8}$$

where

$$\Pi = (\nabla.V + (\nabla.V)^T)^2. \tag{7.9}$$

In present work we consider $\mu_\infty = 0$ and $\Gamma\dot{\gamma} \ll 1$ for Eq. (7.7). Therefore extra stress tensor becomes

$$\boldsymbol{S} = -\mu_0 \left[1 + \frac{n-1}{2}(\Gamma\dot{\gamma})^2\right]\dot{\boldsymbol{\gamma}}. \tag{7.10}$$

The fixed and wave are related as

$$\hat{x} = \hat{X} - \mathfrak{c}\hat{t}, \quad \hat{u} = \hat{U} - \mathfrak{c}, \quad \hat{y} = \hat{Y}, \quad \hat{v} = \hat{V}, \quad \hat{p}(\hat{x}, \hat{y}, \hat{t}) = \hat{P}\big(\hat{X}, \hat{Y}, \hat{t}\big). \tag{7.11}$$

where $(\hat{x}, \hat{y})$and $(\hat{u}, \hat{v})$ are coordinates and velocity in wave frame $(\hat{X}, \hat{Y})$and $(\hat{U}, \hat{V})$ are coordinate and velocity in fixed frame.

$$u = \frac{\hat{u}}{\mathfrak{c}}, \quad x = \frac{\hat{x}}{\lambda}, \quad v = \frac{\lambda\,\hat{v}}{l\mathfrak{c}}, \quad y = \frac{\hat{y}}{l},$$
$$p = \frac{l^2\,\hat{p}}{\mathfrak{c}\lambda\mu}, \quad t = \frac{\mathfrak{c}\,\hat{t}}{\lambda}, \quad h = \frac{L}{l}, \quad \theta = \frac{\hat{T} - T_0}{T_0}. \tag{7.12}$$

The dimensionless form of mixed convective magnetohydrodynamic flow of Carreau fluid is governed by the following equations

$$\frac{\partial u}{\partial x} + \frac{\partial v}{\partial y} = 0, \tag{7.13}$$

$$Re\beta\left(u\frac{\partial u}{\partial x} + v\frac{\partial u}{\partial y}\right) = -\frac{\partial p}{\partial x} + \beta\frac{\partial S_{xx}}{\partial x} + \frac{\partial S_{xy}}{\partial y} - \mathcal{M}^2(u+1) + Gr\theta, \tag{7.14}$$

$$Re\beta^3\left(u\frac{\partial v}{\partial x} + v\frac{\partial v}{\partial y}\right) = -\frac{\partial p}{\partial y} + \beta^2\frac{\partial S_{yx}}{\partial x} + \beta\frac{\partial S_{yy}}{\partial y}, \tag{7.15}$$

$$Re\beta\left(u\frac{\partial\theta}{\partial x}+v\frac{\partial\theta}{\partial y}\right)=\frac{1}{Pr}\left(\beta^2\frac{\partial^2\theta}{\partial x^2}+\frac{\partial^2\theta}{\partial y^2}\right)+Ec\begin{pmatrix}\beta S_{xx}\frac{\partial u}{\partial x}+\beta^2 S_{xy}\frac{\partial v}{\partial y}\\+S_{yx}\frac{\partial u}{\partial y}+\beta S_{yy}\frac{\partial v}{\partial y}\end{pmatrix}, \quad (7.16)$$

where

$$S_{xx}=2\beta\left(1+\frac{n-1}{2}We^2\left(\frac{\partial u}{\partial x}\right)^2\right)\frac{\partial u}{\partial x}, \quad (7.17)$$

$$S_{xy}=S_{yx}=\left(1+\frac{n-1}{2}We^2\left(\frac{\partial u}{\partial y}+\beta^2\frac{\partial v}{\partial x}\right)^2\right)\left(\frac{\partial u}{\partial y}+\beta^2\frac{\partial v}{\partial x}\right), \quad (7.18)$$

$$S_{yy}=2\beta\left(1+\frac{n-1}{2}We^2\left(\frac{\partial v}{\partial y}\right)^2\right)\frac{\partial v}{\partial y}. \quad (7.19)$$

In above equation the dimensionless parameters β (wave number), Re (Reynolds number), We (Weissenberg number), $\mathcal{M}$ (Hartmann number), Pr (Prandtl number), Gr (Grashof number) and Ec (Eckert number) are defined as follows

$$\beta=\frac{l}{\lambda},\ \ Re=\frac{\rho c l}{\mu},\ \ We=\frac{n c}{l},\ \ \mathcal{M}^2=\frac{\sigma {B_0}^2 l^2}{\mu},$$
$$Pr=\frac{\mu c_p}{k_1},\ \ E_c=\frac{c^2}{c_p T_0},\ \ Gr=\frac{l^2\rho g\beta_1 T_0}{c\mu},\ \ Br=PrE_c\,. \quad (7.20)$$

Considering the long wavelength $\beta\ll 1$ and low Reynolds number $Re\to 0$ assumption, Eq. (7.14)-(7.19) reduce into following form

$$\frac{\partial p}{\partial x}=\frac{\partial S_{xy}}{\partial y}-\mathcal{M}^2(u+1)+Gr\theta, \quad (7.21)$$

$$\frac{\partial p}{\partial y}=0, \quad (7.22)$$

$$\frac{\partial^2\theta}{\partial y^2}=-BrS_{yx}\frac{\partial u}{\partial y}, \quad (7.23)$$

in which

$$S_{xx}=0,\ \ S_{yy}=0, \quad (7.24)$$

$$S_{xy}=S_{yx}=\left(1+\frac{n-1}{2}We^2\left(\frac{\partial u}{\partial y}\right)^2\right)\frac{\partial u}{\partial y}. \quad (7.25)$$

Incorporating Eq. (7.25) into Eq. (7.21) and (7.23), following form can be obtained

$$\frac{\partial p}{\partial x}=\frac{\partial^2 u}{\partial y^2}+\frac{3(n-1)}{2}We^2\left(\frac{\partial u}{\partial y}\right)^2\frac{\partial^2 u}{\partial y^2}-\mathcal{M}^2(u+1)+Gr\theta, \quad (7.26)$$

$$\frac{\partial^2\theta}{\partial y^2} = -Br\left(\left(\frac{\partial u}{\partial y}\right)^2 + \frac{n-1}{2}We^2\left(\frac{\partial u}{\partial y}\right)^4\right), \tag{7.27}$$

The non-dimensional form of boundary conditions are

$$\frac{\partial u}{\partial y} = 0, \quad \frac{\partial \theta}{\partial y} = 0, \quad \text{at} \quad y = 0, \tag{7.28}$$

$$u = -1 - 2\pi\varepsilon\alpha\beta\cos(2\pi x), \quad \theta = 0,$$
$$y = h = 1 + \varepsilon\sin(2\pi x). \tag{7.29}$$

7.2 Solution Methodology

Eq. (7.26) and Eq. (7.27) depends upon each other, therefore we will simultaneously solve these equation by Adomian decomposition method

$$u(x,y) = f(x,y)$$
$$+L^{-1}(\mathcal{M}^2(u+1) - Gr\theta) - L^{-1}\left(\frac{3(n-1)}{2}We^2\left(\frac{\partial u}{\partial y}\right)^2\frac{\partial^2 u}{\partial y^2}\right), \tag{7.30}$$

$$\theta = c_3 y + c_4 + L^{-1}\left(\left(-Br\left(\left(\frac{\partial u}{\partial y}\right)^2 + \frac{n-1}{2}We^2\left(\frac{\partial u}{\partial y}\right)^4\right)\right)\right), \tag{7.31}$$

where $L^{-1}$is defined as

$$L^{-1}(.) = \iint (.)dy, \tag{7.32}$$

and

$$f(x,y) = \frac{dp}{dx}\frac{y^2}{2} + c_1 y + c_2, \tag{7.33}$$

where c_1, c_2, c_3 and c_4 are integration constant and can be extracted by the aid of boundary conditions which are given in Eq. (7.28) and Eq. (7.29). The linear terms $u(x,y)$ and $\theta(x,y)$ are decomposed in terms of infinite series as follows

$$u(x,y) = \sum_{m=0}^{\infty} u_m(x,y), \quad \theta(x,y) = \sum_{m=0}^{\infty} \theta_m(x,y), \tag{7.34}$$

and the non-linear terms can be decomposed into infinite series of Adomian polynomials, which satisfy

$$A_m = \frac{1}{m!}\frac{d^m}{d\lambda^m}\left[N\left(\sum_{i=0}^{\infty}\lambda_i u_i\right)\right]_{\lambda=0}, \quad m = 0, 1, 2, 3, \ldots, \tag{7.35}$$

where the non-linear term represented by Nu is as follow

$$Nu = \frac{3(n-1)}{2} We^2 \left(\frac{\partial u}{\partial y}\right)^2 \frac{\partial^2 u}{\partial y^2}. \tag{7.36}$$

Pushing Eq. (7.34) into Eq. (7.30) & Eq. (7.31) and using the boundary conditions (7.28) and (7.29), one can get

$$u_0 = u(h) + \frac{y^2 - h^2}{2}\frac{dp}{dx}, \tag{7.37}$$

$$\theta_0 = -Br\left(\frac{dp}{dx}\right)^2 \left(\frac{y^4 - h^4}{12} + \frac{n-1}{2} We^2 \frac{y^6 - h^6}{30}\left(\frac{dp}{dx}\right)^2\right). \tag{7.38}$$

The other terms of the series can be obtain from the following recursive relation

$$\begin{aligned} u_{m+1} = B_n + L^{-1}\left(\mathcal{M}^2(u_m + Gr\theta_m)\right) \\ -L^{-1}\left(\frac{3(n-1)}{2} We^2 \left(\frac{\partial u_m}{\partial y}\right)^2 \frac{\partial^2 u_m}{\partial y^2}\right), \text{ for } m \geq 0, \end{aligned} \tag{7.39}$$

$$\theta_m = D_n + L^{-1}\left(-Br\left(\left(\frac{\partial u_m}{\partial y}\right)^2 + \frac{n-1}{2} We^2 \left(\frac{\partial u_m}{\partial y}\right)^4\right)\right), \tag{7.40}$$

for $m = 0, 1, 2, \ldots$
Where

$$B_n = b_1(x) + y b_2(x), \tag{7.41}$$

$$D_n = d_1(x) + y d_2(x), \tag{7.42}$$

b_1, b_2, d_1 and d_2 are integration's constants and evaluated from the given conditions. The solution for horizontal velocity and temperature profile can be found as

$$u = u_0 + u_1 + \cdots, \tag{7.43}$$

$$\theta = \theta_0 + \theta_1 + \cdots, \tag{7.44}$$

Now the volumetric flow rate Q is related to the flux F by the following relation

$$Q = \int_0^h (u+1)dy = F + h, \tag{7.45}$$

and time mean volumetric flow rate $\hat{Q}$ in a fixed frame is related as

$$\hat{Q} = \frac{1}{T}\int_0^h (F+h)d\hat{t} = \int_0^1 (F+h)dx = F + 1\,. \tag{7.46}$$

$$\hat{Q} = F + 1 \text{ or } F = \hat{Q} - 1. \tag{7.47}$$

With the aid of Eq. (7.43) and Eq. (7.45) pressure gradient $\frac{dp}{dx}$ can be obtained interms

of mean flow rate $\hat{Q}$. The value of $\frac{dp}{dx}$ is obtained by software "MATHEMATICA" which is graphically illustrated in Fig. 7.3.

By integrating the expression of pressure gradient, one can get the pressure rise as

$$\Delta p = \int_0^1 \frac{dp}{dx} dx. \tag{7.48}$$

7.3 Results and Discussion

In this research mathematical modelling and computation for thermal analysis of mucus flow due to ciliary movement has been made. The mucus rheology is described by the Carreau fluid model. The flow characteristics of mucus are simulated by the velocity field, temperature field and pressure distribution. The mixed convection is utilized to analyze the thermal analysis of the flow field that will arise due to temperature differences of the fluid and the environment. This part of the research is focused to the discussions of different parameters of physical interest like pressure gradient, pressure rise (drop), velocity and heat transfer. In this section, we will analyze the impact of the Carreau fluid parameter We, power law index n, the magnetic parameter $\mathcal{M}$, the thermal Grashof number Gr. The values of other parameters are kept fixed throughout the study, and these parameters with their values are $\alpha = 0.4$, $\beta = 0.4$, $\hat{Q} = 0.5$, $\epsilon = 0.3$.

Pressure rise and pressure gradient

Pressure rise against volume flux are presented in Fig. 7.2a-d. It is depicted from the graphs that pressure rise attains free pumping at $\hat{Q} = 0$ and decreases with the increase in $\mathcal{M}$ for $0 < \hat{Q} < 1$ whereas increases for $\hat{Q} < 0$. Weissenberg number and power law index show that pressure rise attains the free pumping in the region $0.05 < \hat{Q} < 0.25$ and increases for $\hat{Q} > 0.25$. Increasing values of Gr show that pressure rise increases in the whole pumping region.

Consequences of various values of $\mathcal{M}$, We, n and Gr on the pressure gradient are represented in Fig.7.3a-d. It is found that $\frac{dp}{dx}$ reduces at the entrance, middle and exit region of the channel as we increase $\mathcal{M}$, We and n and opposite behavior can be seen for increasing values of Gr. The impact of magnetic parameter $\mathcal{M}$ on the pressure gradient shows that magnetic field helps to increase the favourable pressure gradient for the flow of highly viscous mucus. The impact of Weissenberg number *We* on the

pressure gradient illustrates that favorable pressure gradient increases by the increasing value of shear rate and relaxation time, i.e. when viscous effects are dominant over the elastic effect then favorable pressure gradient mounts. It can also be observed that for shear thickening $n > 1$ of the mucus favorable pressure gradient increases. It is also observed that $\mathcal{M}$, We and n show the significant variation on the entrance and exit of the channel when compared with middle of channel. The increasing values of Gr help to decrease the favorable pressure gradient for the convective flow of mucus.

Velocity profile

The impacts of $\mathcal{M}$, We, n and Gr on velocity profile are represented in Fig. 7.4a-d. It is found that axial velocity is maximum at the middle of channel. Impact of magnetic field $\mathcal{M}$ on axial velocity shows that magnitude of velocity increases as the strength of magnetic field increases, physically it represents that the magnetic field can be used to control the flow of viscous fluid. Figure 7.4b-d indicate that increasing value of We, n and Gr show the significant change in velocity profile at the center of the channel. The increasing values of We reduces the magnitude of velocity profile as shear rate and relaxation time make the fluid thick due to cold environment. The increasing values of power law index $n > 1$ make the mucus more consistent which reduces the magnitude of the velocity profile. The increasing values of Grashof number Gr make the fluid thick as buoyancy forces due to temperature difference are dominant over the viscous forces, therefore magnitude of the axial velocity decreases and flow rate become slow.

Temperature profile

Effects of $\mathcal{M}$, We, n and Br on temperature profile are represented in Fig 7.5a-d which show that magnetic field tends to decelerate the flow and causes to rise in temperature profile and as a result heat transfer through mucus flow increases with the increase in We and n. It is depicted that temperature profile rises with the increase in Br (Brinkman number) which is the product of Eckert and Prandtl number and shows that when the value of Brinkman number Br is less than one temperature difference is dominant over viscous effect. Here Br =0.1, 0.2, 0.3 show that as the effect of viscosity over temperature difference become prominent then the convection process become fast due to closure of molecules and heat transfer increases.

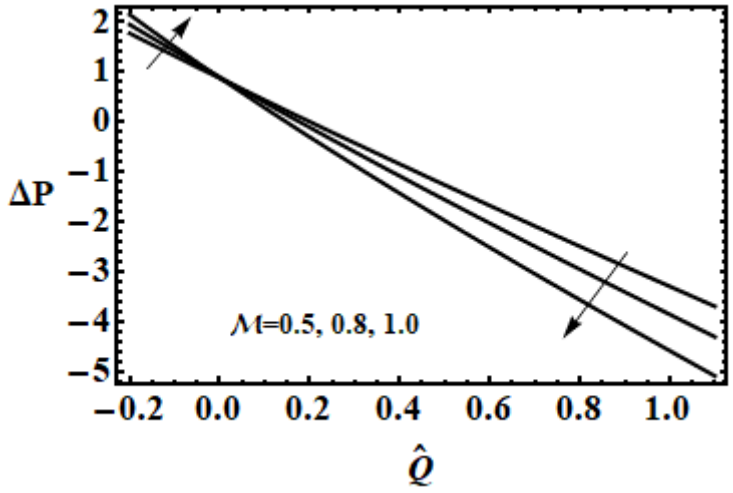

Fig. 7.2a: The effect of Hartmann number $\mathcal{M}$ on pressure rise for $\alpha = 0.4,\ \beta = 0.4,$ $\hat{Q} = 0.5,\ \epsilon = 0.3.$

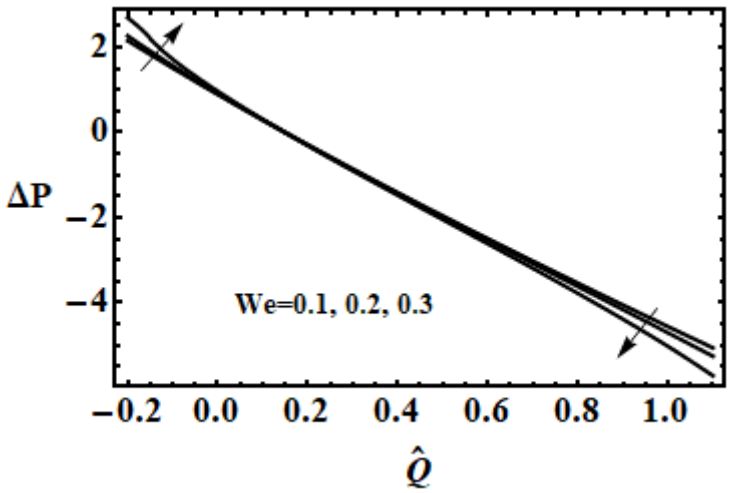

Fig. 7.2b: The effect of Weissenberg number We on pressure rise for $\alpha = 0.4,\ \beta = 0.4,\ \hat{Q} = 0.5,\ \epsilon = 0.3.$

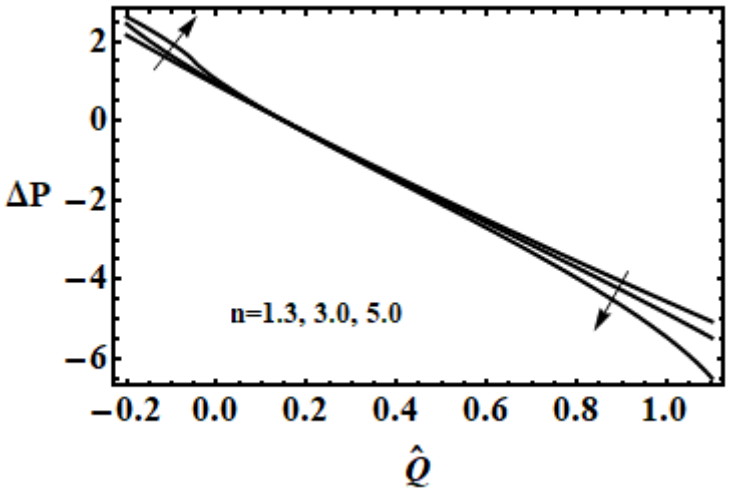

Fig. 7.2c: The effect of power law index n on pressure rise for $\alpha = 0.4,\ \beta = 0.4,$ $\hat{Q} = 0.5,\ \epsilon = 0.3.$

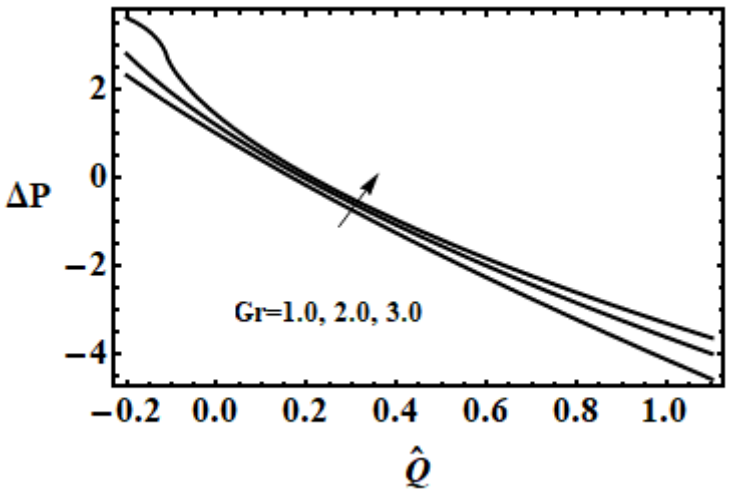

Fig. 7.2d: The effect of Grashof number Gr on pressure rise for $\alpha = 0.4,\ \beta = 0.4,$ $\hat{Q} = 0.5,\ \epsilon = 0.3.$

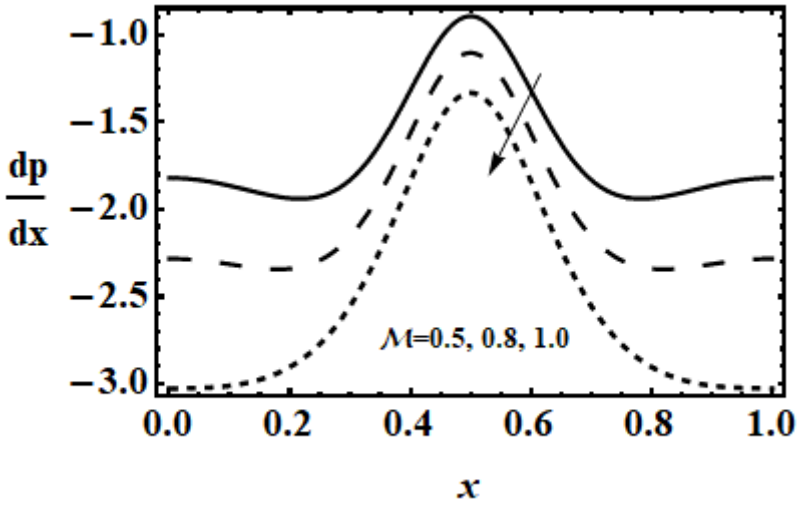

Fig. 7.3a: The effect of Hartmann number $\mathcal{M}$ on pressure gradient for $\alpha = 0.4,\ \beta = 0.4, \hat{Q} = 0.5,\ \epsilon = 0.3$.

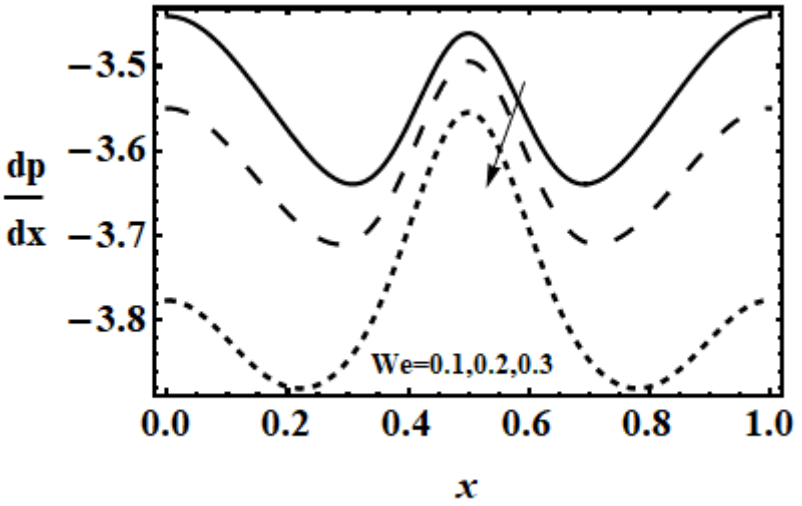

Fig. 7.3b: The effect of Weissenberg number We on pressure gradient for $\alpha = 0.4$, $\beta = 0.4, \hat{Q} = 0.5,\ \epsilon = 0.3$.

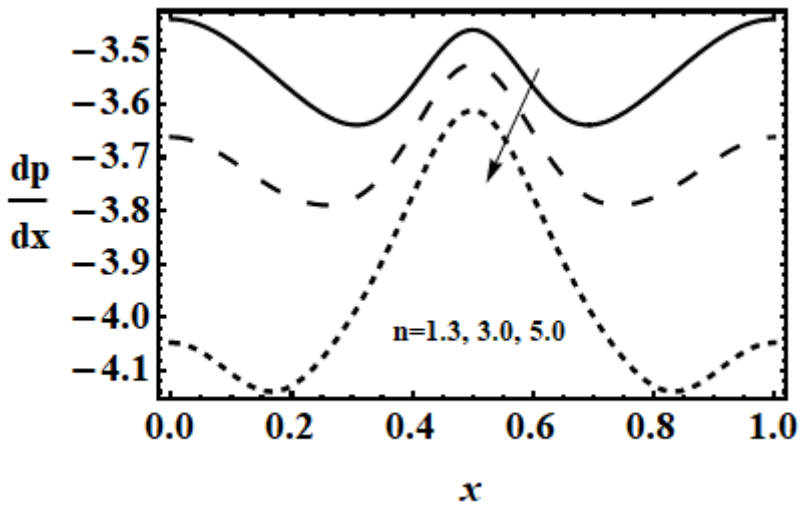

Fig. 7.3c: The effect of Power law index n on pressure gradient for $\alpha = 0.4,\ \beta = 0.4, \hat{Q} = 0.5,\ \epsilon = 0.3$.

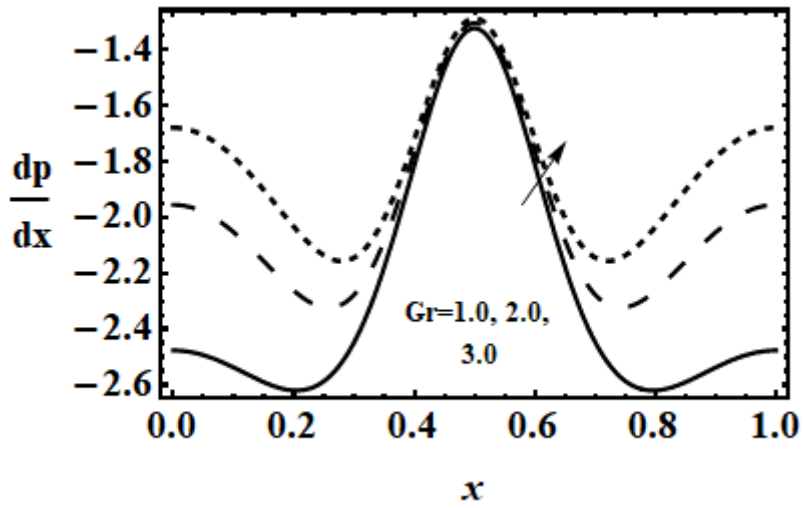

Fig. 7.3d: The effect of Grashof number Gr on pressure gradient for $\alpha = 0.4,\ \beta = 0.4, \hat{Q} = 0.5,\ \epsilon = 0.3$.

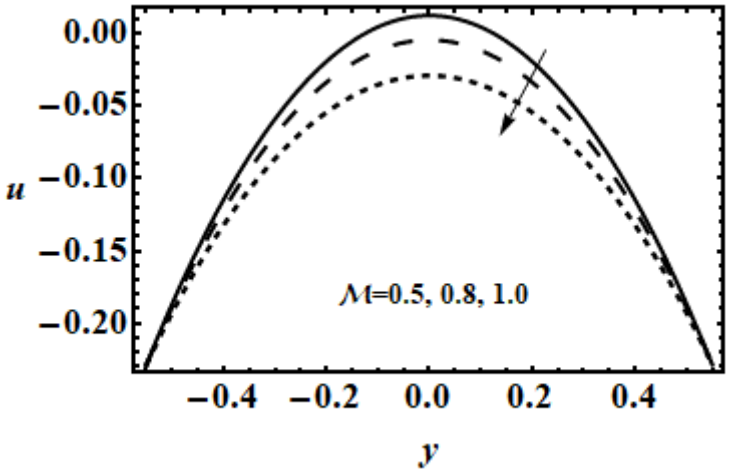

Fig. 7.4a: The effect of Hartmann number $\mathcal{M}$ on velocity for $\alpha = 0.4,\ \beta = 0.4, \hat{Q} = 0.5,\ \epsilon = 0.3$.

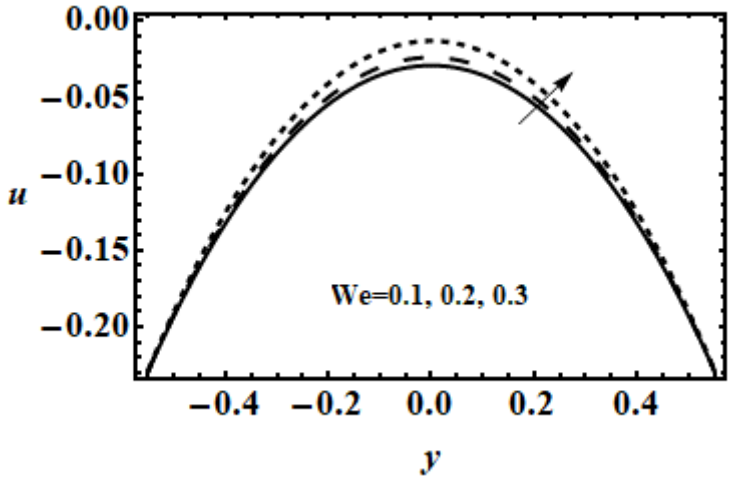

Fig. 7.4b: The effect of Weissenberg number We on velocity for $\alpha = 0.4,\ \beta = 0.4, \hat{Q} = 0.5,\ \epsilon = 0.3$.

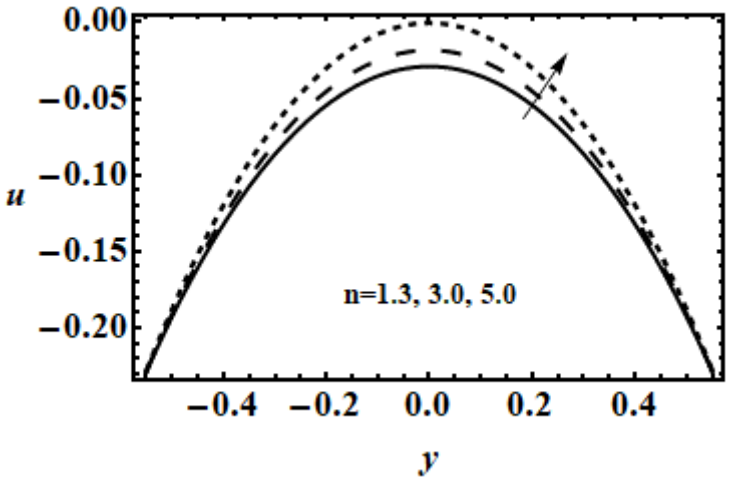

Fig. 7.4c: The effect of Power law index n on velocity for $\alpha = 0.4,\ \beta = 0.4, \hat{Q} = 0.5,\ \epsilon = 0.3$.

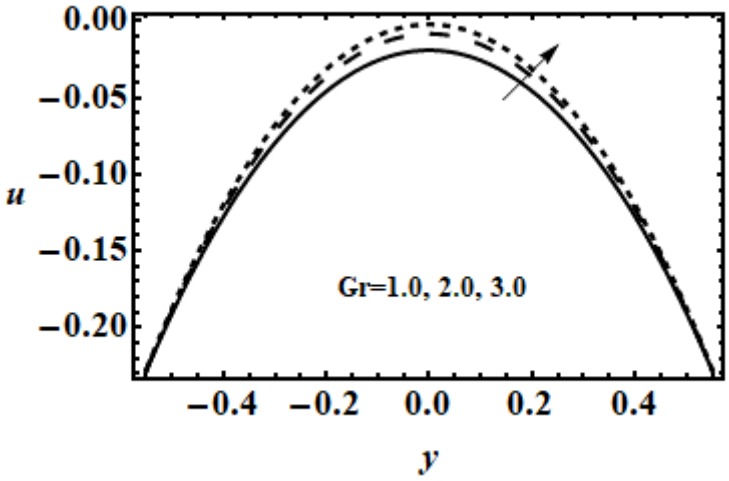

Fig. 7.4d: The effect of Grashof number Gr on velocity for $\alpha = 0.4,\ \beta = 0.4, \hat{Q} = 0.5,\ \epsilon = 0.3$.

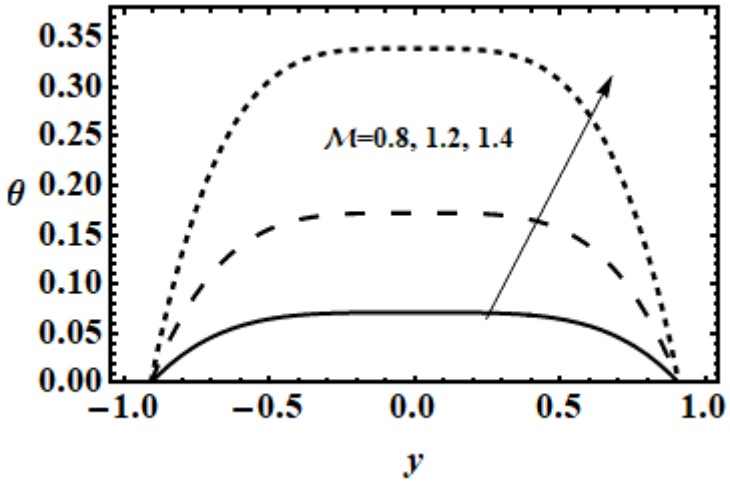

Fig. 7.5a: The effect of Hartmann number $\mathcal{M}$ on temperature profile for $\alpha = 0.4$, $\beta = 0.4, \hat{Q} = 0.5,\ \epsilon = 0.3$.

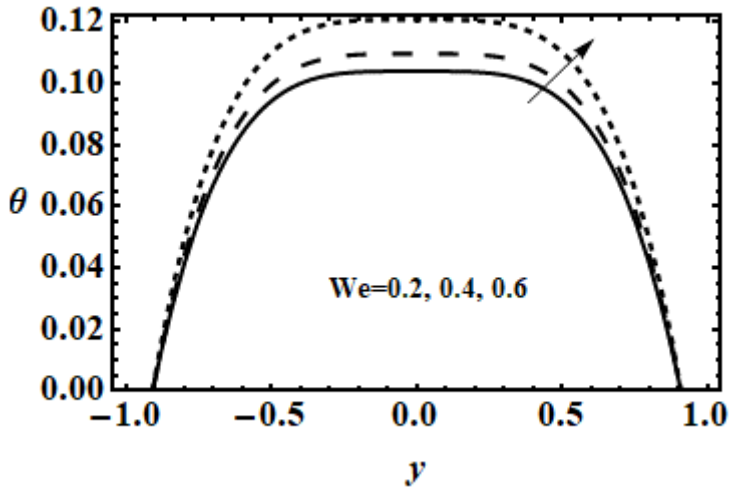

Fig. 7.5b: The effect of Weissenberg number We on temperature profile for $\alpha = 0.4$, $\beta = 0.4, \hat{Q} = 0.5,\ \epsilon = 0.3$.

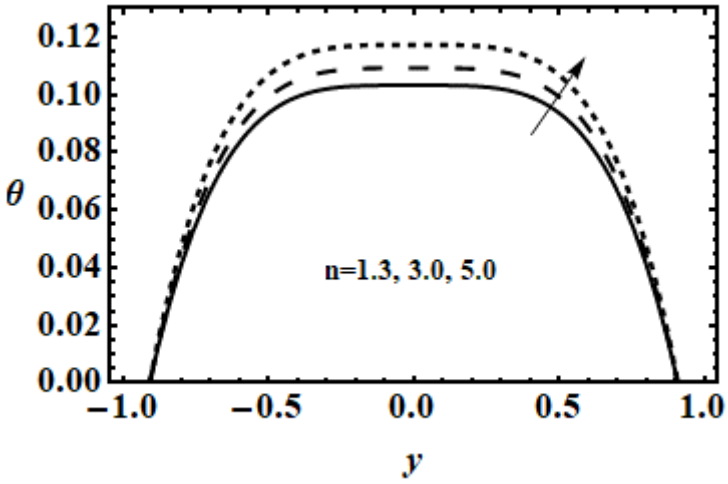

Fig. 7.5c: The effect of Power law index n on temperature profile for $\alpha = 0.4,\ \beta = 0.4, \hat{Q} = 0.5,\ \epsilon = 0.3$.

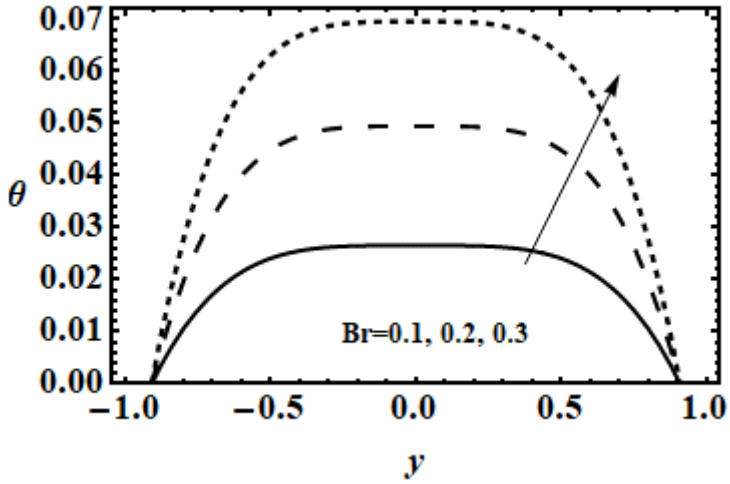

Fig. 7.5d: The effect of Brinkman Br on temperature profile for $\alpha = 0.4,\ \beta = 0.4, \hat{Q} = 0.5,\ \epsilon = 0.3$.

7.4 Conclusion

The mathematical study has been presented for muco ciliary flow affected by the surrounding temperature in the presence of magnetic field. In this research for muco ciliary flow we have considered mixed convective flow of MHD Carreau fluid through a ciliated channel under the action of applied magnetic field. The flow is produced due to effective stroke of metachoronal wave generated by the tip of cilia. The non-dimensional moving boundary value problem is solved by semi analytic technique, Adomian decomposition method and software "MATHEMATICA". The present study shows that results of Siddiqui et al. [43] can be deduced if $We \to 0, Br \to 0$, and $Gr \to 0$ which guarantees that our study is correct. The main findings of this research are summarized as follows:

- Pressure rise reduces with the increasing value of Hartmann number and increases due to Grashof number.
- Favorable pressure gradient increases by the increasing values of Hartmann number $\mathcal{M}$, Weissenberg number We, power law index n and Grashof number Gr.
- Magnitude of the axial velocity decreases by the increasing value of We, Gr and n but increases for the increasing values of $\mathcal{M}$.
- Temperature profile increases by increasing magnetic strength $\mathcal{M}$, Weissenberg number We, power law index n and Brinkman number Br.
- The present research can be beneficial for the designing of artificial cilia that help to propel the viscous fluid. Also, magnetic field effect decelerate and heat transfer effect (Grashof number) significantly accelerates the mucus flow, heat transfer assists whereas magnetic field resists the ciliary induced flow. The current study has neglected porous medium and thermophoresis effect which are also important in biofluid.

Chapter 8

Hall and Ion-slip Effect on Convective Flow of Carreau Fluid in a Ciliated Tube with Ohmic Heating

This study investigates the Carreau fluid flow and heat transfer through a ciliated tube with the effects of Hall current, ionslip and ohmic heating. Mathematical modelling is done using the long wavelength and small Reynolds number approximation. The non-linear momentum equation with Hall and ionslip effect and the non-homogeneous energy equation due to viscous dissipation and ohmic heating effect are solved by Homotopy perturbation method which are solved by software Mathematica. Impact of Hall and Ionslip effect show an increase in velocity profile and the pressure gradient, also performance of thermal energy enhances with the rise in magnetic parameter and power law index of Carreau fluid. Variation of velocity and temperature profile are observed by the graphical result plotted in software "Mathematica".

8.1 Mathematical Formulation

Consider the forced convective Carreau fluid flow in two dimensional axisymmetric tube of length L. The walls of the tube are ciliated internally which causes the fluid flow (due to flogging of cilia) by generating the metachronal wave with the wave speed ƈ and wavelength λ. The shape of the sinusoidal waves in laboratory frame is defined through the following expressions

$$\hat{R} = H(\hat{Z}, \hat{t}) = \pm\left[l + \varepsilon l cos\left(\frac{2\pi}{\lambda}\right)(\hat{Z} - c\hat{t})\right], \tag{8.1}$$

$$\hat{Z} = F(\hat{Z}, \hat{t}) = Z_0 + \varepsilon l \alpha sin\left(\frac{2\pi}{\lambda}\right)(\hat{Z} - c\hat{t}). \tag{8.2}$$

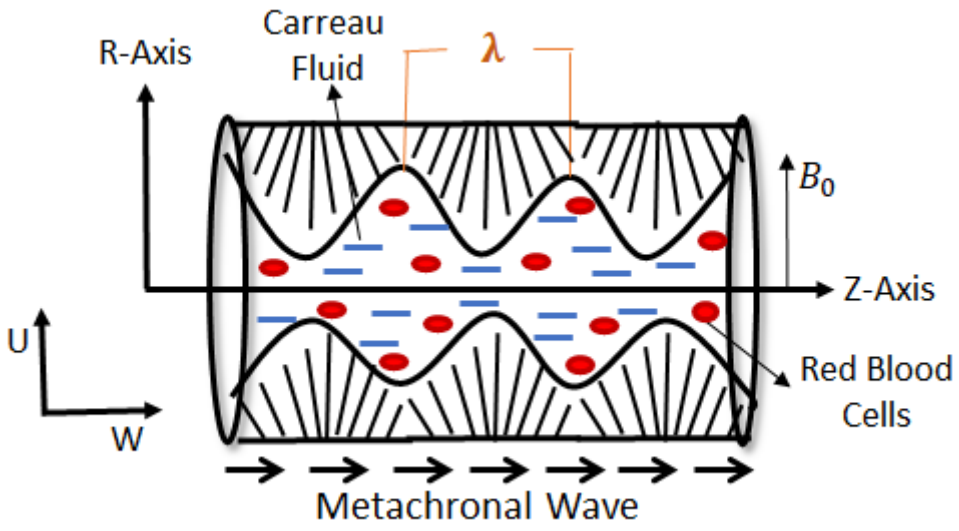

Fig. 8.1: Geometry of problem

Moreover, the tube walls are presumed to be conducted with constant temperature T_0. To detect the plasma (Carreau fluid) flow in a ciliated tube a strong magnetic field is exerted normal to the flow. The shear stress near the tip of cilia is measured by the momentum equation and Lorentz force due to Hall effect that can be calculated from generalized Ohm's law.

$$\boldsymbol{J} = \sigma(\boldsymbol{E} + \boldsymbol{V} \times \boldsymbol{B}) - \frac{\beta_e}{B_0}(\boldsymbol{J} \times \boldsymbol{B}) + \frac{\beta_e \beta_i}{B_0}\big((\boldsymbol{J} \times \boldsymbol{B}) \times \boldsymbol{B}\big), \tag{8.3}$$

$$\boldsymbol{J} \times \boldsymbol{B} = -\frac{\sigma {B_0}^2}{{\alpha_e}^2 + {\beta_e}^2}\Big(\big(\alpha_e \hat{U} + \beta_e \hat{W}\big)\boldsymbol{e_r} + \big(\alpha_e \hat{W} - \beta_e \hat{U}\big)\boldsymbol{e_z}\Big), \tag{8.4}$$

$$\boldsymbol{J}.\boldsymbol{J} = \frac{\sigma^2 {B_0}^2}{{\alpha_e}^2 + {\beta_e}^2}\big(\hat{U}^2 + \hat{W}^2\big), \tag{8.5}$$

where $\beta_e = w_e \tau_e$ and $\alpha_e = 1 + \beta_e \beta_i$.

The momentum and energy equations for the forced convective flow of Carreau fluid [88]

$$\frac{\partial \hat{U}}{\partial \hat{R}} + \frac{\hat{U}}{\hat{R}} + \frac{\partial \hat{W}}{\partial \hat{Z}} = 0, \tag{8.6}$$

$$\rho\left(\frac{\partial \hat{U}}{\partial t} + \hat{U}\frac{\partial \hat{U}}{\partial \hat{R}} + \hat{W}\frac{\partial \hat{U}}{\partial \hat{Z}}\right) = -\frac{\partial \hat{P}}{\partial \hat{R}} + \frac{1}{\hat{R}}\frac{\partial\big(R\hat{S}_{\hat{R}\hat{R}}\big)}{\partial \hat{R}} + \frac{\partial \hat{S}_{\hat{R}\hat{Z}}}{\partial \hat{Z}} - \frac{\hat{S}_{\theta\theta}}{\hat{R}} - \frac{\sigma {B_0}^2}{{\alpha_e}^2 + {\beta_e}^2}\big(\alpha_e \hat{U} + \beta_e \hat{W}\big), \tag{8.7}$$

$$\rho\left(\frac{\partial \hat{W}}{\partial \hat{t}} + \hat{U}\frac{\partial \hat{W}}{\partial \hat{R}} + \hat{W}\frac{\partial \hat{W}}{\partial \hat{Z}}\right) = -\frac{\partial P}{\partial \hat{Z}} + \frac{1}{\hat{R}}\frac{\partial\big(R\hat{S}_{\hat{R}\hat{R}}\big)}{\partial \hat{R}} + \frac{\partial \hat{S}_{\hat{R}\hat{Z}}}{\partial \hat{Z}} - \frac{\sigma {B_0}^2}{{\alpha_e}^2 + {\beta_e}^2}\big(\alpha_e \hat{W} - \beta_e \hat{U}\big), \tag{8.8}$$

$$\rho c_p\left(\frac{\partial \hat{T}}{\partial \hat{t}}+\hat{U}\frac{\partial \hat{T}}{\partial \hat{R}}+\hat{W}\frac{\partial \hat{T}}{\partial \hat{Z}}\right)=k\left(\frac{\partial^2 \hat{T}}{\partial \hat{R}^2}+\frac{1}{\hat{R}}\frac{\partial \hat{T}}{\partial \hat{R}}+\frac{\partial^2 \hat{T}}{\partial \hat{Z}^2}\right)+\hat{S}_{\hat{R}\hat{R}}\frac{\partial \hat{U}}{\partial \hat{R}}+\hat{S}_{\hat{R}\hat{Z}}\frac{\partial \hat{W}}{\partial \hat{R}}$$
$$+\hat{S}_{\hat{Z}\hat{R}}\frac{\partial \hat{U}}{\partial \hat{Z}}+\hat{S}_{\hat{Z}\hat{Z}}\frac{\partial \hat{W}}{\partial \hat{Z}}\quad+\frac{\alpha^2 {B_0}^2}{{\alpha_e}^2+{\beta_e}^2}\left(\hat{U}^2+\hat{W}^2\right). \quad (8.9)$$

where τ_{RR}, τ_{RZ}, τ_{ZR} and τ_{ZZ} are given by the following expression

$$\hat{S}_{\hat{R}\hat{R}}=2\left(1+\frac{n-1}{2}We^2\dot{\gamma}^2\right)\frac{\partial \hat{U}}{\partial \hat{R}}, \quad (8.10)$$

$$\hat{S}_{\hat{R}\hat{Z}}=\hat{S}_{\hat{Z}\hat{R}}=\left(1+\frac{n-1}{2}We^2\dot{\gamma}^2\right)\left(\frac{\partial \hat{U}}{\partial \hat{Z}}+\frac{\partial \hat{W}}{\partial \hat{R}}\right), \quad (8.11)$$

$$\hat{S}_{\hat{Z}\hat{Z}}=2\left(1+\frac{n-1}{2}We^2\dot{\gamma}^2\right)\frac{\partial \hat{W}}{\partial \hat{Z}}, \quad (8.12)$$

$$\dot{\gamma}^2=2\left(\frac{\partial \hat{U}}{\partial \hat{R}}\right)^2+2\left(\frac{\partial \hat{W}}{\partial \hat{Z}}\right)^2+\left(\frac{\partial \hat{U}}{\partial \hat{Z}}+\frac{\partial \hat{W}}{\partial \hat{R}}\right)^2. \quad (8.13)$$

The transformation from fixed to wave frame by using Galilean transformation are given by

$$\hat{r}=R,\ \ \hat{u}=\hat{U},\ \ \hat{z}=\hat{Z}-\mathfrak{c}\hat{t},\ \ \hat{w}=\hat{W}-\mathfrak{c},\ \ \hat{p}(\hat{r},\hat{z},\hat{t})=\hat{P}\left(\hat{R},\hat{Z},\hat{t}\right). \quad (8.14)$$

The following non-dimensional variables are used in Eqs. (8.6)-(8.13).

$$r=\frac{\hat{r}}{l},\ \ u=\frac{\lambda \hat{u}}{l\mathfrak{c}},\ \ z=\frac{\hat{z}}{\lambda},\ \ w=\frac{\hat{w}}{\mathfrak{c}},$$
$$t=\frac{c\hat{t}}{\lambda},\ \ h=\frac{L}{l},\ \ p=\frac{l^2\,\hat{p}}{\mathfrak{c}\lambda\mu},\ \ \beta=\frac{l}{\lambda},$$
$$Re=\frac{\rho \mathfrak{c} l}{\mu},\ \ \mathcal{M}^2=\frac{\sigma {B_0}^2 l^2}{\mu},\ \ E_c=\frac{\mathfrak{c}^2}{c_p T_0},$$
$$Pr=\frac{\mu c_p}{k_1},\ \ Br=PrE_c,\ \ \theta=\frac{\hat{T}-T_0}{T_0}. \quad (8.15)$$

The non-dimensional form of Eqs. (8.6)-(8.13) are as follows

$$\frac{\partial u}{\partial r}+\frac{u}{r}+\frac{\partial w}{\partial z}=0, \quad (8.16)$$

$$\beta^2 Re\left(u\frac{\partial u}{\partial r}+w\frac{\partial u}{\partial z}\right)=-\frac{\partial p}{\partial r}-\beta\frac{1}{r}\frac{\partial (rS_{rr})}{\partial r}-\beta^2\frac{\partial S_{rz}}{\partial z}+\beta\frac{S_{\theta\theta}}{r}$$
$$-\frac{\mathcal{M}^2\beta}{{\alpha_e}^2+{\beta_e}^2}\left(\beta\alpha_e u+\beta_e(w+1)\right), \quad (8.17)$$

$$Re\left(u\frac{\partial u}{\partial r}+w\frac{\partial u}{\partial z}\right)=-\frac{\partial p}{\partial z}-\frac{1}{r}\frac{\partial (rS_{rz})}{\partial r}-\beta\frac{\partial S_{zz}}{\partial z}-\frac{\mathcal{M}^2}{{\alpha_e}^2+{\beta_e}^2}(\alpha_e(w+1)-\beta\beta_e u), \quad (8.18)$$

$$RePr\beta\left(u\frac{\partial\theta}{\partial r}+w\frac{\partial\theta}{\partial z}\right)=\left(\frac{\partial^2\theta}{\partial r^2}+\frac{1}{r}\frac{\partial\theta}{\partial r}+\beta^2\frac{\partial^2\theta}{\partial z^2}\right)+Br\beta\begin{pmatrix}S_{rr}\frac{\partial u}{\partial r}+\frac{1}{\beta}S_{rz}\frac{\partial w}{\partial r}\\+S_{zr}\frac{\partial u}{\partial z}+S_{zz}\frac{\partial w}{\partial z}\end{pmatrix}$$

$$+\frac{Br\mathcal{M}^2}{{\alpha_e}^2+{\beta_e}^2}(\beta^2u^2+(w+1)^2). \tag{8.19}$$

in which

$$S_{rr}=-2\beta\left(1+\frac{n-1}{2}We^2\dot{\gamma}^2\right)\frac{\partial u}{\partial r}, \tag{8.20}$$

$$S_{rz}=S_{zr}=-\left(1+\frac{n-1}{2}We^2\dot{\gamma}^2\right)\left(\beta^2\frac{\partial u}{\partial z}+\frac{\partial w}{\partial r}\right), \tag{8.21}$$

$$S_{zz}=-2\beta\left(1+\frac{n-1}{2}We^2\dot{\gamma}^2\right)\frac{\partial w}{\partial z}, \tag{8.22}$$

$$\dot{\gamma}^2=2\left(\beta\frac{\partial u}{\partial r}\right)^2+2\left(\beta\frac{\partial w}{\partial z}\right)^2+\left(\beta^2\frac{\partial u}{\partial z}+\frac{\partial w}{\partial r}\right)^2. \tag{8.23}$$

Where the wave number β, Weissenberg number We, Reynolds number Re, Hartmann number $\mathcal{M}$, Eckert number Ec and Prandtl number Pr are the dimensionless numbers defined in Eq. (8.15). Incorporating the approximation of long wave length and small Reynolds number ($\lambda\to\infty,\ Re\to 0$), Eq. (8.16)-(8.23) takes the following form

$$\frac{\partial p}{\partial r}=0, \tag{8.24}$$

$$\frac{\partial p}{\partial z}=-\frac{1}{r}\frac{\partial(rS_{rz})}{\partial r}-\frac{\mathcal{M}^2\alpha_e}{{\alpha_e}^2+{\beta_e}^2}(w+1), \tag{8.25}$$

$$\left(\frac{\partial^2\theta}{\partial r^2}+\frac{1}{r}\frac{\partial\theta}{\partial r}\right)=Br\left(S_{rz}\frac{\partial w}{\partial r}\right)+\frac{Br\mathcal{M}^2}{{\alpha_e}^2+{\beta_e}^2}(w+1)^2+Br\left(\frac{\partial w}{\partial r}\right)^2, \tag{8.26}$$

where

$$S_{rz}=-\left(1+\frac{n-1}{2}We^2\dot{\gamma}^2\right)\frac{\partial w}{\partial r}, \tag{8.27}$$

and

$$\dot{\gamma}^2=\left(\frac{\partial w}{\partial r}\right)^2. \tag{8.28}$$

The non-dimensional geometry of the wave is as follow

$$r=h=1+\varepsilon\cos(2\pi z), \tag{8.31}$$

and the associated boundary conditions can be emerge as

$$w(h)=-1-2\pi\varepsilon\alpha\beta\cos(2\pi z),$$

$$u(h)=2\pi\varepsilon\sin(2\pi z)+\beta(2\pi\varepsilon)^2\alpha\sin(2\pi z)\cos(2\pi z),\ \theta(h)=0,$$

$$\frac{\partial w}{\partial r} = 0, \quad \frac{\partial \theta}{\partial r} = 0, \quad at \quad r = 0. \tag{8.32}$$

8.3 Solution of Problem

We have employed Homotopy perturbation method (**HPM**) to evaluate the transformed nonlinear problem defined in Eq. (8.29) under the boundary conditions given in Eq. (8.32). HPM starts with the initial approximation selected by possible unknown constants. Thus, we take the following approximation as an initial guess

$$u_0 = w(h) + \left(\frac{r^2 - h^2}{4}\right)\frac{dP}{dz}, \tag{8.33}$$

where $\frac{dP}{dz}$ is initial pressure gradient.

HPM takes the desire solution in terms of a formal power series by using embedding parameter as a "small parameter". The homotopy structure is expressed as follows

$$(1-q)(L[w(r,z)] - L[u_0(r,z)]) = q(L[w(r,z)] + N[w(r,z)] - g(z)), \tag{8.34}$$

where $q \in [0,1]$ is an embedding constant. Re-writing Eq. (8.29) with the aid of Eq. (8.34) as follows

$$(1-q)\left(\frac{1}{r}\frac{\partial}{\partial r}\left(r\frac{\partial w}{\partial r}\right) - \frac{1}{r}\frac{\partial}{\partial r}\left(r\frac{\partial u_0}{\partial r}\right)\right) = q\begin{pmatrix}\frac{1}{r}\frac{\partial}{\partial r}\left(r\frac{\partial w}{\partial r} + \frac{n-1}{2}We^2 r\left(\frac{\partial w}{\partial r}\right)^3\right) \\ -\frac{\mathcal{M}^2\alpha_e}{{\alpha_e}^2 + {\beta_e}^2}(w+1) - \frac{\partial p}{\partial z}\end{pmatrix}, \tag{8.35}$$

using

$$w = w_0 + qw_1 + q^2 w_2 + \cdots, \tag{8.36}$$

$$\theta = \theta_0 + q\theta_1 + q^2\theta_2 + \cdots, \tag{8.37}$$

$$\frac{\partial p}{\partial z} = \frac{\partial p_0}{\partial z} + q\frac{\partial p_1}{\partial z} + q^2\frac{\partial p_2}{\partial z} + \cdots, \tag{8.38}$$

$$F = F_0 + qF_1 + q^2 F_2 + \cdots, \tag{8.39}$$

Using Eq. (8.33), Eq. (8.36) and Eq. (8.37) into Eq. (8.35) and equating the same power of q on both sides, we get the following system of equations.

8.3.1 Zeroth Order System

$$\frac{1}{r}\frac{\partial}{\partial r}\left(r\frac{\partial w_0}{\partial r}\right)-\frac{1}{r}\frac{\partial}{\partial r}\left(r\frac{\partial u_0}{\partial r}\right)=0, \tag{8.40}$$

$$\frac{1}{r}\frac{\partial}{\partial r}\left(r\frac{\partial \theta_0}{\partial r}\right) = -Br\begin{pmatrix}\left(\frac{\partial w_0}{\partial r}\right)^2+\frac{n-1}{2}We^2\left(\frac{\partial w_0}{\partial r}\right)^4 \\ +\frac{\mathcal{M}^2}{{\alpha_e}^2+{\beta_e}^2}(w_0+1)^2+\left(\frac{\partial w_0}{\partial r}\right)^2\end{pmatrix}, \tag{8.41}$$

and the boundary conditions are

$$w_0=-1-2\pi\varepsilon\alpha\beta\cos(2\pi z),\quad \theta_0=0 \quad at\quad r=h,$$
$$\frac{\partial w_0}{\partial r}=0,\quad \frac{\partial \theta_0}{\partial r}=0,\ \ at\ \ r=0. \tag{8.42}$$

8.3.2 First Order System

$$\frac{1}{r}\frac{\partial}{\partial r}\left(r\frac{\partial w_1}{\partial r}\right)=-\frac{1}{r}\frac{\partial}{\partial r}\left(r\frac{\partial u_0}{\partial r}\right)-\frac{n-1}{2}We^2\frac{1}{r}\frac{\partial}{\partial r}\left(r\left(\frac{\partial w_0}{\partial r}\right)^3\right)$$
$$+\frac{\mathcal{M}^2\alpha_e}{{\alpha_e}^2+{\beta_e}^2}(w_0+1)+\frac{\partial p_0}{\partial z}, \tag{8.43}$$

$$\frac{1}{r}\frac{\partial}{\partial r}\left(r\frac{\partial \theta_1}{\partial r}\right)=-Br\begin{pmatrix}\left(\frac{\partial w_1}{\partial r}\right)^2+\frac{n-1}{2}We^2\left(\frac{\partial w_1}{\partial r}\right)^4 \\ +\frac{\mathcal{M}^2}{{\alpha_e}^2+{\beta_e}^2}(w_1+1)^2+\left(\frac{\partial w_1}{\partial r}\right)^2\end{pmatrix}, \tag{8.44}$$

and boundary conditions are

$$w_1=0,\ \theta_1=0\quad at\quad r=h,$$
$$\frac{\partial w_1}{\partial r}=0,\quad \frac{\partial \theta_1}{\partial r}=0\quad at\quad r=0, \tag{8.45}$$

8.3.3 Second Order System

$$\frac{1}{r}\frac{\partial}{\partial r}\left(r\frac{\partial w_2}{\partial r}\right)=-\frac{n-1}{2}We^2\frac{1}{r}\frac{\partial}{\partial r}\left(r\left(\frac{\partial w_1}{\partial r}\right)^3\right)$$
$$+\frac{\mathcal{M}^2\alpha_e}{{\alpha_e}^2+{\beta_e}^2}(w_1+1)+\frac{\partial p_1}{\partial z}, \tag{8.46}$$

$$\frac{1}{r}\frac{\partial}{\partial r}\left(r\frac{\partial \theta_2}{\partial r}\right) = -Br\left(\begin{array}{c}\left(\frac{\partial w_2}{\partial r}\right)^2 + \frac{n-1}{2}We^2\left(\frac{\partial w_2}{\partial r}\right)^4 \\ + \frac{\mathcal{M}^2}{{\alpha_e}^2 + {\beta_e}^2}(w_2+1)^2 + \left(\frac{\partial w_2}{\partial r}\right)^2\end{array}\right), \tag{8.47}$$

and boundary conditions are

$$\begin{aligned} w_2 = 0, \quad \theta_2 = 0 = 0, \quad at \quad r = h, \\ \frac{\partial w_2}{\partial r} = 0, \quad \frac{\partial \theta_2}{\partial r} = 0 \quad at \quad r = 0. \end{aligned} \tag{8.48}$$

Solving Eqs. (8.40)-(8.48) with the help of software "Mathematica" we have found $w_i,\ \theta_i,\ p_i\ (i = 0,\ 1, 2)$ and the solution for velocity, temperature and pressure gradient are

$$W = \lim_{q\to 1}(w_0 + qw_1 + q^2 w_2 + \cdots), \tag{8.49}$$

$$\theta = \lim_{q\to 1}(\theta_0 + q\theta_1 + q^2\theta_2 + \cdots), \tag{8.50}$$

$$\frac{\partial p}{\partial z} = \lim_{q\to 1}\left(\frac{\partial p_0}{\partial z} + q\frac{\partial p_1}{\partial z} + q^2\frac{\partial p_2}{\partial z} + \cdots\right), \tag{8.51}$$

The volumetric flow rate can be evaluate by the following formula

$$Q = 2\pi\int_0^h r(w(r,z)+1)dr. \tag{8.52}$$

and mean volumetric flow rate in a fixed frame is written as follow

$$\hat{Q} = \frac{1}{T}\int_0^1 Q d\hat{t} = F + \frac{1}{2}\left(1 + \frac{\varepsilon^2}{2}\right). \tag{8.53}$$

8.4 Result and Discussion

This section compromise a detailed discussion on the graphs of pressure rise, pressure gradient, velocity and temperature distribution. The parameters $\mathcal{M},\ \beta_i,\ \beta_e,\ n, We$ and Br represent the Hartmann number, ion-slip parameter, Hall parameter, power law index, Weissenberg number and Brinkman number, respectively. Figs. 8.2a-e show the impact of interested parameters on the velocity field. The consequence of interested parameters on the pressure gradient and pressure rise can be depicted from Fig. 8.3a-e and Fig. 8.4a-e. Fig. 8.5a-e exhibit the impact of selected parameters on temperature profile.

Velocity profile

From Fig. 8.2a it is revealed that the significant variation in velocity can be observed at the center of ciliated tube because in pioseuille flow velocity is high at the axis of tube (i.e $r = 0$). The consequence of magnetic field on the velocity profile shows that the speed of plasma in the axial direction became slow in the region $-0.45 < r < 0.45$ for rising value of Hartmann number. The increasing values of Hartmann number indicate that electromagnetic forces are dominent over the viscous forces and acting along the radial direction therefore causes to decelerate the axial velocity also Fig. 8.2b-c show that axial velocity increases by rising Hall parameter β_e and slip parameter β_i. Increasing values of Hall parameter show that when ratio of frequency of iron particles in plasma and frequency of collision of electrons due to strong magnetic field increases then fluid flow becomes faster in axial direction i.e Hall effect assist the fluid flow in axial direction. Fig. 8.2d indicates that increasing values of Wessenberg number We show that viscous properties of fluid are dominant over the elastic properties and by increasing the amount of elasticity in plasma, fluid become thick and for increasing value of $We < 1$, flow is deccelerated.

Fig. 8.2e illustrates that increasing power law index $n < 1$ make the fluid thin and in results axial velocity increases but for $n > 1$ the fluid (plasma) become discontinouns which is physically not possible in continium fluid mechanics.

Pressure gradient

Fig. 8.3 exhibit the consequential change in pressure gradient for rising value of interested parameters, i.e, Hartmann number $\mathcal{M}$, Hall parameter β_e, slip parameter β_i, Weissenberg number We and power law index n. It is depictted that behaviour of pressure gradient is same for all parameters in the region $z \in [-1, 1]$. Fig. 8.3a indicates that axial pressure gradient decreases by rising Hartmann number $\mathcal{M}$. Since the flow rate is directly proportional to pressure gradient, therefore, it is clear that strong magnetic field opposes flow in axial direction which results a decrease in axial pressure gradient. Fig. 8.3b and 8.3c show that axial pressure gradient increases by increases Hall parameter β_e and slip parameter β_i. It is further noted that axial pressure gradient is reinforced with rising value of β_e and β_i. $\frac{dp}{dz}$ is small in region $z \in [-0.5, -0.2]$ and $z \in [0.2, 0.5]$, whereas attain its maximum at $r - axis$. It can be revealed that flow can move freely with small pressure gradient, whereas high pressure gradient is important to attain the same flux. Fig. 8.3d indicates the impact of Wessenberg number We on

pressure gradient. Since, fluid become more thick for increasing values of weissenberg number $We < 1$, therefore, cilia need more effort to flow the fluid which results increase in pressure gradient. Fig. 3e illustrates the impact of power law index n on pressure gradient. For $n < 1$, the fluid become thin, therefore flow that generates due to motion of cilia can move easily without imposing high pressure gradient. Thus pressure gradient decreases as power law index n increases.

Streamlines

Fig. 8.4a-c, 8.5a-c and 8.6a-c represent the streamlines pattern of cilia-induced flow with the effect of Hartmann number $\mathcal{M}$, Hall prameter β_e and slip parameter β_i, respectively. Since the streamlines show the pattren of fluid flow and internal circulation of streamlines known as trapped bolus, also more boluses indicate fluid is flowing rapidly. Fig. 8.4a-c indicate the influence of magnetic field on trapped bolus. As the magnetic field causes reduction in fluid velocity, it decreases both the number and size of trapping bolus by strong magnetic field. As Hall and slip parameter accelerate the flow hence large size and more trapping blouses create in flow. Therefore, it can be observed from Fig. 8.5a-c and 8.6a-c that the size of trapping boluses rises by larger Hall parameter β_e and slip parameter β_i.

Temperature distribution

Fig. 8.7a-d depict the significance change in temperature profile θ for growing values of various parameters. The trend of temperature profile is same as velocity profile attains its peak at center of tube (i.e $r = 0$). The impact of magnetic field can be observed from Fig. 8.7a. Since the magnetic field resist the fluid flow hence rise in Hartmann number $\mathcal{M}$, results to increase in temperature profile. The resistance in the flow due to magnetic field decreases average kinetic energy, thus from Fig. 8.7b and 8.7c we observe the reduction in temperature with higher values of $\mathcal{M}$, β_e and β_i. The impact of Brinkman number can be observed from Fig. 8.7d which reveals that higher values of Brinkman number Br increases the temperature profile.

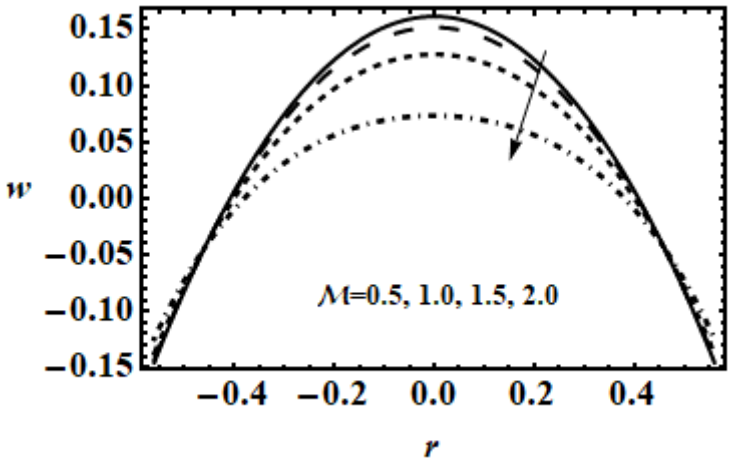

Fig. 8.2a: Impact of Hartmann number $\mathcal{M}$ on horizontal velocity for $\alpha = 0.4, \beta = 0.4, \varepsilon = 0.2, \hat{Q} = 0.2, n = 0.3,\ \beta_e = 0.5, \beta_i = 0.5, We = 0.2$.

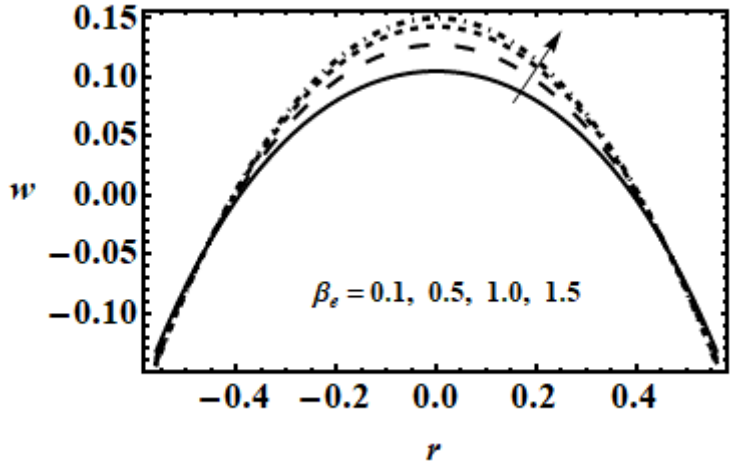

Fig. 8.2b: Impact of Hall parameter β_e on horizontal velocity for $\alpha = 0.4, \beta = 0.4, \varepsilon = 0.2, \hat{Q} = 0.2, n = 0.3, \mathcal{M} = 1.5, \beta_i = 0.5, We = 0.2$.

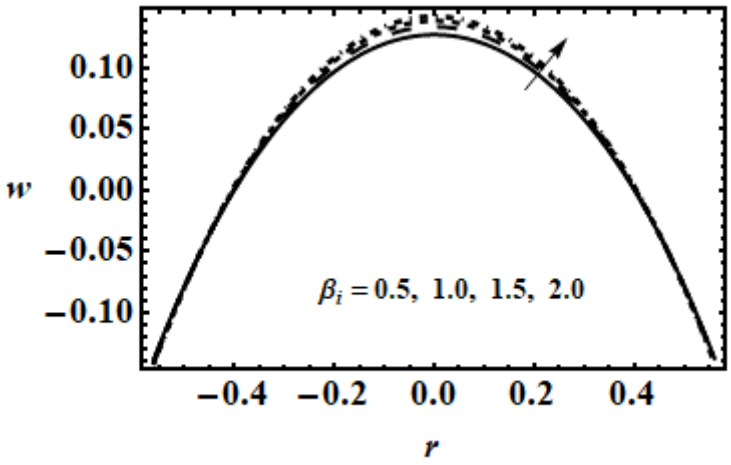

Fig. 8.2c: Impact of Ion-slip β_i parameter on horizontal velocity for $\alpha = 0.4, \beta = 0.4, \varepsilon = 0.2, \hat{Q} = 0.2, n = 0.3, \mathcal{M} = 1.5, \beta_e = 0.5,\ We = 0.2.$

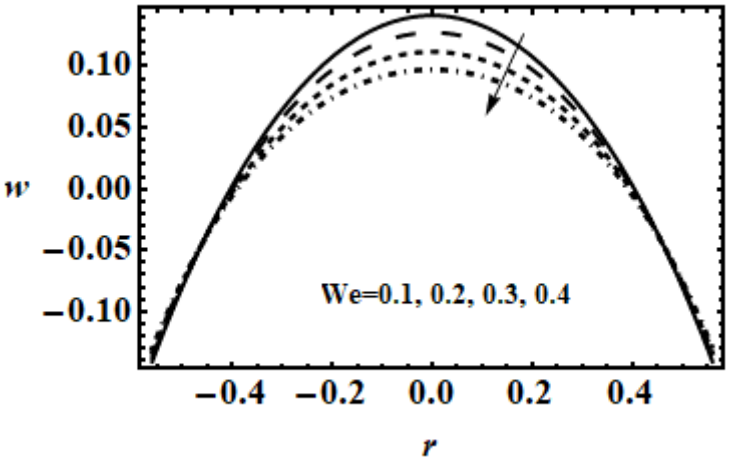

Fig. 8.2d: Impact of Weissenberg We number on horizontal velocity for $\alpha = 0.4, \beta = 0.4, \varepsilon = 0.2, \hat{Q} = 0.2, n = 0.3, \mathcal{M} = 1.5, \beta_e = 0.5, \beta_i = 0.5, We = 0.2.$

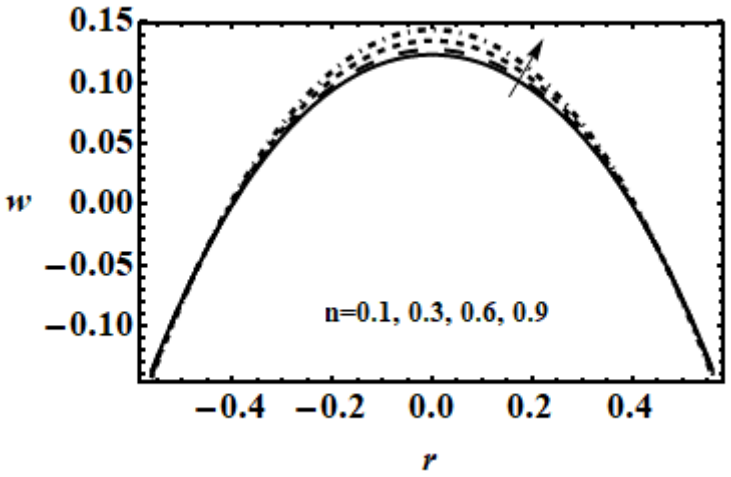

Fig. 8.2e: Impact of power law index n on horizontal velocity for $\alpha = 0.4, \beta = 0.4, \varepsilon = 0.2, \hat{Q} = 0.2, n = 0.3, \mathcal{M} = 1.5, \beta_e = 0.5, \beta_i = 0.5, We = 0.2.$

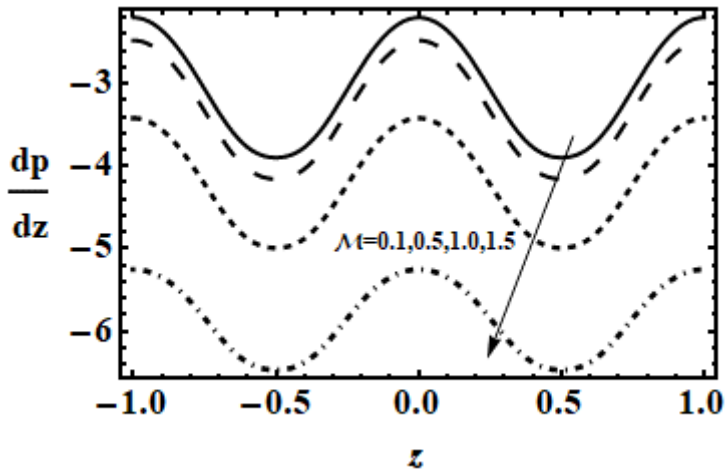

Fig. 8.3a: Impact of Hartmann number $\mathcal{M}$ on pressure gradient.

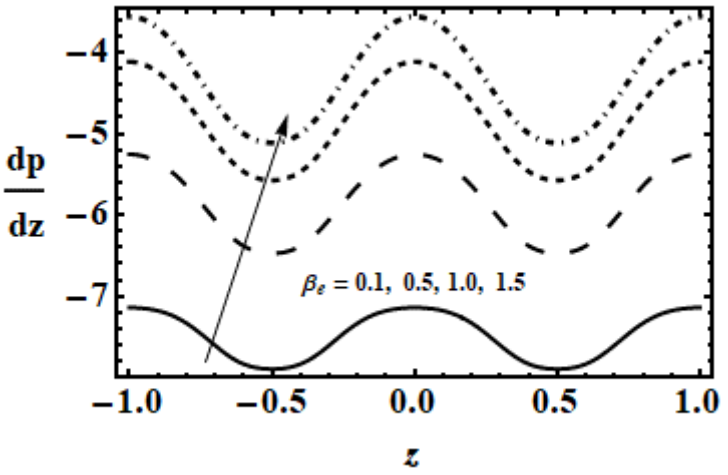

Fig. 8.3b: Impact of Hall parameter β_e on pressure gradient.

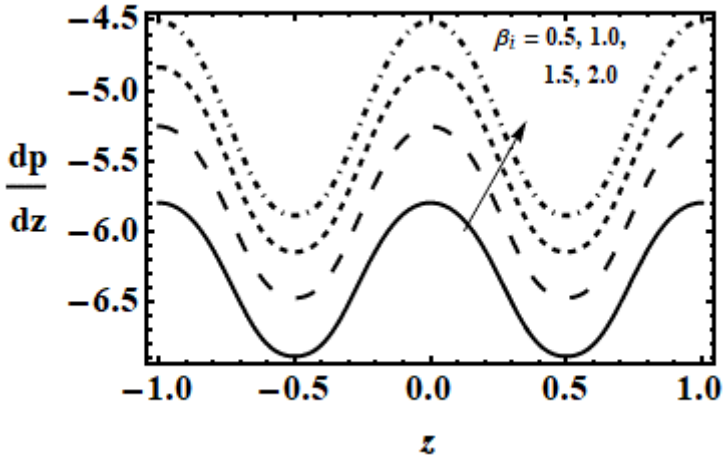

Fig. 8.3c: Impact of Ion-slip parameter β_i on pressure gradient.

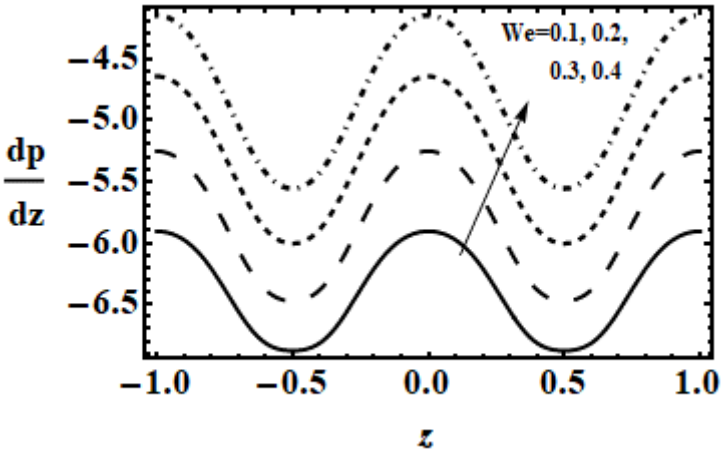

Fig. 8.3d: Impact of Weissenberg number We on pressure gradient.

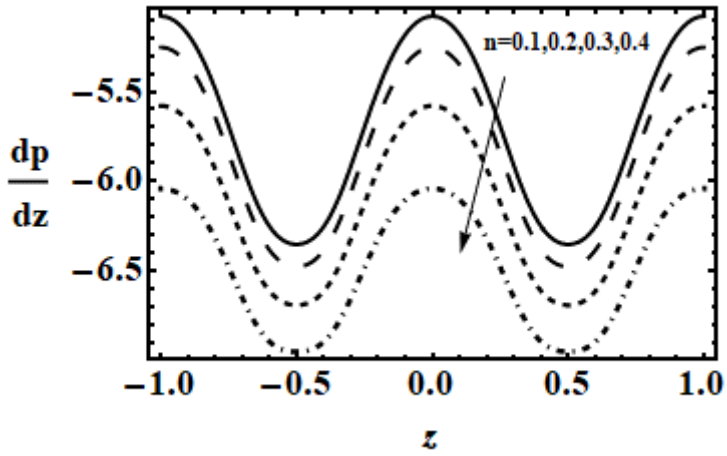

Fig. 8.3e: Impact of power law index n on pressure gradient.

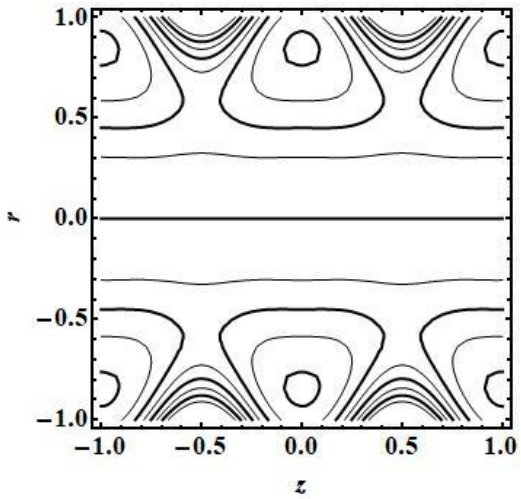

(a) $\mathcal{M} = 0.5$

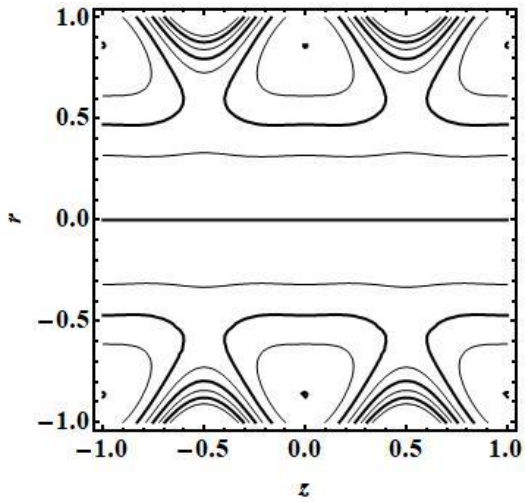

(b) $\mathcal{M} = 1.0$

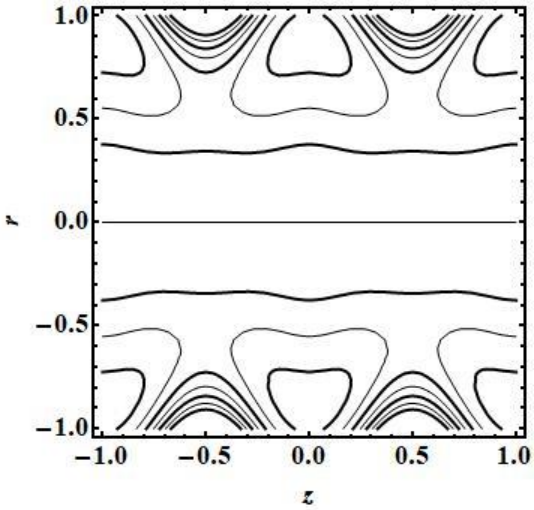

(c) $\mathcal{M} = 1.5$

Fig. 8.4: Impact of Hartmann number $\mathcal{M}$ on stream function for for $\alpha = 0.4,\ \beta = 0.4,$ $\varepsilon = 0.2,\ \hat{Q} = 0.5,\ n = 0.3,\ \beta_e = 0.5,\ \beta_i = 0.5,\ We = 0.2.$

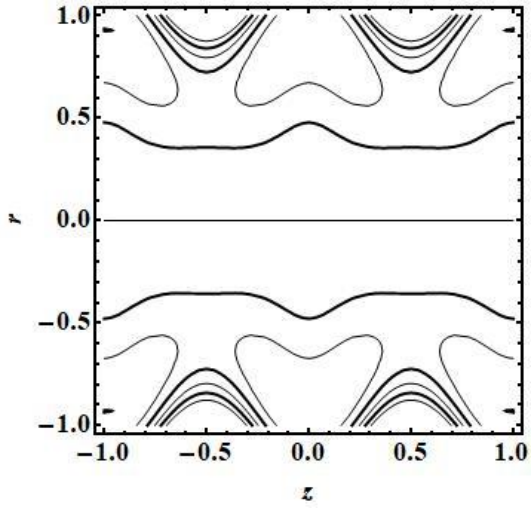

(a) $\beta_e = 0.1$

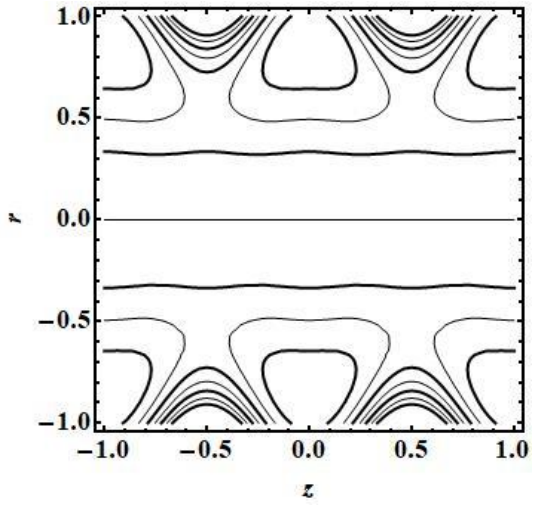

(b) $\beta_e = 1.0$

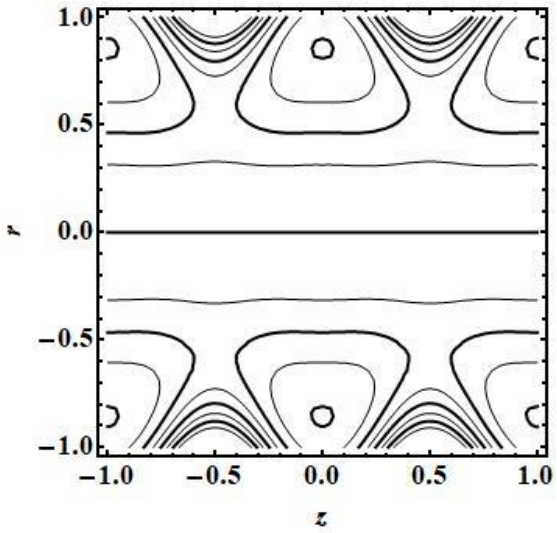

(c) $\beta_e = 2.0$

Fig. 8.5: Impact of Hall parameter β_e on stream function for for $\alpha = 0.4,\ \beta = 0.4,$ $\varepsilon = 0.2,\ \hat{Q} = 0.5,\ n = 0.3, \mathcal{M} = 1.5,\ \beta_i = 0.5,\ We = 0.2.$

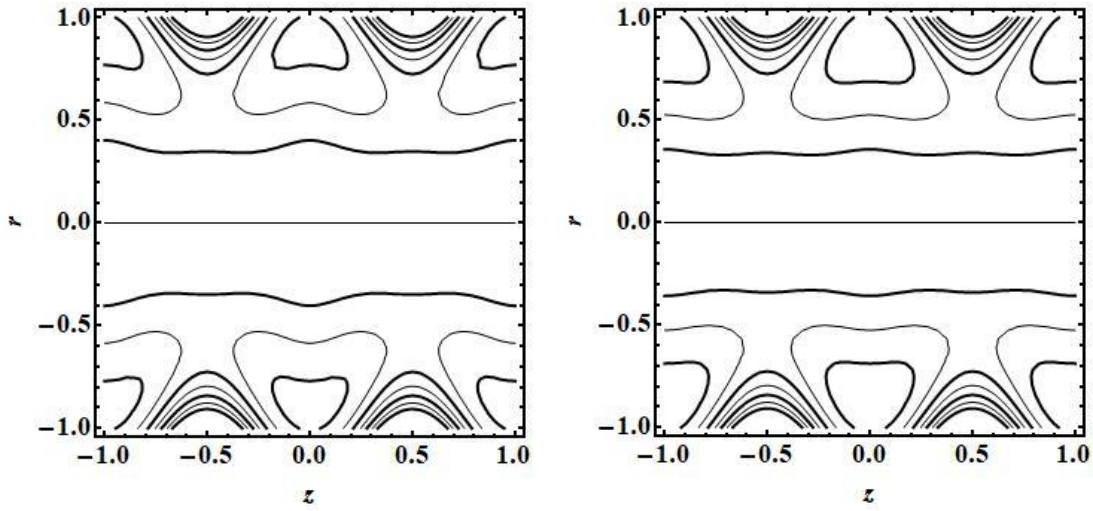

(a) $\beta_i = 0.1$ (b) $\beta_i = 1.0$

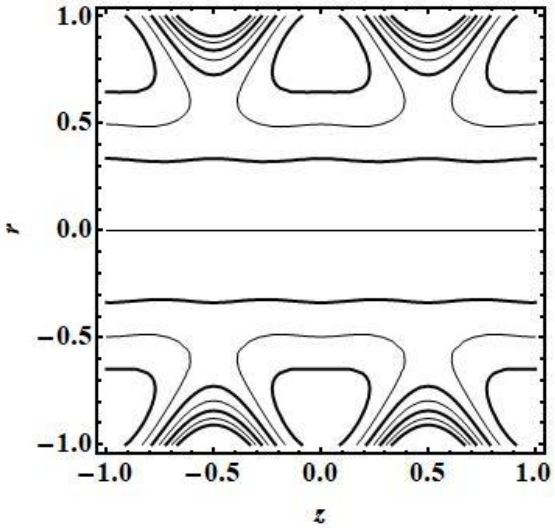

(c) $\beta_i = 2.0$

Fig. 8.6: Impact of Hall parameter β_i on stream function for for $\alpha = 0.4,\ \beta = 0.4,$ $\varepsilon = 0.2,\ \hat{Q} = 0.5,\ n = 0.3, \mathcal{M} = 1.5,\ \beta_e = 0.5,\ We = 0.2.$

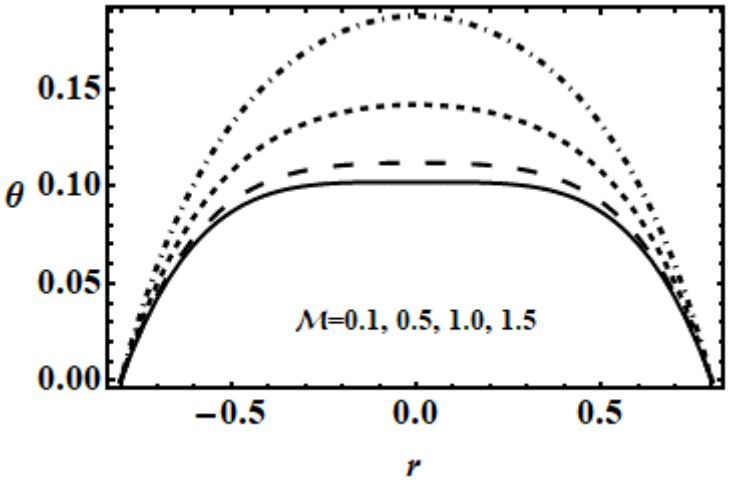

Fig. 8.7a: Impact of Hartmann number on temperature profile for $\alpha = 0.4,\ \beta = 0.4,\ \varepsilon = 0.2,\ \hat{Q} = 0.5,\ n = 0.3,\ \beta_e = 0.5,\ \beta_i = 1, We = 0.2.$

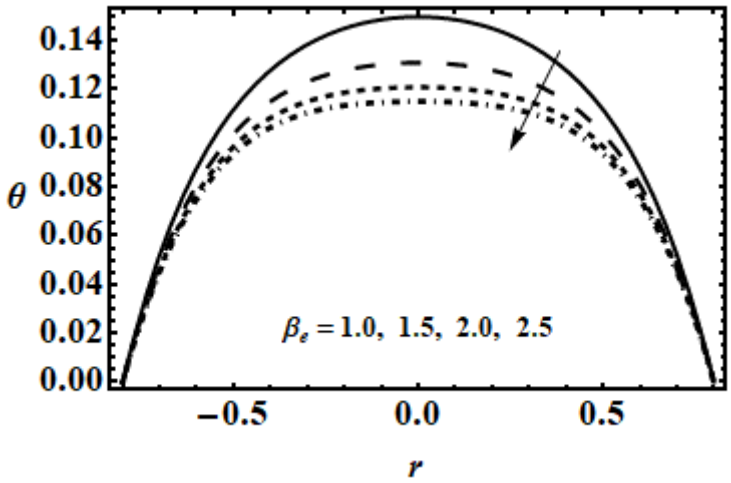

Fig. 8.7b: Impact of Hall parameter on temperature profile for $\alpha = 0.4,\ \beta = 0.4,\ \varepsilon = 0.2,\ \hat{Q} = 0.5,\ n = 0.3,\ \beta_e = 0.5,\ \beta_i = 1, We = 0.2.$

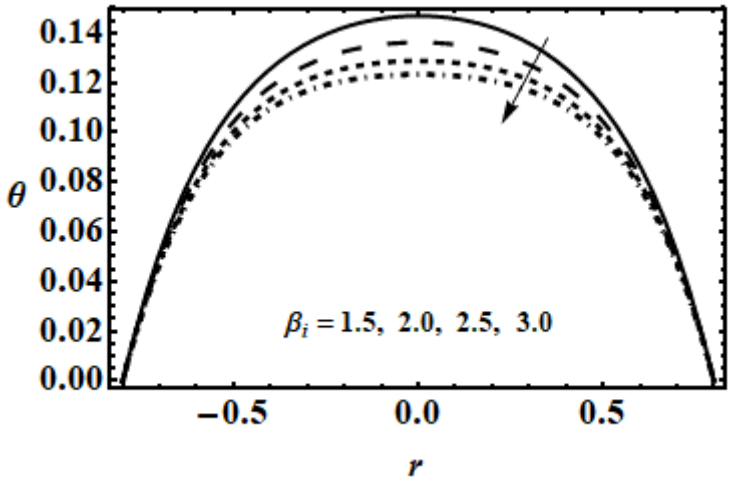

Fig. 8.7c: Impact of ionslip parameter on temperature profile for $\alpha = 0.4,\ \beta = 0.4,$ $\varepsilon = 0.2,\ \hat{Q} = 0.5,\ n = 0.3,\ \beta_e = 0.5,\ , We = 0.2.$

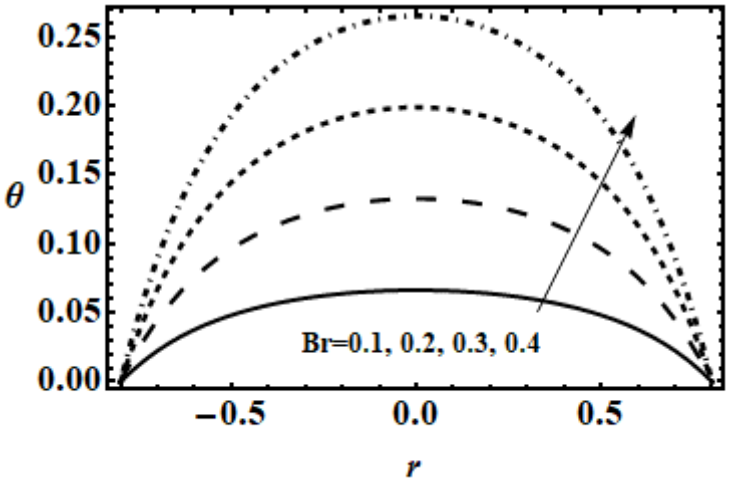

Fig. 8.7d: Impact of Brinkmann number on temperature profile for $\alpha = 0.4,\ \beta = 0.4,$ $\varepsilon = 0.2,\ \hat{Q} = 0.5,\ n = 0.3,\ \beta_e = 0.5,\ \beta_i = 1, We = 0.2.$

8.5 Conclusion

This study has been presented for heat transfer analysis with Hall current, ion-slip effect and the Ohmic heating through a ciliary transport of Carreau fluid in a tube. The dimensionless boundary value problem is evaluated by semi analytic technique Homotopy perturbation method and software "MATHEMATICA". The outcomes are examined for distinct parameters. The attributes of this study are:

- Velocity profile reduces with the larger Hartmann number $\mathcal{M}$ and Weissenberg number We whereas it rises with Hall parameter, power law index n and ion-slip parameter.
- Pressure gradient decreases for larger Hartmann number $\mathcal{M}$ and power law index n and increases with Hall parameter, ion-slip parameter and Weissenberg number We.
- The size of trapping bolus increases with the rise in Hall current β_e and ion-slip parameter β_i while reduces with rising Hartmann number $\mathcal{M}$.
- Temperature profile is enhanced by increasing Hartmann number $\mathcal{M}$ and power law index n and diminished by increasing Weissenberg number We, Hall current β_e and ion-slip parameter β_i.

Chapter 9

Conclusion

This thesis presents the effect of heat transfer in transport of magnetohydronamic flow of two dimensional ciliated channel/tube. It is found that cilia has to work more efficiently in the existence of magnetic field and heat transport in the fluid.

In chapter 1, introduction to cilia and review of literature is discussed regarding to the contribution of various authors in ciliary transport.

In chapter 2, applications of ciliary propulsion is explained by mathematical model of magnetohydrodynamic (MHD) flow through the infinite length of ciliated porous planer surface. Influence of magnetic field and porous medium is higher near the boundary and vanishes away from boundary.

Influence of Hall and ion-slip effect on the ciliary propulsion of viscous incompressible flow in infinite length model embedded in porous medium is evaluated in chapter 3. Impact of Hall and ionslip parameter showed the significant effect on longitudinal velocity as compared to transverse velocity. It is also noted that porosity, Hall and ionslip effect are required to accelerate the ciliary flow.

Chapter 4 presents the mathematical modeling of electrically conducting viscoelastic physiological Johnson-Segalman fluid flow in a ciliated channel. With increase in fluid parameter larger pressure gradient is required to maintain the same flux through a center region of channel, whereas smaller pressure gradient is required with rise in magnetic parameter.

In chapter 5, mathematical modeling of ciliary transport of electrically conducting inertial flow of second grade fluid model is discussed in a two dimensional channel implanted in a porous medium. It is investigated that larger inertial forces caused to accelerate the flow, whereas magnetic forces reduce the longitudinal velocity but dual behavior can be seen through transverse velocity.

Basically, it is concluded that magnetic field decelerated cilia induced flow if it is applied normal to the direction of fluid flow. The impact of electromagnetic forces on incompressible viscoelastic Johnson Segalman fluid and second grade fluid show that magnetic field retarded the flow quickly in second grade fluid as compared to Johnson Segalman fluid.

In chapter 6, influence of porous medium and magnetohydrodynamic (MHD) on the convective viscoelastic physiological Jeffrey fluid model is anticipated through the ciliated channel. It is depicted that larger values of Hartmann number and Jeffrey first viscoelastic parameter reduced the speed in core section of the channel whereas it is elevated with rising permeability parameter and Jeffrey second viscoelastic parameter (retardation parameter) in the core zone. Temperature is enhanced with rising Hartmann number and second Jeffrey parameter whereas it is reduced with permeability parameter and Jeffrey first parameter.

In chapter 7, mixed convective flow of electrically conducting Carreau fluid model is discussed in a vertical ciliated channel. Electromagnetic forces revived whereas heat transfer significantly accelerated the cilia induced flow.

In chapter 8, the impact of Hall current and ion-slip on the convective flow of Carreau fluid is discussed through the two dimensional ciliated tube with ohmic heating. The flow is accelerated in the presence of Hall and ionslip effect but heat transfer in ciliary flow show the decreasing behavior.

Finally, it is concluded that the magnetic field resists the ciliated flow which result the strong elevation in temperature profile. The magnitude of velocity is greater in Jeffrey fluid flow thus more heat can be transfer through Jeffrey fluid compared for Carreau fluid flow in tube or in channel. However, Carreau fluid flow in channel moves with faster speed as compared with tube in the existence of magnetic field thus temperature profile attains maximum rate in channel. This thesis is beneficial to discuss problem occur in mucus in trachea, blood in fallopian tube, cholesterol in veins and arteries and in designing the artificial cilia.

Appendix

$$A_1(x) = \frac{1}{1008000h}(1512000F + h(-504000u_0 + Gh(25200 + Gh^{22} \times (-1320 + 67Gh^2))(F + hu_0))) + \frac{1}{84000h^3}\beta\lambda_2((15 \times (2520 + Gh^2(-228 + 5Gh^2))F^2 - 9h(7000 + 3Gh^{22} \times (-180 + 7Gh^2))Fu_0 + 2h^2(12600 + Gh^2(-1770 + 167Gh^2))u_0{}^2)h' + h^2(12600(F - hu_0) - 60Gh^2(33F + 2hu_0) + G^2h^4(181F + 39hu_0))u_0'),$$

$$A_2(x) = -\frac{1}{756000h^3}(-378000 + Gh^2(37800 + Gh^2(-2430 + 133Gh^2))) \times (F + hu_0) - \frac{1}{21000h^5}\beta\lambda_2((15(-15 + Gh^2)(-84 + 5Gh^2) \times F^2 - h(31500 + Gh^2(-3555 + 167Gh^2))Fu_0 + h^2(12600 + Ah^2(-2220 + 227Gh^2))u_0{}^2)h' + h^2((6300 + Gh^2(-1215 + 118Gh^2))F + h(-15 + Gh^2) \times (420 + 17Gh^2)u_0)u_0'),$$

$$A_3(x) = \frac{1}{56000h^3}G(1400 + Gh^2(-140 + 9Gh^2))(F + hu_0) - \frac{1}{14000h^7}\beta\lambda_2((-15(420 + Gh^2(-98 + 5Gh^2))F^2 + h(10500 + Gh^2(-2310 + 149Gh^2))Fu_0 - 2h^2(2100 + Gh^2(-595 + 72Gh^2))u_0{}^2)h' + h^2(G^2h^4(-71F + hu_0) + 2100(-F + hu_0) - 70Gh^2(-9F + 4hu_0))u_0'),$$

$$A^4(x) = -\frac{1}{16800h^3}G^2(-10 + Gh^2)(-F + hu_0) - \frac{1}{(4200h^7} \times G\beta\lambda^2((15(-9 + Gh^2)F - 9h(-25 + 3Gh^2)Fu_0 + h^{22} \times (-90 + 17Gh^2)u_0{}^2)h' + h^2(Gh^2(8F - 3hu_0] + 45(-F + hu_0))u_0'),$$

$$A_5(x) = \frac{1}{120960h^3}G^3(-F + hu_0) - \frac{1}{3360h^7}(G^2(-F + hu_0)\beta\lambda_2((3F - 2hu_0)h' + h^2u_0')),$$

$$B_1(x) = -\frac{1}{10710470950058880000000000h^4(1 + \lambda_1)} \times [Br(21420941900117760000000000h^6 + (-F + hu_0)\beta\lambda_2((A^9h^{18}(10233330719421F - 13415170239448hu_0)(F - hu_0) - 1486674000G^6h^{12} \times (7370113F - 19503891hu_0)(F - hu_0) - 1159141877712000000G^3h^6(F + hu_0)(-256F + 255hu^0) + 3213141285017664000000000(9F^2 - 5hFu_0 + h^2u_0{}^2))h' + 7h^2(165591696816000000G^3h^6(-F + hu_0)$$

$$-2576996039196000G^6h^{12}(F+hu^0)+454548502861G^9h^{18}$$
$$\times(F+hu_0)+459020183573952000000000(3F+2hu_0))u_0')],$$

$$B_2(x) = \frac{1}{480090240000000000h^8(1+\lambda_1)}[Br(F-hu_0)$$
$$\times\beta\lambda_2((360067680000000G^3h^6(F+hu_0)^2$$
$$-77944680000G^6h^{12}(-F+hu_0)^2+1185163G^9h^{18}(-F+hu_0)^2$$
$$-720135360000000000(3F^2(2+hu_0)+hu_0(3+hu_0)))h'$$
$$-720135360000000000h^2Fu_0'],$$

$$B_3(x) = \frac{1}{3600676800000000000h^{10}(1+\lambda_1)}[Br(-F+hu_0)^2\beta\lambda_2$$
$$\times((-216040608000000000(-3F+2hu_0)$$
$$+360067680000000G^3h^6(-26F+25hu_0)$$
$$-78732000G^6h^{12}(-3891F+3932hu_0)$$
$$+133G^9h^{18}(-438972F+449621hu_0))h'$$
$$+h^2(216040608000000000-360067680000000G^3h^6$$
$$-3228012000G^6h^{12}+1416317G^9h^{18})u_0'],$$

$$B_4(x) = \frac{1}{248935680000000000h^6(1+\lambda_1)}[G^3Br(-F+hu_0)^2\beta\lambda_2$$
$$\times((G^6h^{12}(10685101F-10831802hu_0)$$
$$-444528000000(-204F+181hu_0)$$
$$+5292000G^3h^6(-8767(F+8625hu_0))h'$$
$$+h^2(10224144000000-751464000G^3h^{66}$$
$$-146701G^6h^{12})u_0'],$$

$$B_5(x) = \frac{1}{60011280000000000h^8(1+\lambda_1)}[G^3Br(-F+hu_0)_2{}^2\beta\lambda_2$$
$$\times((1000188000000(-F+11hu_0)$$
$$-81000G^3h^6(-165937F+156106hu_0)$$
$$+7G^6h^{12}(-558740F+554657hu_0))h'$$
$$-3h^2(1000188000000-265437000G^3h^{66}$$
$$+9527G^6h^{12})u_0')],$$

$$B_6(x) = \frac{1}{1584297792000000000h^{10}(1+\lambda_1)}[G^3Br(-F+hu_0)^2\beta\lambda_2$$
$$\times((G^6h^{12}(101393121F-98073227hu_0)$$
$$-30005640000000(-3F+2hu_0)$$
$$+10206000G^3h^6(-24819F+22055hu_0))h'$$
$$+2h^2(15002820000000-14104692000G^3h^{66}$$
$$+1659947G^6h^{12})u_0')],$$

$$B_7(x) = \frac{1}{107872128000000h^6(1+\lambda_1)}[G^6Br(-F+hu_0)^2\beta\lambda_2$$
$$\times((-25200(-2893F+2400hu_0)+G^3h^6(-45924F$$
$$+43127hu_0))h'+h^2(12423600-2797G^3h^6)u_0')],$$

$$B_8(x) = \frac{1}{426746880000000h^8(1+\lambda_1)}[G^6Br(-F+hu_0)^2\beta\lambda_2 \times ((A^3h^6(82529F-74860hu_0)+2646000(-25F +19hu_0))h'+h^2(-15876000+7669A^3h^6)u_0')],$$

$$B_9(x) = \frac{1}{2448460224000000h^{10}(1+\lambda_1)}[G^6Br(-F+hu_0)^2\beta\lambda_2 \times ((-11907000(-3F+2hu_0)+G^3h^6(-144084-F +125069hu_0))h'+5h^2(2381400-3803A^3h^6)u_0')],$$

$$B_{10}(x) = \frac{1}{90091008000000h^6(1+\lambda_1)}[G^9Br(-F+hu_0)^2 \times \beta\lambda_2((1029F-841hu_0)h'+188h^2u_0')],$$

$$B_{11}(x) = -\frac{1}{3129477120000h^8(1+\lambda_1)}[G^9Br(-F+hu_0)^2 \times \beta\lambda_2((4F-3hu_0)h'+h^2u_0')],$$

$$B_{12}(x) = \frac{1}{47112855552000h^{10}(1+\lambda_1)}[G^9Br(-F+hu_0)^2 \times \beta\lambda_2((3F-2hu_0)h'+h^2u_0')].$$

$$C_1(x,y) = +2\sqrt{G}ysinh[2\sqrt{G}y](-1+3Gh^2)+\sqrt{G}ysinh[4\sqrt{G}y](1+3Gh^2) +cos\,h[\sqrt{G}(y-h)](-3+3Gh^2)+cos\,h[\sqrt{G}(y+h)](3-3Gh^2) +cos\,h[\sqrt{G}(y-3h)](1+3Gh^2)-cos\,h[\sqrt{G}(y+3h)](1+3Gh^2) +3\sqrt{G}h(\sqrt{G}y-\sqrt{G}yCosh[4\sqrt{G}h]+Sinh[\sqrt{G}(y-3h)] -Sinh[\sqrt{G}(y-h)]-Sinh[\sqrt{G}(y+h)]+Sinh[\sqrt{G}(y+3h)]),$$

$$C_2(x,y) = -72\sqrt{G}\frac{dP_0}{dx}y+112\sqrt{G}\left(\frac{dP_0}{dx}\right)^2h^2+192\sqrt{G}\frac{dP_0}{dx}h -128G^{\frac{3}{2}}\frac{dP_0}{dx}h^3-144G^{\frac{3}{2}}\left(\frac{dP_0}{dx}\right)^2h^4+76G^{\frac{3}{2}}\left(\frac{dP_0}{dx}\right)^2h^3y +120G^{\frac{5}{2}}\frac{dP_0}{dx}h^4y+20G^2\left(\frac{dP_0}{dx}\right)^2h^5+60\sqrt{G}\left(\frac{dP_0}{dx}\right)^2hy +56G^{\frac{3}{2}}\frac{dP_0}{dx}h^2y-96G^{\frac{5}{2}}\frac{dP_0}{dx}h^3yF_0+96G\frac{dP_0}{dx}yF_0 -32G^{\frac{3}{2}}\frac{dP_0}{dx}h^2F_0-28G^{\frac{3}{2}}yF_0-64G^{\frac{3}{2}}\frac{dP_0}{dx}hyF_0 +24G^{\frac{5}{2}}\left(\frac{dP_0}{dx}\right)^2h^2yF_0+48GG^{\frac{5}{2}}hyF_0{}^2-4G^{\frac{5}{2}}\left(\frac{dP_0}{dx}\right)^2 \times h^6\left(4\sqrt{G}yCosh\left[\sqrt{G}y\right]\left(Cosh\left[\sqrt{G}y\right]\right)^2Sinh\left[Cosh\left[\sqrt{G}y\right]\right]\right),$$

$$C_3(x,y) = 52\sqrt{G}\frac{dP_0}{dx}y-14(8+Gy^2)\sqrt{G}\left(\frac{dP_0}{dx}\right)^2h^2-24(8+Gy^2)\sqrt{G}\frac{dP_0}{dx}h +16(8+Gy^2)G^{\frac{3}{2}}\frac{dP_0}{dx}h^3+18(8+Gy^2)G^{\frac{3}{2}}\left(\frac{dP_0}{dx}\right)^2h^4$$

$$+24G^{\frac{3}{2}}\left(\frac{dP_0}{dx}\right)^2 h^3y - 16G^{\frac{5}{2}}\left(\frac{dP_0}{dx}\right)^2 h^5y - 100\sqrt{G}\sqrt{G}\left(\frac{dP_0}{dx}\right)^2 hy$$
$$+132G^{\frac{3}{2}}\frac{dP_0}{dx}h^2y + 32G^{\frac{5}{2}}\frac{dP_0}{dx}h^3yF_0 - 12(8+Gy^2)\sqrt{G}\frac{dP_0}{dx}F_0$$
$$+4(8+Gy^2)G^{\frac{3}{2}}\frac{dP_0}{dx}h^2F_0 - 152G^{\frac{3}{2}}\frac{dP_0}{dx}hyF_0,$$

$$C_4(x,y) = 72\sqrt{G}\frac{dP_0}{dx}y + 64\sqrt{G}\left(\frac{dP_0}{dx}\right)^2 h^2 - 192\sqrt{G}\frac{dP_0}{dx}h - 64G^{\frac{3}{2}}\frac{dP_0}{dx}h^3$$
$$+64G^{\frac{3}{2}}\frac{dP_0}{dx}h^3 + 128G^{\frac{3}{2}}\left(\frac{dP_0}{dx}\right)^2 h^4 - 272G^{\frac{3}{2}}\left(\frac{dP_0}{dx}\right)^2 h^3y$$
$$-32G^{\frac{5}{2}}\frac{dP_0}{dx}h^4y - 4G^{\frac{3}{2}}\left(\frac{dP_0}{dx}\right)^2 h^3y - 48\sqrt{G}\left(\frac{dP_0}{dx}\right)^2 hy$$
$$-248G^{\frac{3}{2}}\frac{dP_0}{dx}h^2y - 72G^{\frac{5}{2}}\frac{dP_0}{dx}h^3yF_0 - 128\sqrt{G}\frac{dP_0}{dx}F_0$$
$$-128G^{\frac{3}{2}}\frac{dP_0}{dx}h^2F_0 - 16G^{\frac{3}{2}}\frac{dP_0}{dx}hyF_0,$$

$$C_5(x,y) = 48\sqrt{G}\frac{dP_0}{dx}y - 192\sqrt{G}\left(\frac{dP_0}{dx}\right)^2 h^2 - 128\sqrt{G}\frac{dP_0}{dx}h - 128G^{\frac{3}{2}}\frac{dP_0}{dx}h^3$$
$$-128G^{\frac{3}{2}}\left(\frac{dP_0}{dx}\right)^2 h^4 + 304G^{\frac{3}{2}}\left(\frac{dP_0}{dx}\right)^2 h^3y - 40G^{\frac{5}{2}}\frac{dP_0}{dx}h^4y$$
$$-20G^{\frac{3}{2}}\left(\frac{dP_0}{dx}\right)^2 h^3y - 48\sqrt{G}\left(\frac{dP_0}{dx}\right)^2 hy + 224G^{\frac{3}{2}}\frac{dP_0}{dx}h^2y$$
$$-32G^{\frac{5}{2}}\frac{dP_0}{dx}h^3yF_0 - 128\sqrt{G}\frac{dP_0}{dx}F_0 + 96G^{\frac{3}{2}}\frac{dP_0}{dx}hyF_0$$
$$-16G^{\frac{5}{2}}\left(\frac{dP_0}{dx}\right)^2 h^2yF_0 - 48G^{\frac{5}{2}}hyF_0{}^2,$$

$$C_6(x,y) = -72\sqrt{G}\frac{dP_0}{dx}y - 64\sqrt{G}\left(\frac{dP_0}{dx}\right)^2 h^2 + 124\sqrt{G}\frac{dP_0}{dx}h + 192G^{\frac{3}{2}}\frac{dP_0}{dx}h^3$$
$$+128G^{\frac{3}{2}}\left(\frac{dP_0}{dx}\right)^2 h^4 - 112G^{\frac{3}{2}}\left(\frac{dP_0}{dx}\right)^2 h^3y + 4G^{\frac{3}{2}}\left(\frac{dP_0}{dx}\right)^2 h^3y$$
$$+48\sqrt{G}\left(\frac{dP_0}{dx}\right)^2 hy - 20G^{\frac{3}{2}}\frac{dP_0}{dx}h^2y + 8G^{\frac{5}{2}}\frac{dP_0}{dx}h^3yF_0$$
$$+128G^{\frac{3}{2}}\frac{dP_0}{dx}h^2F_0 + 16G^{\frac{3}{2}}\frac{dP_0}{dx}hyF_0,$$

$$C_7(x,y) = 24\sqrt{G}\frac{dP_0}{dx}y + 80\sqrt{G}\left(\frac{dP_0}{dx}\right)^2 h^2 - 64\sqrt{G}\frac{dP_0}{dx}h + 16G^{\frac{3}{2}}\left(\frac{dP_0}{dx}\right)^2 h^4$$
$$+4G^{\frac{3}{2}}\left(\frac{dP_0}{dx}\right)^2 h^3y - 12\sqrt{G}\left(\frac{dP_0}{dx}\right)^2 hy + 18\frac{dP_0}{dx}h^2y + 32\frac{dP_0}{dx}h^3yF_0$$
$$+32\sqrt{G}\frac{dP_0}{dx}F_0 + 32G^{\frac{3}{2}}\frac{dP_0}{dx}h^2F_0 + 28G^{\frac{3}{2}}yF_0 - 32G^{\frac{3}{2}}\frac{dP_0}{dx}hyF_0,$$

$$C_8(x,y) = -4(40+Gy^2)\frac{dP_0}{dx} + 70G\left(\frac{dP_0}{dx}\right)^2 h^2y + 120G\frac{dP_0}{dx}hy - 40G^2\frac{dP_0}{dx}h^3y$$

$$-90G^2\left(\frac{dP_0}{dx}\right)^2 h^4 y - 8G^2\left(\frac{dP_0}{dx}\right)^2 h^3 y + 224G^2\frac{dP_0}{dx}h^4$$
$$-152G^2\left(\frac{dP_0}{dx}\right)^2 h^5 + 4(40+5Gy^2)\left(\frac{dP_0}{dx}\right)^2 h + 72G^2\frac{dP_0}{dx}h^3 F_0$$
$$+60G^2\frac{dP_0}{dx}yF_0 + 60G\frac{dP_0}{dx}yF_0 - 20G^2\frac{dP_0}{dx}h^2 yF_0 - 4(48+6Gy^2)$$
$$\times G\frac{dP_0}{dx}hF_0 - 32G^3h^5 cosh[\sqrt{G}h] + 4G^3\frac{dP_0}{dx}(-5Cosh[\sqrt{G}h]$$
$$+Cosh[3\sqrt{G}h])h^6 - 2(6Sinh[\sqrt{G}h] + Sinh[2\sqrt{G}h])$$
$$-32G^3(Cosh[\sqrt{G}h])^3 h^4 F_0 - 16G^{\frac{5}{2}}\frac{dP_0}{dx}h^4(-10Sinh[\sqrt{G}h]$$
$$+Sinh[\sqrt{G}h])F_0,$$

$$C_9(x,y) = 192\frac{dP_0}{dx} + 228G\left(\frac{dP_0}{dx}\right)^2 h^2 y + 168\frac{dP_0}{dx}h - 232G^2\frac{dP_0}{dx}h^3 y - 112G^{\frac{3}{2}}$$
$$\times\left(\frac{dP_0}{dx}\right)^2 h^4 + 32G^2\left(\frac{dP_0}{dx}\right)^2 h^4 y - 64G^2\frac{dP_0}{dx}h^4 - 32G^2\left(\frac{dP_0}{dx}\right)^2 h^5$$
$$-192\left(\frac{dP_0}{dx}\right)^2 h - 64G^2\frac{dP_0}{dx}h^3 F_0 + 72G\frac{dP_0}{dx}yF_0 - 144G^2\frac{dP_0}{dx}h^2 yF_0$$
$$+192G\frac{dP_0}{dx}hF_0,$$

$$C_{10}(x,y) = -64\frac{dP_0}{dx} - 132G\left(\frac{dP_0}{dx}\right)^2 h^2 y - 176\frac{dP_0}{dx}h - 52G^2\frac{dP_0}{dx}h^3 y - 128G^2$$
$$\times\frac{dP_0}{dx}h^2 y + 18G^{\frac{3}{2}}\left(\frac{dP_0}{dx}\right)^2 h^4 + 256G^2\left(\frac{dP_0}{dx}\right)^2 h^4 y - 32G^2$$
$$\times\left(\frac{dP_0}{dx}\right)^2 h^5 + 64\left(\frac{dP_0}{dx}\right)^2 h + 320G\frac{dP_0}{dx}h^2 - 32G^3h^3 yF_0$$
$$-16G^3\frac{dP_0}{dx}h^4 yF_0 - 248G^2 hyF_0 + 72G^2\frac{dP_0}{dx}yF_0 - 24G\frac{dP_0}{dx}yF_0$$
$$-48G^{2\frac{dP_0}{dx}}h^2 yF_0 + 128G\frac{dP_0}{dx}hF_0 - 40G^2 yF_0{}^2 - 32G^3h^2 yF_0{}^2 - 16Gy,$$

$$C_{11}(x,y) = -64\frac{dP_0}{dx} - 12G\left(\frac{dP_0}{dx}\right)^2 h^2 y + 136\frac{dP_0}{dx}h + 56G^2\frac{dP_0}{dx}h^3 y + 32GG^{\frac{3}{2}}$$
$$\times\left(\frac{dP_0}{dx}\right)^2 h^4 - 96G^2\left(\frac{dP_0}{dx}\right)^2 h^4 y - 64G^2\frac{dP_0}{dx}h^4 + 64\left(\frac{dP_0}{dx}\right)^2 h$$
$$-256G\frac{dP_0}{dx}h^2 - 64G^2\frac{dP_0}{dx}h^3 F_0 + 80G^2\frac{dP_0}{dx}h^2 yF_0 + 64G\frac{dP_0}{dx}hF_0,$$

$$C_{12}(x,y) = 32\frac{dP_0}{dx} + G\left(\frac{dP_0}{dx}\right)^2 h^2 y - 56\frac{dP_0}{dx}h - 6G^2\frac{dP_0}{dx}h^3 y - 5G^{\frac{3}{2}}\left(\frac{dP_0}{dx}\right)^2 h^4$$
$$-64G^2\left(\frac{dP_0}{dx}\right)^2 h^4 y - 32\left(\frac{dP_0}{dx}\right)^2 h + 32G\frac{dP_0}{dx}h^2 + 12G^2 hyF_0$$
$$+24G\frac{dP_0}{dx}yF_0 + 64G\frac{dP_0}{dx}hF_0{}^2 + 20G^2 yF_0{}^2 + 8Gy,$$

$$C_{13}(x,y) = -92G^{\frac{5}{2}}h^4 - 88G^{\frac{5}{2}}h^3y - 88\frac{dP_0}{dx}y - 272\sqrt{G}\left(\frac{dP_0}{dx}\right)^2 h^2 - 14G^{\frac{5}{2}} \times \left(\frac{dP_0}{dx}\right)^2 h^2y^2 - 94G^{\frac{5}{2}}\frac{dP_0}{dx}h^5 - 32\sqrt{G}\frac{dP_0}{dx}h - 8G^{\frac{5}{2}}\frac{dP_0}{dx}hy^2 + 2(16+4Gy^2)G^{\frac{3}{2}}\frac{dP_0}{dx}h^3 + 4G^{\frac{3}{2}}yh + 4G^{\frac{3}{2}}h^2(-6+5Gy^2) + G^{\frac{3}{2}}\left(\frac{dP_0}{dx}\right)^2 h^4(28-7Gy^2) + 54G^{\frac{3}{2}}\left(\frac{dP_0}{dx}\right)^2 h^3y - 34G^{\frac{5}{2}}\frac{dP_0}{dx}h^4y + 11G^{\frac{5}{2}}\frac{dP_0}{dx}h^5y + 100\sqrt{G}\left(\frac{dP_0}{dx}\right)^2 hy + 58G^{\frac{3}{2}}\frac{dP_0}{dx}h^2y - 148G^{\frac{5}{2}}h^3F_0 - 32G^{\frac{5}{2}}\frac{dP_0}{dx}h^3yF_0 + 32G^{\frac{5}{2}}y^2hF_0 - 4(24+3Gy^2)\sqrt{G}\frac{dP_0}{dx}F_0 + 4(44+4Gy^2)G^{\frac{3}{2}}\frac{dP_0}{dx}h^2F_0 + 28G^{\frac{3}{2}}yF_0 - 68G^{\frac{3}{2}}\frac{dP_0}{dx}hyF_0 - 121G^{\frac{5}{2}}h^2yF_0 + 12G^{\frac{5}{2}}y^2{F_0}^2 - 48G^{\frac{5}{2}}h^2{F_0}^2 - 12G^{\frac{5}{2}}hy{F_0}^2,$$

$$C_{14}(x,y) = 92G^{\frac{5}{2}}h^4 - 88G^{\frac{5}{2}}h^3y + 24\sqrt{G}\frac{dP_0}{dx}y + 208\sqrt{G}\left(\frac{dP_0}{dx}\right)^2 h^2 - 9G^{\frac{3}{2}} \times \left(\frac{dP_0}{dx}\right)^2 h^3y + 6G^{\frac{5}{2}}\left(\frac{dP_0}{dx}\right)^2 h^2y^2 + 94G^{\frac{5}{2}}\frac{dP_0}{dx}h^5 + 224\sqrt{G}\frac{dP_0}{dx}h + 32G^{\frac{5}{2}}\frac{dP_0}{dx}hy^2 - 2(48+8Gy^2)G^{\frac{3}{2}}\frac{dP_0}{dx}h^3 + 4G^{\frac{3}{2}}yh + 4G^{\frac{3}{2}}h^2 \times (6-5Gy^2) - G^{\frac{3}{2}}\left(\frac{dP_0}{dx}\right)^2 h^4(156+9Gy^2) + 74G^{\frac{3}{2}}\left(\frac{dP_0}{dx}\right)^2 h^3y - 74G^{\frac{5}{2}}\frac{dP_0}{dx}h^4y - 9G^{\frac{5}{2}}\frac{dP_0}{dx}h^5y - 20\left(\frac{dP_0}{dx}\right)^2 hy + 58G^{\frac{3}{2}}\frac{dP_0}{dx}h^2y + 148G^{\frac{5}{2}}h^3F_0 - 72G^{\frac{5}{2}}\frac{dP_0}{dx}h^3yF_0 - 32G^{\frac{5}{2}}y^2hF_0 + 4(24+3Gy^2) \times \sqrt{G}\frac{dP_0}{dx}F_0 - 48G^{\frac{3}{2}}\frac{dP_0}{dx}h^2F_0 + 28GG^{\frac{3}{2}}yF_0 + 52G^{\frac{3}{2}}\frac{dP_0}{dx}hyF_0 - 121G^{\frac{5}{2}}h^2yF_0 - 12G^{\frac{5}{2}}y^2{F_0}^2 + 48G^{\frac{5}{2}}h^2{F_0}^2 - 12G^{\frac{5}{2}}hy{F_0}^2,$$

$$C_{15}(x,y) = 4\sqrt{G}\frac{dP_0}{dx}y + 2(88+3Gy^2)\sqrt{G}\left(\frac{dP_0}{dx}\right)^2 h^2 - 8G^{\frac{5}{2}}\frac{dP_0}{dx}h^5 + 256\sqrt{G}\frac{dP_0}{dx}h + 16G^{\frac{5}{2}}\frac{dP_0}{dx}hy^2 + 2(100+12Gy^2)G^{\frac{3}{2}}\frac{dP_0}{dx}h^3 + G^{\frac{3}{2}}\left(\frac{dP_0}{dx}\right)^2 h^4(160 + 14Gy^2) - 176G^{\frac{3}{2}}\left(\frac{dP_0}{dx}\right)^2 h^3y - 8G^{\frac{5}{2}}\frac{dP_0}{dx}h^5y + 20\sqrt{G}\left(\frac{dP_0}{dx}\right)^2 hy - 268G^{\frac{3}{2}}\frac{dP_0}{dx}h^2y + 16G^{\frac{5}{2}}\frac{dP_0}{dx}h^3yF_0 + 4(24+3Gy^2)\sqrt{G}\frac{dP_0}{dx}F_0 + 4(24+3Gy^2)G^{\frac{3}{2}}\frac{dP_0}{dx}h^2F_0 - 136G^{\frac{3}{2}}\frac{dP_0}{dx}hy,$$

$$C_{16}(x,y) = -36\sqrt{G}\frac{dP_0}{dx}y + 2(8+9Gy^2)\sqrt{G}\left(\frac{dP_0}{dx}\right)^2 h^2 + 8G^{\frac{5}{2}}\frac{dP_0}{dx}h^5 - 128\sqrt{G}\frac{dP_0}{dx}h$$
$$-128G^{\frac{5}{2}}\frac{dP_0}{dx}hy^2 - 2(36+4Gy^2)G^{\frac{3}{2}}\frac{dP_0}{dx}h^3 + G^{\frac{3}{2}}\left(\frac{dP_0}{dx}\right)^2 h^4(-32+2Gy^2)$$
$$-16G^{\frac{3}{2}}\left(\frac{dP_0}{dx}\right)^2 h^3y - 8G^{\frac{5}{2}}\frac{dP_0}{dx}h^5y + 60\sqrt{G}\left(\frac{dP_0}{dx}\right)^2 hy - 68G^{\frac{3}{2}}\frac{dP_0}{dx}h^2y$$
$$+16GG^{\frac{5}{2}}\frac{dP_0}{dx}h^3yF_0 + 4(8+Gy^2)\sqrt{G}\frac{dP_0}{dx}F_0 - 4(24+3Gy^2)G^{\frac{3}{2}}\frac{dP_0}{dx}h^2F_0$$
$$-56G^{\frac{3}{2}}\frac{dP_0}{dx}hyF_0,$$

$$C_{17}(x,y) = 4G^{\frac{5}{2}}h^4 + G^{\frac{5}{2}}y + 48\sqrt{G}\frac{dP_0}{dx}y + 112\sqrt{G}\left(\frac{dP_0}{dx}\right)^2 h^2 + 18G^{\frac{5}{2}}\left(\frac{dP_0}{dx}\right)^2 h^2y^2$$
$$+2G^{\frac{5}{2}}\frac{dP_0}{dx}h^5 - 224\sqrt{G}\frac{dP_0}{dx}h - 16G^{\frac{5}{2}}\frac{dP_0}{dx}hy^2 - 2(104+8Gy^2)G^{\frac{3}{2}}\frac{dP_0}{dx}h^3$$
$$-4G^{\frac{3}{2}}yh + 4G^{\frac{3}{2}}h^2(2+Gy^2) - G^{\frac{3}{2}}\left(\frac{dP_0}{dx}\right)^2 h^4(148+11Gy^2) + 30G^{\frac{3}{2}}$$
$$\times\left(\frac{dP_0}{dx}\right)^2 h^3y + 50G^{\frac{5}{2}}\frac{dP_0}{dx}h^4y + 25G^{\frac{5}{2}}\frac{dP_0}{dx}h^5y - 60\sqrt{G}\left(\frac{dP_0}{dx}\right)^2 hy$$
$$+134GG^{\frac{3}{2}}\frac{dP_0}{dx}h^2y + 12G^{\frac{5}{2}}h^3F_0 + 40G^{\frac{5}{2}}\frac{dP_0}{dx}h^3yF_0 + 4(8+Gy^2)$$
$$\times\sqrt{G}\frac{dP_0}{dx}F_0 - 4(36+4Gy^2)G^{\frac{3}{2}}\frac{dP_0}{dx}h^2F_0 - 28G^{\frac{3}{2}}yF_0 + 28G^{\frac{3}{2}}$$
$$\times\frac{dP_0}{dx}hyF_0 + 12G^{\frac{5}{2}}h^2yF_0 - 4G^{\frac{5}{2}}y^2{F_0}^2 + 16G^{\frac{5}{2}}h^2{F_0}^2 + 12G^{\frac{5}{2}}hy{F_0}^2,$$

$$C_{18}(x,y) = -4G^{\frac{5}{2}}h^4 + G^{\frac{5}{2}}y - 8\sqrt{G}\frac{dP_0}{dx}y - 48\sqrt{G}\left(\frac{dP_0}{dx}\right)^2 h^2 - 10G^{\frac{5}{2}}\left(\frac{dP_0}{dx}\right)^2 h^2y^2$$
$$-2G^{\frac{5}{2}}\frac{dP_0}{dx}h^5 + 32\sqrt{G}\frac{dP_0}{dx}h - 8G^{\frac{5}{2}}\frac{dP_0}{dx}hy^2 + 2(8-4Gy^2)G^{\frac{3}{2}}\frac{dP_0}{dx}h^3$$
$$-4G^{\frac{3}{2}}yh - 4G^{\frac{3}{2}}h^2(2+Gy^2) + G^{\frac{3}{2}}\left(\frac{dP_0}{dx}\right)^2 h^4(20+5Gy^2) - 30G^{\frac{3}{2}}$$
$$\times\left(\frac{dP_0}{dx}\right)^2 h^3y + 10G^{\frac{5}{2}}\frac{dP_0}{dx}h^4y + 5G^{\frac{5}{2}}\frac{dP_0}{dx}h^5y - 20\sqrt{G}\left(\frac{dP_0}{dx}\right)^2 hy$$
$$-26G^{\frac{3}{2}}\frac{dP_0}{dx}h^2y - 12G^{\frac{5}{2}}h^3F_0 - 4(8+Gy^2)\sqrt{G}\frac{dP_0}{dx}F_0 + 16G^{\frac{3}{2}}$$
$$\times\frac{dP_0}{dx}h^2F_0 - 28G^{\frac{3}{2}}yF_0 - 12G^{\frac{3}{2}}\frac{dP_0}{dx}hyF_0 - 12G^{\frac{5}{2}}h^2yF_0 + 4G^{\frac{5}{2}}y^2{F_0}^2$$
$$-16G^{\frac{5}{2}}h^2{F_0}^2 + 12G^{\frac{5}{2}}hy{F_0}^2,$$

$$C_{19}(x,y) = -20\sqrt{G}\frac{dP_0}{dx}y - 10(8+Gy^2)\sqrt{G}\left(\frac{dP_0}{dx}\right)^2 h^2 + 8(8+Gy^2)\sqrt{G}\frac{dP_0}{dx}h$$

$$-2G^{\frac{3}{2}}\left(\frac{dP_0}{dx}\right)^2 h^4(8+Gy^2)+40G^{\frac{3}{2}}\left(\frac{dP_0}{dx}\right)^2 h^3y+20G^{\frac{1}{2}}\left(\frac{dP_0}{dx}\right)^2 hy$$
$$-20G^{\frac{3}{2}}\frac{dP_0}{dx}h^2y-4(8+Gy^2)\sqrt{G}\frac{dP_0}{dx}F_0-4(8+Gy^2)G^{\frac{3}{2}}\frac{dP_0}{dx}h^2F_0$$
$$+40G^{\frac{3}{2}}\frac{dP_0}{dx}hyF_0,$$

$$C_{20}(x,y) = 8G^2h^3+16G^{\frac{5}{2}}y^2h^3+24Gy-G^3\left(\frac{dP_0}{dx}\right)^2 h^7-160\frac{dP_0}{dx}+16G\frac{dP_0}{dx}y^2$$
$$+110G^2\left(\frac{dP_0}{dx}\right)^2 h^2y+4G^3\frac{dP_0}{dx}h^5y+G\frac{dP_0}{dx}hy-44G^2\frac{dP_0}{dx}h^3y$$
$$-4G^2y^2h-116G^2h^2y+39G^2\left(\frac{dP_0}{dx}\right)^2 h^4y-2(96+Gy^2)G\left(\frac{dP_0}{dx}\right)^2 h^3$$
$$-2(22-3Gy^2)G^2\frac{dP_0}{dx}h^4-(54+Gy^2)G^2\frac{dP_0}{dx}h^5-4(40+5Gy^2)$$
$$\times\left(\frac{dP_0}{dx}\right)^2 h-2(68+7Gy^2)G\frac{dP_0}{dx}h^2-8G^3h^3yF_0-4G^2\frac{dP_0}{dx}h^3F_0$$
$$-20G^2yhF_0+60G\frac{dP_0}{dx}yF_0-104G^2\frac{dP_0}{dx}h^2yF_0-4G^2y^2F_0$$
$$+4(24+3Gy^2)G\frac{dP_0}{dx}hF_0+4(6+5Gy^2)G^2h^2F_0+4G^3h^3{F_0}^2$$
$$-60G^2y{F_0}^2-8G^3h^2y{F_0}^2-4G^3hy^2{F_0}^2,$$

$$C_{21}(x,y) = 8G^2h^3+16G^{\frac{5}{2}}y^2h^3+24Gy-G^3\left(\frac{dP_0}{dx}\right)^2 h^7+32\frac{dP_0}{dx}-8G\frac{dP_0}{dx}y^2$$
$$-70G^2\left(\frac{dP_0}{dx}\right)^2 h^2y-4G^3\frac{dP_0}{dx}h^5y-95G\frac{dP_0}{dx}hy+84G^2\frac{dP_0}{dx}h^3y$$
$$-4G^2y^2h+116G^2h^2y+41G^2\left(\frac{dP_0}{dx}\right)^2 h^4y-2(112+3Gy^2)$$
$$\times G\left(\frac{dP_0}{dx}\right)^2 h^3+2(10+7Gy^2)G^2\frac{dP_0}{dx}h^4-(22-3Gy^2)G^2\frac{dP_0}{dx}h^5$$
$$+4(8+Gy^2)\left(\frac{dP_0}{dx}\right)^2 h-2(68+7Gy^2)G\frac{dP_0}{dx}h^2+8G^3h^3yF_0$$
$$+4(15+2Gy^2)G^2\frac{dP_0}{dx}h^3F_0+20G^2yhF_0-60G\frac{dP_0}{dx}yF_0+24G^2$$
$$\times\frac{dP_0}{dx}h^2yF_0-4G^2y^2F_0-4(24+3Gy^2)G\frac{dP_0}{dx}hF_0-4(6+5Gy^2)$$
$$\times G^2h^2F_0+8G^3h^3yF_0+4G^3h^3{F_0}^2+60G^2y{F_0}^2+8G^3h^2y{F_0}^2+4G^3hy^2{F_0}^2,$$

$$C_{22}(x,y) = -4(-8+Gy^2)\frac{dP_0}{dx}-62G\left(\frac{dP_0}{dx}\right)^2 h^2y-112G\frac{dP_0}{dx}hy$$
$$-152G^2\frac{dP_0}{dx}h^3y$$
$$-102G^2\left(\frac{dP_0}{dx}\right)^2 h^4y+2(208+12Gy^2)G\left(\frac{dP_0}{dx}\right)^2 h^3-64G^2\frac{dP_0}{dx}h^4$$
$$-12G^2\frac{dP_0}{dx}h^5-4(8+Gy^2)\left(\frac{dP_0}{dx}\right)^2 h+2(200+22Gy^2)G\frac{dP_0}{dx}h^2$$

$$-72G^2\frac{dP_0}{dx}h^3F_0 - 60G\frac{dP_0}{dx}yF_0 - 60G^2\frac{dP_0}{dx}h^2yF_0 + 4(48+6Gy^2)G\frac{dP_0}{dx}hF_0,$$

$$\begin{aligned}C_{23}(x,y) \;=\; & 4(24+Gy^2)\frac{dP_0}{dx} - 58G\left(\frac{dP_0}{dx}\right)^2h^2y + 32G\frac{dP_0}{dx}hy + 72G^2\frac{dP_0}{dx}h^3y \\ & +22G^2\left(\frac{dP_0}{dx}\right)^2h^4y - 2(-80+4Gy^2)G\left(\frac{dP_0}{dx}\right)^2h^3 - 64G^2\frac{dP_0}{dx}h^4 \\ & -12G^2\frac{dP_0}{dx}h^5 + 2(40+2Gy^2)G\frac{dP_0}{dx}h^2 - 72G^2\frac{dP_0}{dx}h^3F_0 \\ & -20G\frac{dP_0}{dx}yF_0 + 60G^2\frac{dP_0}{dx}h^2yF_0 + 4(16+2Gy^2)G\frac{dP_0}{dx}hF_0,\end{aligned}$$

$$\begin{aligned}C_{24}(x,y) \;=\; & -8G^2h^3 + 8Gy + G^3\left(\frac{dP_0}{dx}\right)^2h^7 - 96\frac{dP_0}{dx} - 8G\frac{dP_0}{dx}y^2 \\ & -82G^2\left(\frac{dP_0}{dx}\right)^2h^2y \\ & +4G^3\frac{dP_0}{dx}h^5y + 104G\frac{dP_0}{dx}hy + 124G^2\frac{dP_0}{dx}h^3y + 4G^2hy^2 - 4G^2h^2y \\ & +75G^2\left(\frac{dP_0}{dx}\right)^2h^4y - 2(48+Gy^2)G\left(\frac{dP_0}{dx}\right)^2h^3 - 2(34+3Gy^2)G^2\frac{dP_0}{dx}h^4 \\ & -(42+3Gy^2)G^2\frac{dP_0}{dx}h^5 + 4(24+3Gy^2)\left(\frac{dP_0}{dx}\right)^2h - 2(124+9Gy^2)G\frac{dP_0}{dx}h^2 \\ & -8G^3h^3yF_0 - 4(15+2Gy^2)G^2\frac{dP_0}{dx}h^3F_0 - 8G^2yhF_0 - 20G\frac{dP_0}{dx}yF_0 + 44G^2 \\ & \times\frac{dP_0}{dx}h^2yF_0 + 4G^2y^2F_0 - 4(8+Gy^2)G\frac{dP_0}{dx}hF_0 - 4(6+Gy^2)G^2h^2F_0 \\ & -4G^3h^3{F_0}^2 + 20G^2y{F_0}^2 - 8G^3h^2y{F_0}^2 - 4G^3hy^2{F_0}^2,\end{aligned}$$

$$\begin{aligned}C_{25}(x,y) \;=\; & 8G^2h^3 - 8Gy + G^3\left(\frac{dP_0}{dx}\right)^2h^7 + 32\frac{dP_0}{dx} + 8\sqrt{G}\frac{dP_0}{dx}y \\ & +42G^2\left(\frac{dP_0}{dx}\right)^2h^2y \\ & -4G^3((dP_0)/(dx))h^5y + 16G\frac{dP_0}{dx}hy - 4G^2\frac{dP_0}{dx}h^3y + 4G^2y^2h + 4G^2h^2y \\ & +5G^2\left(\frac{dP_0}{dx}\right)^2h^4y + 10G^2\left(\frac{dP_0}{dx}\right)^2h^3y^2 - 2(2-Gy^2)G^2\frac{dP_0}{dx}h^4 \\ & -(10-Gy^2)G^2\frac{dP_0}{dx}h^5 - 4(24+3Gy^2)\left(\frac{dP_0}{dx}\right)^2h + 4(8+Gy^2)\left(\frac{dP_0}{dx}\right)^2h \\ & +2(4+7Gy^2)G\frac{dP_0}{dx}h^2 + 4(1+2Gy)G^2\frac{dP_0}{dx}h^3F_0 + 8G^2yhF_0 + 20G\frac{dP_0}{dx}yF_0 \\ & -8G^2\frac{dP_0}{dx}h^2yF_0 + 4G^2y^2F_0 - 4(6+Gy^2)G^2h^2F_0 - 4G^3h^3{F_0}^2 - 20G^2y{F_0}^2 \\ & +8G^3h^2y{F_0}^2 + 4G^3hy^2{F_0}^2.\end{aligned}$$

$$C_{26}(x,y) = 4(8+Gy^2)\frac{dP_0}{dx} + 50G\left(\frac{dP_0}{dx}\right)^2 h^2 y - 40G\frac{dP_0}{dx}hy + 10G^2\left(\frac{dP_0}{dx}\right)^2 h^4 y$$
$$-2(32+4Gy^2)G\left(\frac{dP_0}{dx}\right)^2 h^3 - 4(8+Gy^2)\left(\frac{dP_0}{dx}\right)^2 h + 2(16+2Gy^2)$$
$$\times G\frac{dP_0}{dx}h^2 + 5G\frac{dP_0}{dx}yF_0 + 20G^2\frac{dP_0}{dx}h^2 yF_0 - 4(16+2Gy^2)G\frac{dP_0}{dx}hF_0$$
$$+4(8+Gy^2)G\frac{dP_0}{dx}hF_0.$$

References

1. Dobell, C. Antony van Leeuwenhoek and his ‘Little Animals’. New York: Harcourt, Brace and Co. 1932, p. 435.
2. Muller OF, (1786). Animalcula infusoria; fluvia tilia et marina, que detexit, systematice descripsit et ad vivum delineari curavit. Havniae: Typis N. Molleri.
3. Kowalevsky A. Entwickelungsgeschichte des Amphioxus lanceolatus. Memoires de l'Academie Imperiale des Sciences de St.-Petersbourg VII. 1867, 11: 1-17.
4. Langerhans P. Zur Anatomie des Amphioxus. Archiv fur Mikrokopische Anatomie 1876, 12: 290-348.
5. Zimmermann KW. Beitrage zur Kenntniss einiger Drusen und Epithelien. Archiv fur Mikroskopische Anatomie 1898, 52: 552-706.
6. Sorokin SP. Reconstructions of centriole formation and ciliogenesis in mammalian lungs. Journal of Cell Science. 1968, 3: 207-230.
7. Porter KR, (1957). The submicroscopic morphology of protoplasm. New York: Harvey Society.
8. Taylor G. Analysis of the swimming of microscopic organisms. In Proceedings of the Royal Society of London A: Mathematical, Physical and Engineering Sciences.1951, 209(1099): 447-461.
9. Reynolds AJ. The swimaming of minute organisms. Journal of Fluid Mechanics. 1965, 23(2): 241-260.
10. Tuck EO. A note on a swimming problem. Journal of Fluid Mechanics. 1968, 31(2): 305-308.
11. Lighthill MJ. On the squirming (twisting) motion of nearly spherical deformable bodies through liquids at very small Reynolds numbers. Communications on Pure and Applied Mathematics. 1952, 5(2): 109-118.

12. Sleigh MA, (1962).The Biology of Cilia and Flagella. Pergamon Press London.
13. Sleigh MA. Patterns of ciliary beating. In Symposia of the Society for Experimental Biology. 1968, 22: 131-143.
14. Blake JR. A spherical envelope approach to ciliary propulsion. Journal of Fluid Mechanics. 1971, 46(1): 199-208.
15. Blake JR. Infinite models for ciliary propulsion. Journal of Fluid Mechanics. 1971, 49(2): 209-222.
16. Brennen C. An oscillating-boundary-layer theory for ciliary propulsion. Journal of Fluid Mechanics. 1974, 65(4): 799-824.
17. Brennen C. Hydromechanics of propulsion for ciliated micro-organisms. 1975, 235-253.
18. Katz DF, (1972). On the biophysics of in vivo sperm transport. Doctoral dissertation, University of California, Berkeley.
19. Lardner TJ and Shack WJ. Cilia transport. Bulletin of Mathematical Biology. 1972, 34(3): 325-335.
20. Blake JR. Flow in tubules due to ciliary activity. Bulletin of mathematical biology, 1973, 35: 513-523.
21. Sanderson MJ and Sleigh MA. The Function of Respiratory Tract Cilia. In The Lung in its Environment Springer US. 1982, 81-120.
22. Fulford GR and Blake JR. Muco-ciliary transport in the lung. Journal of Theoretical Biology. 1986, 121(4): 381-402.
23. Agrawal HL and Anawaruddin. Cilia transport of bio-fluid with variable viscosity. Indian Journal of Pure and Applied Mathematics. 1984, 15(10): 1128-1139.

24. Sleigh MA. Adaptations of ciliary systems for the propulsion of water and mucus. Comparative Biochemistry and Physiology Part A: Physiology. 1989, 94(2): 359-364.
25. Gueron S and Liron N. Ciliary motion modeling, and dynamic multicilia interactions. Biophysical Journal. 1992, 63(4): 1045-1058.
26. Dauptain A, Favier J and Bottaro A. Hydrodynamics of ciliary propulsion. Journal of Fluids and Structures. 2008, 24(8): 1156-1165.
27. Dillon RH, Fauci LJ, Omoto C and Yang X. Fluid dynamic models of flagellar and ciliary beating. Annals of the New York Academy of Sciences. 2007, 1101(1): 494-505.
28. Jayathilake PG, Tan Z, Le DV, Lee HP and Khoo BC. Three-dimensional numerical simulations of human pulmonary cilia in the periciliary liquid layer by the immersed boundary method. Computers & Fluids. 2012, 67: 130-137.
29. Pazour GJ and Witman GB. The vertebrate primary cilium is a sensory organelle. Current Opinion in Cell Biology. 2003, 15(1): 105-110.
30. Siddiqui AM, Haroon T, Rani M and Ansari AR. An analysis of the flow of a power law fluid due to ciliary motion in an infinite channel. Journal of Biorheology. 2010, 24(2): 56-69.
31. Bhatti MM, Zeeshan A and Rashidi MM. Influence of magnetohydrodynamics on metachronal wave of particle-fluid suspension due to cilia motion. Engineering Science and Technology, an International Journal. 2017, 20(1): 265-271.
32. Asghar Z, Ali N andSajid M. Interaction of gliding motion of bacteria with rheological properties of the slime. Mathematical Biosciences. 2017, 290: 31-40.

33. Akbar NS and Khan ZH. Metachronal beating of cilia under the influence of Casson fluid and magnetic field. Journal of Magnetism and Magnetic Materials. 2015, 378: 320-326.
34. Maqbool K, Shaheen S and Mann AB. Exact solution of cilia induced flow of a Jeffrey fluid in an inclined tube. Springer Plus. 2016, 5(1): 13-79.
35. Nadeem S and Sadaf H. Trapping study of nanofluids in an annulus with cilia. AIP Advances. 2015, 5(12): 127-204.
36. Sturgis SH. The effect of ciliary current on sperm progress in excised human fallopian tubes. Transactions of the American Society for the Study of Sterility. 1947, 3: 31–39.
37. Ashraf H, Siddiqui AM and Rana MA. Fallopian tube analysis of the peristaltic-ciliary flow of third grade fluid in a finite narrow tube. Chinese Journal of Physics. 2018, 56(2): 605-621.
38. Ashraf H, Siddiqui AM and Rana MA. Analysis of the peristaltic-ciliary flow of Johnson–Segalman fluid induced by peristalsis-cilia of the human fallopian tube. Mathematical Biosciences. 2018, 300: 64-75.
39. Fulford GR and Blake JR. Muco-ciliary Transport in the Lung. Jornal of Theoretical Biology. 1986, 121: 381-402.
40. Smith DJ, Gaffney EA and Blake JR. Modelling mucociliary clearance. Respiratory Physiology Neurobiology. 2008, 163:178-188.
41. Bottier M, Fernández MP, Pelle G, Isabey D, Louis B, Grotberg JB and Filoche M. A new index for characterizing micro-bead motion in a flow induced by ciliary beating: Part II, modeling. PLoS Computational Biology, 2017, 13(7):
42. Lardner TJ and Shack WJ. Cilia transport. Bulletin of Mathematical Biophysics. 1972, 34: 325–335.

43. Siddiqui AM, Farooq AA and Rana MA. Hydromagnetic flow of Newtonian fluid due to ciliary motion in the channel. Magnetohydrodynamics. 2014, 50: 109-122.
44. Haroon T, Ansari AR, Imran A and Siddiqui AM. On the ciliary transport of an axisymmetric power law fluid through a tube. Mathematics in Engineering Science and Aerospace. 2012, 3(2): 131–142.
45. Handling AC. The role of ciliaryaction in production of pulmonary atelectasis, vacuum in the paranasal sinuses and in otitis media. The Annals of Otology, Rhinology and Laryngology. 1943, 52: 3-19.
46. Handling AC. The relation of ciliary insu¢ ciency to death from asthma and other respiratory diseases. Transaction-American Academy of Ophthalmology Otolaryngology. 1943, 816-833.
47. Afzelius BA. Cilia-related diseases. The Journal of Pathology: A Journal of the Pathological Society of Great Britain and Ireland. 2004, 204(4): 470-477.
48. Ramesh K, Anwar Beg O and Tripathi D. 2018. Cilia-assisted hydromagnetic pumping of biorheological couple stress fluids. Propulsion and Power Research. In press
49. Ally J, Roa W and Amirfazli A. Use of mucolytics to enhance magnetic particle retention at a model airway surface. Journal of Magnetism and Magnetic Materials. 2008, 320(12):1834–1843.
50. Hayat T, Mahomed FM and Asghar S. Peristaltic flow of a magnetohydrodynamic Johnson–Segalman fluid. Nonlinear Dynamics. 2005, 40(4):375–385
51. Kothandapani M and Prakash J. Effect of radiation and magnetic field on peristaltic transport of nanofluids through a porous space in a tapered asymmetric channel. Journal of Magnetism and Magnetic Materials. 2015, 378152–163.

52. Narla VK, Tripathi D, Beg AO and Kadir A. Modelling transient magnetohydrodynamic peristaltic pumping of electroconductive viscoelastic fluids through a deformable curved channel. Journal of Engineering Mathematics. 2018, 111: 127–143.
53. Ramos A. Electrohydrodynamic and magneto-hydrodynamic micropumps, In: Hardt S, Sch€onfeld F, editors. Microfluidics technologies for miniaturized analysis systems. Boston: Springer. 2008, 59–116.
54. Anwar Beg O. 2018. Biomimetic propulsion analogiesaerodynamics of small fliers and microscale beating in internal propulsion, Technical Report, Aero-Mech 3, 94pp, April, University of Salford, Manchester, UK.
55. Sajid M, Ali N, Anwar BO and Siddiqui AM. Swimming of a singly flagellated micro-organism in a magnetohydrodynamic second order fluid. Journal of Mechanics in Medicine Biology. 2017, 17(1):1750009.
56. Mann AB, Shaheen S, Maqbool K and Poncet S. Fractional Burgers Fluid Flow Due to Metachronal Ciliary Motion in an Inclined Tube, Frontiers in Physiology, 2019, 10: 588.
57. Bhatti MM, Zeeshan A. and Rashidi MM. Influence of magnetohydrodynamics on metachronal wave of particle-fluid suspension due to cilia motion. Engineering Science and Technology, an International Journal. 2017, 20: 265-271.
58. Abo-Elkhair RE, Mekheimer KS and Moawad AMA. Cilia walls influence on peristaltically induced motion of magneto-fluid through a porous medium at moderate Reynolds number: Numerical study. Journal of Egyptian Mathematical Society. 2017, 25: 238-251.
59. Siddiqui AM., Manzoor N, Maqbool, K, Mann AB and Shaheen S. Magnetohydrodynamic Flow Induced by Ciliary Movement: An application to

lower respiratory track diseases. Journal of Magnetism and Magnetic Materials. 2019.

60. Vilfan, M, Potoc A, Osterman N, Poberaj I and Vilfan A. Self-assembled artificial cilia. Proceeding of the National Academy of Sciences of the United State of America. 2010, 107: 1844 -1847.
61. Gauger EM, Downton MT and Stark H. Fluid transport at low Reynolds number with magnetically actuated artificial cilia. European Physical Journal E: Soft Matter and Biological Physics. 2009, 28: 231 -242.
62. He Y et al. Finite element analysis of blood flow and heat transfer in an image-based human finger. Comp. Biol Med. 2008, 38: 555-562.
63. Tse O, Pinnau R and Siedow N. Identification of temperature-dependent parameters in laser-interstitial thermo therapy. Mathematical Models and Methods in Applied Sciences. 2012, 22: p.1250019.
64. Infante JA, Ivorra B, Ramos AM and Rey JM. On the modelling and simulation of high pressure processes and inactivation of enzymes in food engineering. Mathematical Models and Methods in Applied Sciences. 2009, 19: 2203-2229.
65. Karampatzakis A and Samaras T. Numerical model of heat transfer in the human eye with consideration of fluid dynamics of the aqueous humor. Physics in Medicine and Biology. 2010, 55: 5653-5678.
66. Tripathi D, Pandey SK and Bég OA. Mathematical modelling of heat transfer effects on swallowing dynamics of viscoelastic food bolus through the human oesophagus. International Journal of Thermal Sciences. 2013, 70: 41-53.
67. Horstmann G, Iravani J, Melville GN and Richter HG. Influence of temperature and decreasing water content of inspired air on the ciliated bronchial epithelium, Acta Oto-Laryngol. 1977, 84:124-131.

68. Zaman A, Ali N, Bég OA and Sajid M. Heat and mass transfer to blood flowing through a tapered overlapping stenosed artery, International Journal of Heat and Mass Transfer. 2015, 95: 1084-1095.

69. Jiang SC, Ma N, Li HJ, Zhang XX. Effects of thermal properties and geometrical dimensions on skin burn injuries. Burns. 2002, 28(8): 713-717.

70. Uddin MJ, Bég OA and Kabir MN. Computational investigation of Stefan blowing and multiple slip effects on buoyancy-driven bioconvection nanofluid flow with micro-organisms, International Journal of Heat and Mass Transfer. 2016, 95: 116-130.

71. Hochmuth R and Deuflhard P. Multiscale analysis for the bio-heat transfer equation---the nonisolated case. Mathematical Models and Methods in Applied Sciences. 2004, 14: 1621-1634.

72. Prek M. Thermodynamical analysis of human thermal comfort. Energy. 2006, 31: 732-743.

73. Mills ZG, Aziz B and Alexeev A. Beating synthetic cilia enhance heat transport in microfluidic channels. Soft Matter. 2012, 45: 11508–11513.

74. Akber NS, Khan ZH and Nadeem S. Metachronal beating of cilia under influence of Hartmann layer and heat transfer. The European Physical Journal Plus. 2014, 129: 176.

75. Akbar NS, Wahid Butt A and Noor FM. Heat transfer analysis on transport of copper nanofluids due to metachronal waves of cilia. Current Nanoscience. 2014, 10(6): 807- 815

76. Sadaf H. Bio-fluid flow analysis based on heat transfer and variable viscosity. Applied Mathematics and Mechanics (English Edition). 2019, 40(7): 1029–1040.

77. Sadaf H and Nadeem S. Fluid flow analysis of cilia beating in a curved channel in the presence of magnetic field and heat transfer. Canadian Journal of Physics. 2020, 999: 1-7.

78. Farooq AA, Shah Z and Alzahrani EO. Heat transfer analysis of a magneto-bio-fluid transport with variable thermal viscosity through a vertical ciliated channel. Symmetry. 2019, 11(10): p.1240.

79. Imran A, Akhtar R, Zhiyu Z, Shoaib M and Raja MAZ. Analysis of MHD and heat transfer effects with variable viscosity through ductus efferentes. AIP Advances, 2019, 9(8): p.085320.

80. Murdock J. Perturbation Methods. Mathematical Tools for Physicists. 2006, 385–415.

81. Adomian G, (1986). Nonlinear Stochastic Operator Equations: Academic Press. Can Diego, CA.

82. Adomian G, (1994). Solving Frontier Problems of Physics: The Decomposition Method Kluwer. Boston MA.

83. He JH. Homotopy perturbation technique. Computer methods in applied mechanics and engineering. 1999, 178(3): 257-262.

84. Hina S and Yasin M. Slip effects on peristaltic flow of magnetohydrodynamics second grade fluid through a flexible channel with heat/mass transfer. Journal of Thermal Science and Engineering Applications. 2018, 10: p.051002.

85. Bég OA, Tripathi D, Sochi T and Gupta PK. Adomian decomposition method (ADM) simulation of magnetobiotribological squeeze film with magnetic induction effects. Journal of Mechanics in Medicine and Biology. 2015, 15: 1550072.1-1550072.23.

86. Bég OA. Nonlinear multiphysical laminar nanofluid bioconvection flows: Models

and computation. In: Sohail A, Li Z, eds. Computational approaches in biomedical nano-engineering. New York, USA: John Wiley Publisher; 2019, 100-130.

87. Thurston GB and Greiling H. Viscoelastic properties of pathological synovial fluids for a wide range of oscillatory shear rates and frequencies. Rheologica Acta. 1978, 17: 433-445.
88. Abdelsalam SI and Bhatti MM. The study of non-Newtonian nanofluid with hall and ion slip effects on peristaltically induced motion in a non-uniform channel. RSC Advances. 2018, 8: 7904-7915.